Contract No. DA-36-039-SC-78902

TIROS I METEOROLOGICAL SATELLITE SYSTEM

FINAL COMPREHENSIVE TECHNICAL REPORT

Volume II

Prepared for the

U.S. ARMY SIGNAL RESEARCH AND DEVELOPMENT LABORATORY

FORT MONMOUTH, N. J.

and the

NATIONAL AERONAUTICS AND SPACE ADMINISTRATION

WASHINGTON, D. C.

ASTRO-ELECTRONICS DIVISION
DEFENSE ELECTRONIC PRODUCTS
RADIO CORPORATION OF AMERICA
PRINCETON, N. J.

AED-339

Issued July 1, 1961

CONTENTS

VOLUME I

CONTENTS (Continued)

CONTENTS (Continued)

CONTENTS (Continued)

CONTENTS (Continued)

CONTENTS (Continued)

CONTENTS (Continued)

CONTENTS (Continued)

CONTENTS (Continued)

VOLUME III

PART 3. TESTS

CONTENTS (Continued)

CONTENTS (Continued)

CONTENTS (Continued)

LIST OF ILLUSTRATIONS

VOLUME I

LIST OF ILLUSTRATIONS (Continued)

LIST OF ILLUSTRATIONS (Continued)

LIST OF ILLUSTRATIONS (Continued)

LIST OF ILLUSTRATIONS (Continued)

LIST OF ILLUSTRATIONS (Continued)

LIST OF ILLUSTRATIONS (Continued)

LIST OF ILLUSTRATIONS (Continued)

LIST OF ILLUSTRATIONS (Continued)

LIST OF ILLUSTRATIONS (Continued)

LIST OF ILLUSTRATIONS (Continued)

LIST OF ILLUSTRATIONS (Continued)

VOLUME III

PART 3. TEST

LIST OF ILLUSTRATIONS (Continued)

LIST OF ILLUSTRATIONS (Continued)

6. Antenna Subsystem

a. General

The satellite antenna subsystem basically provides a means for the reception of command signals from the ground control stations and for the simultaneous radiation of the signals from the two beacon and two television transmitters. It also provides for coupling and matching to the antennas and for isolation between the four transmitters and the two command receivers. This subsystem basically consists of a simple dipole antenna for the command receivers, and two crossed dipole antennas (two frequency) and an associated r-f matching and coupling network for the beacon and television transmitters.

b. Functional Description

The receiving dipole antenna is 0.25 wavelength long, and is vertically mounted on top of the satellite at the spin axis. The antenna is coupled to the two receivers through a 0.5-wavelength transmission line, a T junction and two 3/8 wavelength transmission lines.

The crossed dipole transmitting antennas are mounted under the baseplate, radially oriented and centered on the spin axis. Each dipole element consists of a rod, 0.29 wavelength long at 108 Mc, which is concentrically mounted in a sleeve, one-quarter wavelength long at 235 Mc. The rod and sleeve are joined at the drive end to form a quarter-wave shorted coaxial transmission-line decoupling stub within the sleeve. By correctly proportioning the radiation resistances of the sleeve and the rod extension, the mutual coupling between these elements is used to control the impedance of the sleeve termination. The dipoles are fed in quadrature to provide circular polarization and a nearly isotropic radiation pattern.

The r-f matching and coupling network matches and couples the beacon and television transmitters to the crossed dipoles. It also divides the current to each dipole properly. Separate coupling and matching network sections are used for the beacon (108 Mc) and television (235 Mc) transmitters. Each network section, as shown in Figure 96, is in printed-circuit stripline form and consists of a diplexer and two balun transformers. The diplexer is a transmission-line bridge network which permits the transmitters, connected symmetrically across the bridge input, to be coupled to the antenna, which is connected across the output, without being coupled to each other. The balun transformer serves as a delay line to selectively phase the r-f currents in the dipoles. The two transmission cables, which couple the diplexers to their balun transformers, differ electrically by a quarter wave (90°) to provide quadrative feed to the crossed dipoles.

c. Development

(1) Initial Development

The development of the antenna and r-f coupling networks initially was directed toward quite different requirements than those of the final model. The

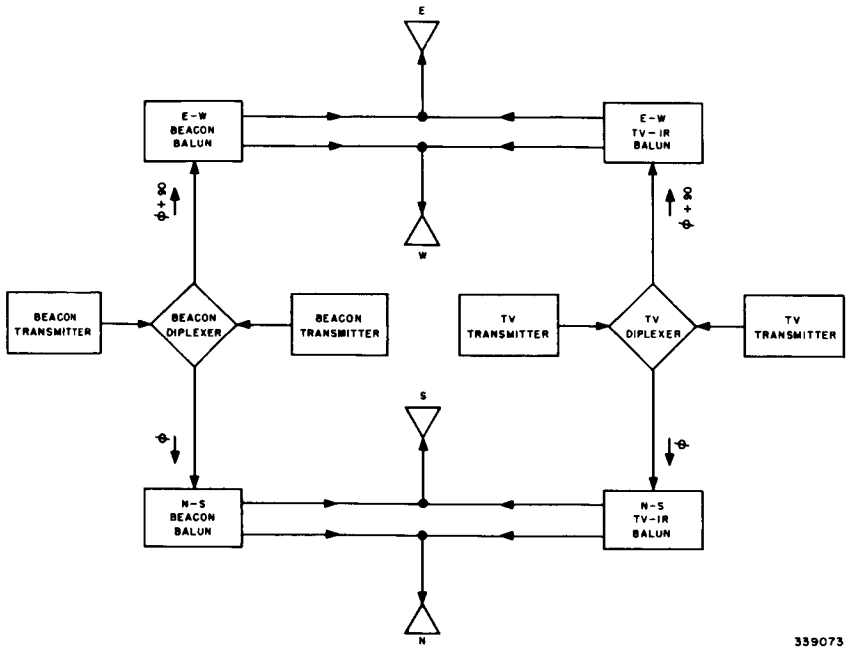

Figure 96. R-F Coupling and Matching Network, Block Diagram

development of these two systems began with a predecessor satellite designed by RCA, which had a radically different form factor than TIROS. The form factor was a major consideration in the development of a workable antenna system. Further, this satellite required only a single electronic channel; i.e., one video tape transmitting system and one beacon transmitter. TIROS was designed for two such channels plus an "infrared experiment" which required a transmitter. Thus the r-f coupling systems for connecting the various transmitters to the antenna system had quite different design goals for the two different projects.

(a) Early Antenna System Requirements.

The initial requirements set up to be met by the antenna and r-f coupling systems are:

1. Circularly polarized radiation from the antenna system.
2. A radiation pattern as nearly isotropic as possible, with minimum distortion caused by satellite shape and external appendages, such as battery arms, etc.
3. Efficient operation in the following frequency bands:

108 Mc (transmission)

235 Mc (transmission)

150 Mc (reception)

4. Simultaneous operation of two transmitters, one in each of the frequency bands listed.

5. Simultaneous operation of a receiver in the 150-Mc band along with the two transmitters listed, with no blocking interference to the receiver from either transmitter.

6. Mechanical and dimensional characteristics of the satellite antenna system within the mechanical and spatial limitations imposed by the form factor of the satellite and its appendages and the limitations imposed by the launching vehicle.

(b) Scale Model Studies.

In order to facilitate initial measurements of both radiation patterns and impedances of various tentative configurations, the scale-modeling technique was used. A scale factor of 5-to-1 was used for obtaining data on the earlier satellite configuration; a 4-to-1 ratio was used on the TIROS satellite configuration. To obtain pattern data, a full-cylinder type accurately-scaled-shape model was used with balanced-dipole radiators. An electrically driven turntable with a mechanically-connected signal-strength recorder was used to plot the patterns. To obtain impedance data, a half-shell model was mounted on a large 1/4-inch thick aluminum sheet which served as a ground plane. This method was used to facilitate the measurement of a single radiating element in the unbalanced form, and thus, reduce the complication of measuring the impedance through a balun. Both a slotted line and a Polytechnic Research and Development Company standing-wave detector were used for measuring the terminal impedance of the various radiating configurations which were tried during the course of the development of the antenna system.

It was decided that, from the standpoints of reliability, more simple construction, and mutual coupling, it would be desirable to concentrate on a single radiating system which would radiate efficiently on both transmitting frequencies, in contrast to a separate radiating system for each frequency. The major problem with this approach, however, was that for a simple dipole of a length which has a reasonable terminating impedance at one of the frequencies, the impedance became unreasonable at the other frequencies, because a range of somewhat over an octave is involved between 108 and 235 Mc. Therefore, it became evident that, in order to solve the impedance problem, some configuration more complex than the simple dipole was necessary.

One solution, which ultimately proved quite satisfactory, was to use a quarter-wave dipole (at the highest frequency) with a parallel-resonant circuit (tuned to the same frequency) connected at the outward end of the dipole, in series with an extension of the dipole. The overall length of the extension would be approximately one-quarter wavelength at the lowest frequency. The result was a reasonably good termination which could be conveniently matched at both the high and low frequencies. In effect, the parallel-resonant circuit formed a trap at the high frequency and prevented

the high-frequency current from traveling beyond the end of the quarter-wave section. In practice, the parallel-resonant circuit was formed by placing a sleeve of one-quarter wavelength, at the high frequency, around a rod which was a quarter wavelength long at the low frequency. The sleeve was electrically connected to the rod at the feedpoint to form a quarter-wave concentric transmission line, shorted at the input end and open-circuited at the other end. The center-conductor or rod portion extending beyond the sleeve was, therefore, conductively isolated from the external portion of the sleeve by the high-impedance path which existed between the outer and inner conductors of the concentric line at the open end of the sleeve. Only mutual coupling exists between the sleeve and the rod portion.

(c) Field Patterns.

With dipoles mounted radially outward from the surface of the satellite, it was evident that two dipoles of a dipole pair would have to be separated by a distance d, which is at least the diameter of the satellite-to-rocket mating surface. This situation dictated the use of separate unbalanced feed lines for each dipole element, which was later found to be a distinct advantage. Straight-forward field pattern calculations can be made in the case of a continuous half-wave dipole in free space from the relation $f(\theta) = \frac{\cos(90 \cos\theta)}{\sin\theta}$ where θ is the angle from the antenna axis. A sufficiently close approximation results, however, if the more simple relation $f(\theta) = \sin\theta$ is used. In the case of the satellite antenna, the current loop or driving point of the quarter-wave dipole pairs, which constitute the half-wave radiating system, were not in proximity to each other, but are separated by d. This condition, in addition to the presence of the satellite itself in the r-f field with its attendant induced skin-circulating currents, resulted in a field-pattern function which differed from that obtained by the free-space dipole to a degree dependent upon d/λ.

Because the initial requirements specified that the radiation be circularly polarized, the radiated field was required to be uniform at any point on the spin axis. This requirement may be theoretically achieved by the use of two crossed dipoles fed in phase quadrature. The resultant field at any point in the plane of the dipoles, obtained from the combined field patterns of the individual dipoles, is equal to the square root of the sum of the squares of the individual fields in that direction. This becomes evident when considering the relation $f(\theta) = \sin\theta$, where θ is the angle measured from the dipole axis. Consider one dipole as a reference axis; its $f(\theta) = \sin\theta$ as stated previously, while the function of the other dipole, measured from the reference axis, is $f(\theta) = \cos\theta$.

The trigonometric identity $\cos^2\theta \quad \sin^2\theta = 1$, therefore shows the validity of using a crossed dipole pair to achieve circular polarization. When using the more precise value $f(\theta) = \frac{\cos(90 \cos\theta)}{\sin\theta}$ for a half-wave dipole, the pattern is not quite circular, but departs from a circle by approximately 5 percent: but, because of the distortion of the field radiated by each dipole pair mounted on the satellite (caused by the previously mentioned d spacing and skin-circulating currents), measurement of the pattern of one dipole pair is necessary to determine the degree of deviation from the $\sin\theta$ dipole pattern. Therefore, measurement of the pattern is also necessary to determine whether the sum field of crossed dipoles on the satellite will be sufficiently circular to satisfy the requirement.

(2) Transmitting Antennas and R-F Coupling Matching Networks

(a) Requirements for TIROS I.

With the redirection of the earlier satellite project, resulting in what became known as TIROS, came a modification of some of the requirements placed on the antenna and coupling systems. (Ref. 12) Items 4 and 5 of the initial antenna requirements were superseded because of an increase in number of overall systems. Item 6, concerning the mechanical and dimensional characteristics, was not changed, but was effectively modified in character because the satellite form factor had been completely changed. A completely new overall study was therefore necessary to determine what form of antenna system would be suitable for use on the TIROS configuration. A new antenna design, which would possibly require a different solution to the impedance matching problem, in addition to increasing the number of transmitters and receivers to be operated simultaneously, also called for a completely new study of the coupling system.

(b) Transmitting Antennas.

Several approaches to the design of a new antenna configuration were considered but most of these were rejected because of mechanical or environmental limitations. One consideration was the use of slot radiators spaced around the periphery of the satellite. However, this method would have pre-empted valuable area required by the sun cells on the surface. Also, the volume required for cavities backing the slots could not be spared inside the satellite. Another consideration was the use of four magnetic loops mounted at the cardinal points on the sides of the satellite and shaped to fit concentrically a few inches outward from the surface. This approach was rejected because of shadowing of the sun cells. It was believed, at that time, that a shadow falling across a group of sun cells would cause an open circuit in that group and reduce the total battery-charging capacity of the sun-cell groups. Therefore, no further consideration of antenna location on side and top areas of the satellite was permitted. Only the bottom area remained acceptable.

With radiating elements on the bottom of such a large conducting mass, the first question which arose concerned the likelihood of an r-f shadow in the topside direction; pattern measurements would determine this. However, there was very little promise of achieving a pattern which would even resemble an isotropic pattern.

One additional initial requirement was that the antenna system be operable during launch to permit tracking of the 108-Mc beacon transmitters. This meant that if a configuration, which would require a fold-in of the dipoles (because of the confining space of the nose cone) was used, it would have to be operable in the folded-in condition as well as in the open condition after the nose cone separation. Restrictions were also imposed on certain areas on the bottom of the satellite, which further limited ideal antenna placement. First, the major area toward the center was required for the mechanical connection to the third-stage rocket; second, unobstructed space was required in front of the two camera lenses and the "downward" viewing path of the

infrared sensor. Essentially, the restrictions and limitations imposed on the design of a radiating system for TIROS were considered to be quite severe.

The straight dipole was the only antenna type considered for the bottom mounting-location. Two different mounting points were considered. One scheme was to use four radiators, each mounted radially from the bottom rim of the satellite; the other was to mount them as close as possible to the rocket attachment ring, protruding angularly outward from the bottom. The latter scheme was chosen and is now in use.

1 Scale-Model Patterns

Scale-model pattern measurements were made by AED personnel, using facilities of the Antenna Laboratory of the RCA Laboratories Division. The previously-mentioned scale factor of four was used; the frequencies used during the test were 432 and 940 Mc. A 48-inch dish, which had a variable-length rotatable dipole feed, was used for the transmitting antenna, and the scale model was used for receiving. A coaxial balun was fabricated to achieve a balanced feed for the two dipoles mounted on the satellite model and to permit the use of a coaxial line to bring the received energy down the supporting mast to the receiver-recorder combination.

The dish was mounted on the side of the building, looking into open space for several hundred feet, entirely clear of any obstacles which might cause reflections. The scale model was placed precisely on the axis of the dish, and sufficiently far from the dish to be in the far-field, to ensure receiving a plane-wave front. To determine the extent which ground reflections might affect the accuracy of the measurements, the model antenna was turned to a null position, and a four-foot square aluminum sheet was moved back and forth under the dish axis. No appreciable change in received signal level was observed at any of the three operating frequencies, thus proving that errors due to ground reflections were negligible.

Initial measurements were made using the same dipole radiating elements for both frequencies. The dipole length was chosen to be a quarter-wave at the highest frequency to ensure that any deviation in the patterns obtained, from that of the ideal dipole pattern, would be the result of the integrated radiating configuration only, and would not be affected by a deviation from the normal aspect directivity of the dipole itself. In other words, if the dipole were longer than a quarter-wave at any of the frequencies involved, the field launched by the dipole would be predistorted and would therefore not follow the sine relation required for achievement of a circular pattern. No attempt was made to effect an impedance match between the dipole pairs and the feedline, other than the previously mentioned stub tuner for tuning out residual reactance at the crystal diode. The balun was carefully checked, however, to ensure that equal currents were flowing in the two dipoles.

From the pattern information obtained with the previous satellite-antenna configuration, the rim mounting method was not expected to be very satisfactory from the standpoint of achieving an isotropic pattern, because the d value (distance of dipole element separation) of the TIROS configuration was exactly four times as great (i.e., 0.8 wavelength) as that of the prior configuration. The previous d value, 0.2 wavelength at the highest frequency, had been large enough to indicate mildly discouraging isotropic possibilities. Although the lowest frequency was not affected appreciably patternwise by the d value for the earlier antenna, this became approximately 0.4 wavelength in TIROS. Nevertheless, patterns were measured with this rim-mounted dipole arrangement, and the results proved what had been suspected; that the d value was much too great to warrant further consideration of this arrangement except as a last resort.

The patterns obtained showed that the shadowing effect which had been anticipated, was not in evidence. Measurements showed that at 235 Mc a pattern which was quite close to isotropic was possible. At 108 Mc a minimum of a few db below isotropic would fall on the spin axis at the bottom, but the radiation off the top would have a broad maximum a few db above the isotropic level; this was the reverse of that which was expected.

2 Scale-Model Impedance Measurements.

Once the pattern measurements revealed a promising dipole configuration, a new half-shell model was fabricated (also at a 4-to-1 scale ratio) with precisely the shape of the new structure. This new model was fitted to the same ground plane, and impedance measurements were made using the same generator and indicator as before, but the Polytechnic Research and Development Company standing-wave detector was used exclusively in preference to the slotted line.

It was quickly determined that the optimum angle between the dipole and the spin axis was 45°, but ±5° was tolerable.

The Smith Chart graphs in Figures 97 and 98 show the impedance at the scale frequencies corresponding to 108 Mc and 235 Mc with varying values of dipole and sleeve dimensions. Note that the 108-Mc impedance increases smoothly with dipole length, somewhat similar to a dipole over an infinite smooth plane, and becomes non-reactive at approximately one-quarter wave with a resistive component of 15 ohms. With increase of length the impedance continues to change smoothly.

An interesting phenomena, concerning the impedance change at the frequency corresponding to 235 Mc emerged, however. This phenomena played an extremely important part in the design of the coupling system. Note that when the coaxial sleeve portion is a quarter wave long, it is

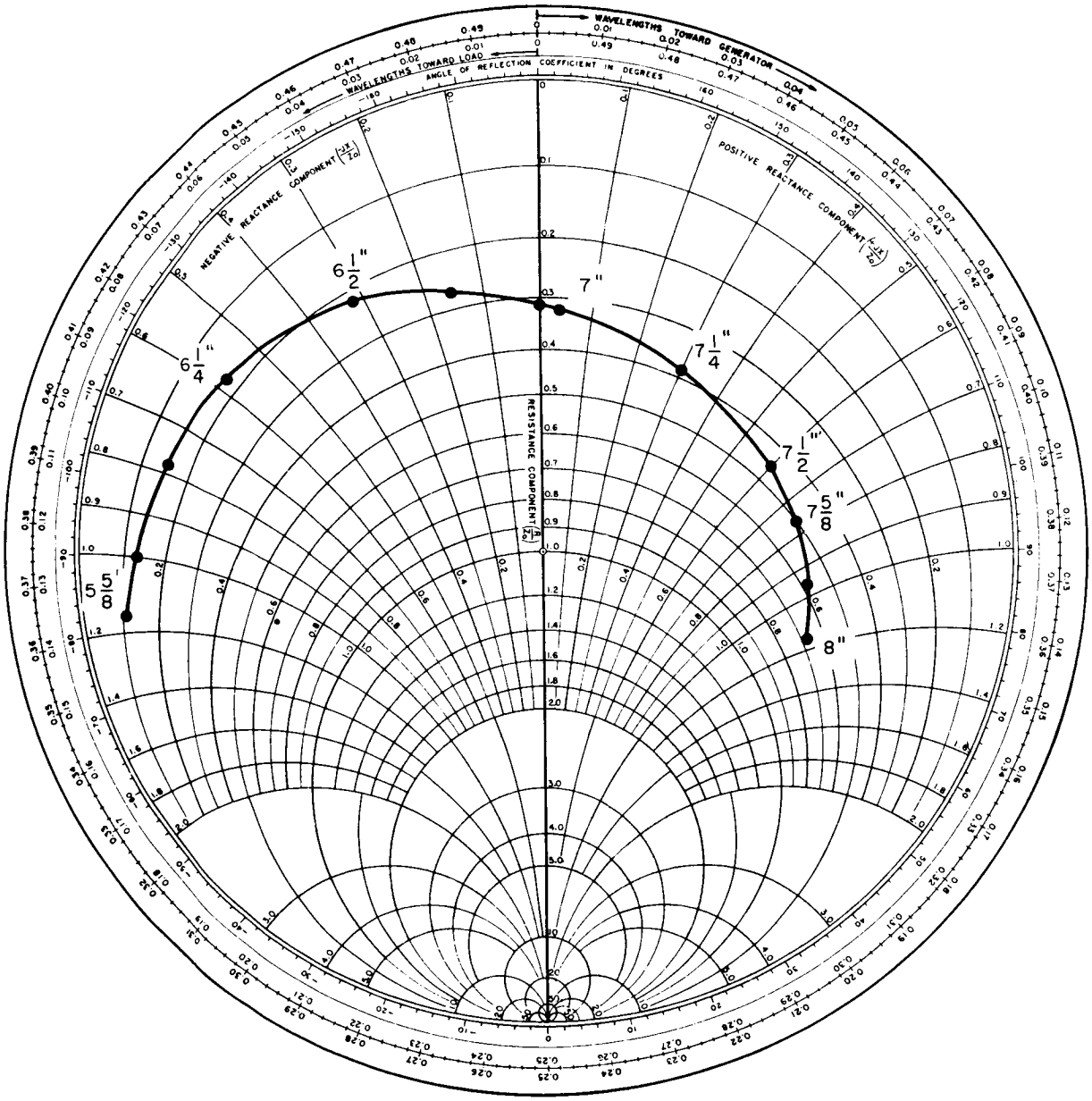

MEASURED AT 432 MC IMPEDANCE
VERSUS TOTAL DIPOLE LENGTH, WITH
CONSTANT SLEEVE LENGTH OF 2 27/32"

339027

Figure 97. Plot of Scale- Model Impedance Measurements (108 Mc)

940 mc.

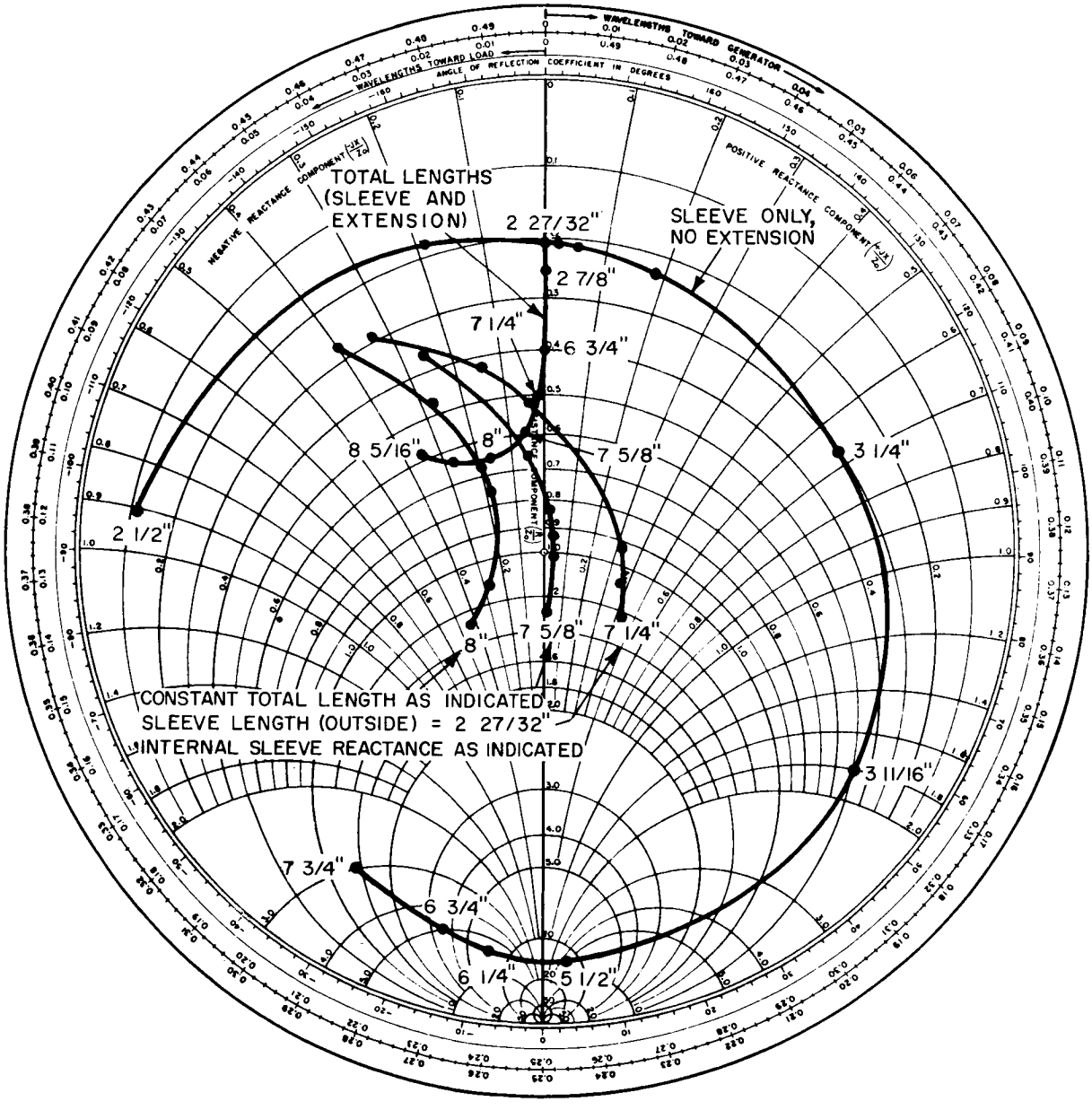

339078

Figure 98. Scale-Model Impedance Measurements (235) Mc)

non-reactive with a resistive component of approximately 10 ohms. As the center conductor is extended toward the length required at 108 Mc, the resistive component of terminating impedance at 235 Mc is seen to increase rapidly without appreciably affecting the reactance until an overall length of 0.6 wavelength is reached. Curves labeled "Constant total length as indicated" show the effect of varying the internal sleeve reactance by varying the internal length of the coaxial portion with given values of center conductor extension length. From this it can be seen that as the extension length is further increased, the resistive component increases, and as a reactive component emerges, it can be cancelled by adjustment of the internal length of the coaxial parallel resonant circuit. Therefore, a 50-ohm non-reactive termination at 235 Mc can be achieved by proper adjustment of the configuration.

The correct length for 235 Mc, however, does not happen to coincide with a non-reactive length at 108 Mc. Actually, the 108-Mc terminating impedance with this arrangement is 25 + j37.5. The manner in which these two impedances influence the design of the coupling system is that, while at one frequency the impedance is 50 + j0, varying the length of a 50-ohm line feeding such a termination will have no adverse effect on the match. This factor leaves complete freedom to choose line lengths in the 108-Mc feed, which by stub and transformer combinations, the terminating impedance of 25 + j37.5 can be transferred to 50 + j0, and thereby achieve a satisfactory match at both frequencies.

3 Full-Scale Model

While the scale-model pattern and impedance measurements were being made, a full-scale model of the TIROS structure was being fabricated. This structure was precise in every detail, including the rib structure for supporting the baseplate. It was constructed of aluminum on a wooden frame. The purpose of the full-scale model was to permit comparison and verification of the measurements obtained with the scale-model technique, and for use in the testing of various dipole mounting configurations in the development of the final hardware.

Measurements taken with this model have shown reasonable agreement with data derived from the scale models. Dipole element dimensions, scaled upward in size from the scale model values, agree quite well with the values determined independently with the full-scale model.

At one time during the development, the group concerned with temperature environment considered placing a reflective skin over the entire bottom. This would result in replacing the ribbed structure environment, for which the antenna system had been designed, with an entirely smooth surface. A sheet aluminum cover was made to fit over the bottom of the full-scale model, and further impedance measurements were made to determine the effect of such a skin on the operation of

the antenna system. Small changes in impedance values were noted, but these would have required only a small change in dipole dimensions if a decision had been made to use such a skin on the final structure.

Subsequent to the pattern and impedance measurements made on the new TIROS configuration, a modification was made in the mechanical mounting configuration which coupled the satellite to the third stage rocket. This modification included enlarging the diameter of the mating surfaces, which in turn necessitated an increased separation distance d between the dipole mountings. It is probable that this change resulted in some degree of change in pattern and impedance. No effort was made to determine the amount of change, however, because, at this late stage of development, it was deemed more practical to make such determinations on the full-scale model.

In the final form of the dipole structure of the prototype and flight models, the coaxial sleeve diameter was changed considerably from that which was measured by the scaling technique. Also, the mounting flange for the dipole in the final model was greatly increased in area; this increased the shunt capacitance at the terminating point. The combination of all of these changes resulted in the necessity for a somewhat longer dipole extension, to increase the resistive component of the 235-Mc terminating impedance to 50 ohms. Also, the composite result at 108 Mc was a change in impedance, from that obtained with the scale model, to a value of approximately 150 - j100 ohms.

(c) R-f Coupling and Matching Networks

1 Initial Studies.

The fundamental r-f coupling and matching system requirements, upon which the initial studies were based, were as follows:

a To supply r-f power to four dipole elements in the 108-Mc and 235-Mc bands; the phase supplied to each element respectively progressing 90° at both frequencies for achievement of circular polarization in both frequency bands.

b To permit coupling of three transmitters in the 235-Mc band and two in the 108-Mc band to the antenna system in an efficient manner with minimum cross coupling. Also, to permit two transmitters in each band (total of four) to be operable simultaneously with no objectionable mutual interference.

c To provide terminal impedance, at each input, of 50 ohms to match the output impedance of the transmitters.

d To provide a terminal impedance, at the four output terminals, N, E, S, W, respectively, of 50 ohms in the 235-Mc band and adjustable in the vicinity of 150 - j100 ohms in the 108-Mc band.

Before attempting to design circuitry to meet these requirements, it was decided to consider the use of r-f transmission line, or distributed constants components, rather than lumped-constants components. It was thought that this approach would be more feasible from the standpoint of environmental stability, and might also prove to have lower circuit loss. With this approach, the circuit shown in Figure 99 was evolved to accommodate two transmitters in each frequency band. This circuit seemed to contain the minimum basic components which could achieve the requirements. The first thought was to fabricate the entire network out of precisely-cut lengths of RG55/U cable, with connections made with BNC connectors. This approach, however, led to a very unwieldy cable-arrangement problem plus a staggering number of BNC connectors. In addition to being unwieldy, this approach would have yielded a very heavy package; a more satisfactory approach was absolutely imperative.

It was thought that perhaps the same basic circuit could be fabricated by using printed-circuit stripline for some of the component parts, and making the interconnections with ordinary coaxial cable and BNC type connectors. This would reduce the physical complexity as well as the number of connectors.

The fabrication technique of stripline components was then investigated to determine: the degree of control which might be obtained over the characteristic impedance of the line; the r-f power loss involved; and the minimum strip-to-strip spacing that could be used to "wind-up" the electrical lengths required. This would avoid the degree of adjacent-strip coupling which might lead to instability.

The first step was to construct a single-length straight-line strip of carefully-cut aluminum foil which was rigidly held between two 1/16-inch aluminum plates by sandwiching the strip between two 1/8-inch sheets of polystyrene. Measurement of characteristic impedance showed very close agreement with that of the design center. The second step was to make a similar test using a stripline fabricated by photo-etching copper-clad, teflon-fiberglass, known as GB-112T, a product of the Continental Diamond Fiber Co. This test showed good agreement and repeatability in both characteristic impedance and electrical length. Terminations were made to BNC chassis connectors and tests were made using a Polytechnic Research and Development Company standing-wave detector.

A further test, using the photo-etched stripline, involved maximizing the length of line in a given area, with a center-to-center strip spacing of 1 cm to determine the degree of mutual coupling between adjacent portions of the folded strip. The criterion of the test was on the basis of the amount of change in characteristic impedance and electrical length of the folded strip compared to a single straight strip with no

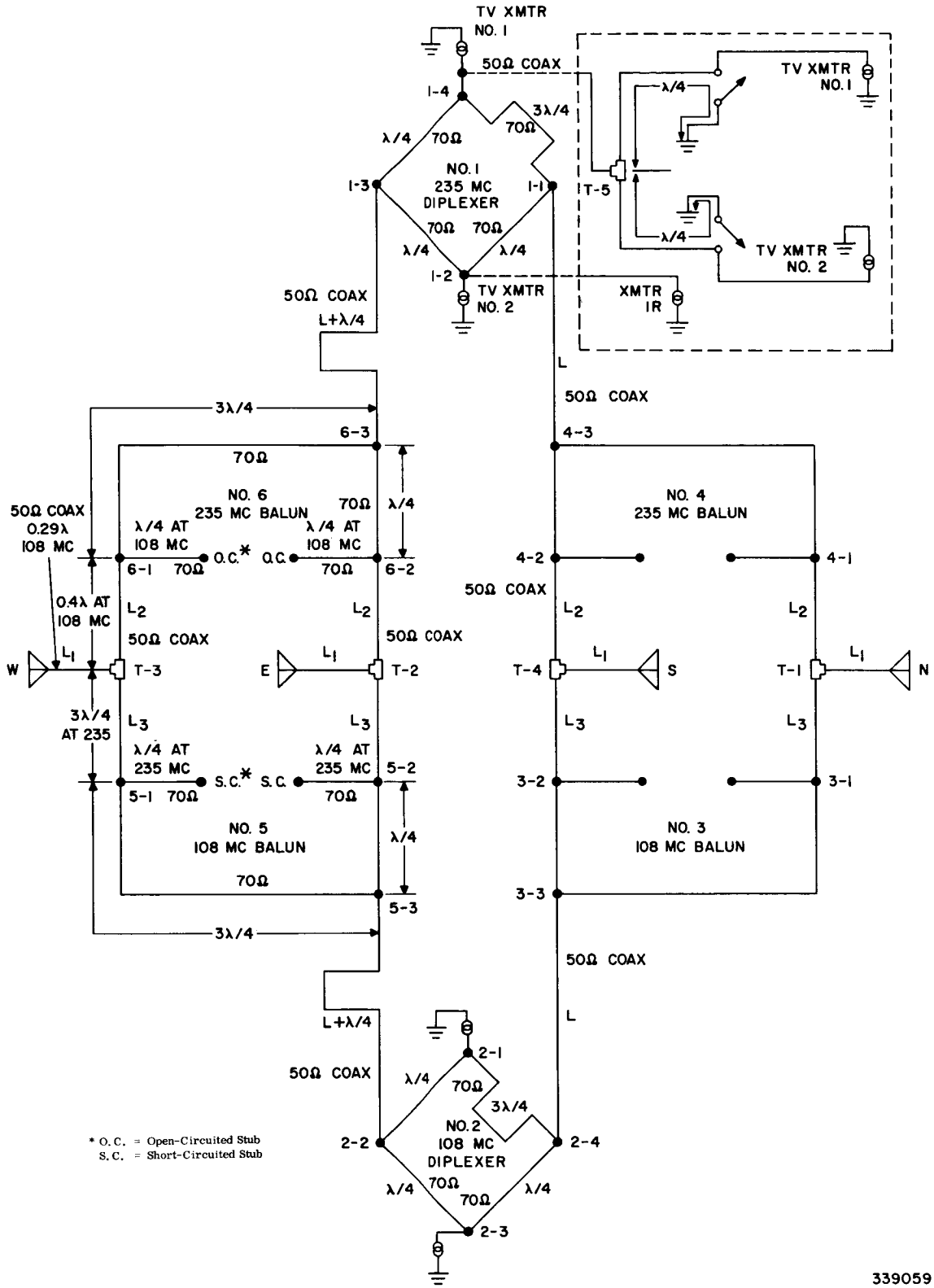

Figure 99(a). R-F Coupling and Matching Network, Schematic Diagram

adjacent strips. With the 1-cm spacing, no effect from mutual coupling was evidenced with lengths up to one wavelength at 108 Mc.

The next step involved fabrication of a hybrid ring or diplexer for the 235-Mc band, using the least possible area for the continuous stripline 1-1/2 wavelength long and with 1 cm spacing. The strip width was designed for a characteristic impedance of 70.7 ohms. With 50-ohm loads at opposite terminals, a voltage standing-wave ratio (VSWR) of 1.02 was obtainable, looking into either remaining terminal. Isolation of 50 db between opposite input terminals was measured, and the insertion loss was approximately 0.5 db. A similar diplexer was then made for 108 Mc. During test, this diplexer produced results which were similar to the 235-Mc diplexer, but with a somewhat smaller insertion loss.

The tests provided evidence that no serious disturbances would result from folding the stripline back on itself to achieve the required lengths in comparatively small areas, while using a 1-cm spacing between folds. The complete proposed circuit would require one diplexer and two baluns for each frequency band. The next study, therefore, was to determine the configuration which would best combine the six components from the standpoints of size, strength, form factor (for integrating with other satellite components), and fabrication technique, including component interconnections. The 108-Mc diplexer required the largest area of the six components, and the 108-Mc baluns were each only slightly smaller. It was then decided to fabricate each component separately and to provide BNC connectors at each termination to permit the interconnections to be made with ordinary coaxial cable. If there had been sufficient time for further development, experiments would have been made to determine whether additional space could have been saved by using closer spacing between strip folds, and possibly by including more than one component on a single board. However, at this point no more time was available for such development. The final fabrication was performed using the 1 cm spacing and separate boards for each component.

2 Final Circuit Design

The r-f coupling and matching networks, Figure 99(a), were originally designed and built to permit the operation of three 235-Mc band transmitters (two simultaneously) with the antenna system. Late in the program, however, after all the satellite models were so equipped, the 237.8-Mc infrared transmitter was removed. This rendered the coaxial switching section for the TV transmitters unnecessary and, accordingly, it was removed as shown by the dotted enclosure in Figure 99. The two TV transmitters were then directly connected to opposite input terminals of the diplexer. To provide a complete description of the design, therefore, the original configuration will be described.

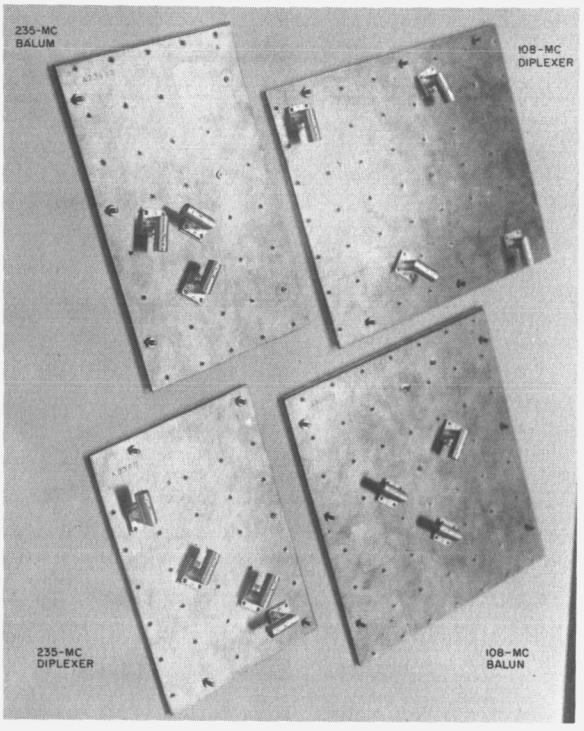

Figure 99(b). R-F Coupling and Matching Networks

To facilitate the descriptions, the system will be considered in two sections, each section being distinguished by the frequency band it serves (i.e., the 235-Mc section and the 108-Mc section). The 235-Mc section is intended to accommodate three transmitters, two operating one at a time at 235 Mc, simultaneously with one at 237.8 Mc. The design center frequency was, therefore, chosen to be 236.4 Mc, the mean of the two operating frequencies. For convenience, however, this section will be referred to as the 235-Mc section.

As shown in Figure 99, each of the four output terminals of the coupling system must actually be a common output terminal of both sections, because the four individual dipole elements must be driven in both frequency bands simultaneously. The objective of each section is to receive energy from two transmitters simultaneously and deliver it to the four dipoles in a 90 degrees progressive phase relationship. The explanation of how this is accomplished will be first described for the 235-Mc section.

The input terminals of the diplexer are 1-2 and 1-4, and the output terminals are 1-3 and 1-1. It is evident from the relationship of the line lengths indicated on the four sides of the diplexer that energy from the transmitter at 1-2 will arrive at the output terminals with the same

relative phase, while energy from the transmitter at 1-4 will arrive at the output terminals with a relative differential phase of 180 degrees. For the moment, the in-phase energy from the transmitter at 1-2 will be discussed. Baluns 6 and 4 are identical, having input terminals 4-3 and 6-3. Stripline 4-3 to 4-1 and 6-3 to 6-1 have lengths of 0.75 wavelength, while lines 4-3 to 4-2 and 6-3 to 6-2 are 0.25 wavelength long. Their differential lengths 4-2 to 4-1 and 6-2 to 6-1 are, therefore, 0.5 wavelength or 180 degrees respectively. Therefore, energy at balun input terminal 4-3 will arrive at 4-1 180 degrees later than at 4.2. Similarly, energy at terminal 6-3 will arrive at terminal 6-1 180 degrees later than at 6-2.

The diplexer output terminal 1-1 is connected to balun 4 input terminal 4-3 with a coaxial cable of arbitrary length L, while diplexer output terminal 1-3 connects to balun 6 input terminal 6-3 with a cable of length L + 0.25 wavelength. This causes energy from the transmitter at 1-2 to arrive at terminal 6-3 90 degrees later than that at terminal 4-3. Therefore, if terminal 4-2 is considered as a 0 degrees phase reference terminal, energy from the transmitter at 1-2 will arrive at terminal 6-2 90 degrees later at 4-1 180 degrees later, at 6-1 270 degrees later, and finally, again at 4-2 360 degrees later. Four identical sets of coaxial lines, $L_1 + L_2$, carry the energy from the four output terminals to each corresponding dipole element. Therefore, the 90 degrees progressive phase relationship between the output terminals is transferred to the dipole terminals without altering the relative phase relationship. Thus, it can be seen that the phase progression of energy from the transmitter at 1-2, arrives at the dipoles in a S, E, N, W order achieving circular polarization in a counterclockwise direction.

When considering that energy from the transmitter at 1-4 will arrive at diplexer output terminals 1-1 and 1-3 with a relative differential phase of 180 degrees (the opposite condition from that of the transmitter at 1-2), and comparing the phase-delay time lengths from terminal 1-4 to 4-3 and to 6-3, respectively, it is apparent that the path 1-4 to 6-3 is 270 degrees longer than the path 1-4 to 4-3. Again, calculating the relative path lengths to the respective balun output terminals and considering terminal 4-2 as a 0 degrees phase reference point, it is apparent that energy from the transmitter at 1-4 will arrive at terminal 6-1 90 degrees later, 4-1 180 degrees later, 6-2 270 degrees later, and finally, again at 4-2 360 degrees later. This phase progression is now in a S, W, N, E order, producing a circularly polarized radiation pattern in a clockwise direction. It is, thus, apparent that opposite screw-sense radiation will result between transmitters coupled to opposing diplexer input terminals.

As described in Paragraph III, A, 6, c, (2), (b), 2 (Scale-Model Impedance Measurements), the dipole extension, in combination with the controllable reactance of the internal portion of the sleeve, permitted adjustment

of each dipole element to a 50 + j0 ohms termination in the 235-Mc band. This adjustment permits complete freedom in the choice of lengths L_1 and L_2, for the purpose of stub and transformer matching of the 150 + j100 ohms dipole termination impedance at 108 Mc to the 50-ohm coupling system, without affecting the matching characteristics in the 235-Mc band.

The basic description of the phasing aspect of the network, for deriving the quadrature feed for the crossed dipoles, will also serve to describe the operation of the 108-Mc section.

The operation of the stubs, which achieve an impedance match at 108 Mc and which provide isolation between the sections (to prevent energy from the transmitters of either frequency band from flowing into the other), will be described in terms of any one dipole, with identical operation at the other three. Arbitrarily using the West dipole for discussion, it may be seen that 235-Mc energy flows from terminal 6-1 to W by means of coaxial lines $L_1 + L_2$, while 108-Mc energy flows from terminal 5-1 to W through $L_3 + L_1$. Energy at 235 Mc will not enter line L_3 because it looks into a high impedance at the junction T-3 in the direction of terminal 5-1. This is because L_3 has a length of an odd multiple of quarter wavelengths at 235 Mc, and a short circuit (for 235 Mc) is placed across the line at terminal 5-1. The short circuit at that point is a result of the reflected impedance of the short-circuited half-wave stub at 235 Mc. Because of the approximate 2-to-1 ratio of the frequencies 235 Mc and 108 Mc, the stub offers a sufficiently high impedance across the line at terminal 5-1 to have negligible shunting effect at 108 Mc. Actually, L_3 is 0.75 wavelength long--the multiple of a quarter wavelength which would physically reach between terminal 5-1 and the junction T-3. Isolations in excess of 40 db have been measured from terminal 1-2 (or 1-4) looking toward terminal 2-1 (or 2-3).

The lengths of lines L_1 and L_2 have been chosen to match the terminal impedance of the dipole, at 108 Mc to 50 + j0 ohms at the junction T-3. Line L_1 transfers the normalized dipole impedance of 2 - j3 ohms to an admittance value of Y = 1 - j1.64 at point T-3. At 108 Mc, line L_2 is a stub, which is shorted at terminal 6-1 and has a length which gives a susceptance, B = +1.64, equal and of opposite sign to the susceptance at T-3, thus cancelling the transferred susceptance and bringing the admittance to Y = 1 + j0. Therefore, the normalized impedance of dipole W is matched to 1 + j0 ohms at junction T-3. The 108-Mc short circuit, at terminal 6-1, is effected by the reflected impedance of the open-circuited 108-Mc quarter-wave stub. Again, the 2-to-1 frequency ratio provided an advantage because this stub was approximately a half wavelength at 235 Mc, and it reflected a negligibly high shunt reactance. across the line at terminal 6-1. The actual lengths are L_1 = 105 degrees and L_2 = 148 degrees, or 0.29 wavelength

and 0.4 wavelength, respectively. These impedance and electrical length values are nominal, and because of small variance between the different TIROS models and the corresponding coupling systems, the actual L_1 and L_2 lengths were cut to fit each individual system in order to achieve the minimum voltage standing-wave ratio (VSWR). A VSWR value of 1.1 or better has been achieved at 108 Mc on all TIROS models.

The simultaneous operation of two transmitters in each band has been described. However, two TV transmitters in the 235-Mc band were to be operated, one at a time, simultaneously with a third transmitter, also in that band. The third transmitter, in the r-f portion of the infrared experiment package, was to be permanently connected to one of the diplexer input terminals (for example, terminal 1-2). Actual photographs of the stripline configurations comprising the diplexers and baluns are shown in Figures 100 through 103. The terminal numbers correspond respectively with those in the schematic diagram of Figure 99.

The system developed for selectively coupling the desired TV transmitter to the diplexer input terminal 1-4 will now be discussed. Considerable study, from the standpoints of reliability and insertion loss, was given to the development of method of selectively coupling the desired TV transmitter to diplexer input terminal 1-4. The straightforward coaxial switching relay, which is used for a conventional "either-or" connection, was eliminated completely from the reliability standpoint. Measurements were made of the impedance of the output circuit of the transmitters, (looking back into the tank circuit from the output terminals), to determine if there was a sufficient difference in the hot-to-cold impedance to enable the use of some type of line-transformer isolation which would become effective merely by turning the transmitter filaments on or off. It was believed that if a termination of 50 + j0 ohms was seen while the transmitter was hot and operating, but either an extremely high or low impedance was seen when the output tube filament was cold, a half-wave or quarter-wave line connected between each transmitter and T junction would automatically decouple the unused transmitter from the line. If this method were feasible, an antenna switching system with 100 percent reliability could be made. This method did not prove feasible, however, because there was an insufficient change in impedance from the hot to cold condition, and also, because considerable detuning of the final r-f tank circuit was required to effect an appreciable change in impedance, and even this changed only the reactive component to any significant degree. Another method which was briefly considered was the paralleling of the two transmitter outputs. This method had the distinct disadvantage of a maximum power loss of 3 db, but it did have the reliability capability of practically 100 percent. It was rejected on the basis that a 3-db loss could not be tolerated.

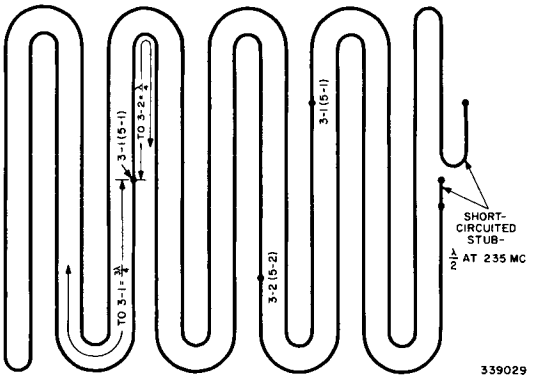

Figure 100. 108-Mc Balun

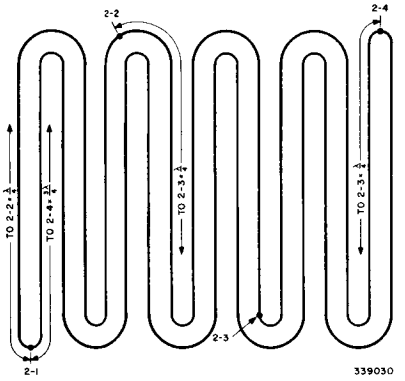

Figure 101. 108-Mc Diplexer

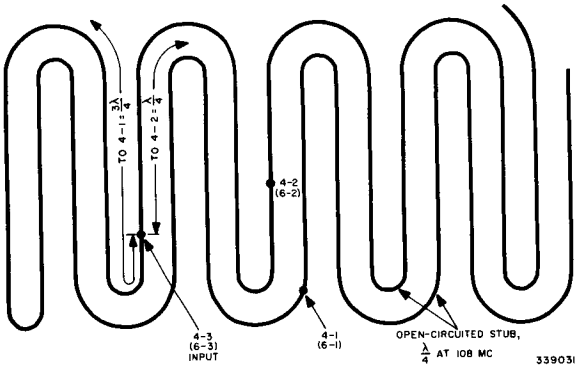

Figure 102. 235-Mc Balun

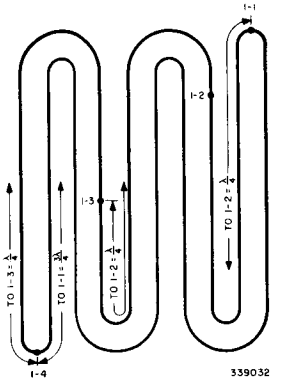

Figure 103. 235-Mc Diplexer

The final method which was developed and actually used was one which employed a double-throw coaxial switching relay, but in an entirely different manner compared with the conventional "either-or" switching method. A conventional coaxial relay was modified by placing a low-inductance short circuit between the outer conductor and the inner conductor of the normally open contact. Also, a continuous connection of the inner conductor was made between the common terminal and the normally closed contact. As a result, reliability of continuity was no longer dependent on the movement of the moveable contact arm. One side of the straight-through portion of each relay was cable-connected to each respective transmitter. The other side of the straight-through portion was connected to a T junction, but with a carefully-cut cable length to effect a quarter-wave line section from the short-circuited point in the relay to the center of the T junction, with the relay energized, or when the contact arm made contact with the normally-open but now-grounded contact. The relay is energized at the same time the opposite respective transmitter is to be operated. The result is that when transmitter number 1 is operating, its output finds a straight-through connection to terminal 1-4 of the diplexer; when looking toward transmitter number 2 from the T junction (T-5), the energy sees an infinite impedance because of the short-circuited quarter-wave line which is effected by relay number 2 placing a short circuit on the output line from transmitter number 2. Thus, transmitter number 2 is effectively decoupled from the r-f line. In the event of failure of the relay to close, the worst condition that can result is a 3-db loss, caused by power absorption by the unused transmitter. If the relay were to fail in closed position, the loss of the transmitter whose r-f would normally go through it would result, but despite the possibility of this condition, the reliability factor is higher with this arrangement than it would have been with the conventional "either-or" switching arrangement.

Again it should be noted that all TIROS I models were equipped in the manner described; the operation was checked and found to be satisfactory. However, with the final change in scope of TIROS I, the infrared instrumentation was deleted, and it became unnecessary to switch the r-f output of the TV transmitters. The two TV transmitters were then connected directly to opposite inputs of the diplexer. The modified coaxial relays and quarter-wave lines were removed and set aside for use in a future TIROS satellite.

(d) Dipole Fabrication and Final Tuning

The fabrication of the final assembly is closely involved with the final tune-up procedure. For this reason, fabrication technique and tune-up procedure will be described simultaneously.

The dipole mounting base, shown as (10) in Figure 104 comprises a stainless-steel flange, silver soldered to a hollow cylindrical sleeve-mounting portion which is made of cold-rolled steel and is internally threaded to receive the tuning stud (16). The dipole itself comprises an aluminum tube forming the sleeve (12), the rod portion (13) forming the inner conductor of the coaxial isolator, the teflon insulating spacers (15), and the teflon tuning slug (14). The rods and the mounting bases are silver plated. The electrical length of the inner portion of the coaxial isolator is adjustable in two ways; by positioning of the stud (16), and by positioning of the teflon slug (14).

The preparations for tune-up include the following:

1. Mounting the four test dipole-mounting bases on the aluminum ring (2), and separating each base from the ring with a teflon insulator (5), which is cut to the shape of the base flange.

2. Having a set of four sleeves similar to that shown in Figure 104, except that each test sleeve is shortened to increase the sliding range on the mounting in order to permit large sleeve-length variations while making tuning measurements.

3. Having a set of four test-dipole rods, as shown in Figure 104, but of shorter length, and having a 2-inch sliding sleeve fitted over the outer end to permit length adjustments during tuning measurements.

4. Having several selected incremental lengths of L_1 and L_2 cables in quadruplicate, from which to select various combinations to vary the matching characteristics of the L_1 L_2 transformer-stub network in order to obtain an impedance match at the L_1 L_2 junction in the 108-mc band.

5. Connecting the components of the coupling system according to the schematic diagram shown in Figure 99 starting with an L_1 length of approximately 105 degrees and an L_2 length of approximately 140 degrees.

6. Fabricating a set of four sleeve and rod assemblies in accordance with Figure 104 leaving both rods and sleeves somewhat longer than required, to allow for subsequent trimming during the tuning procedure.

7. Assembling the test set of dipole sleeves and rods on the mounts, and mounting the antenna ring assembly on the model of the satellite.

The tuning procedure was applied for one dipole pair at a time. In a typical procedure, Hewlett-Packard 608C VHF generator was used as a signal source, and the Polytechnic Research and Development Company (PRD) Standing-Wave Detector

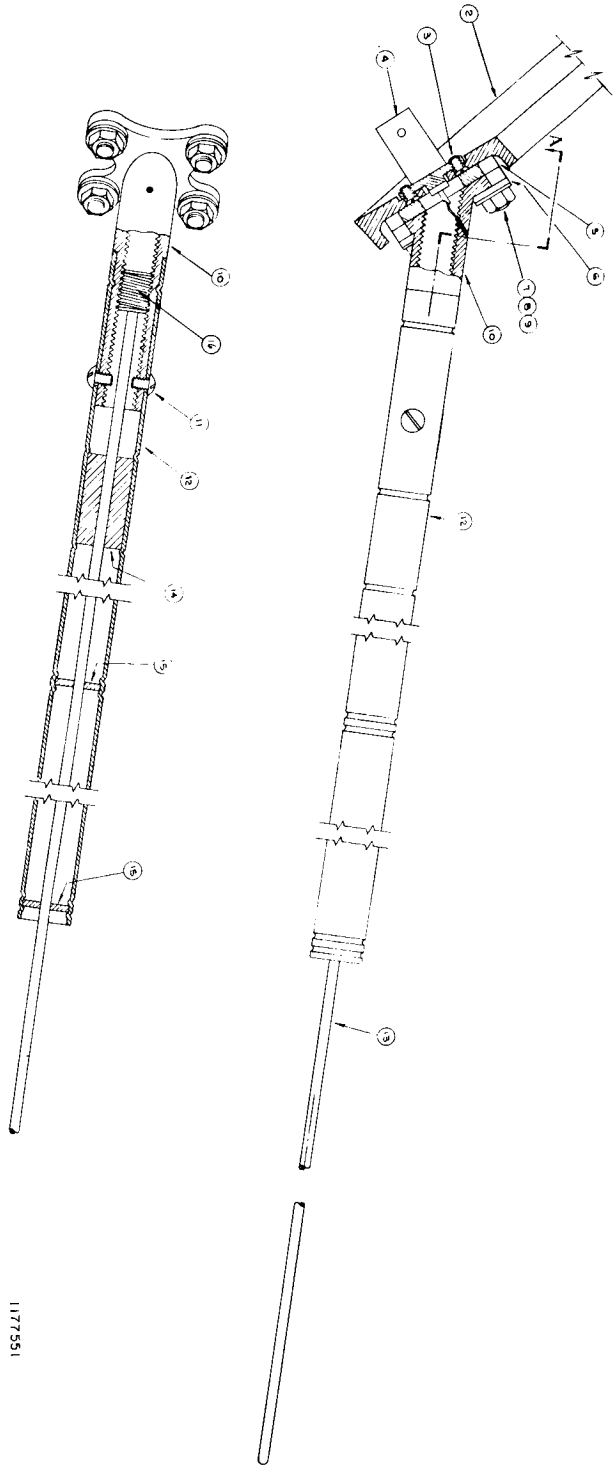

Figure 104. Dipole Transmitting Antenna Assembly

was used, in conjunction with a Hewlett-Packard 415B Standing-Wave Indicator, to measure the Voltage Standing-Wave Ratio (VSWR) and angle of reflection coefficient. For adjustments on the E-W pair, the 235-Mc L + one-quarter wavelength cable was disconnected from terminal 6-3, and the 108-Mc L + one-quarter wavelength cable was disconnected from terminal 5-3. The signal generator was then connected to one of these two terminals, depending upon which frequency adjustment was to be made.

A preliminary adjustment was first made in the 235-Mc band. (The mean frequency of 236.4 Mc was actually used in the adjustments, but 235 Mc will be used for the purpose of description in order to be consistent with previous descriptions.) First, the stud (16) of the rod portion and the teflon slug in the sleeve were both positioned near their center of travel. Preliminary tuning at 235 Mc was then accomplished by adjustment of the outside coaxial-sleeve length (sliding the sleeve on its base), by tuning the internal coaxial portion (screw-adjustment of stud), and by adjusting the rod length (sliding its end-extension sleeve back and forth). These three adjustments are listed in the order of their respective effects on the Voltage Standing-Wave Ratio (VSWR). Symmetrical adjustments should be made simultaneously on each dipole of the pair, and the total sleeve length, the position of stud (16), and total rod length which produces the minimum VSWR should be noted and recorded.

Energy at 108 Mc was then applied to terminal 5-3. At 108 Mc the coaxial sleeve length and the stud position had very little effect on the tuning, except that the stud position affected the total rod length. Beginning with the L_1 length of 105 degrees and L_2 length of 140 degrees, the rod length was varied, by turning stud (16) in combination with various L_2 lengths, until a minimum VSWR was reached while the final rod length was kept within 1/4-inch of the length which was obtained during the preliminary tune-up on 235 Mc. The VSWR obtained with the various lengths of dipole rod was recorded. This procedure was then repeated, using incrementally longer L_1 lengths each time, until the combination which produced the lowest possible VSWR obtainable was determined, while the total rod length was again kept within 1/4-inch of the 235-Mc length. A VSWR value of 1.1 or better was obtained. The L_1 and L_2 cable lengths of this combination were recorded.

Then, two of the four final coaxial sleeves were cut to a length which, when they were pushed all the way onto their mounting bases, provided a total sleeve length which was equal to that obtained with the preliminary 235-Mc adjustment. These two final sleeves were installed in place of the test sleeves, and fastened in place with the screws (11) after the teflon slug (14) was positioned in its central position of travel. The generator was reconnected to terminal 6-3 for 235-Mc input. Again, the rod length and stud position were adjusted for minimum VSWR to check the operation of the final sleeve and to ascertain that the minimum VSWR again occurred with the same rod length as before.

The sleeve was then removed and the position of the stud was determined. Two of the overlength final rods were cut to such a length that, when their studs were in the same position as the test-rod studs, their total length would be 1/2-inch greater than that of the test rods. The test rods were replaced with final rods, and the studs were turned to their previous positions. Again, the VSWR was checked and only the stud positions adjusted for a minimum indication; the extra rod length had no appreciable effect on the VSWR.

The 108-Mc feed was again applied to terminal 5-3, and the rod length was adjusted by turning the stud until a minimum VSWR was obtained. The exact length of the dipole rod was then recorded with the L_1 - L_2 lengths previously recorded. At this point, no further adjustment could be made on the East-West dipole pair until the North-South pair had been adjusted to the same extent. Therefore, the preceding procedures were repeated for the North-South dipole pair, while applying the 108-Mc and 235-Mc energy to terminals 3-3 and 4-3, respectively.

Before finally fastening the dipole elements in place it was necessary to give consideration to a point previously mentioned in the description of coupling circuit operation; i.e., in order for a uniform phase progression to exist around the dipole circuit, all four L_1 sections must be of equal length, and likewise, the four L_2 sections must also be equal. It is likely that, because of small fabrication differences, the best matching combinations on 108 Mc may not be precisely the same for both dipole pairs. That is, somewhat different L_1 and L_2 lengths may have produced the minimum VSWR in the two respective dipole pair circuits. If the L_1 + L_2 length for each pair differed by less than five electrical degrees at 235 Mc, the pattern distortion was considered to be negligible and the final dipole fastening-down would proceed. If a greater than five-degree difference existed, however, a compromise would be made in the matching characteristics of the coupling circuitry between the two dipole pairs.

The stud positions in both dipole pairs were left in a turnable condition for immediate readjustment with a different L_1 - L_2 combination. Also, with some experimentation, a new combination was found for each set which had a differential L_1 + L_2 value of less than five degrees, and still produced a VSWR of approximately 1.1 (maximum of 1.12) at 108 Mc. It was for the purpose of this final compromise tuning at 108 Mc that the dipole studs were left free for adjustment; also, the rods were cut 1/2-inch overlength to allow for adjustments which might have been needed to reach the minimum VSWR obtainable with the compromise L_1-L_2 combination.

Once the final values of L_1 and L_2 were determined, a final set of cables was cut to exact length and the proper BNC connectors were attached. Following this, the final set installed in place of the test set, and final tuning was performed at 108 Mc. When both dipole pairs had been adjusted for minimum VSWR, the exact dipole rod length was measured and recorded.

After obtaining a minimum VSWR at 108 Mc, the stud positions were readjusted, one dipole pair at a time, to achieve a match at 235 Mc. When the match was attained the rod extension was temporarily fastened to the sleeve end with a piece of masking tape to prevent the studs from turning from their final position until they could be permanently soldered. The entire ring-mounting assembly was then removed from the satellite, and the complete antenna system was placed on the soldering bench. One at a time, the sleeves were removed from their mountings and their studs (without being turned), were soldered in place with a high-current clamp-tong type soldering tool, while a damp cloth was would around the flange end of the mounting base to prevent the coaxial connection from being unsoldered. After the studs were soldered, the sleeves were replaced on their mounts and crimp-rolled in place, and the screws were replaced and tightened. Once a sleeve was crimped in place it was no longer removable without destroying it. Therefore, if an error had been made, it could be corrected only by replacing the sleeve.

Because the studs were finally positioned for a match at 235 Mc, the positions could be slightly different from those which produced the correct rod length at 108 Mc. But the 108-Mc lengths had been recorded before turning the studs to the final 235-Mc position, and they were trimmed to make the final overall lengths equal to those recorded at the final 108-Mc tuning.

The entire antenna assembly was remounted on the satellite for the final adjustment at 235 Mc. This last adjustment was made by sliding the teflon slugs to the correct position inside the sleeves. This was actually a fine-tuning adjustment of the internal coaxial-line portion which could be made without changing the length of the dipole rod. Some degree of change was noted between the soldered and unsoldered slugs. This was probably caused by a loosely-fitting thread portion. The primary function of the teflon slug was to tune out any variation resulting from the change in stud-to-mount conduction. Once the optimum slug positions were determined, they were secured in place by rolling a slight crimp in the sleeve at both ends of the slug, as shown in Figure 104. A possible alternative method of crimping might have been to make three or four gentle pricks in the sleeve with a blunted center-punch to slightly deform the sleeve into the teflon.

A final check was made at 108 Mc to determine that the fastened-down assembly provided an impedance match in the vicinity of 1.1 VSWR.

An overall system check was then made; this required reconnecting L and L + one-quarter wavelength cables between the diplexers and their respective baluns. Because of the nature of the circuitry in this system, the energy emerging from the diplexer input terminal opposite the terminal into which the signal is fed is a function of the reflection coefficient at the output terminals. A measure of the ratio of the input signal level to the level at the unused input terminal was, therefore, used directly as an indication of the quality of the impedance match which existed at the output terminals of the diplexer. For a VSWR of 1.1, a 26-db ratio was obtained, while for a VSWR of 1.2 a 20-db ratio was obtained. A ratio of at least 26 db was achieved on all TIROS I models in the 108-Mc band, and at least 20 db for all models in the 235-Mc band. All models were optimized for 235-Mc after the infrared instrumentation was eliminated; a VSWR of at least 1.1 was then obtained at 235 Mc on all models. However, prior to the time the infrared instrumentation was eliminated, optimum adjustments were made for 236.4 Mc, and a 1.1 VSWR was achieved on all models, but with a somewhat degraded match at the two operating frequencies of 235 Mc and 237.8 Mc. Degradation, at the operating frequencies, ranged from 1.15 to 1.25 in the various models after a 1.1 VSWR was achieved at the mean frequency of 236.4 Mc.

(3) Antenna for Command Receiver

The discussion of this receiving antenna will be found in the classified supplement to this report.

d. Tests

(1) Final Radiation Pattern Measurements on Full-Scale Model

After all mechanical and electrical design parameters which had influence on the shape of the radiation pattern were completely finalized, the full-scale model was fitted with an antenna system conforming to the final design parameters. This was done for the purpose of making radiation pattern measurements to determine the degree of success of the development and to obtain information which would be vital to successful satellite-to-ground contact.

In planning the test set-up for the pattern measurements, the space environment was approximated as closely as possible, so that the patterns obtained would have minimum distortion compared to the true space values. Specific attention was given to the following three aspects:

a. Cancellation of the ground-reflected wave so that the measurements would indicate only the direct wave, as would be received in space.

b. Choosing a site in which the space path was clear of obstacles which might introduce undesirable reflections and affect the accuracy of the direct-wave measurements.

c. Raising the satellite model sufficiently high above ground to minimize the ground influence on the radiation resistance.

A rotatable mount, for the satellite model, was fabricated from a tripod-based, cylindrical, plywood pole with a height which placed the model approximately 25 feet above the ground. In terms of wavelength this height was approximately equivalent to 3 wavelengths at 108 Mc and 6 wavelengths at 235 Mc. The down-range antenna was an array which had been specially designed, to achieve cancellation of the ground-reflected wave.

Specifically, the down-range antenna was a two-element, broadside array which was backed with a ground plane spaced a quarter wavelength away; the array plane and the ground plane were parallel to one another. The array was rotatably mounted on the ground plane, and the ground plane could be tilted on its base in a manner which would allow the entire array to be oriented at any angle between 0 and 90 degrees from the horizontal. This type of array was chosen for the down-range antenna because the maximum radiation occurs in the plane normal to the array plane, while the minimum occurs at all points in the array plane; ground-reflected wave-cancellation was thereby achieved by orienting the array plane parallel with the arrival path of the ground-reflected wave.

The down-range antenna was mounted approximately thirty feet from the satellite model, and positioned so that its electrical center was directly in line with the radiation axis of the satellite and the array plane was symmetrically disposed relative to the radiation axis.

When the tilt angle of the array was adjusted to coincide with the arrival angle of the ground-reflected wave (the condition for maximum reflected-wave cancellation), the maximum radiation was pointed upward at an angle which was normal to the arrival path of the ground-reflected wave; therefore, the satellite was not in line with the maximum radiation. However, the ratio of the direct wave to the reflected wave was sufficient to provide excellent discrimination.

A separate dipole array was used for each of the three frequencies, and the ground-plane-to-dipole element spacing was made adjustable to allow it to be pre-set to 0.25 a quarter wavelength at each frequency. The array was rotated to coincide with the polarization plane under observation, and was carefully tested to determine the variation in radiation amplitude versus polarization angle setting. This was done by substituting a standard dipole for the satellite, the dipole being rotatable in the vertical plane. The dipole was turned continuously through 360 degrees, while the down-range array was turned in synchronism so that their respective polarization planes were continually coincident. A maximum variation of $\pm$ 0.2 db was found to exist. This degree of error was considered insignificant, and therefore was not included in the pattern calculations.

The pattern measurement results obtained are shown in Figures 105 through 110 in the form of polar plots of radiated field and total power for both frequency bands for the circularly polarized antenna system. A radiated-field plot is also included for the receiving antenna. Standard spherical coordinate notation has been used throughout, and for convenience, the basic terminology is defined. Figure 111 is included to show the satellite position which was arbitrarily chosen for establishing the reference in the spherical coordinate system.

The terminology used in spherical coordinate system is as follows:

Pattern Plane:	Plane formed by the radius vector and the Z axis
Angle θ :	Angle between the radius vector and the Z axis
Angle ϕ :	Angle between the pattern plane and the horizontal plane (plane formed by X and Z axes)
f θ :	E component lying in the pattern plane
f ϕ :	E component perpendicular to the pattern plane
ρ plane:	Plane containing both f θ and f ϕ and perpendicular to the radius vector

In Figure 111, note that the Z axis intersects the electrical center of the down-range antenna array, and that when $\theta = 0$ degrees, the Z axis and the spin axis are coincident. Also, the pattern plane $\phi = 0$ degrees was chosen in the position in which the wide-angle camera lens was exactly 90 degrees from the horizontal, or directly above the spin axis. Because the dipoles were mounted so that the camera lens fell on the bisector of the angle between two adjacent dipoles, the pattern plane $\phi = 45$ degrees was established when the satellite was rotated clockwise 45 degrees, thus placing a dipole pair in the plane of the pattern.

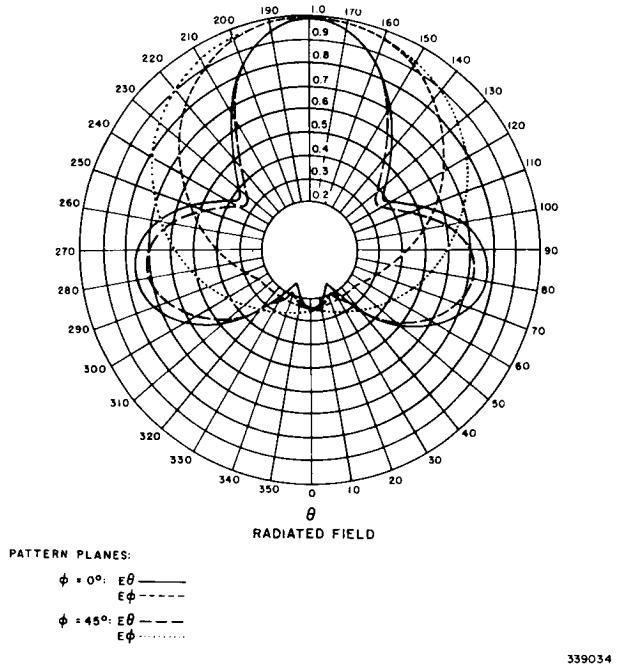

Figure 105. Comparison of Radiated-Field Components, 108 Mc (Actual Satellite)

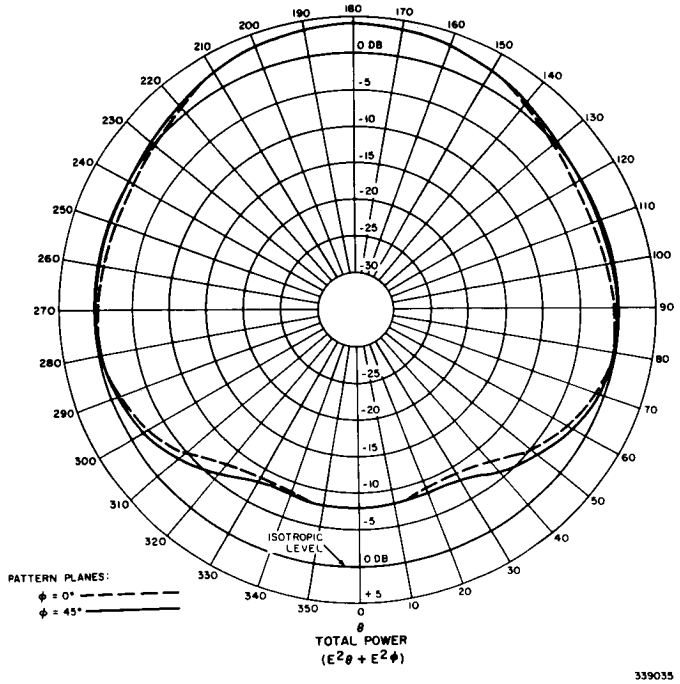

Figure 106. Total-Power Radiation Pattern, 108 Mc (Actual Satellite)

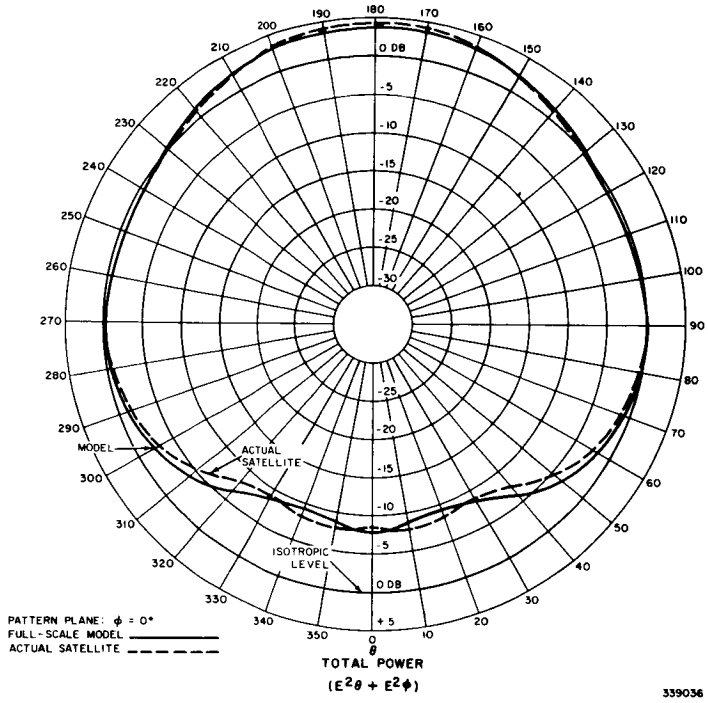

Figure 107. Comparison of Total Power Radiation Pattern, 108 Mc (Actual Satellite versus Full-Scale Model)

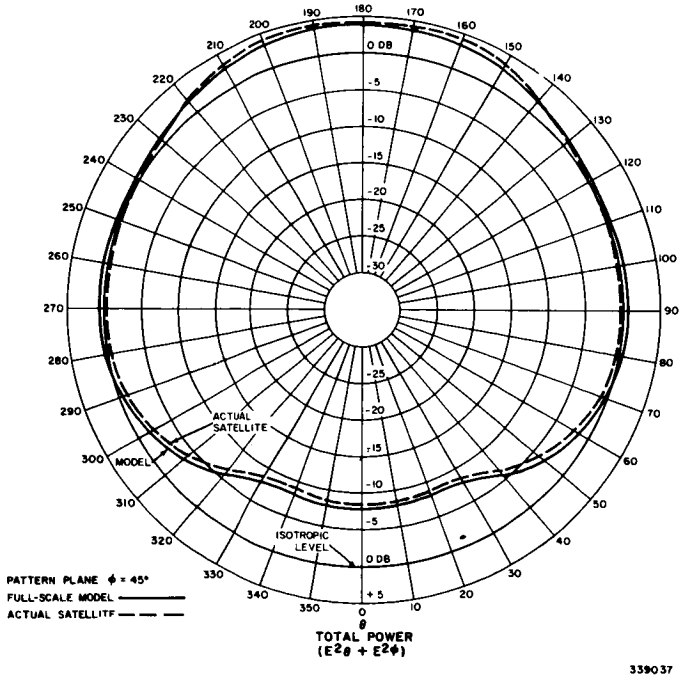

Figure 108. Comparison of Total-Power Radiation Pattern, 108 Mc (Actual Satellite versus Full-Scale Model)

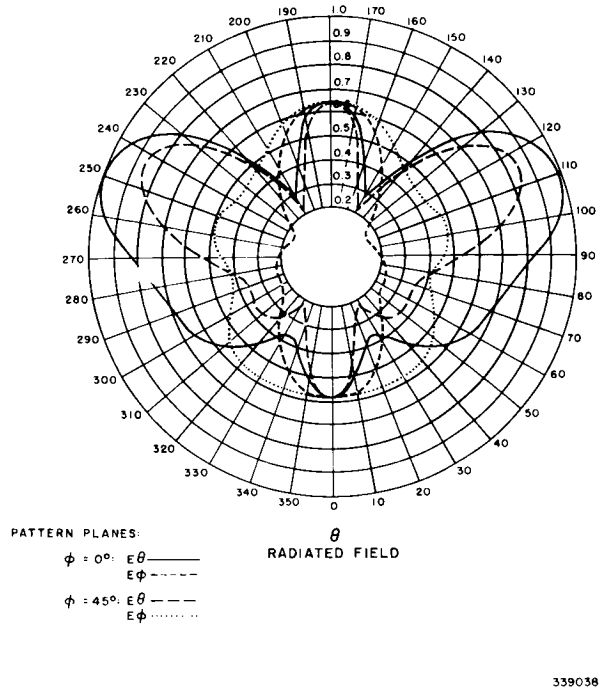

Figure 109. Comparison of Radiated-Field Components, 235 Mc (Full-Scale Model)

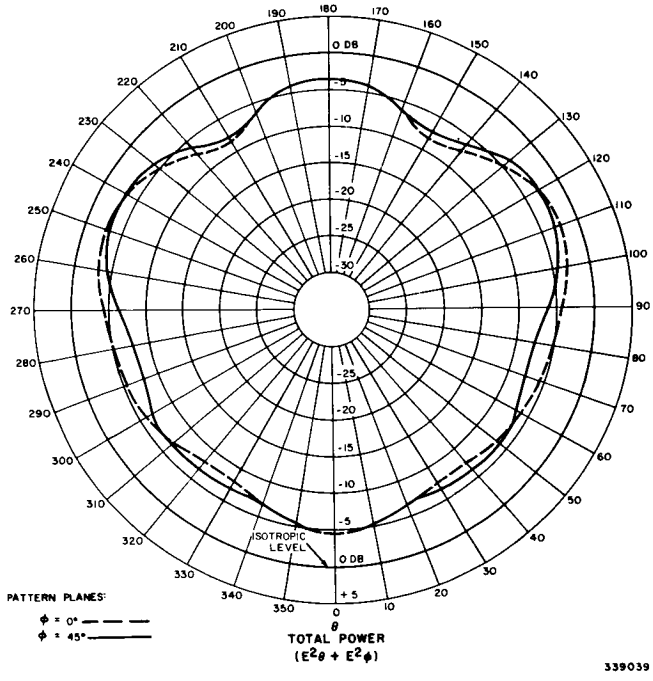

Figure 110. Total-Power Radiation Pattern, 235 Mc (Full-Scale Model)

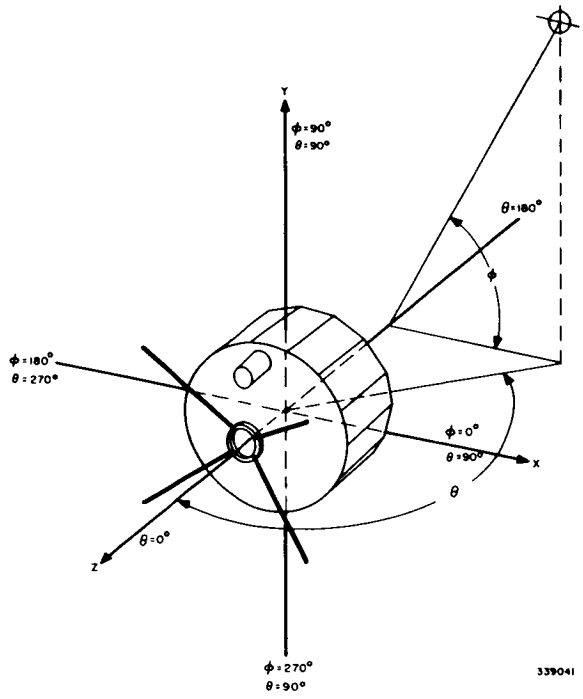

Figure 111. Pattern Coordinate System

Subsequent to the pattern measurements made on the full-scale model, in all three frequency bands, at the test range set up at the RCA Laboratories Antenna Lab, further measurements were made on the radiation patterns in the 108-Mc band, using an actual TIROS airframe and a flight-model set of dipole elements. (Ref. 13) Measurements were made using the satellite alone and also, with the third stage rocket attached as it would be in orbit. The purpose of these measurements was to determine to what effect the rocket might have on the pattern in the 108-Mc band should the rocket and the satellite fail to separate. For this test, a new range set-up was constructed. The same ground-plane-backed broadside array, which was previously used for the down-range antenna, was moved from the RCA Laboratories location and re-used for these measurements. Figure 107 shows a comparison of the total power plot for the 108-Mc radiation between the use of the aluminum and full-scale wooden model at the first test-range setup and the actual flight-model satellite at the second test-range setup. It is believed that the close agreement between the two experiments verifies

the validity of the measurement and emphasizes the care taken in minimizing error accumulation.

The important receiving pattern planes of interest include all values of ϕ from 0 degrees to 360 degrees, with θ as the argument. This pattern deviates only slightly from that of a dipole. A polar plot is shown in the classified supplement of this report.

The degree of decoupling from the transmitting antenna was measured to be from 40 to 45 db. This measurement was first made during the development of the antennas. As a result of this measurement, the receiving antenna was mounted in the neutral plane of the transmitting antennas to improve the transmitter-to-receiver isolation.

7. Dynamics Control

a. Introduction

The TIROS I satellite system was developed around the concept of disc-shaped orbiter, having its axial orientation fixed in space. Stabilization of the axial orientation was accomplished mainly by imparting a moderate amount of spin to the "disc" (consistent with the requirements of the stop-motion photography).

The launching rocket also was spin stabilized, over the latter portion of its trajectory, at a higher rate than that desirable for the satellite. Therefore a means was required to reduce the rate of satellite spin after its injection into orbit. Also, due to the "drag" effect of the earth's magnetic field on magnetic materials in the satellite, it was expected that the spin rate would slowly decline to a value lower than that required for the infra-red experiment. A means of increasing the spin rate, by small amounts, was required. A third disturbance of dynamic tranquility was considered likely from trans-axial torques imparted during rocket-satellite separation, or possible contact with space particles during orbit. These would induce precession, or nutation, which required a means for rapidly damping out such oscillations.

The devices developed, or procured, to perform the dynamics control functions are: (1) The "Yo-Yo" despin mechanism, a portion of which is shown in Figure 112; (2) The TEAM precession damping mechanism, one of which is shown in Figure 113, and (3) a series of spin-up rocket motors, two of which are shown in Figure 114.

b. The Precession Damping Mechanism

The precession damping mechanism designed for TIROS I is essentially a tuned energy absorbing mass (i.e., a "mass-spring resonant system tuned to have a natural frequency precisely equal to the forcing frequency.") This terminology was

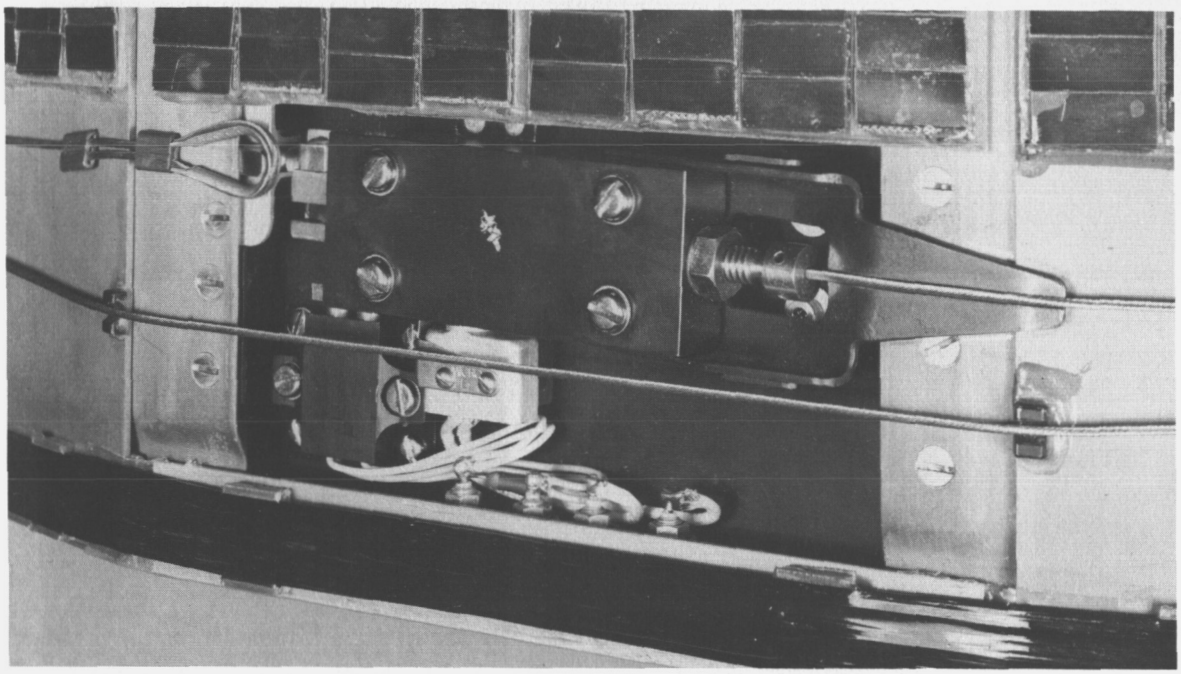

Figure 112. Yo-Yo Despin Mechanism

abbreviated to give it the shorter name: TEAM. In TEAM, the absorbing mass does not itself absorb energy but by its motion produces friction which dissipates energy in the form of heat. Since this motion of the TEAM mass is due to the motion of the satellite, a one-way energy flow occurs (conversion of kinetic energy to heat). This energy conversion process continues until no more precession is present and the body spins about its maximum moment of inertia.

Several methods were considered to absorb or dampen the energy causing this precession. A tube bent in the form of a hoop and half-filled with mercury was considered. The axis of the hoop is located parallel to the satellite spin axis in a plane above or below the center of mass. This mechanical device was developed at the Naval Ordnance Test Station, China Lake, California and extensively analyzed by Space Technology Laboratories. It is a highly effective damping device, but it is difficult to cage (i.e., to prevent it from operating during the ascent of the combined rocket and satellite). During this period of ascent, nutation damping is undesirable because it would tend to increase the "wobble."

Another method of damping considered (very similar to TEAM) consisted of a spherical ball rolling in a tube bent to the proper design radius. This tube was placed in the same position as the rod being used for TEAM. The radius of the tube was greater than that of the rod because of the more complicated motion of the ball. Simplicity of design and sensitivity to nutation are the two main advantages of this method. The major disadvantage is the requirement, that the satellite for which it is used, must possess an inertia distribution such that the polar moment of inertia cannot be less than 1.6 times the moment of inertia about the diameter (assuming that the satellite is a body of revolution). The ball-in-tube could not be used because TIROS I possessed an inertia ratio of approximately 1.45 to 1.

(a)

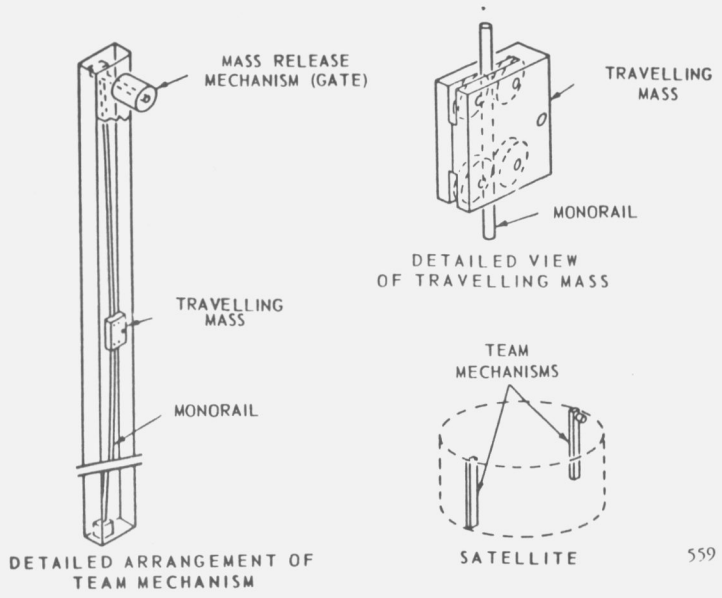

(b)

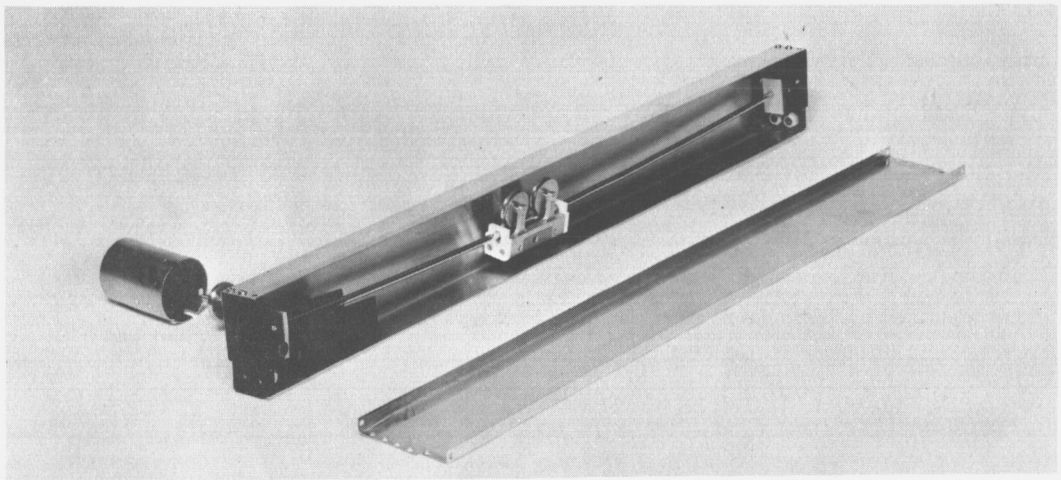

Figure 113. TEAM Precession Damping Mechanism: (a) Outlines of Details, and (b) Photograph

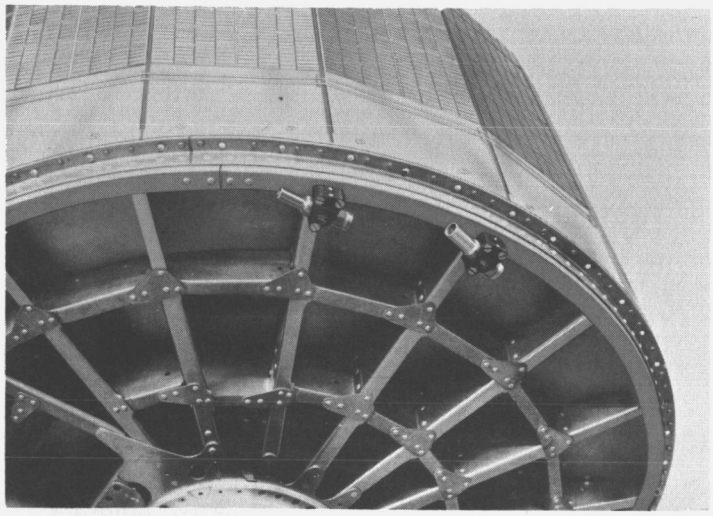

Figure 114. Spin-Up Rockets Mounted on TIROS I Baseplate

(1) Design Analysis

The concept of the design of TEAM was derived from complete analytical studies (discussed in detail in Appendix D) of the motion of a rigid body spinning about an axis which does not coincide with the maximum moment of inertia of the body. The geometry of Figure 115 (which shows a coordinate system X_1, X_2, X_3 fixed to the satellite) was used in the method which is summarized below. There is rotation about one axis (X_3) fixed to the satellite (which is also parallel to the camera optics), while the entire satellite coordinate system rotates about a line fixed in space. This line is in the direction of the total angular momentum of the satellite at the instant of release from the final stage. These two rotations may be combined into one angular velocity vector which does not coincide with either the angular momentum vector or the satellite spin axis.

Before pictures can be taken, it is necessary to reduce the angle between the instantaneous velocity vector (ω) and the satellite spin axis (X_3) to within a small value – approximately 1/2 degree. If energy is removed from the system while a constant momentum is maintained, the desired alignment of the satellite's spin axis and instantaneous angular velocity will take place.

The following equations (based on the derivations from Appendix D) were used for determining the size of a TEAM precession damper and its limitations:

The forcing frequency to which the TEAM is tuned is

$$\dot{\psi} \approx |\dot{\phi} - \omega_3| \tag{1}$$

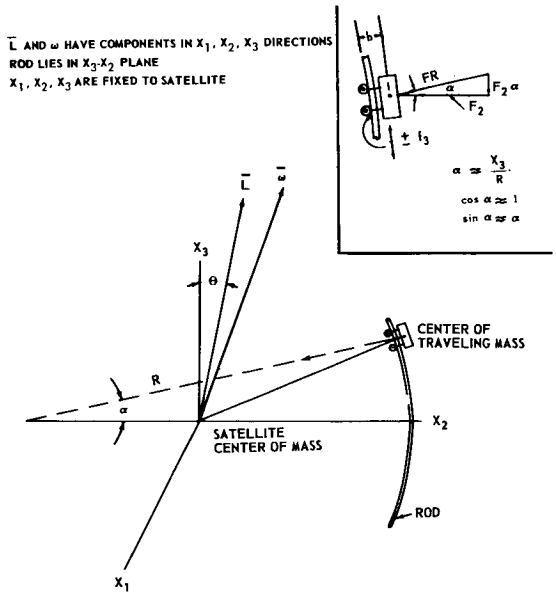

Figure 115. TEAM Precession Damping Mechanism Coordinate System

where $\dot{\psi}$ = forcing frequency, in radians/sec

ω_1, ω_2, ω_3 = components of the satellite's instantaneous velocity vectors resolved into the satellite fixed coordinates, radians/sec

$$\dot{\phi} = \frac{I_3}{I_1}\omega_3, \text{ precession rate, in radians/sec}$$

I_1, I_2, I_3 = principal moments of inertia of the satellite in inch-lb-sec^2

The natural frequency of TEAM is:

$$\omega_n = \omega_3\sqrt{\frac{r}{R}} = \frac{1}{\text{sec}} \qquad (2)$$

where r = distance of rod from the center of mass of the satellite, in inches

R = radius of rod, in inches

The energy which must be dissipated to make the satellite reduce its precession angle from θ_1 to θ_2 is

$$\Delta T \approx \frac{1}{2} \frac{I_3}{I_1} \left[I_3 - I_1 \right] \omega_3^2 \left[\theta_1^2 - \theta_2^2 \right] \tag{3}$$

where ΔT = change in energy of satellite required to produce a change of precession angle from θ_1 to θ_2, in inch-lb

θ_1, θ_2 = maximum and minimum angle the X_3 axis fixed in the satellite makes with the total angular momentum vector, $\overline{L}$, in radians

$\overline{L}$ = total angular momentum vector fixed in inertial space, in inch -lb -sec

For nearly perfect tuning the loss of energy per cycle is

$$4 f (X_3)_{max.} \tag{4}$$

where f = friction force acting on damper traveling mass, in lb

$(X_3)_{max.}$ = half amplitude of motion, in inches

This rate of energy loss is assumed to hold until the amplitude of precession, θ, reduces to a value such that

$$\theta = \frac{f}{B r m \psi^2} \tag{5}$$

where θ = angle that the X_3 axis fixed in the satellite makes with the total angular momentum vector, $\overline{L}$, in radians

$$f = K + \mu m \omega_3^2 r \tag{6}$$

K = static friction, in grams

μ = coefficient of fraction

m = mass of TEAM damper, in $\frac{\text{lb-sec}^2}{\text{inch}}$

$$B = 2 \frac{I_1}{I_3} - \frac{1}{\left(\frac{I_1}{I_3} - 1 \right)^2}$$

Equations (1) through (5) are enough to establish design parameters and allow estimation of the time to damp precession to a value specified by Equation (5). This equation is a relation involving Equations (1), (3) and (4). It is sufficient for many applications in which the angle of precession is several times larger than the threshold value of the damper. An Equation (D-21) of Appendix D which gives a reliable value for the threshold precession angle (i.e., the minimum angle of precession for which the damper just ceases to function) is developed next.

This design procedure for determining the size of the TEAM for the TIROS I satellite according to its specifications is as follows:

$$t = \frac{2\pi\Delta T}{\psi 4 f(X_3)_{max}} \tag{7}$$

where t = time to damp precession from θ_1 to θ_2, in seconds

Let $I_3 = 155$ inch-lb-sec^2

$$\omega_3 = 120 \times \frac{2n}{60} = 12.58 \text{ radians/sec}$$

The initial disturbance is assumed to cause a precession of

$$\theta_1 = 2\frac{1}{2} \text{ degrees}$$

The location of the damper with respect to the spin axis is

$$r = 18 \text{ inches}$$

From Equation (1) the forcing frequency, ψ, is computed. Equation (2) is equated to the forcing frequency to determine the radius of curvature, R, of the rod on which the TEAM mass moves.

$$R = r\frac{\omega_3^2}{\dot{\psi}^2} = 18 \times \left(\frac{12.58}{6.4}\right)^2 = 69.4 \text{ inches}$$

The amount of energy to be dissipated is computed from Equation (3)

$$\Delta T = \frac{1}{2}(1.58)\ (155 - 98)\ (12.58)^2\ [2.5^2 - .5^2]\ \frac{1}{57.3^2}$$

$$\Delta T = 12.9 \text{ inch-lb}$$

The energy loss per cycle as given in Equation (4) depends on the value of the coulomb friction, f. This friction was measured for a TEAM traveling mass weighing 93 grams which is constrained to roll on a monorail as shown in Figure 115.

The friction force is computed for conditions existing in the satellite when it is in orbit by Equation (6).

$$K = 0.135 \text{ grams}$$

$$\mu = 2.00 \times 10^{-3}$$

$$f = 0.035 + 2.00 \times 10^{-3} \times 93 (12.58)^2 \times 18 \times 2.54 \times \frac{1}{980}$$

$$f = 0.035 + 1.41 = 1.45 \text{ gram force}$$

$$f = \frac{1.45}{454} = 3.2 \times 10^{-3} \text{ lb force}$$

The half amplitude of motion, X_3, is 8.25 inches
If the rate of energy loss given by Equation (4) is assumed to apply during the entire damping time, the number of cycles required to absorb the excess energy would be

$$n = \frac{\Delta T}{4 f X_3} = \frac{12.9}{4 \times 3.2 \times 10^{-3} \times 8.25} = 72.5 \text{ cycles}$$

The time per cycle is

$$\frac{2\pi}{\dot{\psi}}$$

Then the total time required to damp precession from a 5° total cone to a 1° total cone would be

$$t = \frac{2\pi}{\dot{\psi}} n = \frac{2\pi}{6.4} \times 72.5 = 71 \text{ sec}$$

The time of 71 seconds for one TEAM damper to reduce precession from 5° to 1° is conservative. This is so because additional energy losses can be expected from impact with the ends during the earlier part of the damping process. Further evidence that the results are conservative will be found in the test results. The importance of the Equations (1) through (7) is that they might readily be applied to a spin-stabilized satellite to obtain an excellent estimate of the time required to dampen precession.

The limiting precession angle θ_{min} is computed below for two conditions, one for the case when the TIROS I satellite is rotating at 120 rpm and the other when the satellite is rotating at 12 rpm. The following values are used in Equations (5) and (6):

For the satellite rotating at 120 rpm

$$f = 3.2 \times 10^{-3} \text{ lb}$$

β = 2.95

m = 93 grams = 5.32×10^{-4} $\frac{\text{lb-sec}^2}{\text{inch}}$

$\dot{\psi}$ = 6.4 radians/sec

r = 18 inches

$\theta_{min} = \frac{f}{\beta r m 2}$ = .16° for ω_3 = 120 rpm

For the satellite rotating at 12 rpm

f = 1.08×10^{-4} lb

β = 2.95

m = 93 grams = 5.32×10^{-4} $\frac{\text{lb-sec}^2}{\text{inch}}$

$\dot{\psi}$ = 0.64

r = 18 inches

θ_{min} = 0.54° for ω_3 = 12 rpm

Both these limiting angles would be well within the tolerance allowed. As the speed of rotation decreases below 12 rpm, θ_{min} increases inversely as the square of the speed for a given mass. The chief reason for this is seen in Equation (6) which shows that friction is made up of a fixed value plus a speed dependent value. At 12 rpm, the speed dependent value represents only 3 percent of the total friction.

If a precession angle, θ, less than 0.54 degree were required, it would be necessary to increase the mass of the damper.

In the present design, the damper mass is less than 0.001 percent of the mass of the satellite. Without going to extremes in attempting to reduce static friction, it would be possible to reduce the minimum angle (by increasing the damper mass) without a severe weight penalty to the whole satellite.

(2) Experimental Results

(a) Measurement of Friction

Two methods were used to determine the amount of friction between the traveling mass and the rod. Experimental models of the TEAM mechanism were constructed to prove the design calculations. One method of measurement was to mount the damper traveling mass on a horizontal rod and then measure the angle to which the rod must be titled to sustain motion of the traveling mass. The resulting friction due to the varying weight loads is shown by the points in the lower left hand corner in Figure 116. This data provides the intercept value of friction, K, which is essentially independent of the normal load. The value of friction determined in this manner is used to compute the threshold value for precession damping in

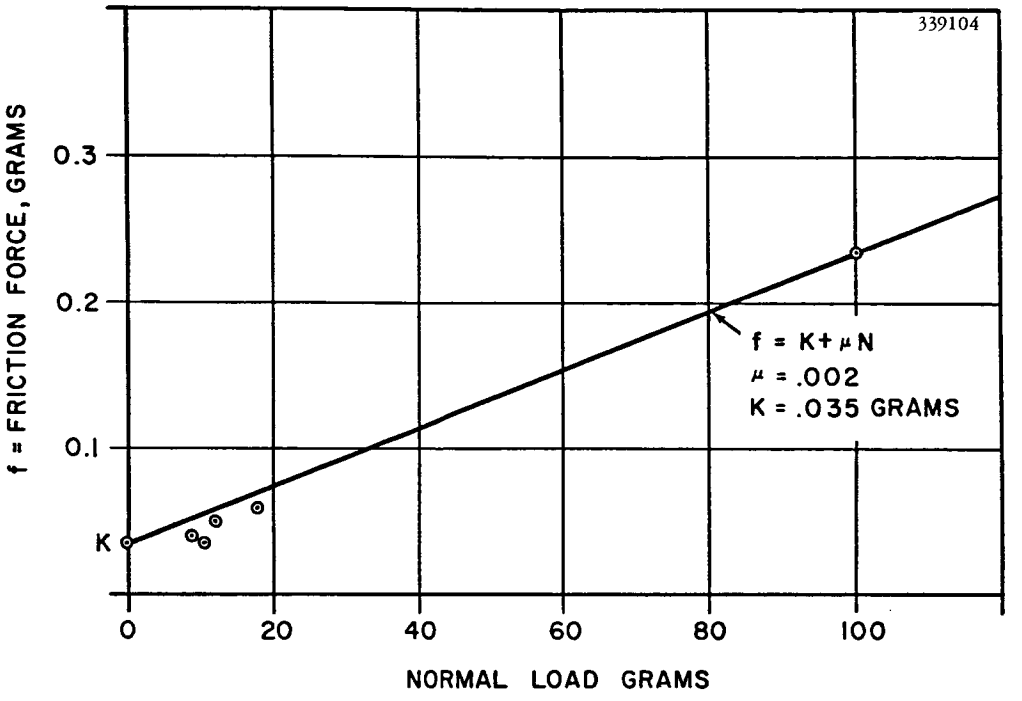

Figure 116. Friction Data for the TEAM Precession Damping Mechanism

Equation (D-21) of Appendix D. It is important to keep the intercept value, K, as low as possible for a satellite rotating at low speeds. Under these conditions, the normal forces are negligible and threshold is determined entirely by K.

For high rotation rates, the friction which arises from normal loads on the damper cart is the most important. To measure the value, μ , of the equation

$$f = K + \mu m \omega_3^2 r,$$

a traveling mass was loaded with a weight which produced a normal force equal to $m\omega_3^2 r$ for

$m = 93$ grams

$\omega_3 = 120$ rpm

$r = 18$ inches

This mass was mounted on a rod bent to the correct radius and the whole assembly mounted on a horizontal plane such that gravity provided the equivalent of the centrifugal force. The mass was given an initial displacement and

its height above a datum plane was recorded on each successive cycle until it came to rest at the lowest point of the rod.

The height lost on each cycle is directly related to friction work done (amount of energy converted to heat) during the cycle and allows μ to be computed from

$$\mu = \frac{\Delta h}{d}$$

Where Δh = lost height, in inches

d = distance traveled during cycle, in inches

The measured data produced an average value of

$$\mu = 2 \times 10^{-3}$$

This is very consistent with the type of bearings used in the damper traveling mass.

The complete friction equation used in predicting damping times and threshold values of precession for the TIROS TEAM damper is

$$f = 0.035 + 2 \times 10^{-3} \frac{m\omega_3^2}{980} r \text{ grams}$$

This equation determined the complete friction versus load curve in Figure 116.

(b) Measurement of Precession Damping

The experimental equipment used to check the design equations developed in Appendix D is shown in Figure 117. The simulated satellite is mounted on a driven shaft by a two-gimbal bearing system and is completely balanced. When the damper is caged and the model is driven at a constant speed, it will spin true about an axis that coincides with the principal moment of inertia, I_3. When a torque impulse is applied to the model in a direction at right angles to the spin axis, the model precesses about an axis corresponding to its total angular momentum. When the dampers are caged, the time required to damp this precession from windage and bearing friction is several minutes. It is shown below that the energy lost from this source is completely negligible compared to that lost to the damper and may be neglected.

The angle of precession is measured by a calibrated optical system. A collimated light source is directed onto a small mirror on the end of the model. When there is no precession, a spot of light appears fixed on a screen set several feet from the model. When the model precesses, the spot moves in a circle at the precession frequency and the diameter is directly proportional to the total cone angle

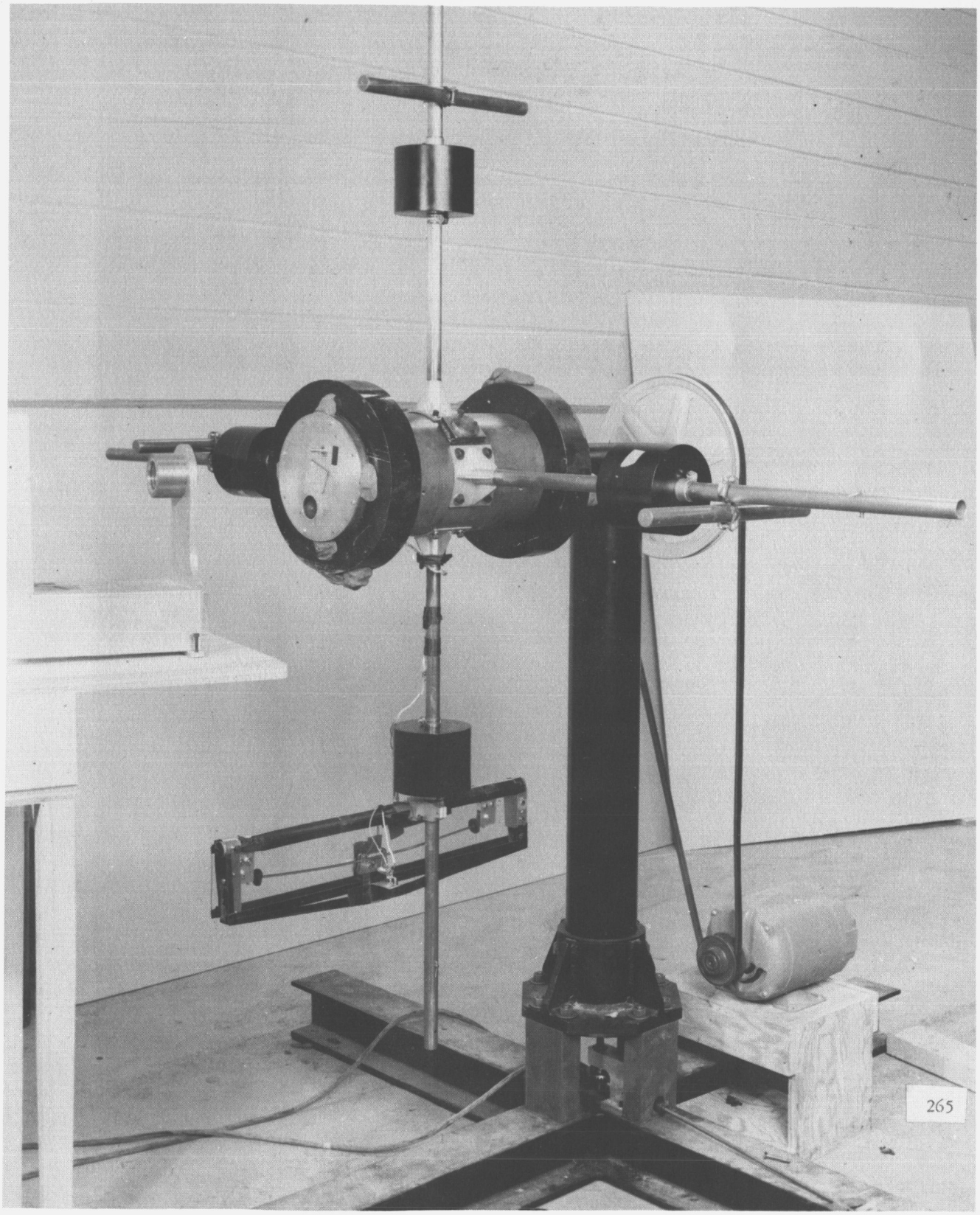

Figure 117. TEAM Precession Damping Mechanism Test Equipment for Checking Analytical Design Derivations

that the model figure axis makes with the fixed angular momentum vector of the system. The calibration was such that a

$$1\text{-inch diameter} = \frac{1}{2}\text{degree total cone angle}$$

The calculations based on the experimental data are as follows:

$$I_3 = 52 \text{ inch-lb-sec}^2$$

$$I_1 = 35.3 \text{ inch-lb-sec}^2$$

$$\omega_3 = 145 \times \frac{2\pi}{60} = 12.58 \text{ radians/sec}$$

The location of the damper with respect to the spin axis was

$$r = 19 \text{ inches}$$

The initial angle was

$$\theta_1 = 1\text{-}1/2 \text{ degrees}$$

and the final angle was

$$\theta_2 = 3/4 \text{ degrees}$$

The time to damp from 1-1/2 to 3/4 degrees was 8 sec

From Equation (1), the forcing frequency, ψ, was computed

$$\psi = \frac{I_3 - I_1}{I_1} \omega_3 = 7.15 \text{ radians/sec}$$

The amount of energy that the damper absorbs between θ_1 = 1-1/2 degrees and θ_2 = 3/4 degrees was computed by equation

$$\Delta T = \frac{1}{2} \frac{I_3}{I_1} \left[I_3 - I_1 \right] \omega_3^2 \left[\theta_1^2 - \theta_2^2 \right] = 1.46 \text{ inches-lb}$$

The friction force developed by the damper was

$$f = K + \mu m \omega_3^2 r = 4.75 \times 10^{-3} \text{ lb force}$$

The loss of energy per cycle by Equation (4) was

$$4f(X_3)_{max} = 0.137 \text{ inch-lb}$$

The number of cycles required to absorb this energy was computed by

$$n = \frac{\Delta T}{4fX_3} = 10.7 \text{ cycles}$$

The period of each cycle was calculated by

$$t = \frac{2\pi}{\psi} = 0.88 \text{ sec/cycle}$$

Therefore the total time required to damp precession was

$$t_{tot} = \frac{2\pi}{\dot{\psi}} n = 0.88 \times 10.7 = 9.4 \text{ sec}$$

as compared to the actual measured total time of 8 sec.

(3) Comparison of Experimental Versus Analytical Results

The small differences between the experimental and analytical results is perhaps somewhat fortuitous when the following factors are considered:

(a) rod end conditions, which result in both additional energy loss through inelastic collisions with the bumpers, and also de-phasing of the cart motion with the forcing input after such collisions.

(b) differences in the total energy (potential and kinetic) of the cart, i.e., when the test vehicle is at the 1-1/2 degree initial and the 3/4 degree final conditions, and

(c) the slightly out-of-tune condition of the damper, which was set at a frequency ratio between 0.90 and 0.95.

In view of the nonlinear nature of the damper behavior, greater differences might easily be expected. However, the method used appears to be quite satisfactory for determining the approximate damping time.

To demonstrate that the amplification of motion is large even for imperfect tuning, Equation (D-20) of Appendix D will be used to compute what the excursion would be if there were no limit stops.

Equation (D-20) gives

$$X_3 = \frac{B\beta^2 r\theta\sqrt{1 - \left(\frac{4f}{\pi B\psi^2 r\theta m}\right)^2}}{1 - \beta^2}$$

for the test condition

$$X_3 = \frac{B\beta^2 r\theta}{1 - \beta^2}$$

Because the accelerating forces on the damper mass are much higher than the friction, the values which apply to the test are

$B = 3.5$ from Equation (D-15) of Appendix D

$\beta = \frac{\dot{\psi}}{\omega n} = 0.945$

$r = 19$ inches

The precession angle θ which would produce a maximum excursion of 8.25 inches is

$$\theta = \frac{1 - \beta^2}{B\beta^2 r}(X_3)\ \text{max.}$$

$$\theta = \frac{1 - 0.8930}{3.5 \times 0.8430 \times 19}\ 8.25 = 0.0157 \text{ radians}$$

$\theta = 0.9$ degrees

The input during most of the damping period was larger than this and, as was observed, the mass did strike the ends.

(4) Functional Description

This TEAM system consists of two similar mechanisms (Figure 113) which are installed vertically along the satellite side-wall, 180 degrees apart. Each mechanism weighs a little under one pound; each traveling mass weighs approximately 3 ounces. A mechanical gate restrains the traveling mass during ascent. This gate is opened automatically by fired squibs at lift-off (separation of satellite from the

third stage), permitting the traveling masses to roll freely along the rods. A manual method of firing the squibs from the ground station is provided for back-up in case of malfunction. The traveling masses are tuned to the frequency of the satellite and rapidly absorb the energy causing the precession and convert it from kinetic energy to thermal energy. This thermal dissipation of energy continues until the traveling masses "rest" at the center of the rods. At this moment, the satellite is stabilized.

c. The Despin (Yo-Yo) Mechanism

At the time of injection into orbit, the TIROS I satellite was spinning at the same rate as its carrier rocket (nominally 120 rpm). To slow the satellite to its operational spin rate, nominally 12 rpm, a despin mechanism of the Yo-Yo type (originally used by Jet Propulsion Laboratory for the Pioneer IV satellite) was developed at RCA. This mechanism consists primarily of weights temporarily secured to the satellite housing, and connected to cables wrapped (once) around the housing. When the masses are released, they are accelerated to a high linear velocity by the action of the cables attached to the satellite. When the cables unhook themselves from the satellite, the masses and cables carry with them about 90 percent of the initial angular momentum of the spinning satellite. Since the satellite inertia is essentially unchanged, the loss in angular momentum represents a 90 percent loss of angular speed.

(1) Design Analysis

The Yo-Yo mechanism was designed from modified equations based on the principles utilized in designing the Pioneer IV mechanism. (Reference 14) A summarized development of the design equations is given here:

The ratio of the final (desired) spin rate to the initial spin rate is expressed as:

$$\frac{\omega_F}{\omega_I} = \frac{\bar{I}}{A}\left[1 - \sqrt{\left(\frac{A}{\bar{I}} - 1\right) \div \left(\frac{AC}{B^2} - 1\right)}\right]$$

in which ω_F = final spin rate, in rpm

ω_I = initial spin rate, in rpm

I = moment of inertia of the satellite with no despin masses, in inch-lb-sec^2

I = moment of inertia of the satellite with despin masses, in inch-lb-sec^2

$A = I + m(\ell + a)^2 + \rho\ell\left(a\ell + a^2 + \frac{\ell^2}{3}\right)$

$B = m\ell(\ell + a) + \rho\ell^2\left(\frac{\ell}{3} + \frac{a}{2}\right)$

$C = \ell^2\left(m + \frac{\rho\ell}{3}\right)$

and m = mass of satellite with despin mechanism, in $\frac{\text{lb-sec}^2}{\text{inch}}$

ℓ = length of despin cable from securing hook on satellite to the center of gravity of the despin weight, in inches

a = distance from the satellite spin axis to the pivot point of the cable, as it is released from the hook, in inches

ρ = linear density of the cable, $\frac{\text{lb-sec}^2}{\text{inch}^2}$

A set of design curves calculated from this equation, for the following parameters is shown in Figure 118. ℓ = 129.8 inches; a = 20.66 inches; $\rho = 2.38 \times 10^{-6}$ lb-sec^2/in^2 (the mass density per unit length of one-sixteenth inch diameter cable).

(2) Functional Description

The Yo-Yo device (Figure 119) designed for TIROS I consists of two weights, each of which is attached to a cable, which in turn is attached to the satellite. The cables are wound (once) around the satellite housing, and the weight is then secured, in a niche, by a squib-actuated, sliding pin. The "free" end of each cable is looped over an open hook, attached to the satellite. A photograph of one niche, with the weight in its launch position, is shown in Figure 112.

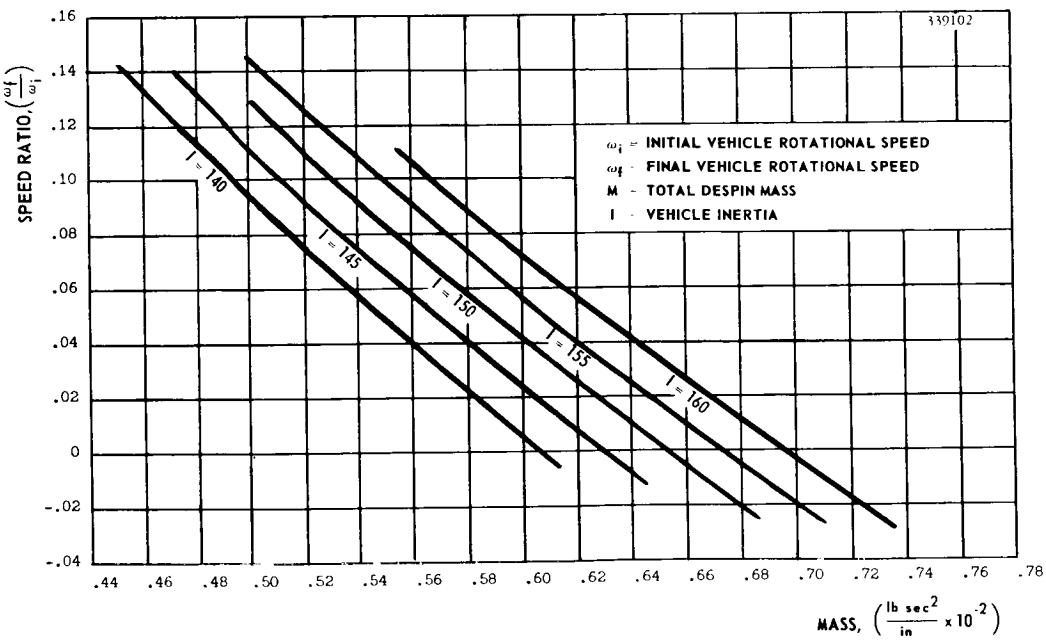

Figure 118. Final Speed Ratio versus Total Despin Mass for Several Satellite Inertias

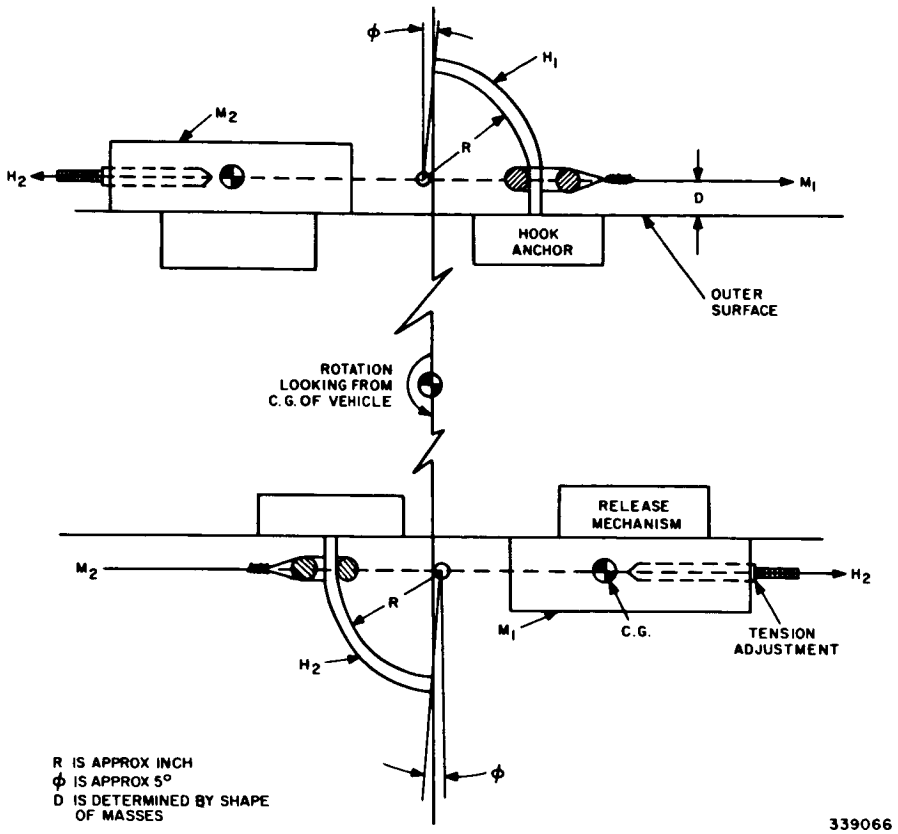

Figure 119. Yo-Yo Mechanism (Hooks, Cable, and Attachments)

Upon separation of the satellite from the carrier rocket, an electronic Yo-Yo control circuit (described in Volume IV, page III-34) was switched into operation. After counting off an eight-minute interval, this circuit fired the weight release squibs of the Yo-Yo mechanism. The retaining pins were thus disengaged, permitting the weights to swing free. These quickly swing outward (due to centrifugal force) until, at the points where the cables attained radial orientation, the cable loops slip off their retaining hooks; the cables and weights then separate completely from the satellite and carry off into space about 90 percent of the angular momentum of the satellite.

d. The Spin-Up Rockets

Of several methods conceived to increase the spin rate of the TIROS I satellite (e.g., electromagnetic, gas jets), the use of small rocket motors appeared to offer

greatest simplicity of design and reliability of performance. A spin-up of 3 rpm would be required at intervals not too specifically known, but which would be well within the capability of nine firings during the operational life of the satellite. The spin-up design, then, called for nine pairs* of rockets mounted just below the outer edge of the satellite baseplate, each of a pair being separated 180 degrees, and firing in opposite directions. These rockets were developed to RCA specifications and supplied by the U. S. Flare Corporation.

(1) Rocket Design

The specifications for the rockets are as follows:

1. Impulse: 1.42 ± 0.1 lb-sec
2. Force (thrust): 5 lbs maximum
3. Time: 0.284 sec or more
4. Test Requirements: Indicated below
5. Envelope Size: 3/4 x 3/4 x 2 inches, maximum
6. Weight: 0.06 lbs maximum
7. Ignition: 1 ampere or less of direct current
8. Gas Cone: Within the space limitations above, it is required that the gas ejected from the nozzle be contained within a cone of 30°, so that the gas particles do not contact the surface adjacent to the rocket
9. Propellent: The propellent is a standard formula (developed for the U. S. Navy in the public domain) called Arcite 377. Its approximate formula is:

Polyvinyl Chloride QYNU	20%
Di-vetyl Azelate	20%
$NH_4 ClO_4$	60%
Anti-oxidant	0.5%
Carbon Black	1.0%
Detergent	0.2%

The method of manufacture permitted variation of grain length and orifice (nozzle) diameter which are the two most important parameters. Table 5 lists the differences in rpm, time and peak thrust differences due to varying these two factors. The quality control and manufacturing standards of the spin-up rockets were the main reason for their reliability as indicated in the test results explained below.

*On the basis of reduced magnetic drag predicted late in the TIROS I design, the number of rocket pairs was reduced to two, which proved operationally ample.

TABLE 5. FLYWHEEL TEST DATA FOR SPIN ROCKETS

Test No.	Date	Nozzle I.D. (inches)	Grain Length (inches)	Ignition Pellet Type*	Pressure (inches Hg)	RPM	T Time (sec)	Peak Thrust (lbs)	Percent Nominal	Remarks
1	4/16	0.125	0.500	1	30.00	110	long	low	59	chuffed
2	4/20	0.125	0.750	2	30.00	143	1.000	6.11	77	---
3	5/1	0.125	0.875	2	30.00	100	OK	?	52	only 1 motor fired
4	5/1	0.125	1.000	2	30.00	---	---	---	---	lost head closures
5	---	0.125	0.875	1	30.00	215	OK	high	114	mech. tach.
6	---	0.125	0.875	1	30.00	215	OK	high	114	mech. tach.
7	5/15	0.130	0.875	1	30.00	250	---	---	---	---
8	5/15	0.135	0.875	1	30.00	166	0.340	---	---	---
9	5/15	0.140	0.875	1	30.00	156	0.360	---	---	---
10	5/20	0.135	0.875	1	1 mm	?	---	---	---	---
11	5/20	0.135	0.875	1	1 mm	253	0.080	---	134	---
12	5/20	0.135	0.875	1	1 mm	260	0.080	---	137	---
13	5/22	0.135	0.875	1	1 mm	246	?	---	faulty	instrumentation
14	5/22	0.135	0.750	1	1 mm	236	---	---	---	---
15	5/22	0.150	0.875	1	1 mm	260	---	---	---	---
16	5/22	0.135	0.750	1	1 mm	233	0.340	---	---	---
17	5/22	0.150	0.875	1	1 mm	160	0.340	---	---	---
18	5/22	0.135	0.875	1	1 mm	260	0.320	---	---	---
19	5/22	0.135	0.875	1	1 mm	260	0.310	---	---	---
20	5/22	0.135	0.875	1	1 mm	256	0.310	---	---	---

*Type 1 pellet is a 12-2M with a spider Head, type 2 is a 12-2M without a Spider Head.

All grain coatings were 90/10; all closures were 2.5 mil aluminum.

(2) Rocket Test Requirements

Test requirements for the spin-up rockets were specified by RCA to be as follows:

(a) Impulse Tests

It was recommended that the impulse of the rockets be measured in a vacuum by attaching them to a flywheel of suitable size and measuring the speed change upon firing.

(b) Environmental Tests

Vacuum Environment:	0.1 micron
Temperature Range:	+60° to -20°C
Vibration:	20 g rms, 20 to 2000 cps
Static Acceleration:	50 g
Shock:	15 g, 11 ± 1 millisec duration

(c) Reliability Tests

One or no failures out of a group of twenty will be considered a success. Two or less failures out of a 100 units fired consecutively out of the total quantity ordered (approximately 150 units) will be considered as acceptable.

Failure: The rockets will be considered as having "failed" because of failures to ignite; impulse above or below 1.42 +0.1, -0 lb-sec; thrust above 5 lbs: and cone of gas exceeding 30 degrees.

(3) Rocket Test Results

The initial rocket tests, conducted at U. S. Flare Corporation, Saugus, California, were observed by one AED and two U. S. Flare Corporation representatives. These tests conducted on 40 separate rockets, in and out of vacuum, indicated that the impulse and reliability specifications would be met. (Reference 15) Table 5 lists the results of 20 firings. Electrical resistance tests of 16 rockets fired showed residual low resistance which would require a circuit that disconnects the battery circuit from the firing circuit. However, the low resistance readings may have been due to condensation on the products of combustion. Although this condition may not exist in orbit, the satellite rockets were fired by pulses rather than direct power because low resistance of rockets would result in a power drain. The stored energy required to fire the spin rockets was determined at this time by using a capacitor-checkage ignition system. A 0.3-ampere current is the amount required to fire the rocket squibs.

Further rockets tested, under vacuum with thermal cycling, by U. S. Flare Corporation did not meet the environmental specifications because of failure to ignite. After an AED investigation, it was found that the method of thermal cycling to meet the temperature extremes was produced by subjecting the rockets to a hot and cold blast of air. This method caused moisture to condense on the propellant grains, which then would not ignite.

AED then recommended that the vendor conduct tests in a vacuum at room temperature. One hundred consecutive successful firings were thus obtained and fulfilled the primary requirement for acceptance. Thrust variation exceeded the specification, but stayed within a range of ± 10 percent rather than plus 7 percent minus zero.

The temperature environmental tests were conducted on six spin rockets and six Atlas Powder Company piston motors by AED at Princeton in the vacuum chamber. The six motors, approximately evenly spaced on the periphery, were mounted at the end of three intersecting arms which placed each rocket close to the walls of the vacuum chamber. The rockets were connected to a battery through six toggle switches which were actuated by the six piston motors. Thermocouples were placed on each rocket and the chamber was temperature-cycled under a constant chamber pressure of 25-microns of mercury. The temperature-cycling consisted of four and a half cycles with the chamber contents reaching +55° five times and -10°C four times. At both of these extremes the temperature was held for a period of 20 minutes. The piston motors and rockets were then fired sequentially at 55°C and all fired successfully.

Five of the above rockets were also tested previously and cycled twice at the above pressure but between the limits of -20°C and +55°C.

Tests were also conducted to determine the effect of expanding gases of the rockets on the lenses and solar cells. These tests indicated that no serious deposits on any part of the satellite would occur.

These design and test results were confirmed when approximately seven weeks after launch a pair of spin rockets were successfully fired. The spin rate of TIROS I increased from 9.4 to 12.85 rpm (the design value was 3 rpm).

(4) Functional Description

Nine pairs of spin-up rockets (originally) were installed around the periphery of the satellite, and connected to an ignition control circuit capable of sequentially firing each (diametrically opposite) pair. Upon ground command, a 0.3 ampere pulse would be generated in the selected rocket-pair ignition circuit. A late design modification left only two pairs of rockets on the satellite. One each of these pairs is shown in the photograph of the rocket baseplate, Figure 114.

SECTION III A.8.

8. Satellite Structure

a. General

The approach to an implementation of the structural design of TIROS I was based on the special dynamic and thermal requirements of its structure. Various problems of fabrication and testing, and detailed stress and vibration analysis were solved after extensive investigation and experimental confirmation. Verification of the approaches used to solve the structure problem was obtained when TIROS I was space-borne.

The structural design was required to be completely strain-controlled because of: (1) the close tolerance on parallelism of camera axes after subjection to severe launch accelerations and vibrations; and (2) the brittleness of the silicon solar cells in the power supply. Fabrications and finishes were dictated by thermal requirements of high conductivity and emissivity. (Reference 16)

The payload weight and radial distribution were itemized, the shears and bending moments for each rib determined, and the envelope of maximum bending plotted. Maximum stresses were determined for the maximum vertical load in all members and their attachments. The sections were then sized by using an allowable working stress based on this criteria. The material used was selected on the basis of especially considering the buckling potential in the lower rib flanges and at the connections among flanges in the non-symmetrical intersections.

The structure was tested for 80 percent of ultimate loading by hydraulic jacks working through a "whiffle-tree" arrangement. Five cycles of five minutes each were performed, the alignment check being made before and after the set of five cycles. Static tests, using forty strain gages, gave results within ±15 percent of calculated values.

The first four vibration modes were determined by the Stodola iteration process, programmed for an IBM-650 computer. The first or "umbrella" fundamental was calculated and was verified experimentally. Higher mode frequencies were checked qualitatively, and extensive probing during vibration test indicated acceptable amplification factors.

b. Design Criteria

Initially the following design criteria were considered to be of utmost importance in designing a suitable structure:

1. Launching Rocket Interfaces and Volumetric Limits
2. Ascent Static and Vibrational Loads
3. Power Supply Area and Solar Cell Fragility
4. Orbital Temperature Variation Limits

5. Spin Stabilization

6. Separation

The launching rocket finally selected for TIROS I was the Thor-Able. It was necessary again to coordinate the volumetric requirements of the satellite with the capabilities of the rocket and its nose cone (heat shield). During this period, several satellite projects had this rocket assigned, and a general-purpose nose-cone configuration (somewhat like a swollen thumb) was evolved. The extending antennas of TIROS Satellite would be required to telescope, squeeze, or bend into this available volume. It was decided that a satellite configuration having a flat plane could be made compatible with the rocket (third stage), since the two flat mating surfaces thus available could be joined together by means of an oversize band strap and a key.

To evolve a precise load schedule, both steady-state and vibrational, for the satellite proved to be more difficult to achieve. It was apparent that there were predictable steady-state load schedules implicit in the selection of rocket stages, sequences and orbits. After thorough research into vibrational input level information, it became apparent that consistent information on this subject was lacking. Nevertheless, a qualification test specification was established which was based on the best available knowledge.

The area requirement of the power supply was readily determined because the normal orbit, duty cycle, and power levels were known. It was also known that solar cells required interwiring such that breakage of a few cells would not greatly reduce the power supply. Since the actual mechanical properties of the solar cells were unknown, experiments were conducted on both single cells and five-cell shingles. The chief result of these experiments was the determination of the limiting beam deflection of the shingle. This value was then used to determine the limit stress of 3000 lb/in^2 of the support structure. The types of support structure that were considered to produce this requirement were foamed plastic laminate, honeycomb structure, a monocoque hemisphere, and the final choice. The plastic configuration and that of metal or paper honeycomb were disallowed because of the necessity of thermal access to the balance of the payload. The solar cells in full sunlight had to be capable of conducting heat through the whole payload and thence dissipating it to the space sink in order to maintain power output. Similar reasoning eliminated the hemisphere because the back of one array of cells might not radiate nor conduct readily to the main mass.

After considering the thermal effects of the structure on the performance and life of the solar cell areas, it seemed natural to progress to the general consideration of thermal variation. The range of temperatures which would satisfy the operational requirements of the various payload components was firmly established. However, the exterior and interior surfaces and joints had to be designed to limit the temperature variation within the satellite. Basically, the heat sources within the satellite transfer heat directly to the baseplate, and since the entire device is spin-stabilized in inertial space, selection of the geometry radiative-absorptive coating was directed at dissipating heat from the mass accummulator. Since the external heat source is the sun, considerable effort was expended to protect the solar cells by discovering a

coating that would mask out the spectrum band above the visible which merely heated the satellite without contributing to power. To distribute the solar heat input internally the main mass, baseplate and sideplates would have to be painted black. Once these selections were made, an orbital temperature variation history was analytically generated.

The final criteria of design was that of satellite separation proper. Although the satellite has a passive role (to react against a trapped spring), it was of utmost importance to allow sufficient space for the severed band strap to be withdrawn.

Once all of these criteria became known, it was possible to consider the configuration that would meet all requirements. The initial shapes considered were:

1. an anvil at the rocket head, with a thin baseplate and spherical solar cell dome;
2. a honeycomb pill box, again anvil mounted;
3. an investment-cast assembly, with possible chemical milling; and
4. a centrifugally cast base, similar to a centrifugal compressor impeller, with a spun-embossed top for solar cell mounting.

The choice of the configuration that would meet the TIROS I requirements was then limited by the following desired design features:

1. Lightweight
2. Rigidity in solar cell support
3. Preservation of camera alignment
4. Thermal flux surfaces
5. Utilization of material strength
6. Ease of manufacture and rework
7. An open baseplate mounting surface to accommodate any required shift of components due to interference or balancing requirements

The type of structure which appeared to fit all the above requirements was a standard, sheet-metal aircraft-type fabrication. This structure would have to meet the final rocket (Thor-Able vehicle) requirements. These specific requirements were:

1. Because the satellite was to be spin-stabilized in space, a disc-shaped configuration was chosen. As a design goal, the ratio of polar to transverse moment of inertia was chosen as 1.6. The actual ratio of the moment of inertia of the orbiting satellite was 1.45 to 1 which was near the design goal ratio.

2. Total payload weight, compatible with the Thor-Able rocket and a 51° orbit at 450 miles, was 270 lbs (of which 25% was allotted to the structure).

3. Final payload configuration geometry to be compatible with the rocketry and the shroud.

c. Design Details

The TIROS I satellite fabricated aluminum-alloy structure was roughly cylindrical in shape, approximately 42 inches in diameter and 25.5 inches high. The structure after installation in the payload is shown in Figure 120. The structure consists basically of a reinforced bottom (baseplate, Figure 121) and a cover. This cover consists of the top (upper) plate, frame and 18 side panels (Figure 122). The two sections are joined by fifty-four, stainless, non-magnetic, socket-head screws and fifty-four anchor nuts, of the same material and attached to the cover.

Nearly all of the payload components are mounted directly over radial reinforcing ribs beneath the baseplate which is of sheet metal structure except for the machined hub section. These ribs, shown in Figure 121, are contoured in accordance with the average load and moment forces generated along them. The baseplate, a tension skin 0.064-inches thick, gives peripheral support to the integrated top and side panel assembly.

The hub central to the base structure is rough machined and bolted to the underside of the baseplate, and finish machined after the baseplate and cover are assembled. This procedure provides accuracy of squareness and concentricity to the very close tolerances that are required for dynamic balancing by accommodating the dynamic balancing machine collets.

Six inner radial ribs emanate from the central hub and are attached to an inner ring; and 18 tapered cross-section radial ribs at 20 degree increments also attach to the inner ring. These 18 ribs take up and transmit the bending moments developed in the baseplate. Three of the 18 radial ribs are reinforced by a 0.040-inch channel effective at radial stations of 4.50 and 6.50 inches. These reinforcements are in the regions of the cameras where no yielding is desired. Radially outboard, at distances of 10.5 inches and 15.5 inches respectively, cross-members are fastened between the radial ribs through gusset plates. The cross-members provide necessary support of the plate and protect against excessive deflections. An assembly of angles around the periphery form the lower plate rim. The rim and the radial ribs are attached through spin-up rocket brackets and 3/16-inch bolts.

Special case ribs appear at 0 degrees, 20 degrees, 320 degrees and 340 degrees. (Angular orientation is designated in Figure 121). These ribs are modified to take the infrared equipment load. Ribs at 0 degrees and 340 degrees join ribs at 20 degrees and 320 degrees, respectively, at a radial distance of 7.63 inches. The ribs begin to unload at this point, and to compensate for this, 0.062-inch gussets are provided to add more compression area in this heavily loaded region.

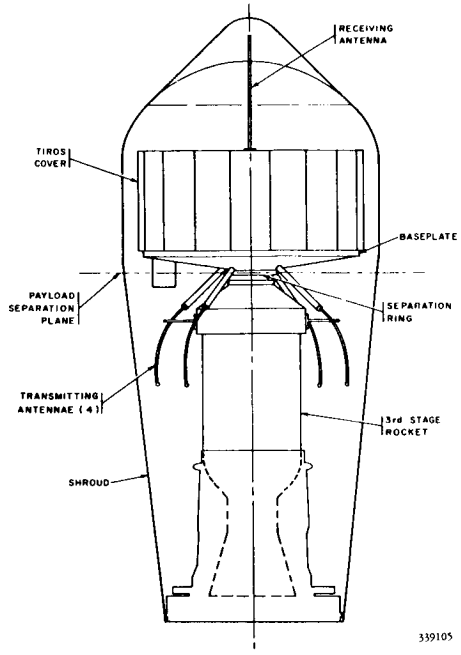

Figure 120. Installation of Payload Rocket

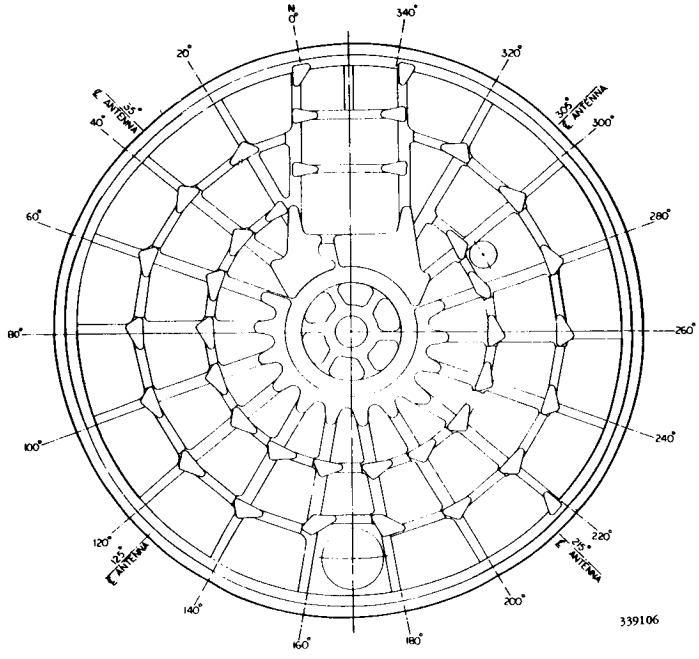

Figure 121. Baseplate Assembly

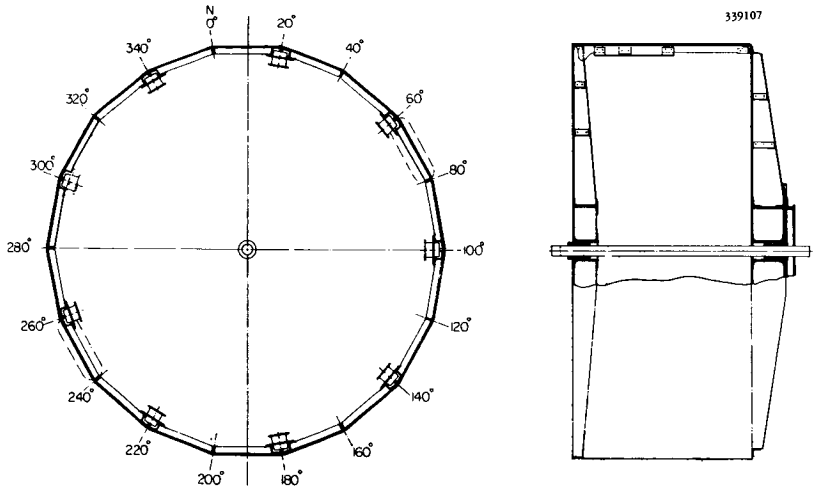

Figure 122. Structural Assembly

The construction of the upper plate assembly is similar to that of the lower-plate assembly in that six inner radial ribs emanate from an upper hub and are attached to an inner ring. Eighteen radial ribs, which support the upper plate and transmit bending moments, are also attached to the inner ring at 20 degree intervals.

Around the periphery of the upper plate assembly, 18 channels form the upper rim. The 18 side panel posts consist of extruded "T" sections. Provision is made on alternate posts for the installation of attitude sensors. These posts are slotted as shown, and are reinforced at the slot area. Precession dampers are attached to two posts.

There are 18 side panels (0.064 x 19 x 7 inches each) bolted to the posts and the upper and lower rims with studs. The side panels have a number of holes for the electrical connections to the solar cells. One panel has an opening for an infrared camera, and two panels are shortened to provide room for the despin mechanism.

The one objective in the design of the upper or cover structure was to provide support area for the silicon solar cells. Because the mechanical properties of these cells were (effectively) unknown, experimentation was carried out on both single cells and five-cell shingles. The primary result of this experimentation was the determination of the limiting beam deflection of the shingle. From this value the limit stress for the cover structure was set at 3000 lb/in^2.

In order that the entire cover should be sufficiently rigid to limit deflections in the shingles to a very low value, a heavy support structure was required. In future efforts, there is probably little that can be done to reduce the weight of optical unit supports; but, for solar cell supports, many newer possibilities now exist. Particularly, the concept that the entire structure have the rigidity to support a shingle need not be followed; rather, only localized rigidity under a group of cells is required. Such ideas lead readily to very light-weight structures, as frame-and-film types at 0.3 to 0.7 lb/ft^2 as compared to approximately 2.0 lb/ft^2 for TIROS.

Although the structure is designed predominantly for high stiffness to maintain the mounting faces for the optical components within the required tolerance and to provide a suitable support for the brittle solar cells, it also possesses adequate strength to withstand the severe launching accelerations. In general, the working stresses were maintained slightly below the yield level, consistent with buckling considerations at loads as high as 50 g in the axial direction, and 30 g radially. However, the top and side structure, where the solar cells are mounted, have stress levels reduced to 3000 lb/in^2.

The TIROS I payload was originally to have been launched by a Jupiter C rocket, but changes by the cognizant agencies finally resulted in the use of a Thor-Able combination. The general program schedule did not allow all of the permitted changes to be reflected in the structural design. Thus a number of assumptions as to structural requirements were incorporated in the design approach. This situation resulted in adherence to requirements undoubtedly more severe than necessary in many instances.

The items of major interest are:

Longitudinal acceleration:	50 g steady state
Transverse acceleration:	30 g steady state
Vibration in three planes:	7 g rms, 20 to 2000 cps
Rotation about longitudinal axis:	200 rpm
Angular deceleration:	200 rpm to 10 rpm in 0.5 sec
Temperature:	0 to 50°C
Pressure tolerance:	5×10^{-5} mm Hg or better
Balance:	6 ounce-inches at 200 rpm

Detailed environmental test specifications are given in Appendix C.

Also, there were no primary resonance frequencies near 77 cps. The tolerance on alignment of camera axes and spin axis preempted all other structural requirements; after injection into orbit, these three axes were to be parallel within 7 minutes of arc.

This tolerance, in conjunction with the stiffness requirement for the solar cells means that the basic design is "strain-controlled," making deflection the independent variable, and the only allowable procedure was now to size the sections using a well-chosen limiting stress. A value of 30,000 lb/in^2 was selected for the aluminum alloys used (yield strength of 42,000 lb/in^2). Margins of safety are detailed for all significant sections in Table 6.

Because the body is spin-stabilized in orbit, the slow-down effect of the earth's magnetic field on this rotating conductor is of concern. After model testing, the qualitative requirements that, whenever possible, the structure should consist of insulated segments, was added. This condition was met for the cover, but because the stiffness-weight limits of the baseplate could not be accomplished, a one-joint angle-section rim was used.

TABLE 6. DETAIL STRESS ANALYSIS MINIMUM MARGINS OF SAFETY

Item	Minimum Margin of Safety
1. 1173022E-2 Rib (Radius 6.50")	+0.11
2. 1173022E-2 Rib (Radius 15.50")	+0.22
3. 1173022E-5 Rib	+0.26
4. 1173022E-4 Rib	+0.03
5. Attachment: -2 Rib to Inner Ring Assembly	+0.16
6. Same as 5, Except in Region of Cameras	+0.07
7. Attachment: -2 Rib to -4 Rib	+0.21
8. Loading of Special Case Ribs (Radius 7.63")	+0.05
9. Loading of Special Case Ribs (Radius 4.50")	+0.34
10. Upper Skin Panel No. 3	+0.09
11. 1173023E-2 Rib (Radius 11.50")	+0.22
12. Upper Plate Center Ring	+0.42
13. Upper Separation Ring -(M_{1-1})	+0.19
14. Upper Separation Ring -(M_{2-2})	+0.07

Other important areas were those of materials, finishes, and fabrication. These were chosen only after extensive survey and experimentation with several possibilities; because production schedule allowed time for only one approach.

The use of a non-conductor, such as Fibreglass, for the basic structure was briefly considered for minimizing the magnetic drag effect. However, calculations readily showed that this type of material could not meet the requirements of stiffness, weight and volume. Considering the metals, the field narrowed very rapidly, to the aluminum alloys as having a maximum or adequate rating in each of the following requirements: non-magnetic, stiffness-to-weight ratio, compatibility with the thermally-required finishes, availability of material in both mill and fabricated forms, availability of equipment and capacity for fabrication techniques, and availability of engineering design techniques and capacity.

The alloys finally used were 2024-T4 sheet and formed parts, and 7075-T4 extrusions. These parts were finished by black anodize, black epoxy paint, bright Iridite, or Martin Hardcoat to provide the α/ϵ ratios of the thermal requirements. Many parts carried different finishes on different areas, creating an extensive identification and handling problem.

Fabrication was carried out according to the best aircraft practice, with 100 percent inspection at each step, extensive use of alignment fixtures and the rigid application of the RCA Workmanship Standards.

An important part of the design work involved stress analysis. Following some initial estimates for the base, the weights of the equipment were distributed along the radial members at a radius equal to the distance of the equipment centers-of-gravity from the center. Shears and bending moments were determined at all points of loading for each of the radial ribs. The maximum bending moment was conservatively assumed to be acting on all the ribs simultaneously and to be relieved by the rim and cross members. These bending moments were determined by making the rotational deflections of the structure consistent at all points where the rim and cross-member ribs attach to the radial ribs. The torsional stiffness of all the ribs was assumed to be zero. The maximum stresses were calculated for 50 g vertical load. The various members of the baseplate and their attachments were analyzed and margins of safety were computed.

In a like manner, section properties were calculated for the elements of the top plate assembly. Skin panels, ribs and cross-members and their attachments were investigated and margins of safety were determined for an allowable stress of 3000 lb/in^2. Also, the effect of a 30 g ultimate side load on the baseplate was computed; the side panels and posts were checked for margins of safety; and a check was made of centrifugal loads, hoist loads, and of the hoist fitting installation and the upper separation ring.

Excerpts of typical calculations in the Detailed Stress Analysis are (Reference 16) given in Appendix E.

d. Vibration Analysis

The main objective in the vibration analysis and testing was to ensure that the final structure and its load, as a spring-mass system, had no significant resonances near the input frequencies of the last stage rocket.

The important forcing frequencies were expected to be in the ranges of 75 to 85 cps and 550 to 650 cps. The fundamental for the baseplate was therefore chosen to be in the range of 55 to 60 cps, comfortably lower than 75 cps.

Symmetrical or "umbrella" mode shapes were treated in the analysis. (Reference 17) Calculations for these modes were carried out by the Stodola iteration process, and were programmed for an IBM 650 digital computer. Of the several cases considered, three were reported as having significant application:

Case No. 3 – Based on the weight data for a typical rib and moment of inertia, given in Table 7.

Case No. 7 – Same as Case No. 3, but considering the baseplate outer rim fully restrained by the side panels.

Case No. 8 – Calculation was made to see if any significant differences would occur in flight vibration and in ground vibration. Moments of inertia were calculated under a 1-g load for this case.

Only the first four vibration modes were calculated because: (1) the frequencies of the higher modes were far above any possible input frequencies from the rocket; (2) the top test frequency available was 2000 cps; and (3) there was no point in using computer time to produce inapplicable results.

The Stodola iterative process essentially consists of assuming a deflected mode shape, y, calculating the inertia forces, and from these, the new deflections. The process is repeated until the values of y converge to the desired degree of accuracy.

Typical results of this analysis are shown in Figure 123. The calculated fundamental was 57.9 cps and an experimental vibration survey indicated 55 cps as an excellent agreement, both values being within the range specified. The vibration survey did not show any significantly large amplitudes above 200 cps, which is in good qualitative agreement with the analysis. There were no significant differences in the results of the three cases noted above, indicating that the restraint imposed by the cover on the base plate deflections was negligible.

e. Test

The structure for the TIROS satellite was required to pass environmental tests according to RCA specifications. Static loading tests were designed to check the structural integrity under the acceleration forces of these specifications and, of equal importance, to check the actual deflections and stresses against the allowable values.

Table 7. CASE III INITIAL VIBRATION DATA

Station	Distance (x)	Differential Weight (lbs.)	I(in.^{4})	Station	Distance (x)	Differential Weight (lbs.)	I(in.^{4})
0[1]	0.00	0.0775	0.41500	32	8.00	0.0669	0.19300
1	0.25	0.1544	0.40909	33	8.25	0.0389	0.18634
2	0.50	0.1539	0.40322	34	8.50	0.0383	0.17972
3	0.75	0.1533	0.39735	35	8.75	0.0377	0.17310
4	1.00	0.1315	0.39148	36	9.00	0.0372	0.16648
5	1.25	0.1097	0.38561	37	9.25	0.0366	0.15986
6	1.50	1.3596	0.37974	38	9.50	0.0360	0.15324
7	1.75	0.1085	0.37387	39	9.75	0.0355	0.14662
8	2.00	0.1080	0.36800	40	10.00	0.0349	0.14000
9	2.25	0.1074	0.36100	41	10.25	0.0344	0.13434
10	2.50	0.1068	0.35400	42	10.50	0.1213	0.12872
11	2.75	0.1063	0.34700	43	10.75	0.2082	0.12310
12	3.00	0.1057	0.34000	44	11.00	0.2076	0.11748
13	3.25	0.1052	0.33300	45	11.25	0.2071	0.11186
14	3.50	0.0671	0.32600	46	11.50	0.2065	0.10624
15	3.75	0.0290	0.31900	47	11.75	0.2060	0.10062
16	4.00	0.0285	0.31200	48	12.00	0.2054	0.09500
17	4.25	0.0279	0.30409	49	12.25	0.2048	0.09075
18	4.50	0.0373	0.29622	50	12.50	0.2043	0.08650
19	4.75	0.0468	0.28835	51	12.75	0.2037	0.08225
20	5.00	0.0737	0.28048	52	13.00	0.2031	0.07800
21	5.25	0.1006	0.27261	53	13.25	0.2026	0.07375
22	5.50	0.1001	0.26474	54	13.50	0.2020	0.06950
23	5.75	0.0995	0.25687	55	13.75	0.2015	0.06525
24	6.00	0.0989	0.24900	56	14.00	0.2009	0.06100
25	6.25	0.0984	0.24200	57	14.25	0.2003	0.05675
26	6.50	0.0978	0.23500	58	14.50	0.1023	0.05250
27	6.75	0.0973	0.22800	59	14.75	0.0042	0.04825
28	7.00	0.0966	0.22100	60	15.00	0.0036	0.04400
29	7.25	0.0961	0.21400	61	15.25	0.0030	0.03975
30	7.50	0.0956	0.20700	62	15.50	4.5114	0.03550
31	7.75	0.0950	0.20000				

[1] Station "0" is 4.50 inches from center line

$$\Delta M_{24} = 53505 \left(\frac{dy}{dx}\right)_{24} - 1801 \left(\frac{dy}{dx}\right)_{44} - 1365 \left(\frac{dy}{dx}\right)_{62}$$

$$\Delta M_{44} = -1801 \left(\frac{dy}{dx}\right)_{24} + 15195 \left(\frac{dy}{dx}\right)_{44} - 883 \left(\frac{dy}{dx}\right)_{62}$$

$$\Delta M_{62} = -1365 \left(\frac{dy}{dx}\right)_{24} - 883 \left(\frac{dy}{dx}\right)_{44} + 11729 \left(\frac{dy}{dx}\right)_{62}$$

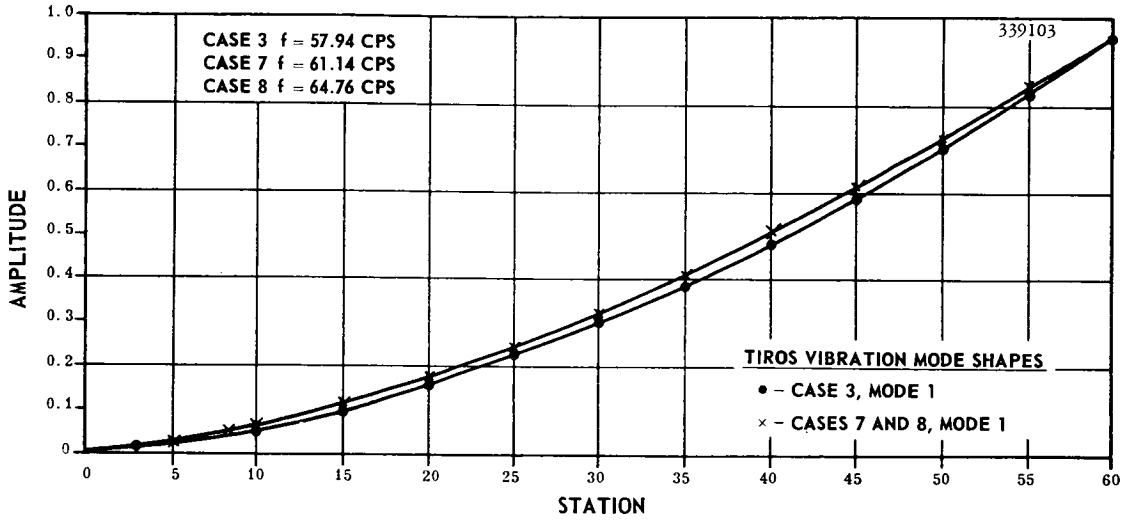

Figure 123. Results of Vibration Analysis

The investigation was limited to those areas of known or anticipated criticality as to stress or deflection, e.g., the lower flanges of the radial ribs. Dynamic vibration testing was performed to determine the transmissibility of the structure from the input at the separation ring to the mounting location of each component, and general structural resonances and the overall structural integrity.

(1) Static Loading Test

Two static loading tests, as required in Appendix C, were employed on the prototypes:

1. Prototype baseplate only (to 80 percent of the design load).
2. Prototype complete structure, i.e., baseplate and cover (to 80 percent of the design load).

A static-loading fixture (Figure 124) for the TIROS I satellite was designed and built to simulate the launching acceleration forces over the range from one to 50 g's. This fixture consists of six elements:

1. A set of mass distribution plates, corresponding to the payload components, such as cameras, tape recorders, etc. These are shown in Figure 125.
2. A pressure bag, made of Mylar, for uniform distribution of the load on the top surface of the satellite, and a manometer to indicate the bag pressure. The bag is shown in Figure 126.

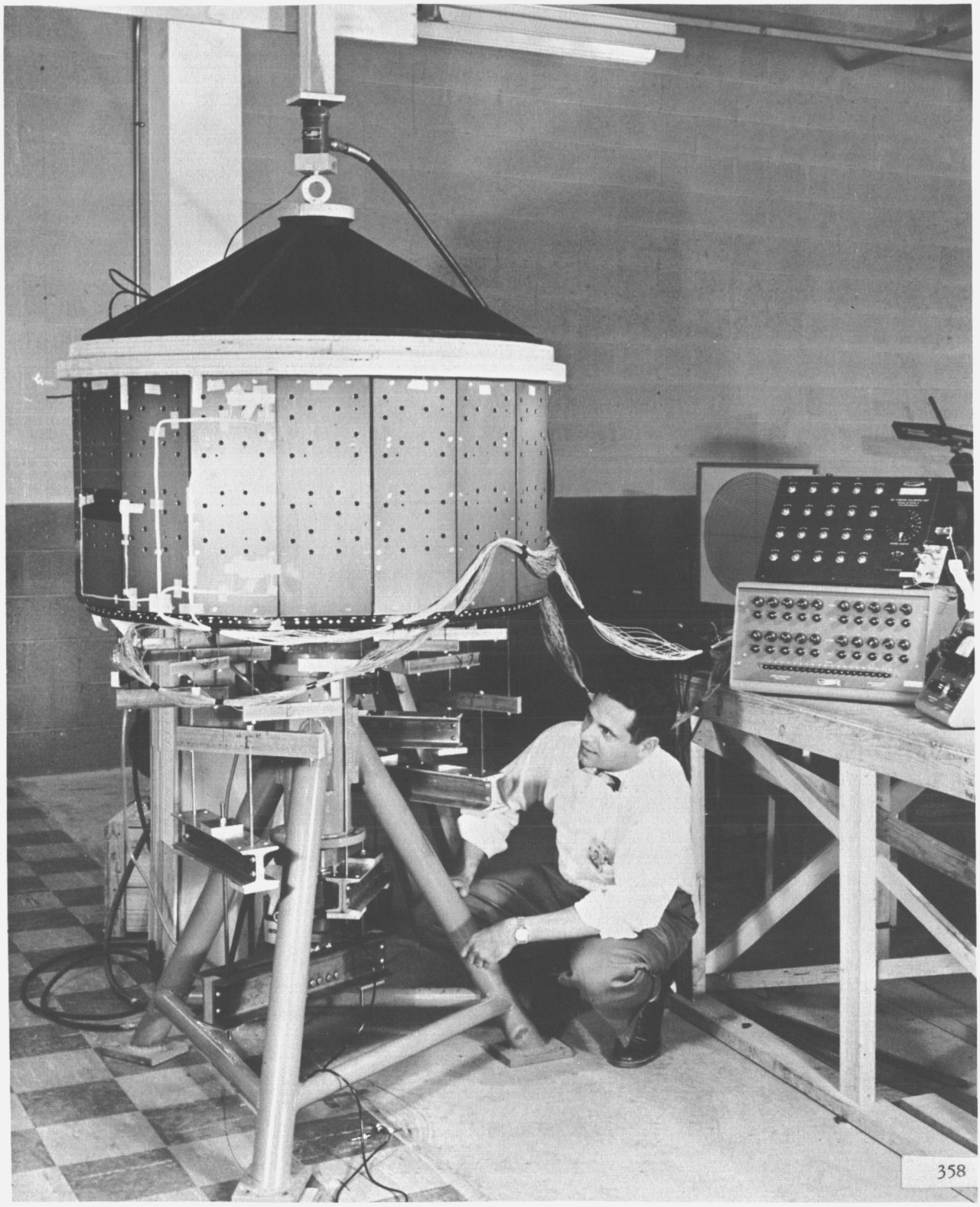

Figure 124. A TIROS I Housing in Place on the Structural Loading Test Fixture; the Strain Gage Instrumentation is Located on the Bench at the Right

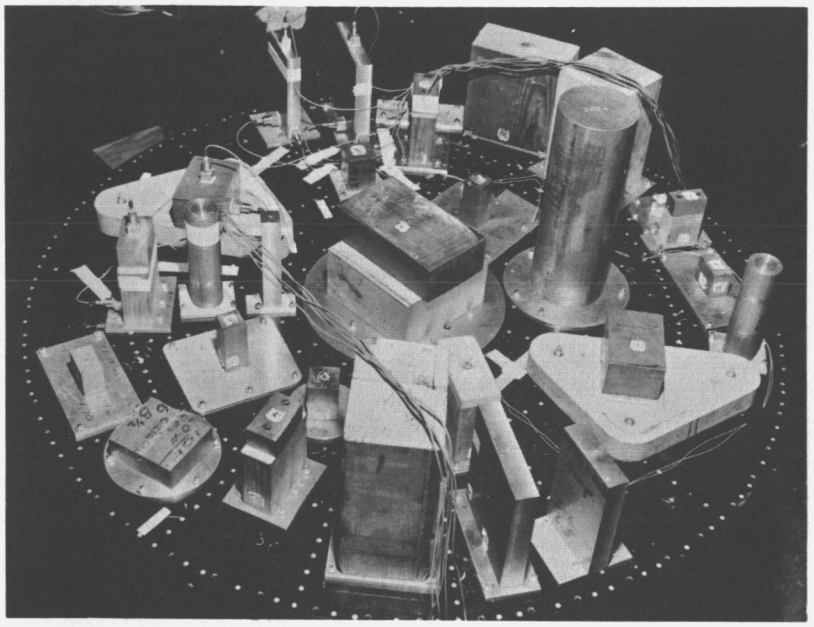

Figure 125. Mass Distribution Plates on Satellite Baseplate

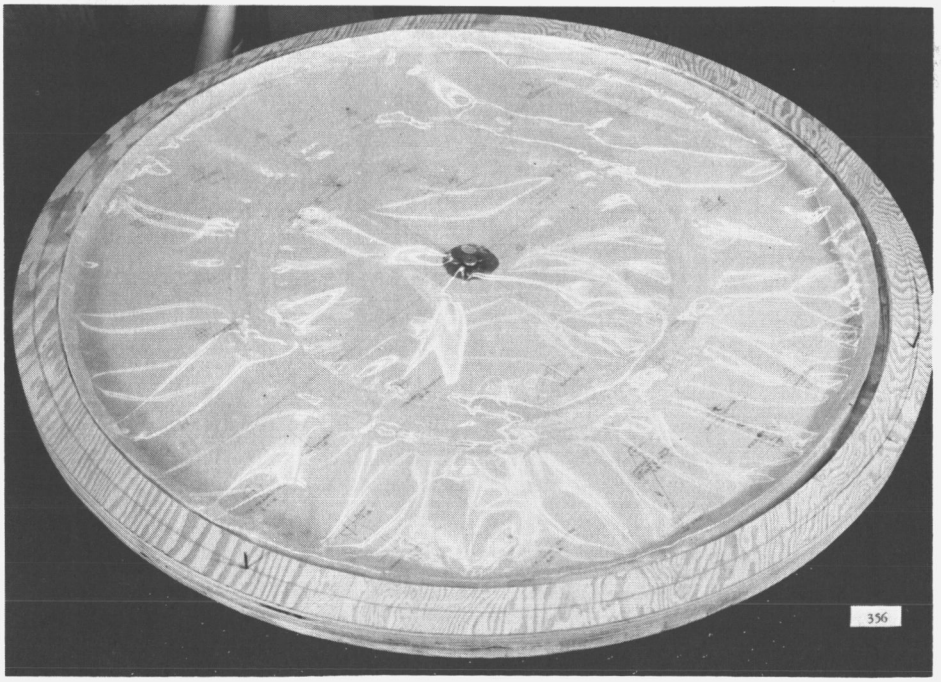

Figure 126. Mylar Pressure Bag

3. Strain gages and instrumentation. About 60 strain gages (gage factor 1.92 ± 2 percent) are used. Some of these are shown in position on the satellite side panels in Figure 124. The associated 40-channel bridge and balance (for the upper and lower surface strain gages) arranged for direct readings in lbs/in^2 are shown on the bench at the right in Figure 124.

4. Two hydraulic jacks, one for loading the pressure bag and one for the "whiffle-tree." These are shown in Figure 124, one above and one below, in line with the satellite axis.

5. Two Morehouse-type force transducers.

The baseplate was set upon a large surface plate in the machine shop, being supported on the separation ring as it would be on the third stage rocket. The profile of the plate was determined by tramming with a 0.0001-inch height gage at a large number of points in the vicinity of the camera and infrared equipment mounting areas. The structure was then loaded to 80 percent of design load (9400 lbs) for five cycles of five minutes each, removed from the test rig, and the baseplate trammed again.

Stress readings were taken for increments of load up to 80 percent of the design load or 40 g. The experimental stresses were extrapolated to a 50 g load and compared with the detailed stress analysis. The compressive bending stresses in several of the lower plate radial ribs were measured near their attachment to the lower plate inner ring, where maximum radial rib stresses were anticipated. Stress reading at four of the six ribs showed good agreement with the calculated stresses. At a typical location the compression bending stress was 36,400 lbs/in^2 for a 50-g load. This was 12 percent higher than the maximum calculated stress. The maximum bending stress on the rib was, however, still within the allowable stress level needed to prevent failure of the rib. Strain gages were located on and near the radial rib at Θ = 180 degrees to verify the load distribution calculated in the stress analysis. The shear stress in a radial rib at a radius of nine inches was 5200 psi for a 50-g load. This corresponds to a shear load in the rib web of approximately 572 pounds and is within five percent of the calculated shear load for that station. The stress in the skin, above the radial rib at Θ = 180 degrees was measured at 3000 psi for a 50-g load and was much lower than the calculated stress. Other stresses measured on the top skin at the radial rib at Θ = 160 degrees and at the special rib at Θ = 200 degrees were also proportionately lower than calculated. This indicates that the skin is more effective in taking load than had been assumed in the stress analysis. The results of the static test indicate that the TIROS payload structure would be able to withstand the design vertical 50-g load without failure by excessive permanent deflection. The results of the static test show that the method of stress analysis applied here is satisfactory for this type structure.

(2) Dynamic Vibration Test

The vibration testing, in order to meet the requirements of RCA TIROS Specification TSP-T1-100B, was conducted in several phases:

1. A survey was made of the entire structure with dummy loads.
2. Components, such as transmitters, cameras, etc., were subjected to "third-level" inputs for prototypes and "first-level" for flight models.
3. The entire prototype assembly was subjected to an input level depending on the number of assemblies to be tested.
4. The flight assemblies were given first-level inputs only.

The dependency of the input level on the number of identical items to be tested resulted from the reliability requirement. This was stated in such terms that satisfactory reliability could be achieved by using second-level input on two prototypes or third-level inputs on one prototype. The various levels of input used in vibration testing were based on the first-level as specified for flight models at 7-g rms random noise with bandwidth limited from 20 to 2000 cps, for 2 minutes in each of three mutually perpendicular planes. The dynamic requirements other than vibration were not subject to multiplication of input levels.

The vibration testing was conducted on a 5000-lb force, Calidyne unit that was fitted with a specially designed fixture having no resonance below 2000 cps. This fixture carried a third stage separation ring, making the mounting for the payload structurally identical to that on the actual rocket.

The initial tests were a manually controlled frequency sweep of 1/2 g rms, and then at 2 g rms, along the thrust axis to search out potentially dangerous resonances. Later tests included both sinusoidal frequency sweeps, and random noise as specified previously.

The vibration tests indicated primary resonances in the umbrella mode at 55 cps and in the rocking mode at 18.5 cps. The fundamental at 55 cps agrees well with the calculated value of 57.9 cps, and the magnitude of these values completely satisfies the requirement that the satellite show no resonances near the 77 cps expected from the third-stage rocket. The other rocket forcing frequency of around 600 cps was also avoided in that all of the payload resonance peaks above about 75 cps were rather low. These conditions were considered as conservative because the actual components were more compliant than the rigid dummy masses.

The amplification factors at various locations ran as high as 10 on the prototype, and were of a sharp peaking nature. Addition of minor stiffening and of a few radial ties at the top of the components brought the amplification down to an acceptable range of 3 to 4.

SECTION III A.9.

9. Thermal Design

a. General

The objectives of the temperature-control subsystem of TIROS I were to maintain the temperatures of the satellite functional components within the allowable design temperature range of 0° to 50°C, except for the solar-cell temperature, which was to be held as close to the lower temperature limit as possible. The method of control was to be effective for a period of at least 90 days from launch and, mainly because of satellite weight limitations, was to be passive (i.e., to have no moving parts). Coatings and finishes would be depended upon in great measure to maintain acceptable thermal conditions. Such finishes were required to be stable in the space environment and, those used externally were required to maintain this stability under illumination by the sun (for a period of one year).

Solution of the thermal problem involved three main areas of investigation: (1) analysis of the heat flow problem, (2) development of suitable surfaces, and (3) experimental verification of the thermal design.

b. Analysis of the Heat Flow Problem

A satellite in space, just as the more common material bodies on earth, must obey the Law of Conservation of Energy, (i.e., the change in heat content of a body must equal the net energy entering the body).

(1) Thermal Sources

The first phase of the thermal analysis was to definitize the significant sources, in order to establish the amount of energy which would have to be dissipated by the TIROS I satellite structure to meet the requirements. The chief ambient thermal sources of supply are the sun and earth (the fluxes received from the stars and moon are negligible). The remainder of the sky constitutes a vast thermal sink, whose radiant output is equivalent to that of a black body ranging from 4° to 30°K.

The radiant flux from the sun (solar constant), just above the earth's atmosphere, has a mean average value of 0.14 watt per cm^2 with a color spectrum approximately that of a 6000°K black body. A seasonal variation of radiant flux from the sun (direct solar energy) of 3.5 percent is due to the eccentricity of the earth's orbit around the sun.

The earth, as a thermal source, provides radiant energy to a satellite by (1) reflection of solar flux (albedo) (ρ) with little selective change in color temperature of 5600°K and (2) thermal emittance (earth radiation, earth shine), which has an average color temperature of 260°K.

The internal source of heat is that due to the heat dissipated by the satellite electrical components. After investigation, the average heat dissipation rate was found to be 20 watts which was insignificant when compared to the external source of heat.

(2) Radiation Input

The amount of heat impinging on the various external surfaces of the satellite had to be determined. The analysis revealed that the factors which influenced the amount were (1) geometry of the satellite and (2) launching site requirements. At the time of the thermal analysis the major aspects of TIROS I geometry were fixed by the mating requirements of the satellite to the vehicle and shroud, as well as by the dynamic and functional considerations. The launching site requirements determined the orbit inclination angle, aiming-point latitude, and date of launch. Further constraints on the remaining parameters stem from the need to satisfy the requirements of solar power conversion and television inputs. The hour of launch determined the initial values of the projection of the direct solar flux impinging on the several exterior surfaces; as well as the fractional time in the sun, within the limits set by the orbit inclination angle. To a lesser extent, the received flux due to the albedo of the earth could be influenced by the time of launch. The precessions of the satellite orbit and the sun, which are not at our disposal, then take over to determine the course of subsequent radiative inputs.

Equations (developed in Appendix G) were then derived to calculate precisely the continually varying values of radiation impingement on these several surfaces. These equations were defined readily in terms of the spin axis because the satellite is spin-stabilized, its spin axis fixed in inertial space.

(3) Thermal Response of the Satellite

The second phase of the thermal analysis involved the determination of the thermal response of the satellite structure to the heat radiation impinging on the satellite surfaces. Because of the absence of air around the satellite, conduction and convection to the surrounding sky is negligible, and practically all heat transfer occurs by radiation.

Early studies were conducted to determine the type of thermal design that could be incorporated into the satellite structure to obtain the desired thermal response. Initially, two extreme philosophies of thermal design were considered: (1) an isothermal design and (2) an adiabatic design.

At one end of the thermodynamic scale is the isothermal design in which all of the various parts of the satellite would be in such good thermal communication with one another that, at any instant of time, the entire satellite could be assumed to be at a single temperature. This, of course, would minimize (1) the orbital temperature fluctuations of the solar cell surfaces at the expense of somewhat larger fluctuations for the interior package; and (2) it would have the important effect of lowering the long-term average temperature of the top solar cell surface, while at the same time raising the average baseplate temperature. This thermal communication of the various parts with one another would be accomplished by both radiation and conduction. Calculations indicated that it would be exceedingly difficult to achieve sufficiently close coupling to arrive at the isothermal state, and it would be undesirable to do so

because the baseplate would tend to become too warm (or at any rate warmer than necessary) during the periods when the satellite is in the sun for a large percentage of each orbit.

At the other end of the thermodynamic scale is the adiabatic design in which the interior component package would be thermally isolated as completely as possible from the exterior surfaces. This would provide maximum protection for the interior against orbital day-night temperature variations, and would provide a means of setting the long-term average temperature of the electrical components at various levels by properly choosing the thermal resistance between the interior packages and the various external surfaces. This method as applied to TIROS I (which was distinguished from previous satellites by the larger percentage of surface area covered by the solar cells) would because of the relatively low ratio of thermal mass of the skin to the surface area of the skin, provide the solar cell surfaces with almost no protection against orbital day-night temperature variations. Therefore, during each orbit, when the spin axis was within 40 degrees or less of the sun vector, the surface temperatures (especially the top surface temperature) would be high enough to cause a serious impairment of the cells. A method would have to be found that would (1) insure against the tendency of the baseplate to run too cold and (2) remove the internal heat dissipation.

After analyzing these two extremes of thermodynamic design, the following conclusions were reached:

1. Because of its large area to mass ratio, the satellite top surface would tend to become too hot during the day part of each orbit if it was required to reject all its own incident energy by radiation from its exterior surface. Therefore, it was desirable to allow some of this energy to be conducted to and dissipated by the rest of the satellite.

2. While the top would become too hot, the baseplate with the electrical components would be rather cool as a result of the low fluxes of energy impinging on this surface. Therefore, it was desirable to receive some additional thermal energy from the top and sides (which receives a high rate of incident energy) and from the components which contribute to the internal heat because of their operating temperatures.

In order to achieve these desired results, a compromise between the extremes of solely isothermal or solely adiabatic design was chosen. By incorporating the following features in the structural design, sufficient radiation coupling was introduced to achieve the desired compromise:

1. Maximum possible internal radiant energy interchange. This was accomplished by:

   (a) Blackening all interior surfaces, with the possible exception of a very few components.

(b) Doing everything possible to minimize the thermal resistance between the outer and inner skin surfaces. Since a double skin of any kind, which would serve as a radiation barrier, would not be suitable, a sheet metal (aluminum skin), reinforced by ribs where necessary, was chosen.

(c) Maximizing the radiating area to the top and sides by filling the interior space of the satellite (as much as possible) with structures which are conductively well bonded to the baseplate.

2. An aluminum side skin. This was required to be:

(a) Approximately 0.040 inches thick to provide efficient radiation coupling from the top to the sides and from the sides to the baseplate.

(b) Capable of conducting electricity to the baseplate because of r-f requirements, and possessing as low a thermal resistance as possible at the joint.

(c) Electrically insulated (because of r-f requirements) from the top plate at the joint, but having as low a thermal resistance as possible.

(d) Segmented (because of eddy-current requirements) into at least 20 sections which are electrically insulated from each other but not from the baseplate. This restriction could become less critical after determination of the hysteresis loss that causes slow-down of the satellite.

3. A baseplate, the underside of which must radiate readily to the sky at a temperature essentially the same as the average baseplate temperature. To accomplish this, the thermal resistance between the inner and outer surfaces must be as low as possible (which rules out a double skin). Indications were that an aluminum baseplate stiffened by ribs well bonded thermally to the baseplate would be required.

4. Individual treatment of certain critical components having restricted operating temperatures (if studies indicated this was required).

(4) Thermal Energy Equations

The thermal equations for a satellite structure, which would contain the above features, were derived for the satellite top, sides, and baseplate (including components) by considering each section as isothermal. As stated previously, the temperature of the orbiting satellite at any time is a function of the time in the sun, the satellite orientation angle between the solar field and the normal to the orbital plane. Since the date and time of launch was not firm at the time of the derivation of these equations, it was not deemed wise to calculate the temperature as a function of

time after launch. Instead, the equations were derived as a function of the angle α for the two extreme conditions, 100 percent sun-time orbit and 64 percent sun-time orbit. The energy equations were then written for the external energy inputs as well as the internal radiation coupling. Conduction coupling was not considered because early analytical models included approximations of the conduction coupling which proved to be negligible due to the relative thinness of the sides. Each section has two equations, one for the orbital day and one for the orbital night.

The daytime condition for the satellite top is*

$$M_T C_T \frac{dT_T}{d\theta} = A_T \epsilon_T \mu_T + A_T \alpha_T \rho_T + A_T \alpha_T Q \cos \alpha + K_{TC} \sigma T_C^4$$

$$- K_{TS} \sigma T_S^4 - (A_T \epsilon_T + K_{TC} + K_{TS}) \sigma T_T^4$$

The nighttime condition for the satellite top is

$$M_T C_T \frac{dT_T}{d\theta} = A_T \epsilon_T \mu_T + K_{TC} \sigma T_C^4 + K_{TC} \sigma T_S^4$$

$$- (A_T \epsilon_T^4 K_{TC} + K_{TS}) \sigma T_T^4$$

The daytime condition for the satellite components is

$$M_C C_C \frac{dT_C}{d\theta} = A_B + {}_B \mu_B + A_B \alpha_B \rho_B + K_{TC} \sigma T_T^4 + K_{SC} \sigma T_S^4$$

$$(A_B \epsilon_B + K_{CS} + K_{CT}) \sigma T_C^4$$

The nighttime condition for the satellite components is

$$M_C C_C \frac{dT_C}{d\theta} = A_B \epsilon_B \mu_B + K_{TC} \mu T_T^4 + K_{SC} \sigma T_S^4$$

$$(A_B \epsilon_B + K_{CS} + K_{CT}) \alpha T_C^4$$

*Note that T, S, B, and C used as subscripts represent the satellite top, sides, base, and components, respectively. However, the classic symbols for absolute temperature and specific heat (T and C, respectively) are also used in these equations, but not as subscripts.

The daytime condition for the satellite sides is

$$M_S C_S \frac{dT_S}{d\theta} = \pi A_S \epsilon_S \mu_S + \pi A_S \alpha_S \rho_S + A_S \alpha_S Q \sin \alpha + K_{ST} \sigma T_T^4 + K_{CS} \sigma T_C C_4 - (\pi A_S \epsilon_S + K_{CS} + K_{TS}) \sigma T_S^4$$

The nighttime condition for the satellite sides is

$$M_S C_S \frac{dT_S}{d\theta} = \pi A_S \epsilon_S \mu_S + K_{ST} \sigma T_T^4 + K_{CS} \sigma T_C - (\pi A_S T + K_{CS} + K_{TS}) \sigma T_S^4$$

where:

M_T, M_S, M_C	=	the mass of the top, sides and components respectively
C_T, C_S, C_C	=	the specific heat of the top, sides and components respectively
A_T, A_B	=	area of the top and base respectively
A_S	=	projected area of sides
α_T, α_S, α_B	=	solar absorptivity of the top, sides and base respectively
ϵ_T, ϵ_S, ϵ_B	=	emissivity of the top, sides and base respectively, in watt/cm^2
μ_T, μ_S, μ_B	=	earth shine to top, sides and base respectively, in watt/cm^2
ρ_T, ρ_S, ρ_B	=	albedo to top, sides and base respectively, in watt/cm^2
K_{TS}	=	top to sides radiative coupling factor
K_{TC}	=	top to components radiative coupling factor
K_{SC}	=	sides to components radiative coupling factor
Q	=	direct solar energy
θ	=	time

To solve these equations directly for the TIROS I satellite was impractical, if not impossible, because of its complex geometry with non-linear boundary conditions. The approach taken was to begin with a simple model and add complexity both in geometry and in thermal properties of the geometric elements until all of the desired five design features (within certain limits) were incorporated into the satellite structure.

For the initial calculation of the temperatures of the top, sides, and baseplate, the interior volume of the satellite was assumed to be entirely occupied by the components. Furthermore, the component package was considered to be isothermal when calculating the transient state (i.e., 64% sun time). The values of emissivity and absorptivity of the surfaces were determined as shown in Appendix H.

Radiation coupling factors were then assumed, based on an examination of the satellite geometry and surface properties. These assumed values were: $K_{TS} = O$, $K_{TC} = 5.75\ ft^2$, $K_{SC} = 11.0\ ft^2$.

The term radiation coupling factor, as used in TIROS I, can be defined in the following manner:

$$Q_{1-2} = A_1 \epsilon' \phi_{1-2} \sigma (T_1^4 - T_2^4)$$

where: A_1 = area of the first body, in cm^2

ϵ' = some function of the emissivities of both bodies, in $watt/cm^2$

ϕ_{1-2} = angle factor from first body to second body, in radians

T_1 = absolute temperature of first body, in °K

T_2 = absolute temperature of second by, in °K

The coupling factor from the first body to the second body is therefore:

$$K_{1-2} = A_1 \epsilon' \phi_{1-2}$$

where: K_{1-2} = coupling factor, in ft^2.

The coupling factors form a symmetrical matrix and $K_{1-2} = K_{2-1}$. Therefore, on the TIROS I satellite, $K_{TS} = K_{ST}$, $K_{SC} = K_{CS}$, and $K_{TC} = K_{CT}$.

The values of the direct solar flux and albedo energy inputs for the transient state (64% sun time) were calculated for each surface and averaged for the illuminated portion. The earthshine for the transient state was averaged over the complete orbit. For the steady state (100 per cent sun time) these energy-input values are constant over the complete orbit.

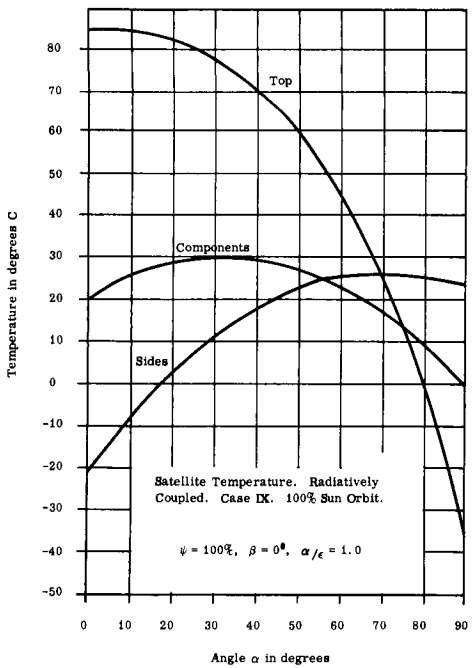

Figure 127. Steady-State Temperatures for a 100% Sun Orbit, with $\beta = 0$, as a Function of which is the Angle between Satellite Spin Axis and the Sun Vector

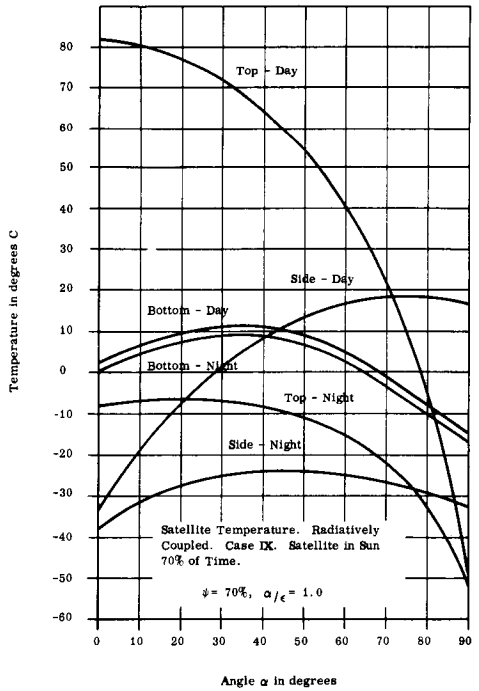

Figure 128. Day-Night Temperature Variation for a 70% Sun Orbit, as a Function of α.

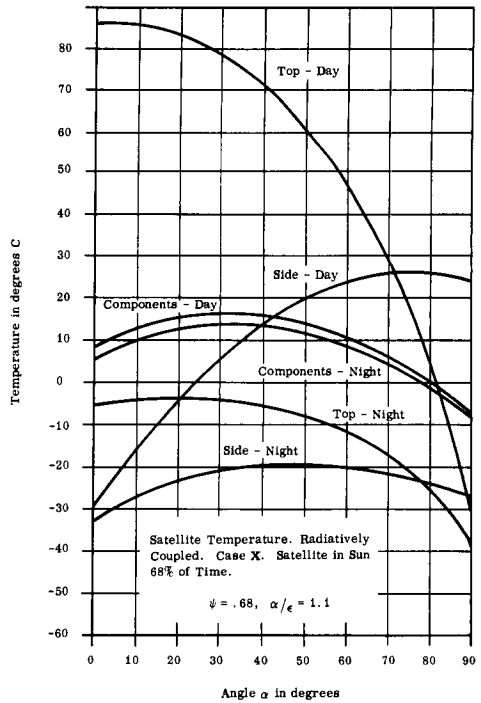

Figure 129. Day-Night Temperature Variation for a 68% Sun Orbit, as a Function of Angle α.

The six simultaneous equations, containing the above values, were then solved by an iterative process on an IBM 650 computer. The results are shown in Figures 127 and 128 for an absorptivity/emissivity ratio of the solar cells of 1.0. Figure 129 shows the resulting temperature change of the space environment caused the absorptivity/emissivity ratio to change from 1.1 to 1.0.

c. Development of Suitable Surfaces and Surface Coating

The surface radiative properties, which already have been mentioned without definition, are the effective absorptivities to the radiant energy input, and emissive powers for thermal radiation of the surfaces. Initial analysis had indicated that, to maintain a desirable operating temperature, the absorptivity/emissivity ratio would have to be accurately measured and that a change of 0.1 in the gross value of α/ϵ of the exterior surfaces would provide changes in the order of 10°C for the interior of the TIROS I satellite.

The equipment used initially for these measurements was a Perkins Elmer Model 112U spectrometer which was modified to keep surface materials at a temperature of 100°C. Spectral measurements between 2 and 15 microns were then made of the emitted flux. This method required extrapolation of the spectral emission curve for 30 percent of the temperature domain, (i.e., when the emitted flux was greater than 15 microns).

Another modification of the spectrometer consisted of a goniometer table mounted at the exit slit to enable total spectral reflectivity measurements to be made. Thus, for opaque materials, direct reflectivity measurements of the spectral absorptivity of the sun over the solar spectrum could be obtained. This type of measurement, however, proved to be too time consuming.

A simple, accurate, and rapid technique (Figure 130) to measure directly the α of a surface to the solar flux was developed by RCA to offset the difficulties indicated in the previous two methods. In this setup, a thin plate, with a given coating on both sides, was suspended in a vacuum to reduce the thermal conduction through the air. The plate is surrounded by walls that are matted to minimize internal reflections and are cooled by liquid nitrogen to reduce incident thermal radiation. To minimize conduction losses, the wires used to suspend the sample were long and thin and of low emissivity. The thermocouple junction was designed to minimize the total heat input and to spread it over a large central area of the sample to minimize further the temperature drop at the junction. A carbon-arc searchlight, that simulated solar flux, was used to illuminate, as uniformly as possible, one side of the sample. For an isothermal plate of negligible thickness at thermal equilibrium, with a total incident radiation intensity (I) the ratio of absorptivity (α) to emissivity (ϵ) is approximately:

$$\alpha/\epsilon = 2\sigma T_E^4/I$$

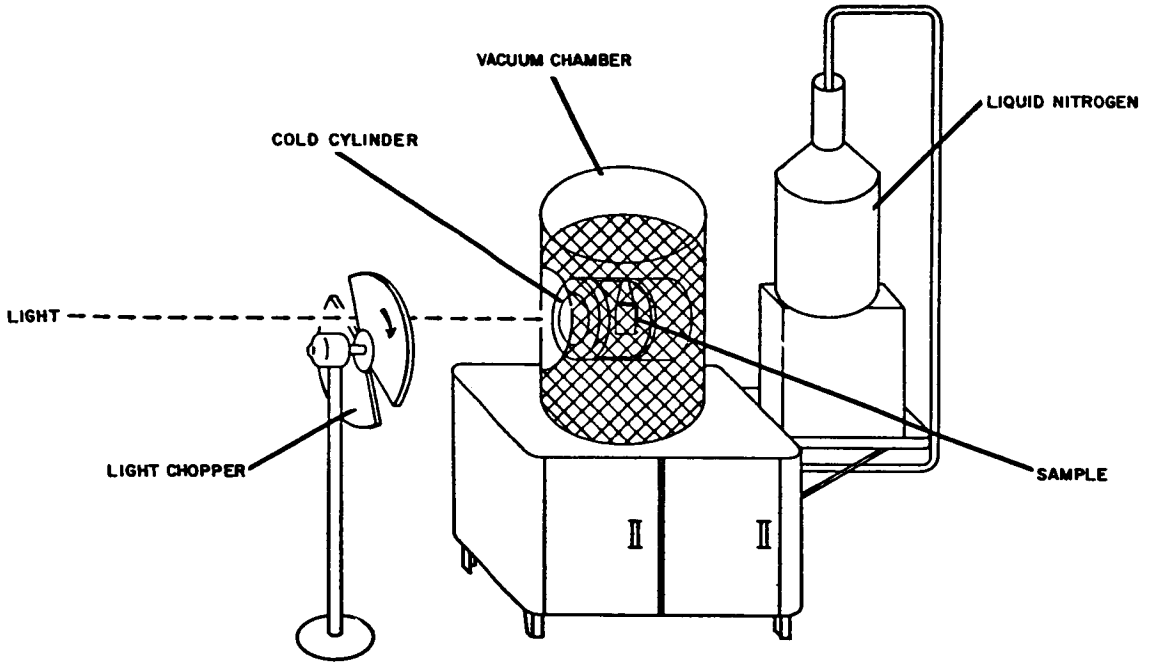

Figure 130. Schematic of Direct Measurement of α/E Apparatus

Where:

α = absorptivity

ϵ = emissivity

σ = Stefan-Boltzmann constant

T_E = measured equilibrium temperature, in °C

I = total incident flux, in watt/cm^2

By recording the temperature as a function of time, the thermal emissivity could be determined separately, when the specific heat of the sample was known. The results of these two methods were compared for a number of samples and the results compared favorably. Since the thermal method was much faster, it was used more extensively toward the final phase of the project. Refer to Appendix H for a more detailed description of this method.

The surface and surface coatings selected as a result of these experiments to produce the desired α/ϵ ratio for the baseplate top, and sides were as described below (also refer to Appendix I):

(1) Baseplate

The baseplate of the TIROS I satellite is a tension skin of aluminum, 0.064 inches thick, reinforced on the exterior surface by tapered ribs extended radially from

the center. Due to shadowing by the ribs near the hub, the effective α/ϵ in this area approaches that of a black body, regardless of the base materials and coatings employed. This radial conduction of the skin, therefore, essentially caused the baseplate to be in an isothermal state despite the heat loads of the components which are thermally connected to the skin.

The external side (bottom) of the baseplate acts as a radiator; that is, it emits heat from the rest of the satellite by radiation to surrounding space. To control the amount of heat emission, the emissivity of the baseplate bottom surface was made as low as possible (0.15) by using an iridite finish. The baseplate bottom could have been painted black to increase the emissivity rate.

Because of the complex geometry of the bottom of the baseplate, the gross value of emissivity had to be determined by experiment. An experiment was conducted in a closed chamber maintained at a pressure of 5×10^{-5} mm Hg. (Ref. 18). In this experiment, a known amount of energy was absorbed by the top side of the baseplate and the external side was allowed to have a radiant exchange with a cold black wall of known temperature. The resulting temperature of the baseplate was a measure of the external emissivity which was 0.4 ± 0.05.

To thermally connect (conductively couple) the components to the baseplate, the mounting surfaces of both the baseplate and components were made as flat as possible. Furthermore, all components were mechanically secured to the baseplate with screws in an attempt to reduce contact resistance. Initially, bonding the components with a high conductivity epoxy to the baseplate was considered; but the resulting malfunctions that could arise from component environmental testing disallowed bonding.

Certain components had to be individually analyzed to ensure good conductive coupling with the cool baseplate to preclude the development of hot spots. For example, the voltage regulator could dissipate up to 10 watts of power in two power transistors. Therefore, for this unit a special thermal path had to be designed to couple the power transistors to the baseplate. The vidicon cameras do not operate efficiently above 40°C; therefore, they were decoupled radiatively from the vehicle top by using an iridite finish on their exterior surfaces. This finish has a reflectivity of 0.85 (to infrared energy) which forces the vidicons to become more closely conductively coupled to the cool temperature of the baseplate.

(2) Top and Sides

Solar cells cover 70 percent of the top and 60 percent of the sides of TIROS I. Uncoated silicon solar cells have an unfortunate α/ϵ ratio of approximately 3:1 ($\alpha = 0.90$, $\epsilon = 0.30$). This α/ϵ ratio would tend to cause the cells to run at too high a temperature for efficient conversion of solar power to electrical power. The solar cells, therefore, had to be coated with a material that would lower its α/ϵ ratio, protect the cells from the other environmental factors, and guarantee high transmissivity in the spectral region of high solar cell activity. Plastic materials were considered

for the coatings. From a thermal standpoint, many plastics possess large numbers of absorption bands in the intermediate infrared spectrum, and high transmissivity in the visible spectral region. They would be ideal as coatings for the thermal protection of silicon solar cells. Their susceptibility, however, to rapid outgassing and depolymerization at the reduced pressures and intense high energy radiation at orbit altitudes, are undesirable factors which precluded their use in TIROS I.

The silicates, in general, possess high visual transparency and a wide absorption band in the neighborhood of 9.0 microns. An investigation of the practicality of coating solar cells with a controlled evaporation of SiO-SiO_2 in conjunction with interference films to reject those portions of the solar spectrum not utilized by the solar cells was undertaken by the Bausch & Lomb Optical Company. The results have proved to be highly satisfactory.

For the first TIROS satellite model, lead development time required that an alternative solar-cell coating technique be used (see Appendix I); thin glass plates cemented to the individual solar cells were used. A 15-layer interference film which rejects the blue portion of the solar spectrum is superposed on the glass cover. Radiation tests with dosages of 8×10^5 Roentgens of Co_{60} (1.1, 1.3 mev) and 1×10^6 Roentgens of X-rays (40 to 250 kev) produced negligible deterioration. The dosages correspond to an anticipated cumulative dosage of 1 year for TIROS I. Figure 131 shows the effectiveness of the coatings in increasing the ϵ of the solar-cell coating composite in contrast to that of the uncovered cell.

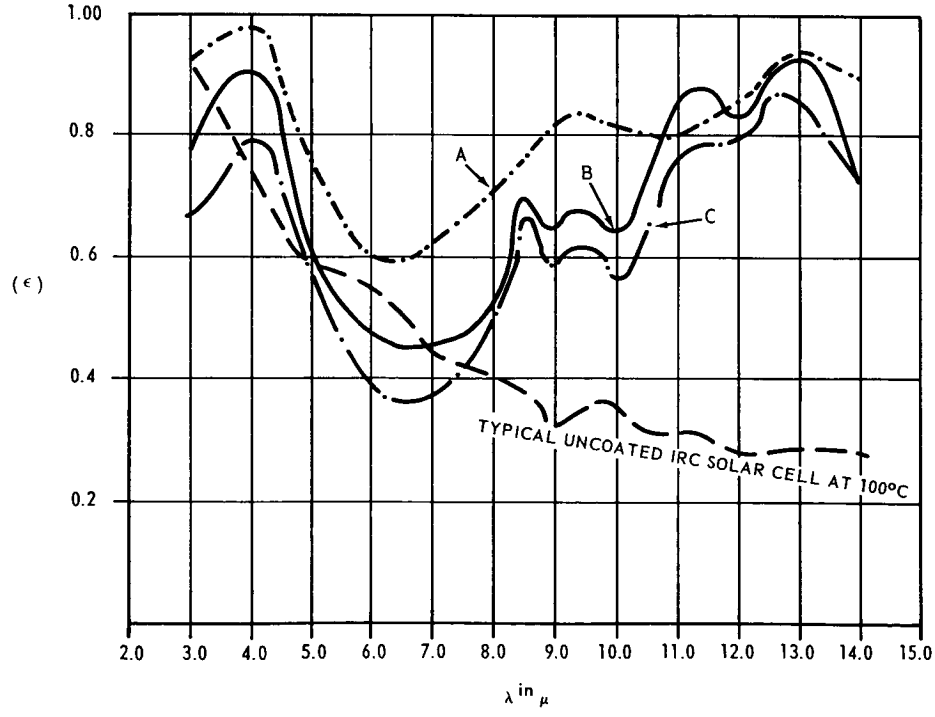

Figure 131. Effect of Coating upon the Effective Emissivity of Solar Cells

Since the top of the vehicle is a round area and the solar cell modules are rectangular in shape, the cells would not cover all of the satellite's top surface. The uncovered areas were coated with "rokide", a low α/ϵ material. This had the effect of lowering the gross value of α/ϵ of the total top surface, thus lowering the top temperature.

d. Experimental Verification of Thermal Design

To verify the results of the analytical results, a thermal vacuum test was conducted at the Signal Corps vacuum chamber at the Evans area of Fort Monmouth. This test was designed to simulate as closely as possible a real orbital condition. The orbital condition chosen for this test was the 100 per cent sun orbit with the angle α (between the sun vector and the satellite spin axis) equal to zero, and the angle θ (between the sun vector and the normal to the plane of the orbit) also equal to zero. The vacuum during the test varied from 2×10^{-5} to 5×10^{-5} mm of Hg. Specifically, this test was conducted to give experimental values of the radiation coupling factors which were to be used in the thermal energy equations. The resulting temperatures, based on these values, for the top, sides, and bottom then could be compared to those of the analytical program.

During the chosen orbit, direct solar energy is incident only on the top surface of the satellite. This input was simulated during the test by a heating plate which radiated only to the top of the satellite. The face of this heater was painted black to minimize multiple reflections. Furthermore, the heater was spaced about 6 inches from the top surface of the satellite with a reflecting shroud around the peripheral area between the heater and satellite to minimize edge effects.

The temperature of the heater was brought to 278°F, which gave a radiant heat input to the vehicle top of

$$Q = \sigma \epsilon \phi_{H-T} T_H^4$$

where:

σ = 0.174×10^{-8}, Stefan-Boltzmann constant

ϵ = 0.9, emittance of the heater

ϕ_{H-T} = 0.9, shape factor from heater to top of vehicle

T_H = 728, average temperature of heater in degrees Rankin

Q = $(0.174)\ (0.9)\ (738)^4 \times 10^{-8}$

= 418 Btu/hr-ft^2

= 123 watts/ft^2

This heat energy input is approximately the solar constant.

During this orbit, the spinning side surface and the bottom of the vehicle will see both the earth and outer space. In the chosen orbit, the albedo input to the vehicle is essentially zero while the earthshine is appreciable. By averaging the inputs for the sides and bottom, they could be approximately simulated by cooling the vacuum chamber walls to -128°F. Although the heater temperature was held at the proper value of 278°F, the walls could not be cooled below an average value of -78°F due to the large heating load in the chamber. The temperatures were then allowed to go to steady state and were then recorded by 22 thermo couples located throughout the satellite.

The analytically-determined component temperature for the simulated orbit, shown in Figure 127 was 21°C, while the experimentally-determined component temperature was 18°C. These close results give a high degree of confidence to the entire analytical program.

By using the outside surface temperatures of the tops and sides, the following coupling factors were calculated:

Coupling factors between top and sides: $K_{TS} = 2.7$

Coupling factors between top and components: $K_{TC} = 2.0$

Coupling factors between sides and components: $K_{SC} = 4.5$

These new coupling factor values were used in the general equations. The results indicated that component temperatures were not changed at all, the top was slightly lower in temperature and the sides were slightly higher.

Since the electronic system was designed to operate between 0 and 50°C, it was required to test the system between these limits. This was the isothermal test where the satellite was placed in a vacuum chamber at 5×10^{-5} mm of Hg and held for 7 days at 20°C, 7 days at 0°C and 7 days at 50°C. During this time, the electronics system was operated successfully through its normal orbital duty cycle.

e. Actual Determination of Satellite Temperature

Thermal analysis sets the requirements for the surface radiative characteristics; measurements determine how closely these have been met by surface coating developments. Thermal tests evaluate the soundness of the entire program. Verification of the design effectiveness, however, could be obtained only from the telemetered temperature data from TIROS I in orbit. Eight thermistors in two completely redundant systems were situated at various locations in the TIROS I satellite to provide adequate information on the temperature distributions. Telemetered temperature data indicated excellent agreement with the predicted time-temperature distributions for the several surfaces and interior components.

10. Integration of Satellite Components

a. Subsystem Integration Problems

Integration of the TIROS I subsystems was started on the original electrical prototype satellite, T-1, in conjunction with the prototype (Princeton) ground station. As soon as the more advanced prototype, T-2, was available, it was substituted for the T-1, and was utilized for the remaining part of the integration, test, and evaluation program. Satellite T-1 was the original electrical prototype. It was used only during the study of the original mechanical layout and electrical integration problems. A typical series of problems encountered included system logic errors, grounding problems, inadequate filtering and decoupling, and incompatibility of units. Several units required changes as a result of the investigation. Handling techniques and test procedures were developed as a result of the test made on this model. (This model was later rebuilt as a complete prototype and designated model T-1A.) The advanced prototype, T-2, showed several of the same type of problems encountered in T-1 because of minor harness and grounding changes. Subtle logic errors continued to be located, but before the flight models were completed, a foolproof logic system had been developed. The T-2 satellite was primarily used as a test prototype for the environmental tests required for the program. The results of this were excellent, since there was not a serious failure on any flight model during their tests that could be attributed to design problems.

b. Mechanical Integration

A review of the components to be assembled showed the satellite to be a two-system payload with two of each of the major components. This indicated that a symmetrical type of arrangement was possible.

A layout of the baseplate pattern was made on a stable glass cloth and the components then laid out on this pattern, attempting at all times to locate units so that at least two or more of the mounting bolts would be through rib flanges. The glass cloth was then used as a layout template to maintain interchangeability.

Since the batteries are the major component containing magnetic material, they were mounted symmetrically around the spin axis, as close to the center as possible. This arrangement places nine packs of seven cells each in a two level package having a 1-1/2-inch axial clearance hole through the center. This hole is necessary to permit insertion and removal of a 1-inch shaft for handling and balancing of the satellite. Since the batteries are heavy (40 lbs. per set) and are heat producing, they were mounted directly to the baseplate for structural integrity and the shortest possible thermal path to the cold baseplate.

The position of both cameras is dictated by the structure design since each of these units mounts over a cutout in the baseplate. Both cameras were shim mounted to provide parallelism with the spin axis within 2 minutes angular displacement.

The units requiring the most space are the two tape recorders which are contained in sealed pressure vessels in the shape of a hemisphere 13 inches in diameter. These units were then positioned and the clocks which are also pressurized, but in domed cylinders, were positioned next.

All other components were located generally in such a position that the shortest possible wiring harness would be required. This harness was pre-fabricated on a wiring board and positioned on the baseplate after a few of the basic units had been bolted in position. The harness was secured at intervals generally not exceeding 5 inches and also at critical points of sharp change in direction, by the use of nylon cable clamps. Wherever the harness entered or attached to a component, it was anchored either by clamping or by the use of an epoxy adhesive.

Preliminary tests had indicated the need for special mounting procedures for various components. Some were isolated electrically from the baseplate by the use of mylar sheet and special flanged bushings of epoxy impregnated fiberglass, others required special grounding by means of removing the black anodized finish to reduce the resistance to a minimum value.

The hardware used throughout the assembly is stainless steel, non-magnetic socket head type screws, and either standard all metal lock nuts or anchor nuts of the same material. The washers are of aluminum.

Since many of the components are higher than either one or both of their base dimensions, vibration was a serious consideration. This problem was overcome by the use of lightly stiffened sheet metal brackets used to tie together the upper ends of all critical units. These brackets served primarily as dampers or ties to join units of differing resonant frequencies together and thus caused them mutually to act as dampers for each other.

The cover assembly carries only three sets of components other than the solar cells which were described in a separate section of this manual. The precession dampers were mounted diametrically opposite to eath other and were fastened at the upper and lower extremities of the cover.

The Yo-Yo or despin devices were also mounted opposite to each other and were located at the bottom of the cover side panels, the only external area of the cover not covered with solar cells. The nine sun-angle sensors were mounted in the modified T-posts.

This general arrangement provided an assembly which was dynamically balanced about its own spin or mechanical axes within 4 per cent of the total weight of 263.25 pounds.

B. GROUND STATION COMPONENTS

B. GROUND STATION COMPONENTS

1. Introduction

Ground operations for the TIROS I Satellite consisted, in general, of: (1) tracking the satellite's position; (2) commanding the satellite's instrumentation to perform specific functions in a given order; and (3) receiving, storing, and processing data received from the satellite. These operations were performed and coordinated by a ground complex (diagrammed in Figure 132) including* two primary Command and Data Acquisition (CDA) stations, located at Kaena Point, Hawaii and Fort Monmouth, New Jersey, respectively; a secondary CDA station located at the RCA Space Center, near Princeton, New Jersey; and selected stations of the NASA Minitrack Network. The satellite pre-launch checkout equipment was converted (immediately after launch) to a CDA station of somewhat limited capability. It remained at the launch site in a ready status for only a short time; and then was returned to RCA for modification for a future satellite project.

---

* The ground complex included other facilities involved in the satellite command program and data processing. However, those mentioned here were those in direct communication with the satellite.

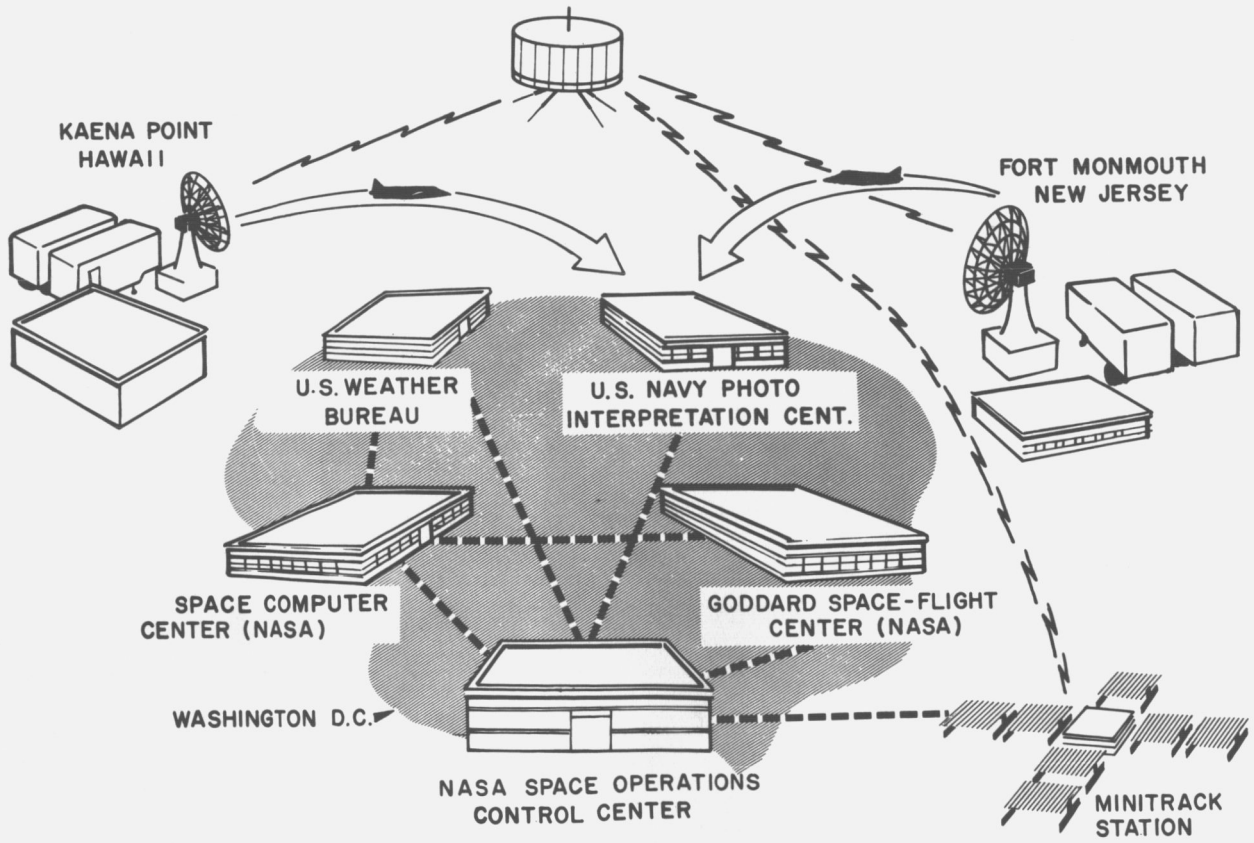

Figure 132. TIROS I Ground Complex, Functional Diagram

Functionally, each CDA station was divided into four basic sections; namely, the satellite command and control equipment, the data receiving components, the data processing and display components, and the recording devices. Figure 133 is a simplified block diagram of the ground station equipment. The functions of the primary ground stations were as follows:

a. To transmit radio signals to the satellite for programming its operation and data transmission.

b. To receive signals carrying the television, attitude, and telemetry data from the satellite.

c. To extract the television, attitude, and telemetry data from the carrier signals.

d. To record the received data and to provide a means of identifying that data.

e. To relay the recorded attitude and telemetry data, along with station status reports, to the NASA TIROS Technical Control Center in Washington, D.C.

The secondary CDA station at Princeton, was equipped with the same functional systems as each primary CDA station, but was equipped with an experimental tracking antenna, which is described in another part of this report. The Princeton station monitored the satellite response to commands from Fort Monmouth and was directed to go "on the air" for back-up command and recording several times during TIROS I operations.

The Cape Canaveral (converted Go, No-Go) station was intended to provide extended coverage of the area in which pictures could be taken by the satellite and returned directly to the ground, if thought desirable. An original concept in providing this back-up station was to establish an alternate station in the event of a failure at Fort Monmouth.

2. Functional Description

The command and control equipment controlled the satellite functions by means of an amplitude-modulated command transmitter. Nine audio control tones, each representing a different command function, were used for modulating the command transmitter. Three modes of operation were provided for commanding the satellite; they were: manual-operate, manual-start, and automatic. In manual-operate, which was used only during test, all satellite commands were initiated manually. During manual-start operation, only the program sequences were started manually; once the sequence started, the commands within the sequence were initiated automatically. In automatic operation, the initiation of all sequences and commands within a sequence were transmitted without manual intervention.

The TV picture (and sun-angle data) receiving circuit consisted of two receivers, connected in polarization diversity to minimize signal fading due to satellite spin and attitude. The telemetry receiving circuits consisted of four receivers, each pair of which were connected in polarization diversity. Two of the receivers were tuned to the upper telemetry frequency, and two were tuned to the lower telemetry frequency. The telemetry information was recorded on two-channel Sanborn Recorders.

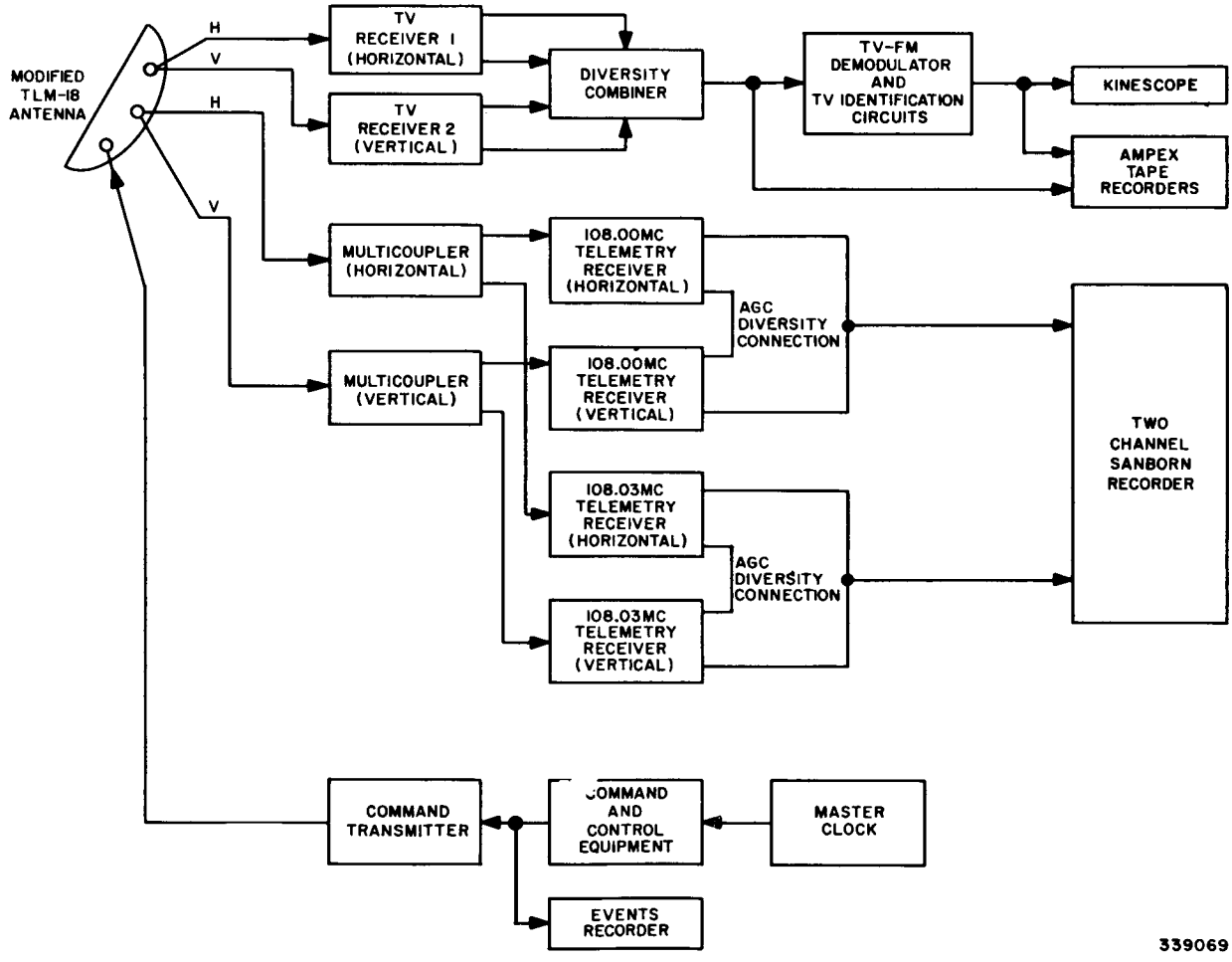

Figure 133. Primary Ground Station Components, Simplified Block Diagram

Each TV picture received was displayed on a kinescope, mounted in the display unit. A panel, framing the kinescope, was equipped with legends and numbers that were illuminated to indicate, for each TV picture, the mode (direct camera or tape playback), camera source (1 or 2), frame number, sun angle, and orbit number. The mode and camera source information was derived from outputs of the command and control equipment. The frame number was generated by a binary counter, which was stepped by the vertical sync pulse of each TV picture received. The frame number, consisting of six binary bits, and the mode and camera source data, consisting of three binary bits, were stored in a shift register from which a serial output and a parallel set of outputs were taken. The parallel output controlled read-out lamps which were photographed along with the kinescope display; the serial output keyed oscillators to record the camera source and frame information on magnetic tape. A parallel set of outputs comprising the binary-coded sun-angle data from the sun-angle computer were recorded on another channel of the magnetic tape. The orbit number was displayed by means of manually-set, illuminated dials. A camera, mounted on the display units, was used to photograph each picture displayed on the kinescope and the associated illuminated identification data.

The recording devices used at the primary TIROS I ground stations were two Ampex Model FR104 tape recorders and an Esterline-Angus Model AW events recorder. The events recorder provided a real-time recording of the initiation of the various satellite commands and of other vital ground system operations. The tape recorders recorded the TV pictures received from the satellite and the related identification information. Each recorder, which used one-half inch wide tape at a running speed of 60 inches per second, was capable of four-channel operation. The tape recorders were remotely controlled by the command and control equipment to start automatically at the beginning of each ground-to-satellite contact.

3. Physical Configuration

At the time of ground station fabrication, it was not known whether one or both CDA stations would be mounted in vans. Accordingly, both stations were designed for van mounting. Eventually, the station at Kaena Point used van-mounted equipment; the system delivered to Fort Monmouth was installed in a building.

Among the several factors considered before a final physical configuration was selected, were ease of maintenance and ease of cooling. Two conventional methods of mounting—bathtub and horizontal chassis with front panels—were investigated but rejected because they proved to be wasteful of space and hard to cool, and did not lend themselves to the front-only accessibility which was required in the vans. A third method, in which two vertical chassis were mounted perpendicular to the front panel, was selected. The vertical chassis were arranged so that the tubes faced inward and the wiring faced outward. The overall assemblies were mounted on roll-out slides. This combination of chassis arrangement and roll-out slides facilitated maintenance and trouble-shooting. The vertical mounting of the chassis provided a chimney effect which assisted materially in cooling.

The roll-out assemblies, to be compatible with van mounting, were mounted in vertical racks which had an overall height of 65-3/8 inches. The components which comprised each ground station were mounted in 16 of these vertical racks. The location of the components within the racks is shown in Figure 134.§

The TIROS I ground equipment for Kaena Point was mounted in the same Government-furnished V-51 vans that had been used for the Signal Corps SCORE project. Each van was equipped with a three-ton air conditioning system, a 60,000 BTU gasoline heater, and a 208-volt, 60-cps, 3-phase, 4-wire power system. The same distribution ducts were used for both the air conditioning and heating systems. Certain modifications and additions had to be made to the power system in order to ready the vans for TIROS use. A detailed description of the vans and the equipment layout within the vans is included in another section of this report.

4. The Satellite Command and Control Equipment

a. General

The satellite command and control equipment provided a reliable means for turning on the command transmitter, programming the antenna to follow the predicted path of the satellite, turning on the TV and data recorders, initiating the transmission of control tones to the satellite, and turning off the equipment at the end of a satellite-to-ground contact.

Design and development of the TIROS command and control equipment was facilitated by the experience gained during development of the JUNO satellite command system which was started in March 1958. Initially, several types of command systems, developed at the breadboard level, were abandoned because their design could not be modified to meet changes in JUNO requirements. During June and July of 1958, RCA successfully developed a command system which not only met the requirements of that date, but also seemed flexible enough to accommodate any future changes in requirements.

When the responsibility for the satellite system was transferred from ARPA to NASA, the JUNO satellite project became the TIROS project. At the start of project TIROS, it was hoped that the JUNO command system would be suitable for use in TIROS. However, as the nature of the TIROS project became better known, it became apparent that the variable programming requirements would prohibit the use of the JUNO system.

Accordingly, that system was abandoned and RCA began studies to determine what type of command and control system would best meet the requirements of TIROS.

Because of the weight and size limitations of the satellite, it was anticipated that the major design problems would be encountered during development of the satellite components of the command and control system. Therefore, initial design efforts on

---

§ This illustration is printed on a fold-out page located at rear of this volume.

the ground station components were postponed pending further information on design of satellite components. As soon as the basic approaches to the satellite design were established, and the requirements for the ground system were known, design studies for the command and control equipment were begun.

As part of the initial studies, RCA evaluated commercially available equipments to determine their adaptability to the TIROS I system, and a design for the ground station components of the command and control equipment was gradually formulated. The design of these components was based on already proven techniques. Complete commercially available equipments were used wherever possible. Duplication of design in certain equipments was used to provide even greater ground station reliability.

Construction of a prototype model of the ground station command and control equipment began in January 1959 and was completed in May 1959. On June 5 of that year the prototype equipment was moved to the Princeton Ground Station where it was used for testing the satellite equipments.

The ground station components of the satellite command and control equipment were contained in three racks. Racks 1 and 3 (Figure 135) were identical; each contained a full set of programming equipment. Rack 2 (Figure 136) contained the timing equipment, program selector, and power control switches and relays.

b. Functional Operation

Figure 137 is a functional block diagram of the TIROS I command and control equipment. Functionally, the equipment consisted of two separate programming circuits, one program selector, and one timing circuit. The timing circuit, consisting of the master clock, the WWV receiver, and the frequency standard, was common to both programming circuits. The program selector provided selection of the outputs of either of the two programming circuits.

The ground station components of the satellite command and control equipment provided for the selection of three types of programs: automatic, manual-start, and manual-operate. Briefly, the system operation for these three types of programs was as follows:

1. Automatic. During automatic operation the program was setup in advance on the control equipment. Each program sequence was started in response to an alarm signal from the master clock and proceeded to its conclusion without the aid of an operator.
2. Manual-Start. Durting manual-start operation, the program was also set up in advance. The only difference between manual-start and automatic was that pushbutton controls were used in place of the master clock for initiating the alarm signals.

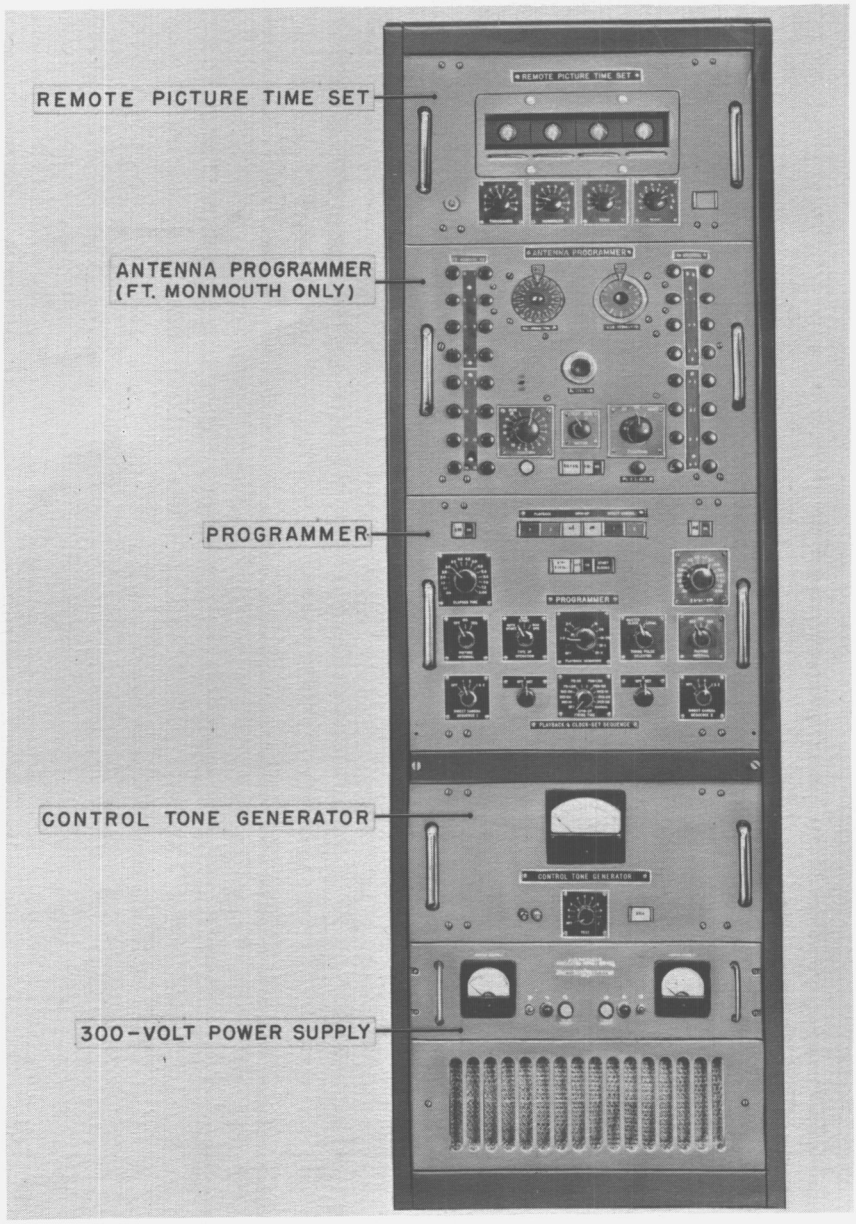

Figure 135. Sqtellite Command and Control Equipment, Racks 1 and 3

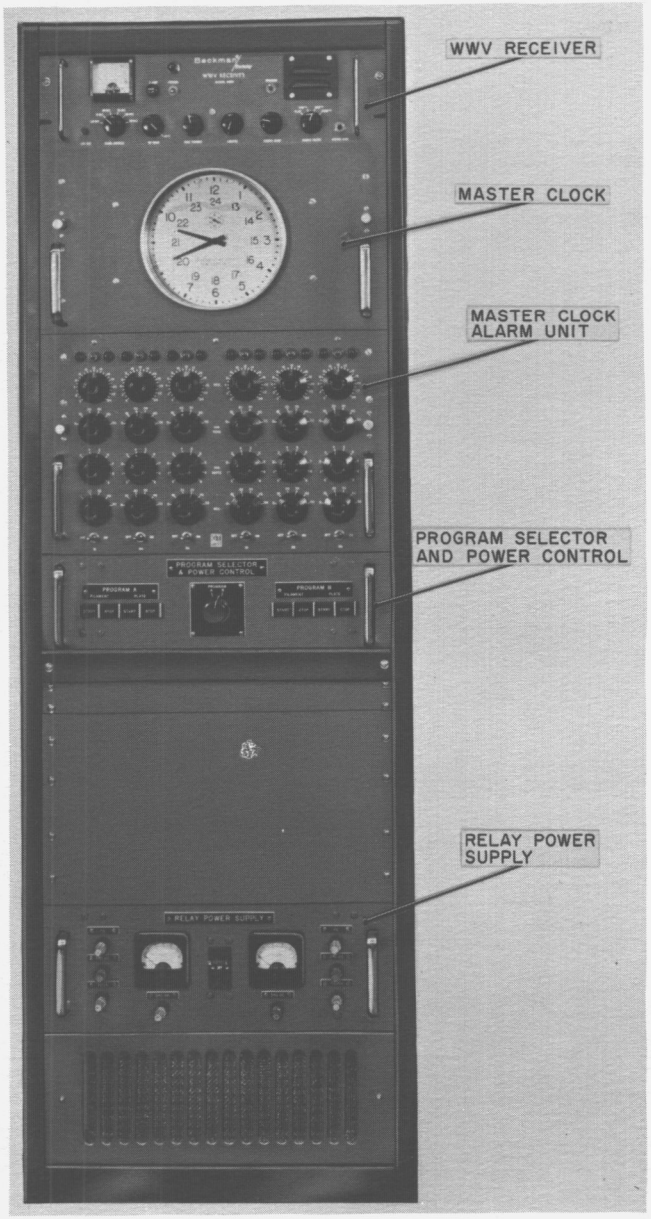

Figure 136. Satellite Command and Control Equipment, Rack 2

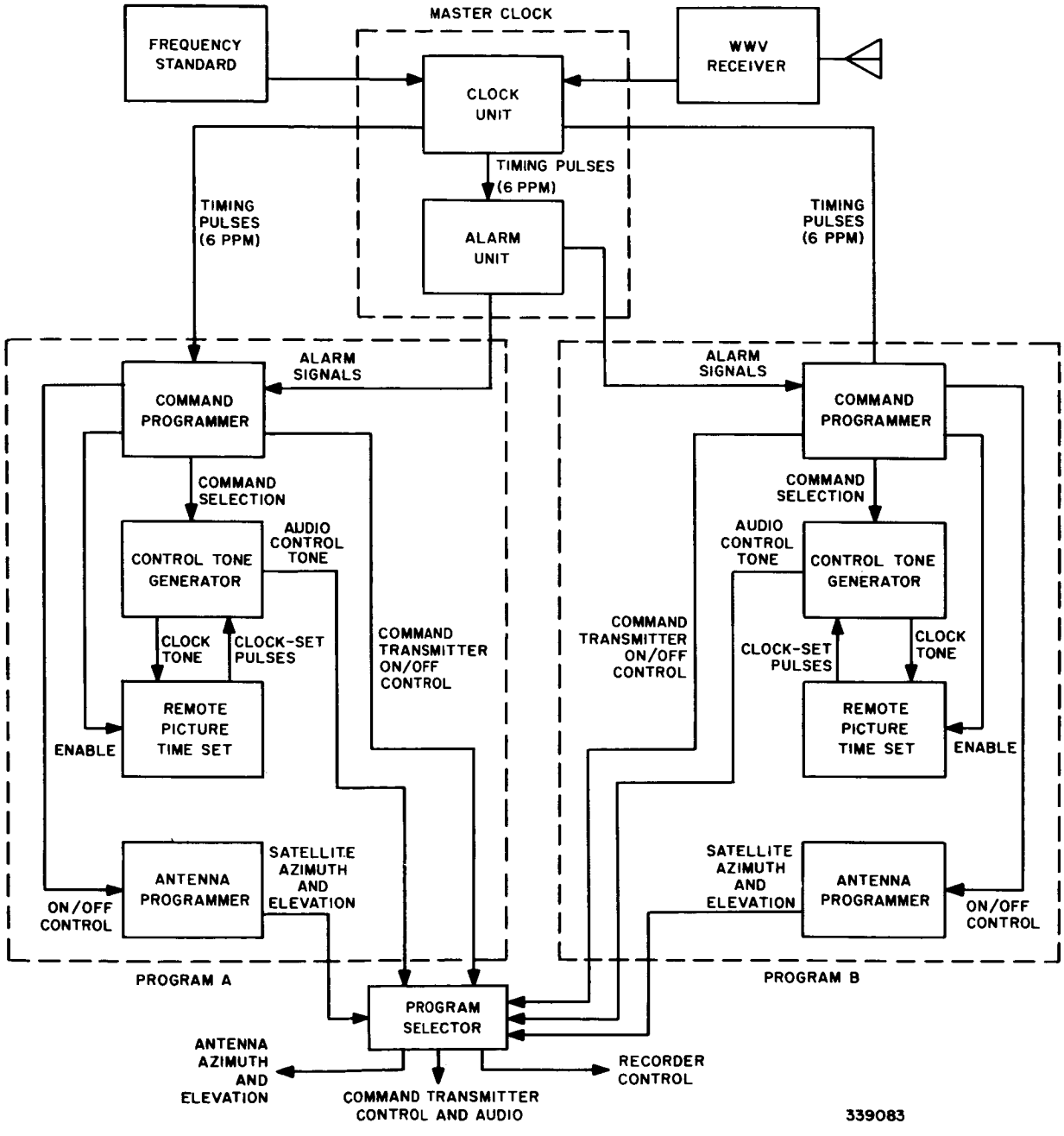

Figure 137. Satellite Command and Control Equipment, Block Diagram

3. Manual-Operate. During manual-operate, a presetup program was not used. Instead, the program sequences were initiated by means of push-buttons which were also used to carry each sequence through to completion.

The two separate programming circuits permitted two complete programs to be setup in advance. These programs could be setup for consecutive orbits or could be setup to provide alternate programs for the same orbit. The program sequences used in TIROS I and the alarms which controlled these sequences are as follows:

1. Direct Camera Sequence I.- Direct camera sequence I was controlled by alarm number 1. This program sequence was used when the TV pictures were to be taken while the satellite was in range of a ground station. When the satellite was in the direct camera sequence, the pictures were transmitted directly to ground, bypassing the satellite's tape recorders. Either one of the satellite cameras could be commanded to take pictures at either a 10-second or a 30-second interval. Picture taking commands could be alternated from one camera to the other at an interval of 30 seconds. The length of the sequence could be varied between 0.5 minute and 8.0 minutes.
2. Playback and Clock Set Sequence. -The playback and clock set sequence, initiated by alarm number 2, commanded the satellite to read-out pictures which had been recorded on the satellite's tape recorders since the last ground-to-satellite contact. Also during this sequence, set pulses were sent to the vehicle clocks and, at the conclusion of the set pulses, a start pulse (alarm number 3) was sent to the clocks.
3. Direct Camera Sequence II.- Whenever this sequence was programmed, it followed directly after the playback sequence. The same variations of program were provided as in direct camera sequence I.

In addition to the functions listed for each sequence, any one of the program sequences could also include the sending of a "fire spin-up rockets" command. A control tone could be automatically transmitted at the time preselected on the spin-up control, or the command tone could be transmitted in response to the operation of a manual control switch.

c. Master Clock

(1) General

The master clock generated the alarm signals required for initiating the various sequences of a program during automatic operation. Responsibility for the design of the master clock was subcontracted to the General Time Corporation.

The master clock consisted of two separate units: a clock unit and an alarm unit. (See Figure 138.) The clock unit, a spring-reserve type electric clock, normally operated on 115-volt, 60-cps line voltage. In the event of power failure or a temporary interruption in the line voltage, the clock could run on the spring-reserve energy. The spring stored enough energy to run the clock for 72 hours.

The alarm unit contained six independent alarm circuits which could be set manually (in hours, minutes, and tens-of-seconds) to provide an alarm delay of up to 24 hours. Each alarm circuit contained stepping switches which were driven by the short d-c pulses which were generated by the clock unit at 10-second intervals. When the stepping switches of an alarm circuit reached the positions corresponding to the preset alarm time, a set of contacts closed and an alarm was sent to initiate the associated programming sequence.

(2) Functional Description

Figure 139 is a block diagram of the master clock. The input to the clock motor is normally 60-cps, a-c power from a tuning-fork controlled frequency standard; however, in cases of power failure the clock will run on spring reserve energy. The 60-cps input can be interrupted to permit setting of the clock by the WWV time standard.

The pulse cam is ganged to the clock motor and operates a microswitch, causing the switch to close six times per minute. Each time the switch closes, a d-c pulse is sent to the stepping switches in the alarm unit and causes the switches to advance one position. When the stepping switches advance to the positions which correspond to the time set on the front panel time set dials, the d-c input to the dials is applied through the stepping switches to the associated programmer where it initiates the related program sequences.

The schematic of the master clock is shown in Figure 140[§]. Detailed circuit description of the clock is included in Instruction and Operating Handbook TIROS I Meterological Satellite System. (Reference 20)

d. Control Tone Generator

The discussion of the control tone generator involves classified information and is included, therefore, in the classified supplement to this Report.

e. Remote Picture Time Set

The discussion of the remote picture time set involves classified information and is included, therefore, in the classified supplement to this Report.

f. Antenna Programmer

(1) General

The antenna programmer (Figure 141) was used only in the CDA station at Fort Monmouth, New Jersey and in the CDA station at Princeton, New Jersey. (The antenna at Kaena Point, Hawaii was programmed by existing facilities.) The programmer controlled the tracking antenna in azimuth and elevation along the path of the satellite. Making use of orbit predictions eliminated the need for horizon scanning at the beginning of each pass, thus effecting faster antenna lock-on. Fast lock-on insured receipt of a minimum amount of data when satellite-to-ground contact time was short.

The predicted accuracy for the satellite-position data input to the antenna programmer was about 2 degrees. Since the beam width of the tracking antenna was approximately 8 degrees, it was decided that the programmer accuracy should be ±2

[§] This illustration is printed on a fold-out page located at rear of this volume.

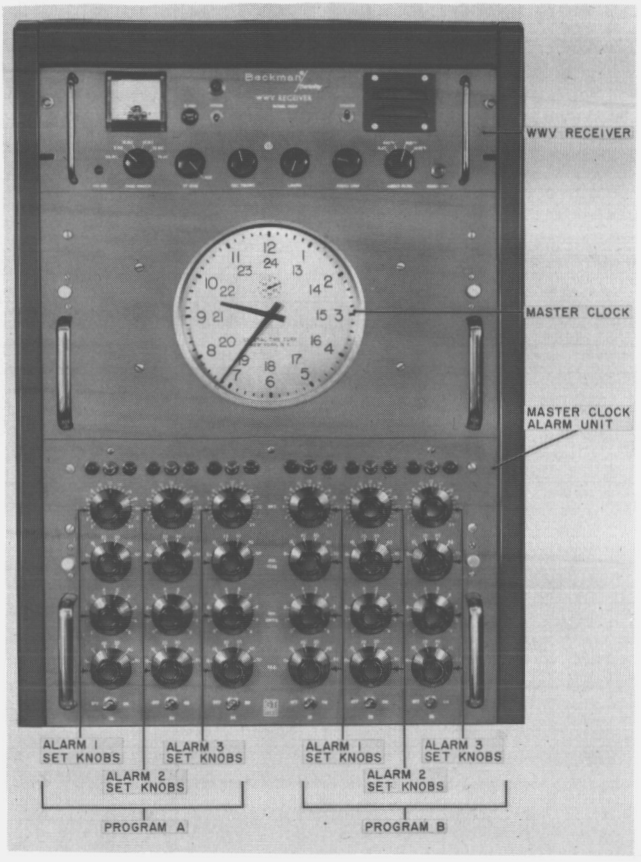

Figure 138. Master Clock and WWV Receiver, Front View

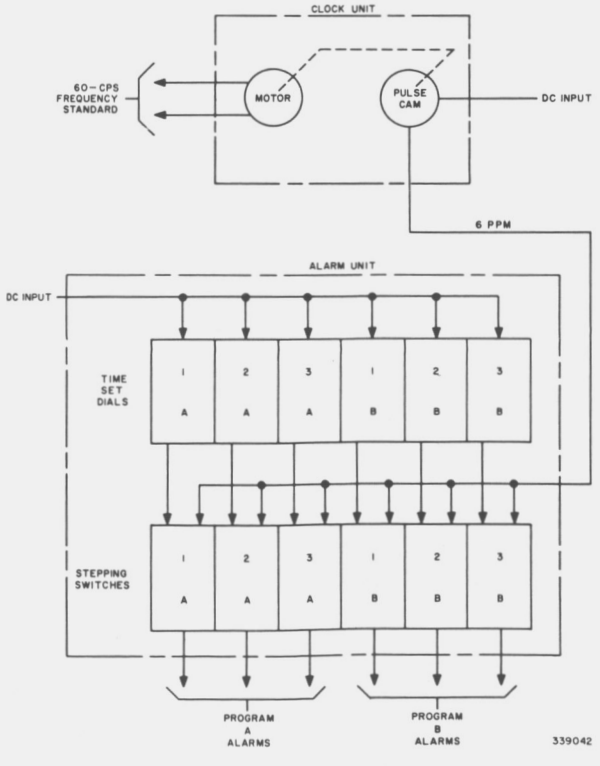

Figure 139. Master Clock, Block Diagram

degrees. Computations indicated that if accurate satellite position data could be obtained at one minute intervals, the maximum deviation between the actual satellite path and the chord of this path would be much less than 2 degrees except for positions within a circle subtending a few degrees directly overhead. Since very few passes were expected to enter this circle, and since the need for the programming function (i.e., loss of tracking signal) was expected to be at a minimum for this position, RCA concluded that linear interpolation of the satellite-position data would meet the accuracy requirements for the programmer.

Accordingly, the programmer was designed around a function generator which consisted of a two-gang, 15-turn precision potentiometer. The potentiometer was provided with a tap at each turn. One gang of the potentiometer produced azimuth information while the other provided elevation information. By rotating this device at one rpm, and by applying accurate position information to each tap, a fifteen-minute program with linear interpolation between minutes was obtained.

Two synchros, positioned by two servos which followed the function generator voltages, produced the azimuth and elevation drive signals for the antenna. Operating the entire servo system on 60-cycle a-c eliminated the difficulties due to amplifier and voltage drifts associated with d-c servos. Tachometer feedback provided sufficient stability to the loops without the addition of compensating networks which would necessitate d-c operation or conversion.

The design of the antenna programmer was chosen, not because it was considered the ultimate or most desirable means for accomplishing the function; but rather, because it was considered to be the simplest way, and perhaps the only way, in which this essential requirement could be met within the scheduled time for development of the equipment.

(2) Functional Description

Figure 142 is a block diagram of the antenna programmer. The antenna programmer consists of a two-gang program potentiometer, two similar servo circuits, and 32 control potentiometers for setting in azimuth and elevation information. The position of the two-gang potentiometer is controlled by a constant speed, 1-rpm motor. The 32 control potentiometers, 16 for azimuth and 16 for elevation, are manually set to the azimuth and elevation information which is received from the NASA Space Operations Control Center.

When the azimuth information is being set in, the function switch is set to "azimuth" and the preset control and preset amplifier are connected into the circuit. Prior to setting the azimuth information into each of the 16 potentiometers, the preset pushbutton is depressed and the information for each succeeding channel is set in by use of the preset control. That is, before setting channel (potentiometer) O, the preset pushbutton must be depressed and the preset control adjusted until the azimuth indicator reads the value to be set into channel 1. Similarly, after channel O has been set, but before channel 1 is set, the preset control must be readjusted so that the azimuth indicator reads the value to be set into channel 2. Use of this

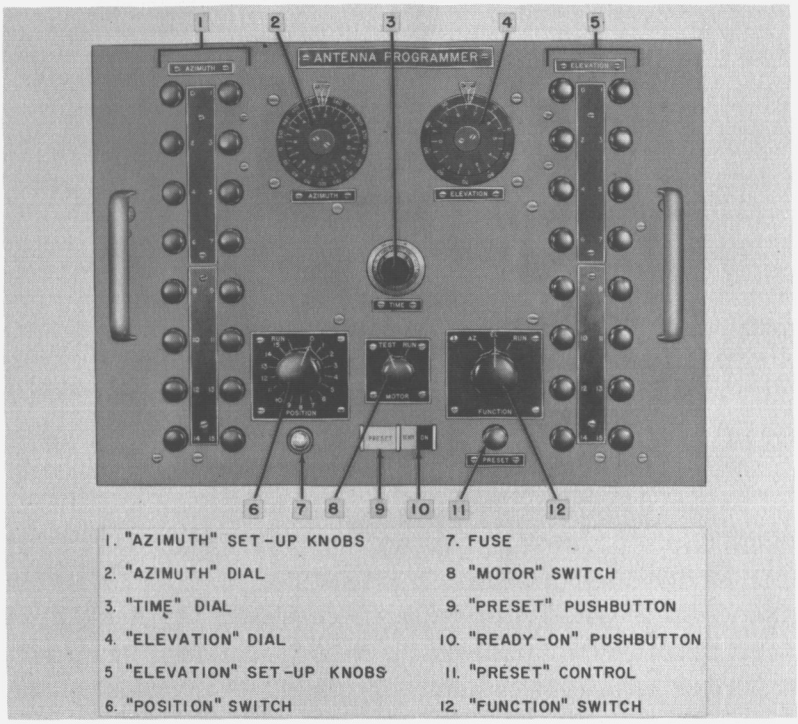

Figure 141. Programmer, Front View

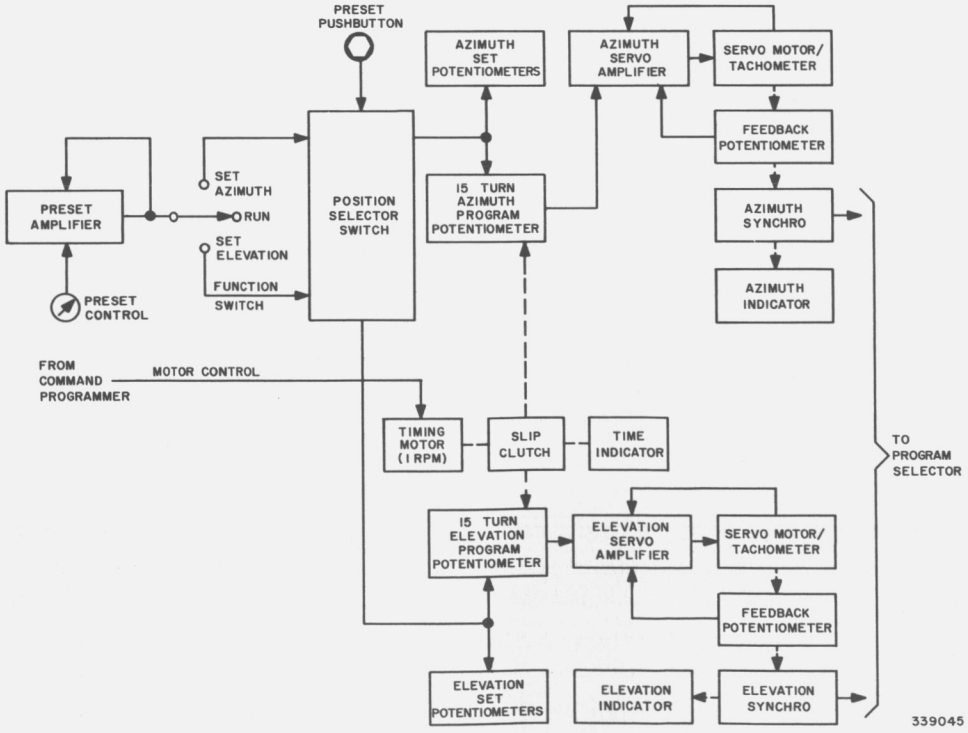

Figure 142. Antenna Programmer, Block Diagram

technique reduces the interreaction of successive channels and thus permits the azimuth information to be set in accurately without several readjustments.

The same technique is used for setting in the elevation information. Once the available azimuth and elevation information has been set in, the function switch is set to run and the preset circuit is disconnected. Operating voltage from the control programmer drives the 1-rpm timing motor. The motor is ganged, through a slip clutch, to the two-gang program potentiometer. One gang of the potentiometer is in the azimuth channel, the other gang is in the elevation channel.

The two-gang potentiometer, driven at a 1 rpm constant rate, produces azimuth and elevation outputs that are linear interpolations of the position voltages between any two of the 16 azimuth or 16 elevation inputs. These voltage outputs drive servo systems whose outputs are connected to the antenna through relays energized by the program selector.

As mentioned in the general discussion, the linear output does not acutally provide precise satellite path information. However, because of the antenna beam-width, this information is accurate enough to permit reliable pick-up of the satellite.

Velocity feedback from the azimuth and elevation tachometers to the associated servo amplifiers stabilizes servo operation. Position feedback from the feedback potentiometers to the servo amplifiers keeps the servos in sync with the position-voltage outputs of the two-gang program potentiometers.

The schematic diagram of the antenna programmer is shown in Figure 143§. Circuit analysis of the antenna programmer is contained in the "Instruction and Operating Handbook TIROS I Meterological Satellite System."

g. Program Selector and Power Control Unit

The program Selector and power control unit (Figure 144) provided selection of either Program A or Program B for transmission to the satellite. In addition, the unit contains switching circuits for controlling filament and plate voltages to the two programmer circuits. Figure 145 is the schematic diagram of the program selector and power control unit.

h. Relay Power Supply

(1) General

The relay power supply (Figure 146) generated the 24 volts required for energizing the relays in the ground station command and control equipment and provided for distribution of 115-volt, 60-cps, a-c to these same components. The power supply is fused to provide protection for the load circuits. Design and development of the relay power supply was based on the use of standard circuits.

§ This illustration is printed on a fold-out page located at rear of this volume.

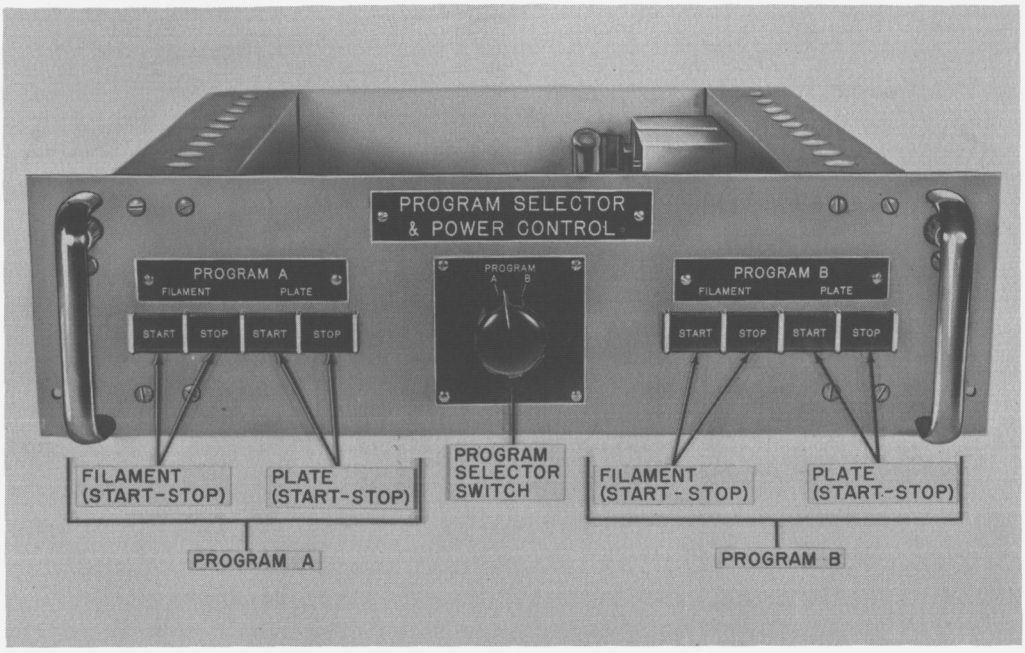

Figure 144. Program Selector and Power Control Unit, Front View

(2) Functional Description

Figure 147 is a block diagram of the relay power supply. The relay power supply receives 115-volt, 60-cps, a-c power from an external source. This a-c power is applied through fused lines to the d-c supply circuit and to various components of the command and control equipment.

The d-c supply circuit is fed by power transformer T401. The a-c output of the transformer is full-wave bridge rectified and filtered. The resultant d-c is applied through the normal position of switch S401 and through ammeter M401 to the using components in racks 1, 2 and 3. As in the case of the a-c voltage, the load lines are fused for protection purposes. A voltmeter is provided for monitoring the output voltage level. Two relay power supplies are included in the ground equipment. Each can, under emergency conditions, handle the total load. Switch S104 can be set to "spare" which transfers the load to the output of the remaining power supply. The schematic diagram of the relay power supply is shown in Figure 148.

i. Command Transmitter and Transmitter Control Panel

Collins Model 242F-2, 200-watt, amplitude-modulated, VHF transmitters were used as the command transmitters. Two of these transmitters were located at each ground station; only one of the two transmitters could be used at any given time.

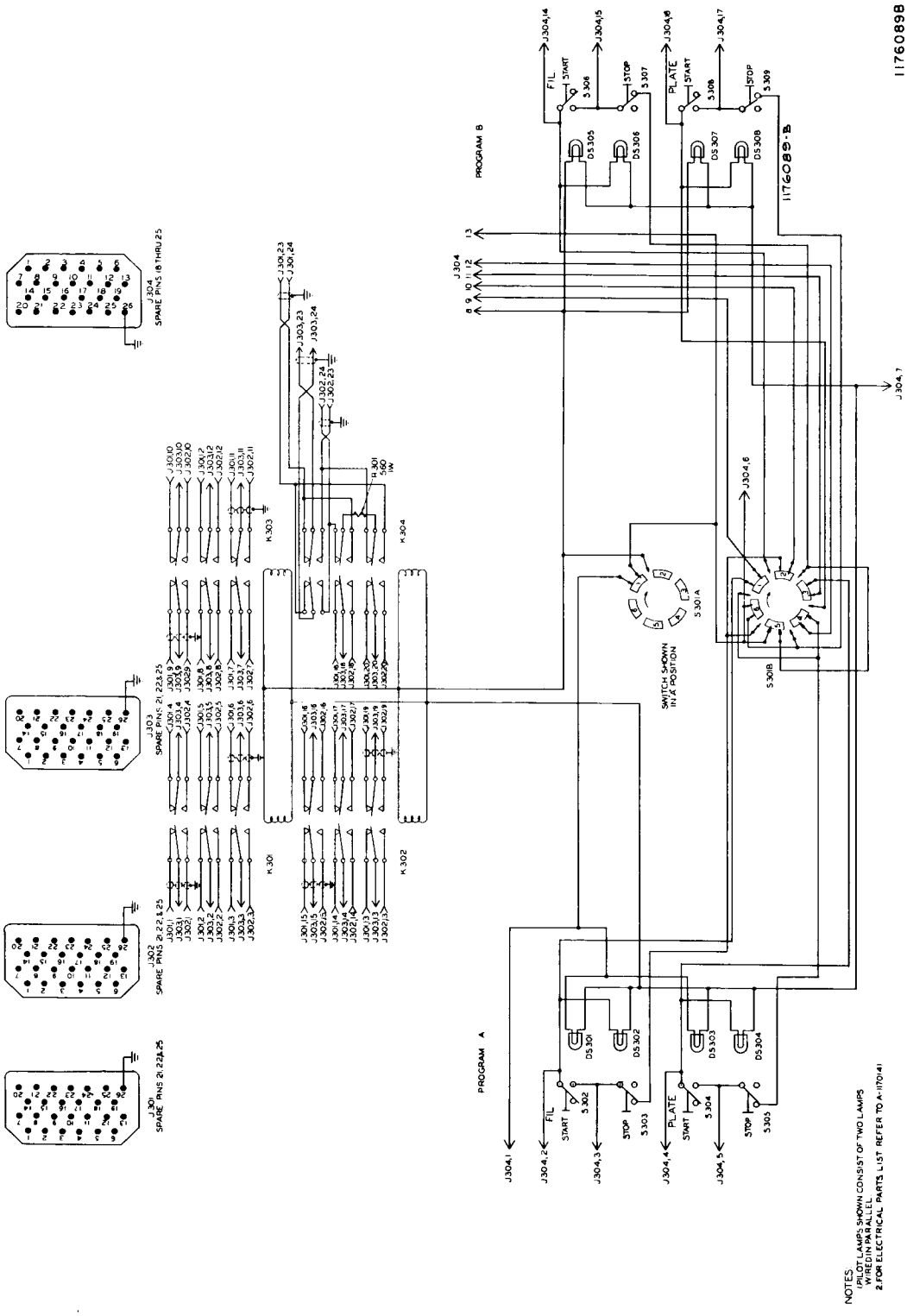

Figure 145. Program Selector and Power Control Unit, Schematic Diagram

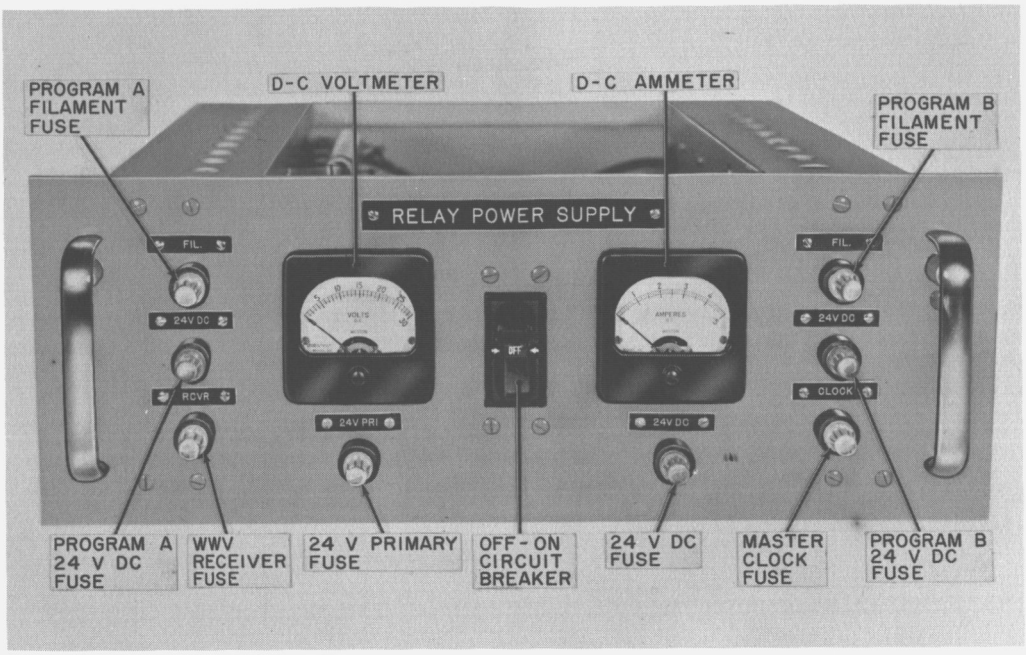

Figure 146. Relay Power Supply, Front View

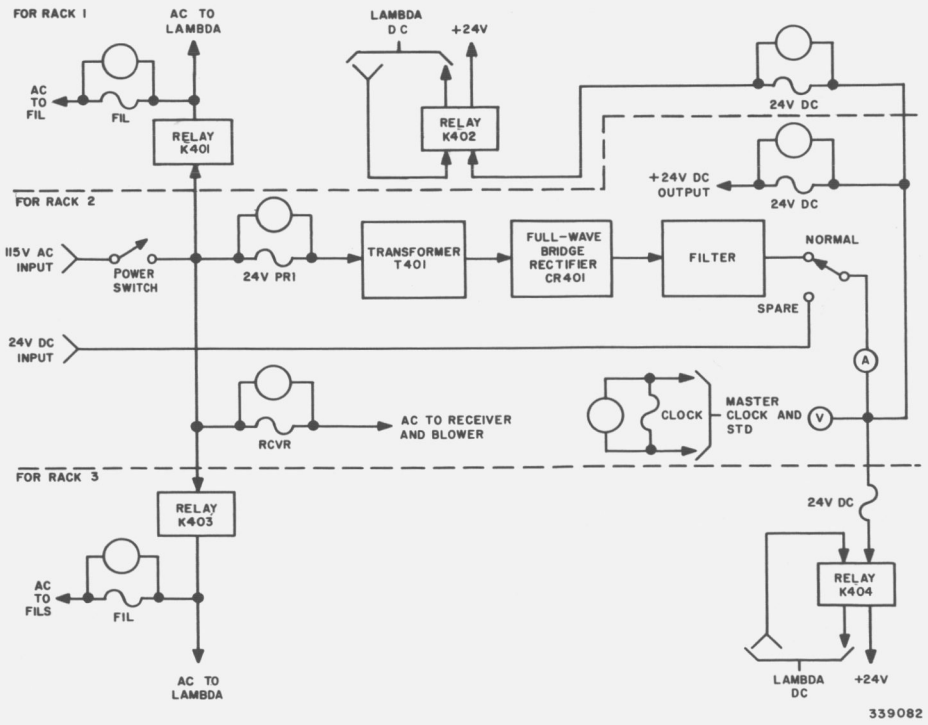

Figure 147. Relay Power Supply, Block Diagram

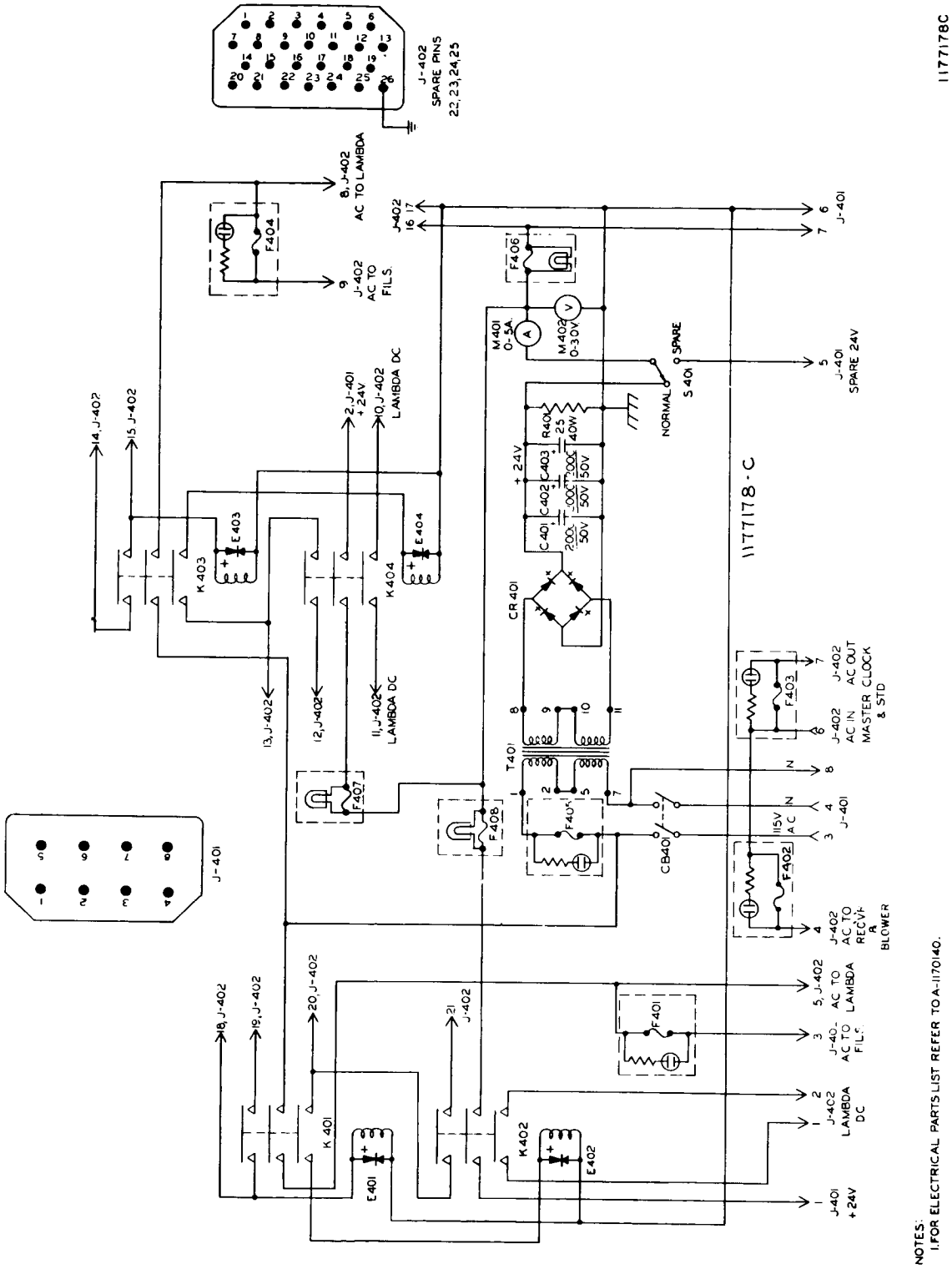

Figure 148. Relay Power Supply, Schematic Diagram

The transmitters were operated remotely because it was required that they be located within 100 feet of the transmitting antenna to avoid excessive power loss in the r-f cabling.

Switching of the antenna from one transmitter to the other was accomplished by the use of a remotely operated coaxial switch. A low-pass filter, installed at the output of the coaxial switch, reduced spurious radiation above the command frequency. The 4X-150B r-f output amplifier tubes normally supplied with the transmitter were replaced with 4X-250B output tubes to ensure ample reserve power output and long tube life at an output power of 200 watts.

Each command transmitter was equipped with an r-f detector that was used for alignment purposes. A portion of the output of the detector, smoothed to a d-c level, was metered to indicate transmitter power output. The detector output also contained the detected command tones which were amplified and used to drive a loudspeaker in the transmitter control panel. The loudspeaker output permitted audio monitoring of the outgoing command tones.

The characteristics of these transmitters are listed in the "Handbook of Maintenance Instructions for Collins 242F-2 Transmitter."

Since the Collins 242F-2 transmitters were designed for remote operation, no difficulties were encountered in devising a suitable transmitter control panel. The transmitter control panel provided the following:

(1) Meter indications of percent r-f power output from transmitter

(2) Audible indications that the transmitter was being modulated

(3) Manual selection of transmitter A or B

(4) Manual selection of channel 1 or 2 (redundant transmitter crystals)

(5) Transmitter primary power on-off switch

(6) Test button for test operation of transmitter

The schematic for the transmitter control panel is shown, along with the schematic for the clock set-pulse demodulator, in Figure 153.

j. Command Programmer

(1) General

The command programmer (Figure 149) provided the means for setting-up and storing the desired satellite program. When an alarm signal was received, the command programmer supplied related portions of this stored information to the control tone generator, antenna programmer, remote picture time set, tape recorders, and command transmitter.

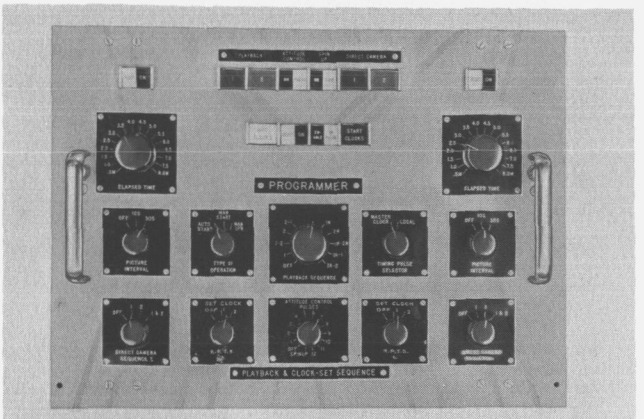

1. "ELAPSED TIME" SELECTOR, DIRECT CAMERA SEQUENCE I
2. "READY-ON" PUSHBUTTON, DIRECT CAMERA SEQUENCE I
3. "SET CLOCK" PUSHBUTTON
4. "READY-ON" PUSHBUTTON, PLAYBACK SEQUENCE
5. "PLAYBACK 1" PUSHBUTTON
6. "PLAYBACK 2" PUSHBUTTON
7. "ON-PULSE" PUSHBUTTON, ATTITUDE CONTROL
8. "ON-FIRE" PUSHBUTTON, SPIN-UP ROCKETS
9. "DIRECT CAMERA 1" PUSHBUTTON
10. "DIRECT CAMERA 2" PUSHBUTTON
11. "ENABLE-IR PULSE" PUSHBUTTON
12. "START CLOCKS" PUSHBUTTON
13. "READY-ON" PUSHBUTTON, DIRECT CAMERA SEQUENCE II
14. "ELAPSED TIME" SELECTOR, DIRECT CAMERA SEQUENCE II
15. "PICTURE INTERVAL" SELECTOR, DIRECT CAMERA SEQUENCE I
16. "DIRECT CAMERA SEQUENCE I" SELECTOR, CAMERA 1, 2, OR 1 AND 2
17. "TYPE OF OPERATION" SELECTOR
18. SET CLOCK R.P.T.S. A
19. "PLAYBACK SEQUENCE" SELECTOR
20. "ATTITUDE CONTROL PULSES" SELECTOR
21. SET CLOCK R.P.T.S. B
22. TIMING PULSE SELECTOR
23. "DIRECT CAMERA SEQUENCE II" SELECTOR, CAMERA 1, 2, OR 1 AND 2
24. "PICTURE INTERVAL" SELECTOR, DIRECT CAMERA SEQUENCE II

Figure 149. Command Programmer, Front View

Primary design considerations for the command programmer were ease of operation and reliability. Time-sequential, push-button control of the program sequences, such as used in project SCORE, was ruled out because of the great possibility of human error in timing such operations.

A cam and stepping-switch controlled system, such as the system that RCA had developed for project JUNO, was also considered. During the setting-up and testing of the JUNO system it was found that adjustment of the cams and followers was a very tedious operation and that, unless they were very carefully tightened, the cams and followers tended to creep out of adjustment.

After analysis of these two subsystems, RCA concluded that the TIROS system should be more automatic than the SCORE system, but less complex and more flexible than the JUNO system. Accordingly, the TIROS programmer was designed to permit presetting of program sequences and to permit automatic read-out of these programs at preselected, electrically-computed times. This design reduced the possibility of human error by affording the opportunity to check the preset programs and by eliminating the need for operator control during a satellite-to-ground contact.

Other design features included provisions for manually controlling the entire program, and for manually starting each of the program sequences. These features

were not intended to be used under normal conditions; they were included to provide for control of the satellite before its path was accurately known and to provide a means of checking out the ground station equipment.

(2) Functional Description

Figure 150 is a block diagram of the command programmer. The programmer has three separate channels; one channel for controlling direct camera sequence I, a second channel for controlling the playback sequence, and a third channel for controlling direct camera sequence II. The time to be allotted for each direct camera sequence is set-up by use of front panel selector switches. In addition, the time interval between picture taking commands is controlled by front panel selector switches. Another control permits selection of the camera to which the commands are to be sent. The programmer contains delay and control circuits to ensure that the satellite systems are warmed up before commands are sent to them.

A program sequence can be initiated either automatically by alarm signals from the master clock or manually by use of front panel switches. Timing of the command programmer functions, normally controlled by 6-ppm* timing inputs from the master clock, can also be controlled either manually or by use of an internal 6-ppm clock generator.

The 6-ppm inputs from the master clock are applied to the start-relays in each of the three channels. When alarm 1 is received, the start-relay in the direct camera sequence I picks up and routes the 6-ppm inputs to the stepping switch of that channel. A d-c voltage, applied through the hold relay and closed contacts of the start-relay, causes that relay to lock-up. Each pulse advances the stepping switch one step. When the switch steps to the position corresponding to the setting of the front-panel time selector switch, the hold-relay opens momentarily and de-energizes the start-relay. This removes the 6-ppm inputs from the stepping action. Normally, the time selector switch is set to a time interval which does not allow the stepping switch to reach the time set in before the playback sequence begins. When the playback sequence begins, the direct-camera-start relay is de-energized by a momentary opening of its hold circuit, stopping direct camera sequence I. By stopping direct camera sequence I in response to the initiation of the playback sequence, the possibility of overlaps and gaps in the transmission of program data is eliminated.

During the time interval between the pick-up and drop-out of the start relay, an energizing voltage is applied through the picture interval selector and the camera selector to the associated oscillator, direct 1, or direct 2, of the control tone generator and to the recording system. Also during this interval, a control voltage, sent to the program hold circuit, turns on and holds on the command transmitter, and an enabling signal is sent to the antenna programmer.

*ppm = pulses per minute

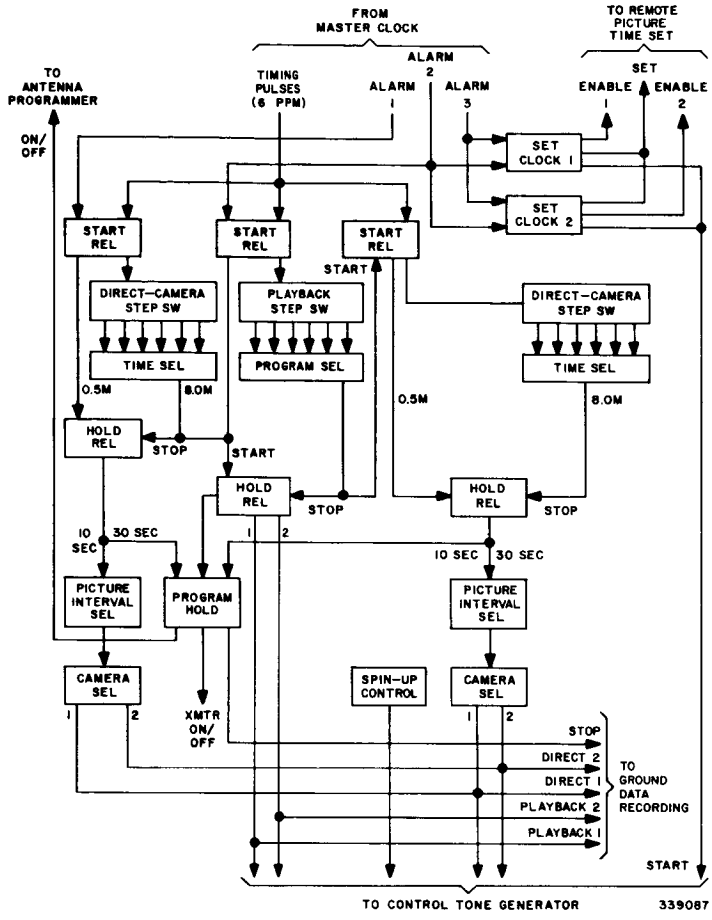

Figure 150. Command Programmer, Block Diagram

The satellite TV cameras are commanded to take a picture by interrupting the control voltage applied to the control tone generator. Interruption of the control voltage is accomplished by the picture interval selector. The selector provides two interruption rates: one rate provides for pictures to be taken at 10-second intervals; the other rate provides for pictures to be taken at 30-second intervals. When the selector is set to the 10-second position, it is connected to every tap of the stepping switch; when set to the 30-second position, the selector is connected to every third tap of the stepping switch.

The alarm 2 input starts the playback sequence and stops direct camera sequence I. Operation of the playback sequence circuit is similar to operation of the direct camera circuit except that, since cameras are not being programmed, there is no picture interval selector. A second difference is that instead of providing control

over the duration of the sequence, a program selector is included to control the sequence of tape playback.

Setting of the satellite clocks is also accomplished during the playback sequence. Clock set is initiated 10 seconds after the satellite has been set to the playback mode. The clock-set time occurs either 10 or 40 seconds after alarm 2 depending on the programmed sequence. The start clock command is initiated by alarm 3. Outputs of the set clock circuits consist of enabling and set signals which are applied to the remote picture time set, and a start signal which activates the clock set oscillator in the control tone generator.

Direct camera sequence II, when called for, is started at the conclusion of the playback sequence by an output from the program selector. Operation of the sequence II circuit is the same as the operation of the direct camera sequence I circuit.

A spin-up selector switch, included in the command programmer, permits selection of either manually or automatically initiated spin-up commands. In addition, the switch permits selection of a specific time within any one of the program sequences for automatically sending the spin-up command.

Figure 151§ is the schematic diagram of the command programmer.

k. Clock Set-Pulse Demodulator

(1) General

The clock set-pulse demodulator, used in conjunction with the back-up Berkeley counters, provided an accurate count of the set pulses sent to the satellite clocks. The need for this unit was established when malfunctions were detected in the remote picture time set unit.

The counters in the remote picture time set unit occasionally skipped counts, causing errors in the number of set pulses sent to the satellite. As a check on the number of pulses actually sent to the satellite, it was decided to monitor and to count the number of set pulses that were applied to the control tone generator. Later, it was decided that it would be better to monitor the set pulses at the output of the command transmitter. By monitoring the pulses at that point, the actual number of set pulses, including any transients which might act like set pulses, could be counted. In addition, monitoring the pulses at that point eliminated the possibility of counting pulses which were lost in the control tone generator or command transmitter circuits and not actually transmitted to the satellite.

The command transmitter was originally equipped with a crystal detector which provided a sample of the control tone intelligence to the speaker system in the transmitter control panel. The clock set-pulse demodulator separated the clock-set

§ This illustration is printed on a fold-out page located ar rear of this volume.

pulses from the other control tones. The output of the demodulator was connected to the back-up Berkeley counter in Rack 12 of the ground station equipment. The design of the clock set-pulse demodulator was essentially the same as the demodulator used in the satellite. It was deemed advantageous to use this design because it had been extensively tested in satellite operations and because it would provide demodulator action similar to that which would be occurring in the satellite.

(2) Functional Description

Figure 152 is a block diagram of the clock set-pulse demodulator. A 600-ohm line-to-line transformer is bridged across the balanced line which carries the tones from the transmitter to the monitoring speaker on the transmitter control panel. The secondary of the transformer feeds a two stage feed-back amplifier which, in turn, drives two bandpass filters. One filter is tuned to the tone frequence of the clock 1 set pulses; the other filter is tuned to the clock 2 set pulse tone frequency.

The pulse selector switch determines which filter output will be applied to the half-wave rectifier. The switch was included in the circuit because it was not considered necessary to provide simultaneous counting of both sets of clock set pulses. The unbypassed half-wave rectifier drives a monostable multivibrator which produces a 2.2-millisecond pulse of 10-volts amplitude. The output of this multivibrator drives the Berkeley counter.

Figure 153 is the schematic diagram of the clock set-pulse demodulator.

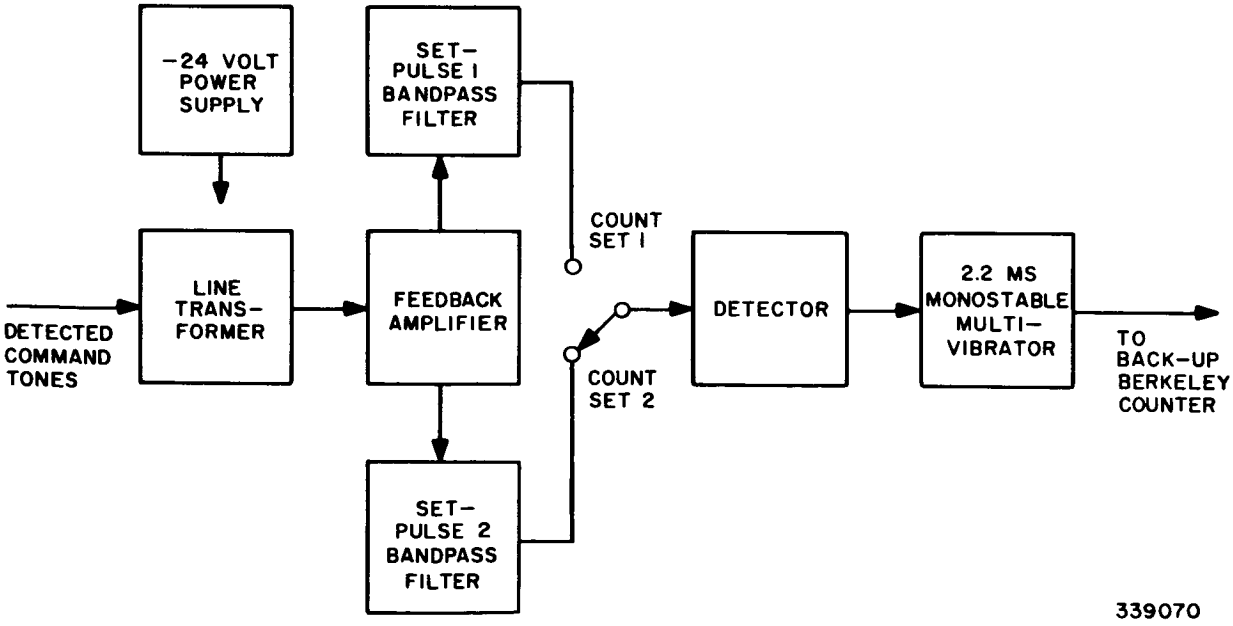

Figure 152. Clock Set-Pulse Demodulator, Block Diagram

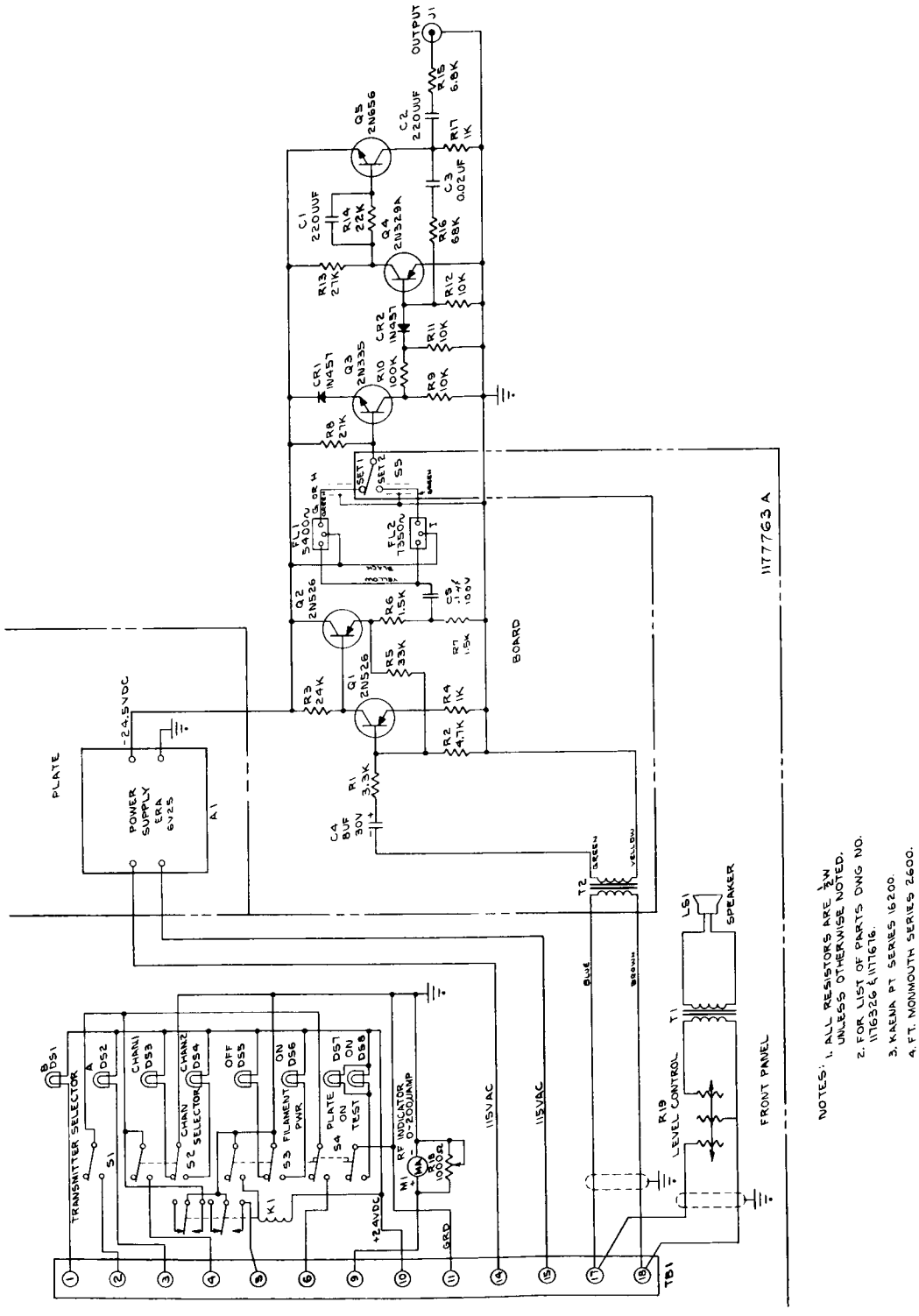

Figure 153. Transmitter Control Panel and Clock Set Pulse Demodulator, Schematic Diagram

5. Data Receiving Components

a. Introduction

The data receiving components consisted of the TV receivers, the beacon and telemetry receivers, and the TV diversity combiners. Except for the TV diversity combiners, the equipments selected for use as data receiving components were in either military or commercial use at the start of the TIROS I contract. The TV diversity combiners, developed by RCA as a means of ensuring more reliable satellite-to-ground communications, provided polarization diversity connection for the horizontal and vertical TV receivers. Polarization diversity for the beacon and telemetry receivers is accomplished by interconnecting the AGC's of the vertical and horizontal receivers for each of the beacon frequencies.

b. TV Receivers

The two TV receivers installed at each ground station were either Nems-Clarke Model 1411 or Nems-Clarke Model 1412. Although Model 1412 was considered to be a superior receiver, that model was not available in sufficient quantity; therefore, most of the TV receivers were Model 1411. At the Fort Monmouth installation, bandpass filters added to the TV receivers prevented interference from the command transmitter. Characteristics of the receivers are listed in the applicable Nems-Clarke Receiver Specifications.

One of the TV receivers was connected to the horizontal and the other was connected to the vertical feed of the TLM-18 antenna. The signal outputs and the AGC voltages of each receiver were connected to a diversity combiner. The diversity combiner selected the stronger of the two signal outputs for application to the succeeding stages of the TV reception circuits. Use of the polarization diversity combination minimized fading of the signal from the satellite.

c. Beacon and Telemetry Receivers

The beacon and telemetry receiving circuits consisted of four R-390A receivers, two Tape-Tone frequency (108 to 14 Mc) converters, two multicouplers, and two F192/U, 108-Mc bandpass filters. Two of the R-390A transmitters were tuned to 14.00 Mc; the other two were tuned to 14.03 Mc. One receiver of each frequency group was connected to a multicoupler which, in turn, was connected to the horizontally polarized feed from the antenna system; the other receiver and multicoupler of each group was connected to the vertically-polarized feed from the antenna system. The two receivers of each frequency group were connected together in polarization diversity combination. Figure 154 is a block diagram of the beacon and telemetry receiving circuits. The Tape-Tone converters, modified by the addition of crystal ovens, provided a frequency stability of ±0.001 percent. Since the R-390A receivers provided very stable operation, acquisition of the satellite beacons was easily achieved.

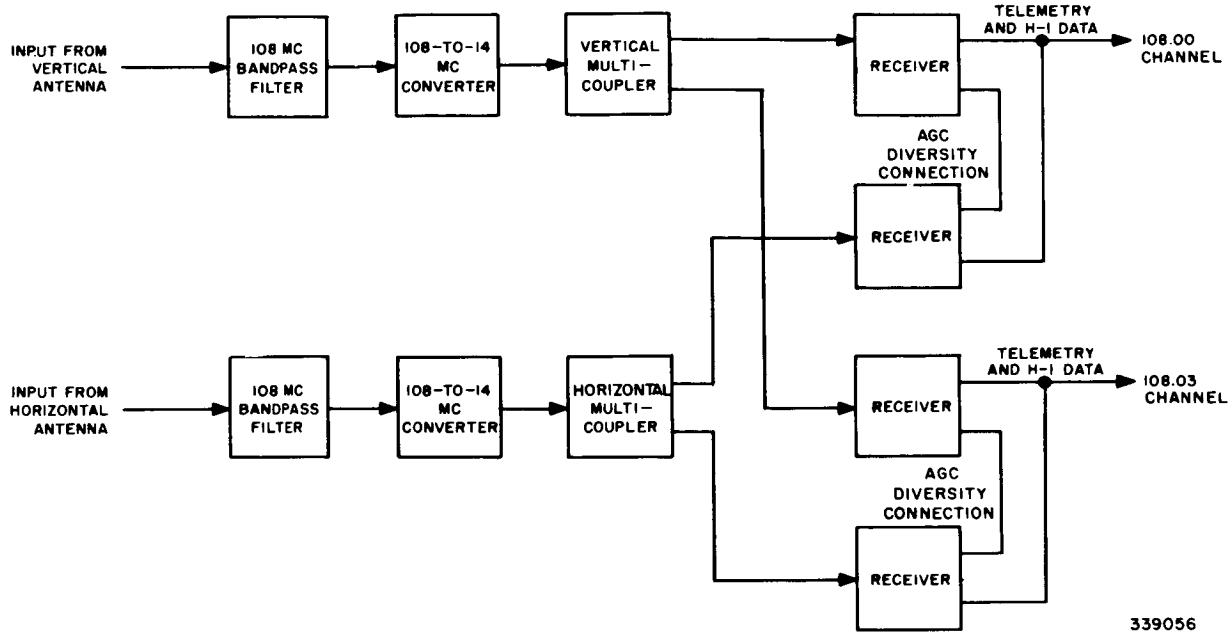

Figure 154. Beacon and Telemetry Receivers, Block Diagram

At Kaena Point, the Tape-Tone converters were rack-mounted in vans. At Fort Monmouth, the converters were mounted in the antenna pod as an integral unit which also contained the 108-Mc bandpass filters. The filters provided 40 db of attenuation to the command transmitter frequency while resulting in an insertion loss of only 1 db. The F192/U bandpass filters were used in this application instead of notch filters because of the availability of the F192/U as government-furnished equipment.

d. Diversity Combiners

(1) General

Both the TV and telemetry receivers were connected in polarization diversity. Early in the TIROS I project, it was recognized that, due to the circularly polarized radiation system of the satellite, the use of the circularly polarized tracking systems which existed on the TLM-18 antennas would result in a high probability of deep nulls in received signal level. Use of the available capability for switching from left to right circular polarization was considered but rejected as being impractical. Since separate horizontal and vertical quarter-wave probes were available in the waveguide system for the TLM-18 antenna, it was decided to bring the horizontal and vertical outputs to separate receivers and then to sum the outputs of the receivers. Calculations indicated that use of horizontal and vertical ground polarization against

circular polarization of the satellite, regardless of satellite attitude, would result in a maximum loss of 3 db. This loss is acceptable when compared to losses encountered in systems using circular against circular polarization or systems using circular polarization against either horizontal or vertical polarization. Figure 155 is a result of statistical analysis of the problem of antenna polarization.

RCA contacted various manufacturers in an effort to purchase a diversity combiner which would meet the TIROS I specifications. The only available combiners were of the base-band type in which the receiver noise band, outside of the intelligence band, is used to control the outputs of the receivers. The transfer from one polarization (receiver) is dependent upon the signal-to-noise ratio in each receiver. When the signal-to-noise ratio of the two receivers is equal, the summed output of the two provides a 3-db gain over the individual ratios.

The base-band type of combiner could not be used for TIROS I because of the bandwidth limitations of the receivers and the nature of the subcarrier television signal. The video bandwidth of the receivers is 150 kc while the highest first order sideband of the video subcarrier is 147.5 kc. The limited receiver bandwidth made it impossible to obtain a noise band outside of the intelligence band that would provide adequate control without interference from the subcarrier higher order sidebands. Thus, it was decided to use a diversity combiner which operated by sampling the receiver AGC voltage. Since a combiner of this type was not available, RCA undertook the task of developing one.

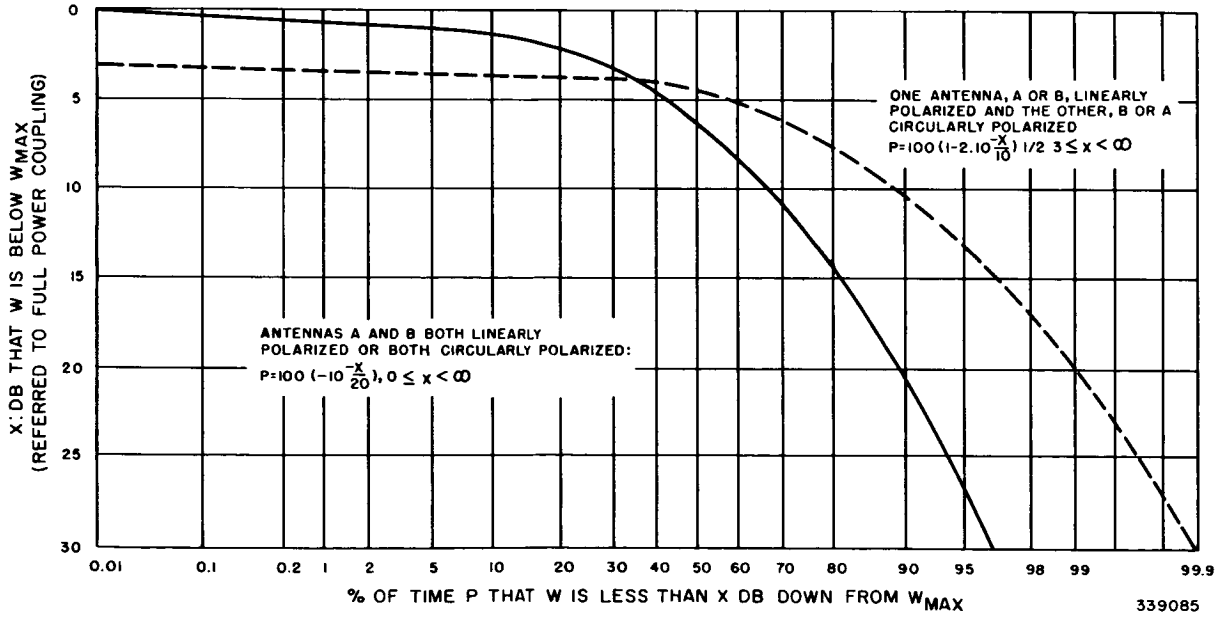

Figure 155. Probability Distribution of Transmission Efficiency

The basic design of the AGC diversity combiner is based on a broadcast band combiner. In addition to combining the outputs of the two receiving channels, whenever the difference in signal level between channels was less than 1 db, the combiner had to select the better signal, when the difference exceeded 1 db while blocking the poorer signal. A prime objective in the development of this combiner was to provide isolation between channels to prevent degradation of the better signal by the poorer signal. Although the original concept provided a 3-db gain in the signal-to-noise ratio, the rate of change of signal level, due to satellite spin, resulted in the combiner acting like a flip-flop for selecting the better signal. Thus, the 3-db improvement feature could not be utilized.

(2) Functional Description

Figure 156 is a block diagram of the diversity combiner. The combiner receives the video signal along with its corresponding AGC voltage from each of two receivers. The video signals are applied through an attenuator directly to the grids of the cathode-coupled combining tube. The signal on the combiner grids is limited to 0.1 volt peak-to-peak to ensure minimum distortion and to reduce cross-modulation between the video subcarrier and the sun pulses. The AGC voltage, amplified and inverted by one section of direct coupled amplifier V3, is applied to the grids of V4. The cathode-coupled combiner tube V4 senses the greater AGC level and passes the corresponding input signal. A 2-db change in signal level causes complete cut-off of one receiver output and full output from the other receiver. The output of V4 is amplified by V5 to provide unity gain through the diversity combiner. An AGC balance control is included to permit balancing of the two outputs of V3 when the inputs to the receiver are equal.

Figure 157 is the schematic diagram of the diversity combiner.

6. Data Processing and Display Components

a. General

The data processing and display components received and demodulated the TV transmission from the satellite and recorded the pictures on film and magnetic tape. A high degree of reliability was required for these functions because of their prime importance. In addition to tape recording of the TV pictures, the data processing and display components provided for tape playback of the TV pictures. This feature permitted the generation of duplicate pictures, both positives and negatives, which facilitated meteorological interpretation. The components of this system also provided identification and orientation information for each picture. This information consisted of the frame number, camera identification, picture-taking sequence, and sun angle.

Originally, the data processing and display components were designed to handle and receive TV pictures at two readout rates; namely, a one-second picture readout and a two-second picture readout. The Ampex tape recorders were equipped to operate at 120 ips so that they would provide the 200-kc bandwidth necessary for the

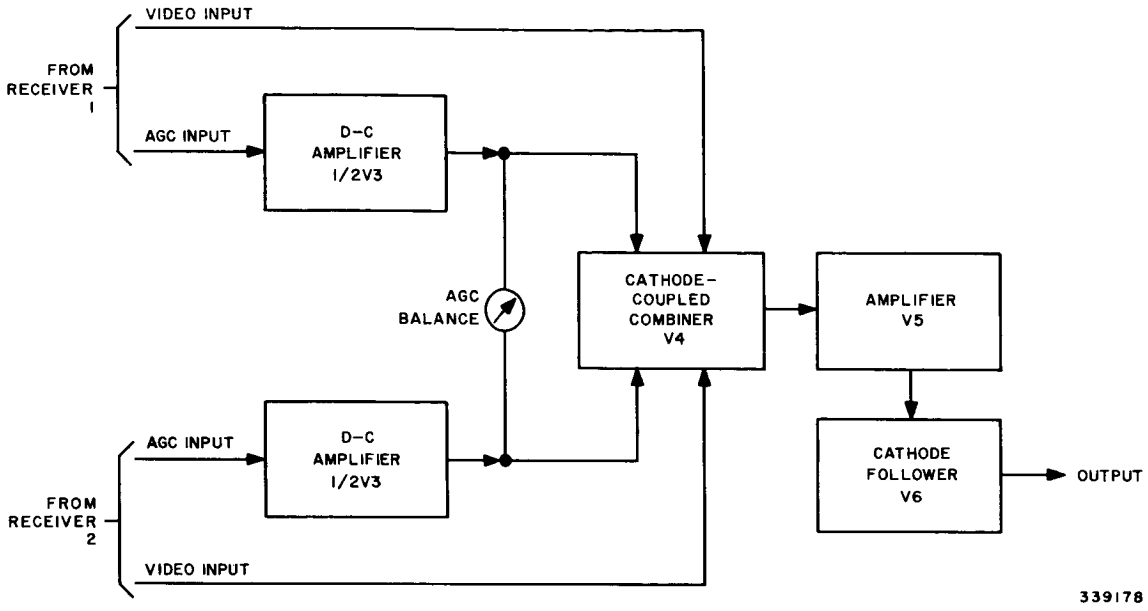

Figure 156. Diversity Combiner, Block Diagram

one-second picture readout. Similarly, the various amplifiers and sweep circuits were designed to operate at either of the two rates. Selection of the rate response was to be controlled by relay switching circuits. When the one-second picture readout requirement was cancelled, the switching circuits were deleted but all other design features were maintained.

b. Functional Description

Figure 158 is a block diagram of the data processing and display components. The input signal is a composite of the frequency multiplexed TV subcarrier and the sun pulse signals from the TV diversity combiner. The sun pulses are separated from the subcarrier by means of a high-pass and a low-pass filter; the sun pulses are passed by the 10-kc bandpass filter while the subcarrier is passed by the high-pass filter. The sun pulse data is fed to the tape and computer control where the 10-kc pulses are filtered and detected. The detected envelopes of these pulses are applied to the sun-angle computer.

The TV subcarrier is demodulated in the TV-FM demodulator. In addition to demodulating the TV subcarrier, the demodulator circuit serves as a vertical sync generator. The video output of the TV-FM demodulator is applied to the horizontal sync separator, a monitor scope, and the video amplifier of the kinescope display and video amplifier unit.

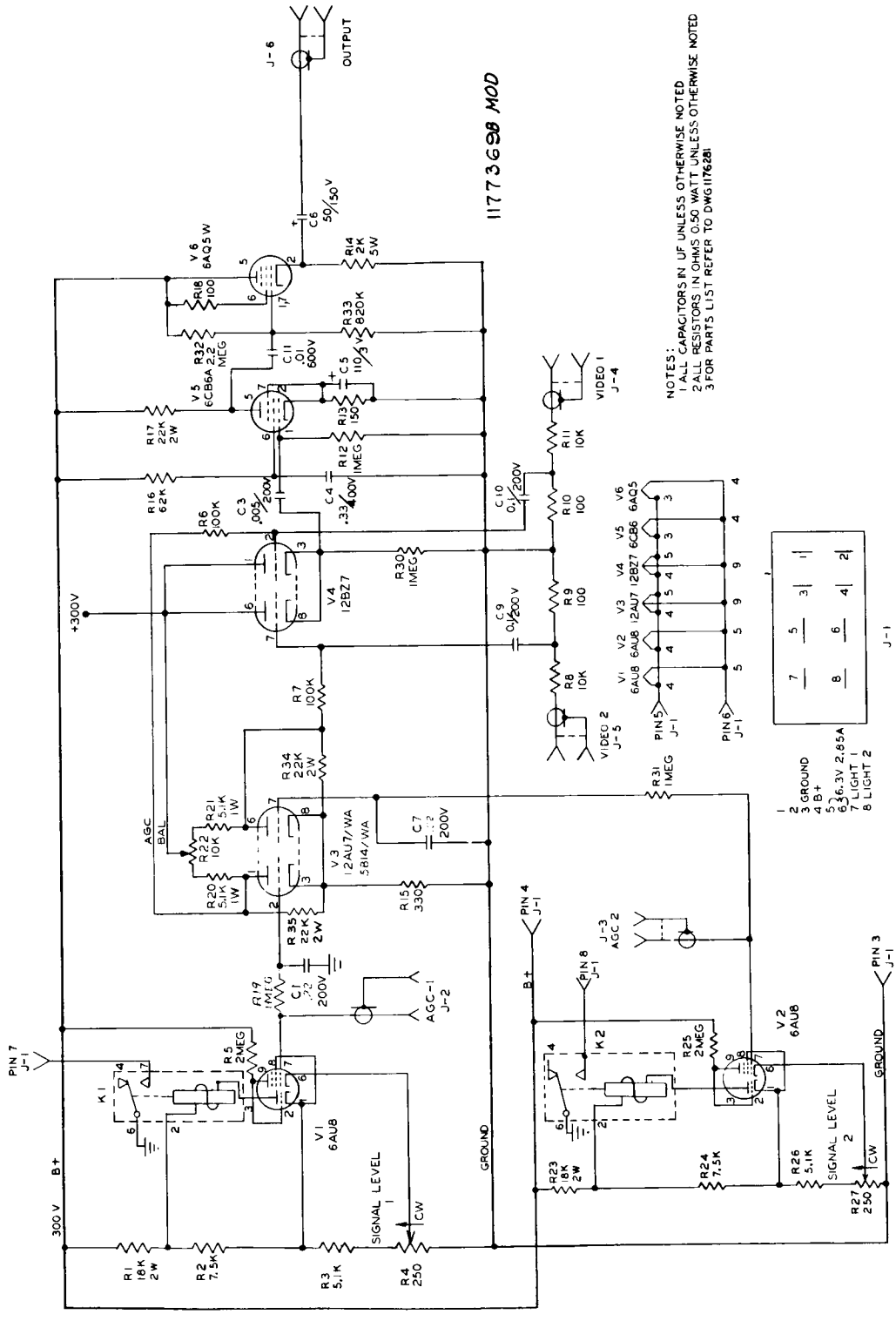

Figure 157. Diversity Combiner, Schematic Diagram

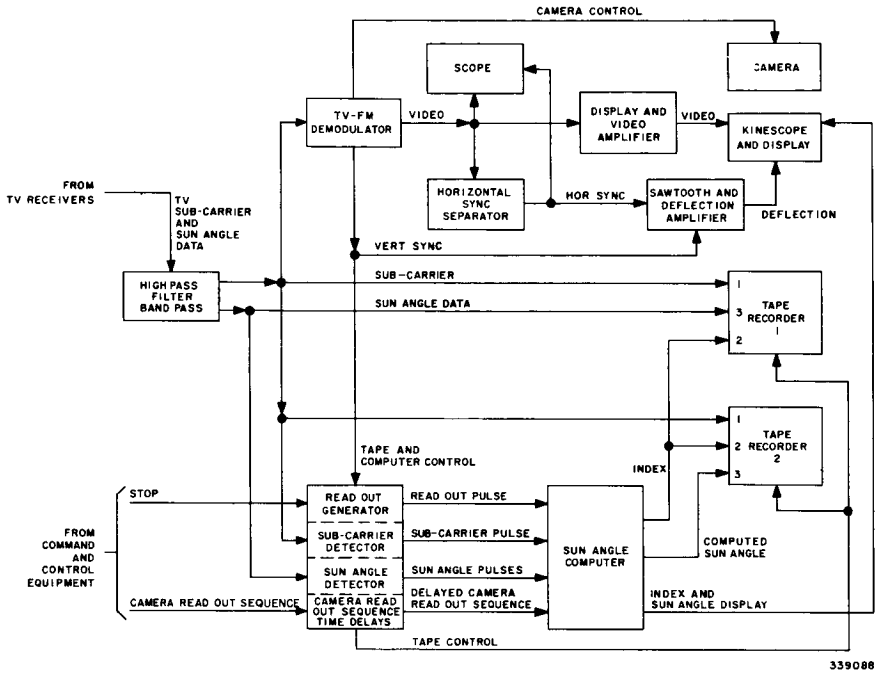

Figure 158. Data Processing and Display Components, Block Diagram

The output of the horizontal sync separator and the vertical sync output of the TV-FM demodulator are applied to the sawtooth and deflection unit. In turn, the sawtooth and deflection unit provides the vertical and horizontal deflection currents to the yoke of the kinescope.

c. Display and Video Amplifier

(1) General

The display and video amplifier provided final amplification of the TV video and displayed the TV picture on a kinescope. In order to provide a film recording of the received TV picture, the kinescope display had to be of a nature that would permit the presentation to be photographed. (Figure 159 shows the display and video amplifier mounted in its associated rack.)

The choices of the kinescope and film type were dependent upon each other since the spectral response of each had to be similar and the resolution and transfer function of the combination had to be satisfactory for the task. After making analyses of various types of kinescopes and films, a 5ZP-16 kinescope was selected for use in combination with Kodak 35-mm television recording film. The 5ZP-16 kinescope provided resolution in excess of 500 lines as did the 35-mm recording film. In addition, a series of tests were conducted to determine what techniques should be

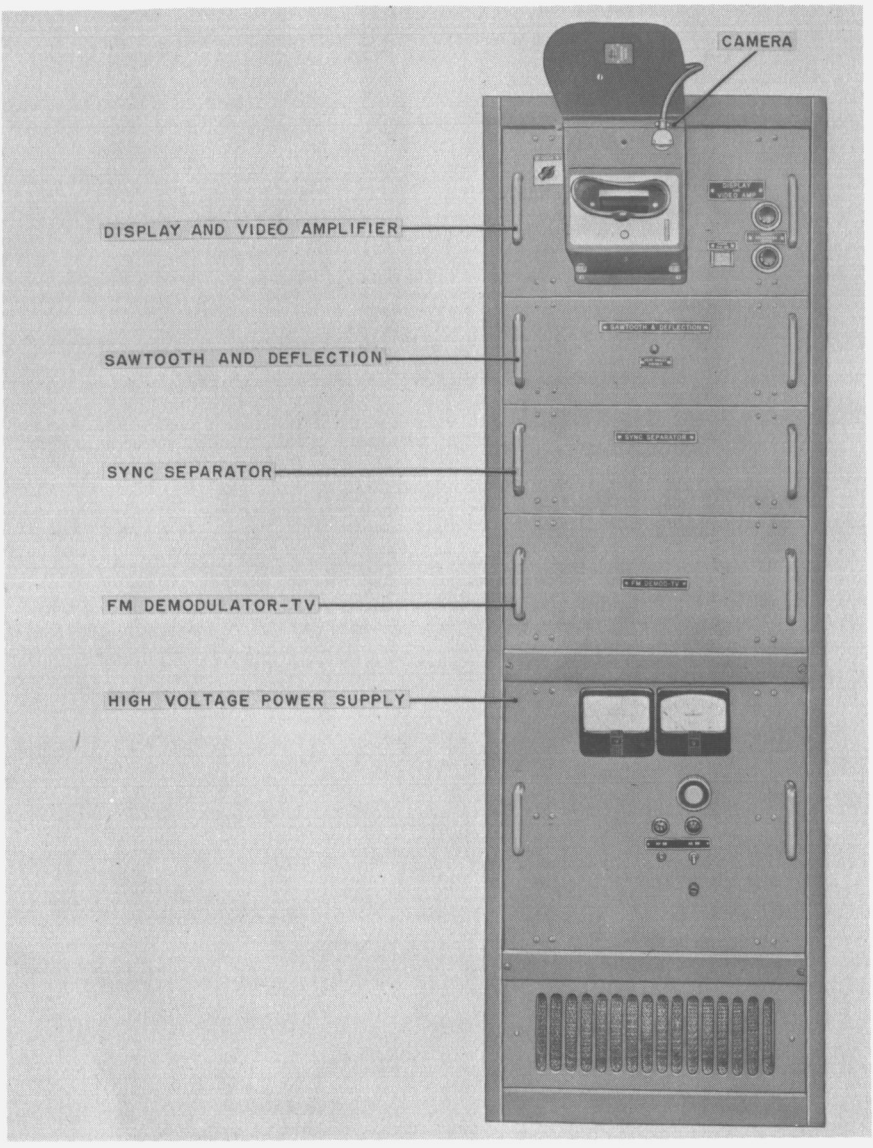

Figure 159. Video Monitor Rack

used to optimize the kinescope-to-film transfer function. Results of these tests showed that the system gamma, a slope of the transfer function, could be made equal to unity by correctly adjusting the exposure time of the film, the developing time of the film, and the beam current of the kinescope. The combination of matched resolutions and correct system adjustment permitted reconstruction of the TV pictures with a minimum amount of degradation.

The camera used for handling the television recording film, a Beattie-Coleman, was the only available automatic camera with double frame capability that also met the other requirements of TIROS I. The kinescope deflection yoke, a motor-stator type, when used with the 5ZP-16 resulted in about 5-percent pin cushion distortion when the yoke was driven with linear sawtooth current waveforms. It was decided that this degree of accuracy was adequate and that no correction was required.

The video amplifier of the display and video amplifier unit was designed to have a frequency response down to d-c, in order to accommodate the signals from the low-speed television system used in TIROS. Although the need for d-c response could have been eliminated by clamping the video signals to the line rate, use of the clamping technique creates many problems which are not found in amplifiers having a d-c response. These problems would have been particularly pronounced because of the aperiodic nature of the TV signals.

Early TIROS I requirements prescribed a picture readout time of one second when the satellite was in a direct camera sequence. In turn, this readout time dictated a 125-kilocycle upper frequency limit for the video amplifier. Accordingly, the video amplifier was designed to provide good response to signals between d-c and 125 kc. The voltage required to drive the 5ZP-16 at the one-second readout time was determined to be 20 volts peak-to-peak.

Later TIROS I requirements prescribed a two-second picture readout time (1/2 frame-per-second). This reduction in frame rate dropped the driving voltage requirement of the kinescope to 10 volts peak-to-peak and reduced the band-pass requirements for the amplifier to 62.5 kc. Although the gain of the amplifier was reduced to meet this new 10-volt requirement, the bandpass was not reduced from the original 125 kc. Thus the video amplifier provided a bandpass which was more than adequate for its intended use.

A chopped circuit added to the video amplifier, eliminated the need for zero adjustment of the d-c amplifier.

(2) Functional Description

Figure 160 is a block diagram of the display and video amplifier unit. The chopper stabilized d-c amplifier, a wide-band, high-gain amplifier with a single-break 60 db/octave cut-off, permits stable operation with feedback. The nominal video input to the d-c amplifier is 1 volt peak-to-peak; the ratio of Z_f to Z_i is set to provide a closed-loop gain of 10. This gain increases the signal level to the 10-volt peak-to-peak level that is required for driving the kinescope at the two-second readout time. The gain of the d-c amplifier can be varied by changing the value of either Z_f or Z_i. (In the actual circuit, Z_f is in the form of a T attenuator in which the shunt arm can be changed.)

The 60-cps chopper, used to reduce the d-c drift of the d-c amplifier, has a very low frequency response; its gain at d-c is approximately 650. The response curve of the 60-cps chopper is shown in Figure 161. The frequency response of the chopper-stabilized d-c amplifier is shown in Figure 162.

The output of the d-c amplifier is connected to the grid of the 5ZP-16 when a positive image (negative photo) is desired and to the cathode of the 5ZP-16 when a negative image (positive photo) is desired.

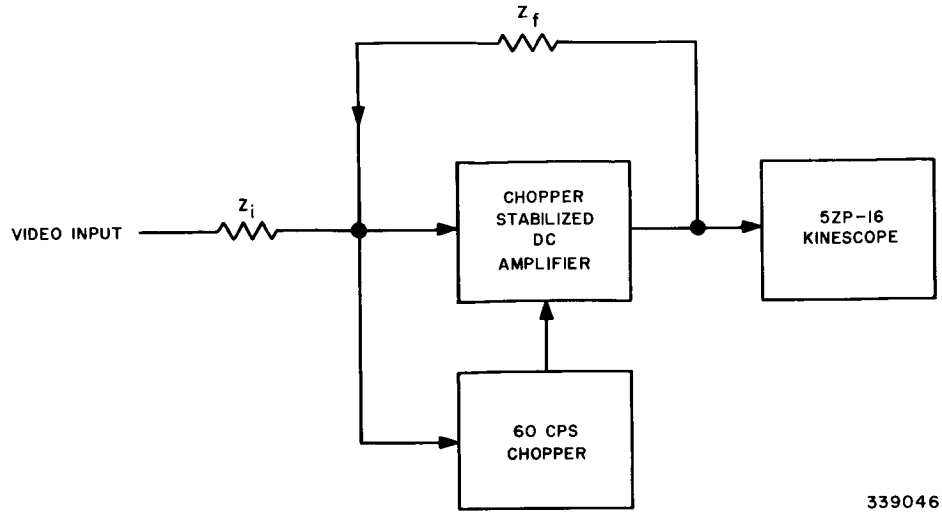

Figure 160. Display and Video Amplifier, Block Diagram

Figure 163 § is the schematic diagram of the display and video amplifier. For a detailed circuit description of the display and video amplifier, refer to "Instruction and Operating Handbook TIROS I Meteorological Satellite System." (Reference 20)

d. Sawtooth Generator and Deflection Amplifier

(1) General

The sawtooth generator and deflection amplifier provided linear sawtooth current waveforms for the horizontal and vertical deflection coils in the yoke of the 5ZP-16 kinescope. (Figure 159 shows the sawtooth generator and deflection amplifier mounted in its associated rack.) The unit consisted of two nearly identical circuits. One circuit supplied the waveforms to the horizontal deflection coil; the other circuit supplied the waveforms to the vertical deflection coil. The sawtooth generator section of each circuit produced a linear sawtooth waveform in response to each sync pulse that it received. The deflection amplifier section of each circuit amplified the waveforms to the required level. In the case of the current waveform for the vertical coil, this level was 0.5 amperes peak-to-peak. In the case of the waveform applied to the horizontal coil, the current level was to 1.5 amperes peak-to-peak. Because of the nature of the TV signals, the sawtooth generator sections were to respond to sync pulses which were aperiodic, and the deflection amplifiers were directly coupled.

Basically, the sawtooth generator sections were operational amplifiers with a capacitor connected into the feedback path. A simplified functional diagram of one of these sawtooth generators is shown in Figure 164.

§ This illustration is printed on a fold-out page located at rear of this volume.

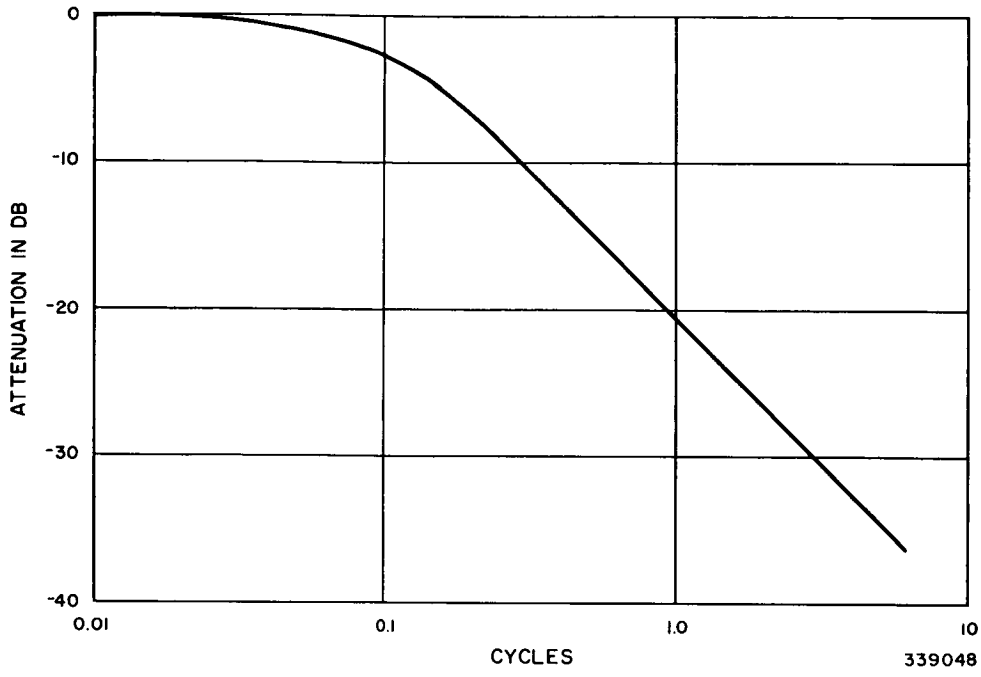

Figure 161. Frequency Response of 60-Cps Chopper

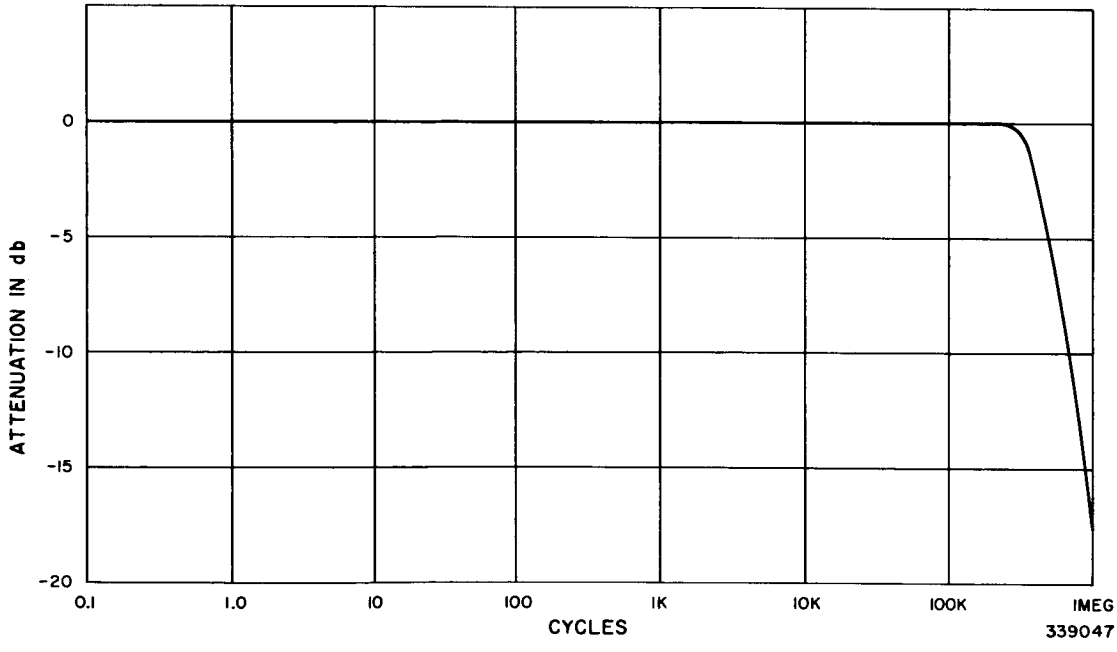

Figure 162. Frequency Response of Chopper Stabilized D-C Amplifier

When a positive voltage is applied to the input, e_1, output voltage e_o is a linear ramp function with a negating slope. The amplifier will continue to integrate and voltage e_o will continue to go negative until it reaches the potential of the bias voltage applied to feedback diode V1. When this occurs, condensor C is short circuited by the diode forward resistance, and the resistance of the feedback network becomes nearly zero. Since the gain of the amplifier is equal to the feedback impedance over the input impedance (R), the amplifier gain drops to nearly zero. The output voltage, e_o, will remain at the bias voltage level as long as the positive voltage appears at e_i. A negative voltage applied to e_i will be integrated and a positive slope, or a positive ramp function will be produced until e_o reaches the potential of bias e_{b2}. When this potential is reached, diode V2 conducts and causes the integration to stop. Thus, one diode limits the upper voltage level while the other diode limits the lower voltage level.

If a voltage waveform as shown in Figure 165a is applied at e_i, the voltage e_o will be as shown in Figure 165. Integration occurs and the linear sawtooth is formed until the voltage output reaches either of the bias voltage levels. When either e_{b1} or e_{b2} is reached, the integration stops and the voltage output remains constant until an integration voltage of opposite polarity is applied to e_i. The negative pulses of the waveform shown in Figure 165b correspond to the retrace times of the vertical and horizontal deflection current. Because the amplitude of each of these retrace pulses is always great enough to permit the integration to reach e_{b1}, the slope and positions of the trace is unaffected by the periodicity of the pulses. The voltage limit e_{b2} prevents the circuit from going into saturation when there are no retrace pulses. In operation, the voltage waveform shown in Figure 165a is adjusted so the sweep appears as in Figure 165c. In this figure the integration never quite reaches e_{b2}. This operation is true only for the horizontal integrator, where the sync pulses are essentially periodic for the duration of one frame. In the case of the vertical integrator, the pulses can occur at 4-, 10-, or 30-second intervals while the sweep time remains at 2 seconds. Thus, in the vertical circuit the integration always reaches e_{b2} and awaits the retrace pulse before the next sweep begins.

Originally the sawtooth generators were designed with the provision for applying a sweep-correction voltage to summing point S. This correction voltage would have permitted the slope of the sweep to be corrected during the sweep itself. Later this was found to be unnecessary because of the adequate tape speed stability of the tape recorder. The vertical and the horizontal sawtooth generator circuits are identical except for the value of the RC time constants.

As in the case of the sawtooth generator sections, the horizontal and vertical deflection amplifiers were nearly identical. The primary difference between the two amplifiers was that parallel connected transistors were used in the horizontal amplifier to provide a higher current output. Figure 166 is a simplified functional diagram of a deflection amplifier circuit. The kinescope yoke windings are constructed for use in a push-pull circuit. The output voltages of the sawtooth generator, e_s, is amplified and then applied to the base of the transistor which drives 1/2 of the yoke winding. This transistor has a large amount of feedback in the emitter circuit. The other 1/2 of the yoke winding is driven by transistor T-2. The emitter

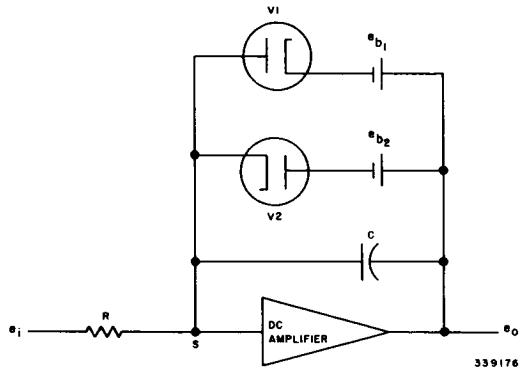

Figure 164. Sawtooth Generator Circuit, Functional Diagram

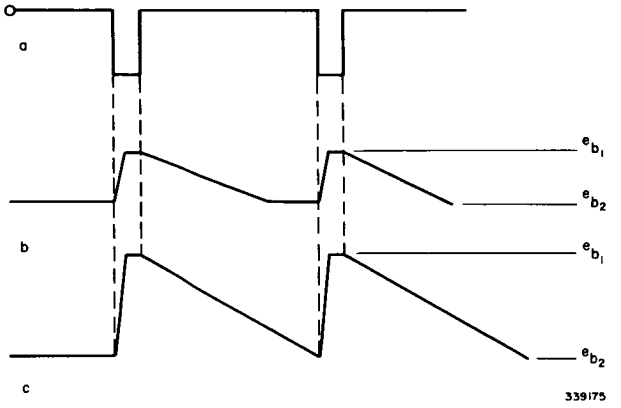

Figure 165. Sawtooth Generator Waveforms

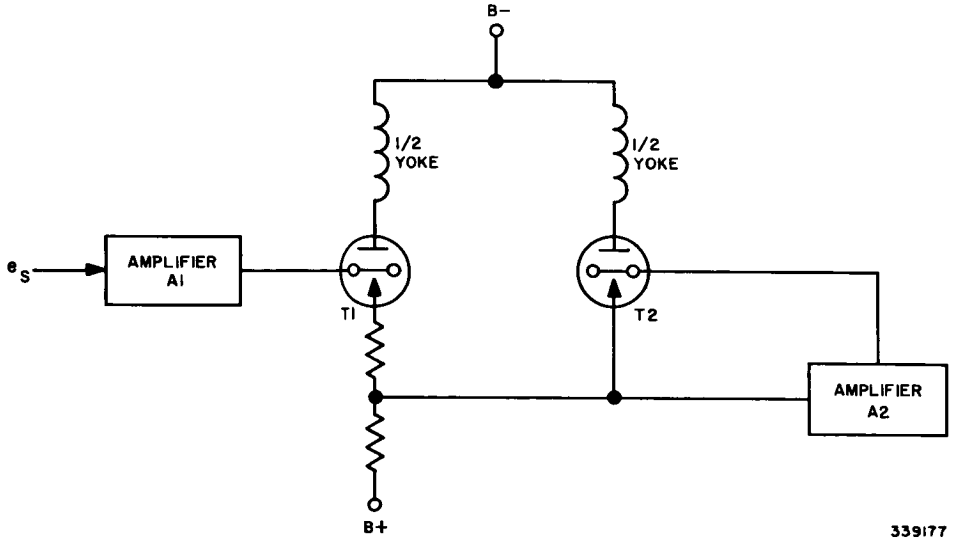

Figure 166. Deflection Amplifier, Functional Diagram

currents of both transistors flow through a common resistor which develops a voltage e_f. Voltage e_f is held constant by the action of amplifier A2. For example, if the emitter current of transistor T-1 increases, the amplifier detects this increase and applies a voltage to the base of transistor T-2, which decreases the emitter current of that transistor.

This circuit was made relatively insensitive to voltage and temperature variations by mounting both transistors on the same heat sink and by using the same source of operating voltage for both transistors.

(2) Functional Description

Figure 167 is a block diagram of the horizontal section of the sawtooth generator and deflection amplifier unit. Except for RC time constants the vertical section is identical; therefore, only the horizontal section is discussed. The horizontal sync pulse inputs drive a one-shot multivibrator; the pulse width of the multivibrator output is set to the desired retrace time. The multivibrator output is coupled through a diode clamp and a disconnect diode to the summing point of the operational amplifier. Adjustment controls in the clamp and disconnect circuit provide for control of the retrace slope and also the sawtooth slope. The sawtooth slope determines the picture width.

The d-c amplifier section of the operational amplifier drives two cathode followers. Each of these cathode followers is driven with a slightly different d-c offset. This difference in offset provides the diode bias (represented by the batteries in Figure 164). The amount of d-c offset is controlled by the horizontal gain control. Sawtooth outputs are applied through a cathode follower and horizontal centering control to the deflection amplifier section of the circuit.

The sawtooth inputs to the deflection amplifier are applied through an isolation emitter follower to the push-pull amplifier which drives the yoke of the kinescope. Phase inversion is obtained by amplifying the emitter feedback of one section of the push-pull amplifier and applying it to the base of the other section. Balance of the push-pull amplifier is controlled by adjustment of the horizontal balance potentiometer.

The schematic of the sawtooth generator and deflection amplifier is shown in Figure 168 §. For a detailed description of circuit operation, refer to Instruction and Operating Handbook TIROS I Meteorological Satellite System. (Reference 20)

e. Horizontal Sync Separator

(1) General

The horizontal sync separator provided synchronizing pulses to the horizontal sawtooth deflection circuitry. These pulses were in phase and locked to

§ This illustration is printed on a fold-out page located at rear of this volume.

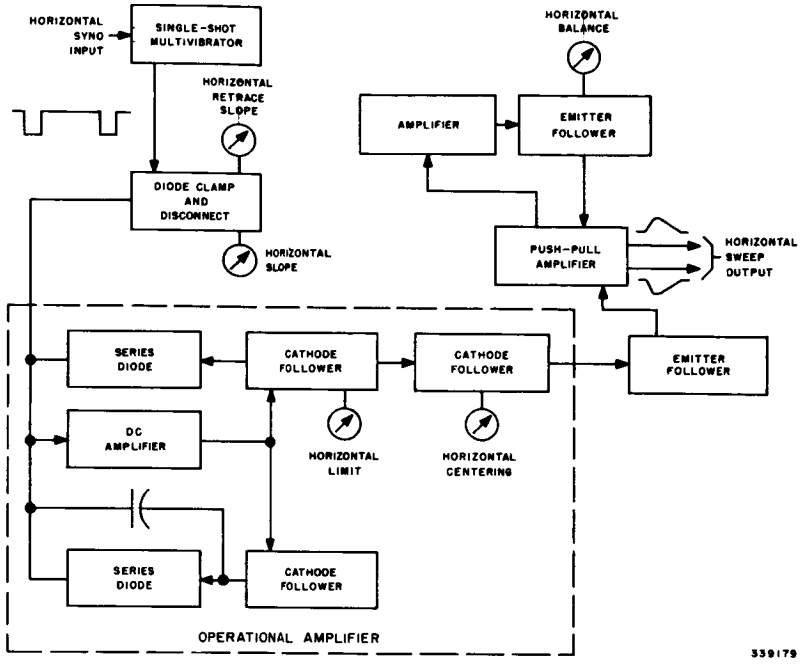

Figure 167. Horizontal Circuits, Sawtooth Generator and Deflection Amplifier, Block Diagram

the prospective video horizontal rate. The operation of the sync separator was unique because it provided these synchronizing pulses in response to video signals which were aperiodic in nature. That is, the horizontal rate or horizontal signal was non-coherent from frame to frame even though the frequency within each frame was the same. (Figure 159 shows the sync separator mounted in its associated rack.)

In the earlier bread-board system, a driven sync separator was tried. The driven sync separator merely clipped the sync pulses from the video signal and used them to drive a multivibrator whose output corresponded to the horizontal sync information. For high signal-to-noise ratios this type sync separator proved to be adequate. However, it was found inadequate for signal-to-noise ratios realistic for the TIROS I system, where the noise box occasionally exceeded the sync tip level of the video signal. Each time that a high level noise box was received, the driven sync separator generated a false trigger, or one extra horizontal line. For the predicted signal-to-noise ratios for TIROS I, these false triggers were expected to occur in quantities of several per frame. Accordingly, the development work on a driven type of separator was abandoned.

The second type of sync separator investigated, a fly-wheel type, was a phase-locked oscillator that provided good sync separation and was not affected by the high level noise boxes.

(2) Functional Description

Figure 169 is a functional block diagram of the horizontal sync separator. The video input (Figure 170a) is applied to the sync clipper where it is clipped at the level indicated. Some of the noise exceeds this clipping level and appears at the output of the clipper along with the sync pulses. A typical output of the sync clipper is depicted by waveform f1 of Figure 170b. This waveform is split by the phase inverter to provide two out-of-phase inputs to the multiplier. The multiplier or phase detector multiplies the clipped video signal with the symmetrical square-wave output of the flip-flop divider (waveform f2 of Figure 170). The product of these two signals, the output of the multiplier, is shown in Figure 170c. If the phase relationship of the two waveforms is correct, the d-c component of the waveform output is zero.

The output of the multiplier is applied through a low-pass filter, amplified, and then applied to a voltage-controlled oscillator. The frequency of the oscillator output is then divided in half by a flip-flop to ensure that the waveform f2 (the output of the divider) is perfectly symmetrical. These elements, the multiplier, filter, amplifier, oscillator and divider, constitute the phase locked loop. The noise bandwidth and the frequency response of the system are determined by the characteristics of the low-pass filter. The closed loop frequency response of the system is approximately 10 cps. This response determines the length of time that it takes for the phase lock loop to pull into phase with the incoming signal. With a 10-cps frequency response, the pull-in time is equivalent to approximately 25-horizontal lines. The low noise bandwidth of this system permits the phase lock to be maintained even when the signal-to-noise ratio is down to 0 db. It was deemed advantageous to sacrifice the 25 lines at the beginning of each frame for pull-in, in order that good horizontal sync should be maintained.

The output of the flip-flop divider is also applied to the one-shot multivibrator. The square-wave is differentiated and triggers the multivibrator to produce sync pulses which are 10 microseconds in duration. These pulses are then amplified and applied to the sawtooth generator and deflection amplifier. The output amplifier is designed to drive a 75-ohm terminated coaxial cable.

Figure 171[§] is the schematic diagram of the horizontal sync separator. Adjustments for the sync separator include setting the frequency of the voltage-controlled oscillator with zero voltage input, and adjusting the loop gain and the zero setting of the d-c amplifier. The "frequency adjust" potentiometer R42, adjusts the frequency to exactly twice the horizontal frequency when the input is grounded by the closing of switch S-1. Potentiometer R65 provided for zero adjustment of d-c amplifier V12. This adjustment is made so that the voltage at the junction of resistors R66 and R67 is zero when the input grids are grounded. Loop-control R68 adjusts the overall loop gain so that the transient response of the system is critically damped. This adjustment is made by observing the transient behavior of the feedback voltage when a signal is applied to the input.

[§]This illustration is printed on a fold-out page located at rear of this volume.

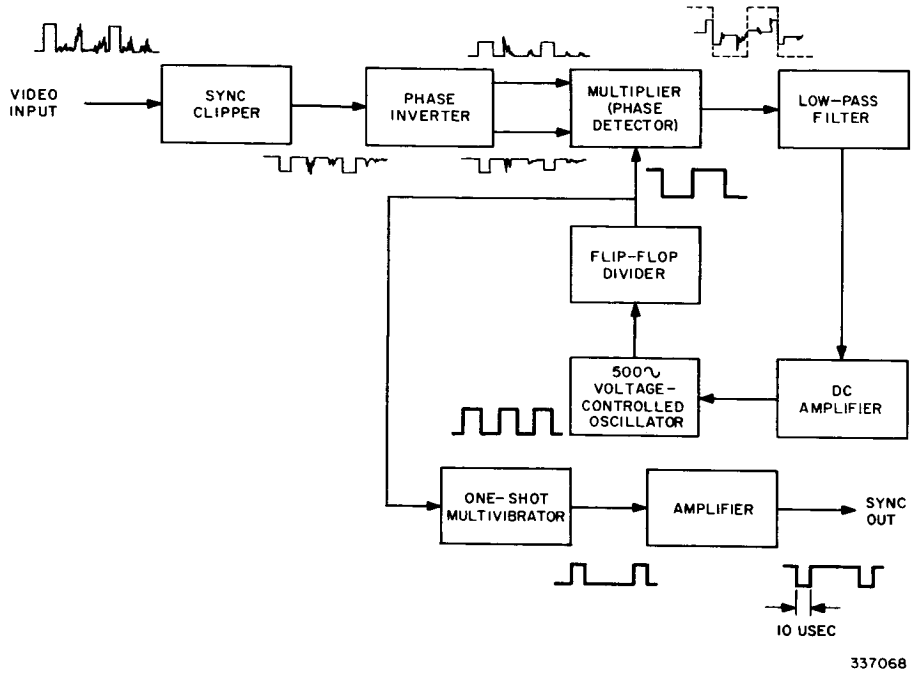

Figure 169. Horizontal Sync Separator, Block Diagram

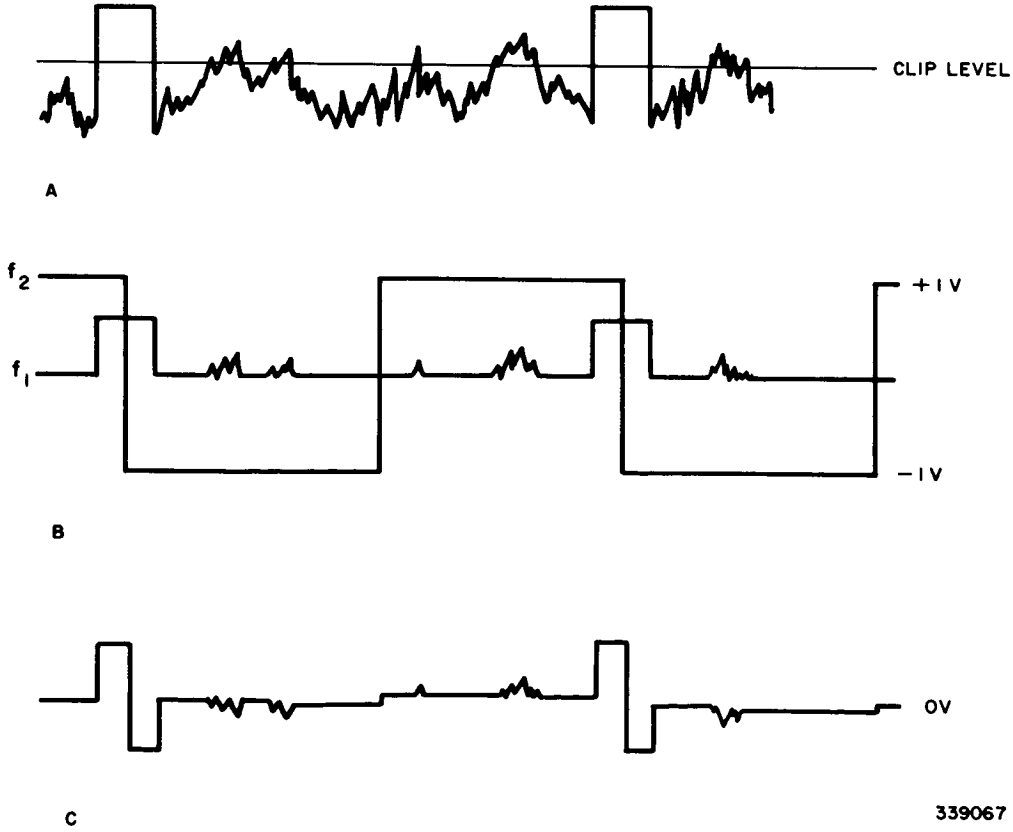

Figure 170. Horizontal Sync Separator, Waveforms

f. TV-FM Demodulator

(1) General

The TV-FM demodulator received the modulated video subcarrier, demodulated the subcarrier, and provided a stable low-impedance video output signal. In addition, this chassis provided the control of the recorder camera shutter and the vertical synchronizing pulses. A pulse counting type of demodulator was selected for use in TIROS because of its stability and because of the linear operating characteristics that it provided. This type of demodulator had been used successfully on commercial video tape recorders in which the relative frequency spectrum relationships of the video signal, carrier, and modulation components were the same as those found in TIROS I. The TV-FM demodulator was divided into three sections; namely, the demodulator section, the camera shutter control, and the vertical synchronizing circuits. (Figure 159 shows the TV-FM demodulator mounted in its associated rack.)

The demodulator section consisted of three basic sub-sections. These sub-sections were the frequency detecting circuits, the low-pass filter, and the d-c amplifier. The original design of the frequency detecting circuits included two vacuum tube limiter stages, a pulse standardizer, a phase inverter and a plate rectifier or detector. In the course of testing and development, four stages of diode limiters were used to replace the two vacuum tube limiters. This change resulted in a better signal-to-noise ratio, and an improvement in the reduction of the noise produced by asymmetry in the pulse standardizing circuit and by even-harmonic distortion of the signal. Another change made as a result of knowledge obtained during testing and development was the replacement of the single high-voltage, Zener diode, used as the plate rectifier, with two lower-voltage Zener diodes connected in series. This change was made to overcome the noise produced by the high-voltage Zener diode whenever it passed into or out of the Zener region of operation.

Development of the low-pass filter was the next major problem. This filter had to attenuate the carrier while passing the modulation signal. Development of a suitable filter was difficult because of slight deviations from symmetry which existed in the carrier signal. Even though the carrier frequency was doubled by the full-wave plate rectifier, the deviation in symmetry caused the rectified signal to retain a fairly large component of the original carrier frequency.

This condition meant that the filter had to pass the high video components at 60 kc and attenuate the carrier components at 70 kc while maintaining a linear phase characteristic in the pass band. A Tchebycheff filter was finally selected as the best possible solution to the filter problem.

The d-c amplifier was basically the same as the one designed for use in the display and video amplifier. The primary difference was that the gain of the d-c amplifier was altered by changing the value of the feedback resistors. The camera shutter control and vertical synchronizing circuits functioned as expected during

tests. However, operational experience indicated that a much narrower bandwidth was required in the shutter control and vertical synchronizing circuits. The narrower bandpass was needed to prevent noise bursts, which proved to be much stronger than originally expected, from triggering the circuits.

(2) Functional Description

Figure 172 is a block diagram of the TV-FM demodulator. The input signal (3 volts peak-to-peak) is clipped to one volt peak-to-peak by the diode clipper. The signal output from the diodes approximates a square wave. This signal is fed to a 1.25 microsecond shorted delay line; the delay line provides an output of positive and negative 2.5 microsecond pulses at a pulse rate which is directly proportional to the incoming frequency. The delay line output is connected to the phase inverter which provides outputs of equal amplitude and opposite phase. The signals are fed to a push-push plate detector which is essentially a full-wave rectifier. The detector's output frequency is double that of the input. The average level of the output of the detector is proportional to the input frequency. The detector output is passed through a low-pass Tchebycheff filter which has a flat response from 0 to 62.5 kc. The filter serves as an integrator to establish a d-c level which changes at a rate corresponding to the frequency modulation.

The video output of the low-pass filter is fed into a chopper-stabilized d-c amplifier. Feedback from the output cathode follower reduces the overall gain of the d-c amplifier to approximately 10. The video output is applied to the sawtooth generator and deflection amplifier unit. Relay K6 shorts the video input to the d-c amplifier in the absence of the carrier to prevent noise feed-through.

Direct video can be fed to the d-c amplifier circuit for test purposes. The d-c restorer provides d-c restoration for the direct video input. Relays K1 through K5 provide for all necessary switching functions; these relays are operated from the monitor control panel.

Timing for the camera shutter and the vertical sync are provided when a video signal is received. The output of the diode clipper is applied to the rectifier and integrator through a bandpass filter, which is centered at 85 kc. The positive output of the integrator is amplified and inverted and then applied to the Schmidt trigger circuit. In addition, when the positive input is received by the amplifier, relay K6 picks up and operates the camera shutter. The Schmidt trigger output operates a pulse shaper which produces a 10-microsecond square-pulse output. The pulse is amplified to provide a negative-going vertical sync output. Figure 173§ is the schematic diagram of the TV-FM demodulator.

§ This illustration is printed on a fold-out page located at rear of this volume.

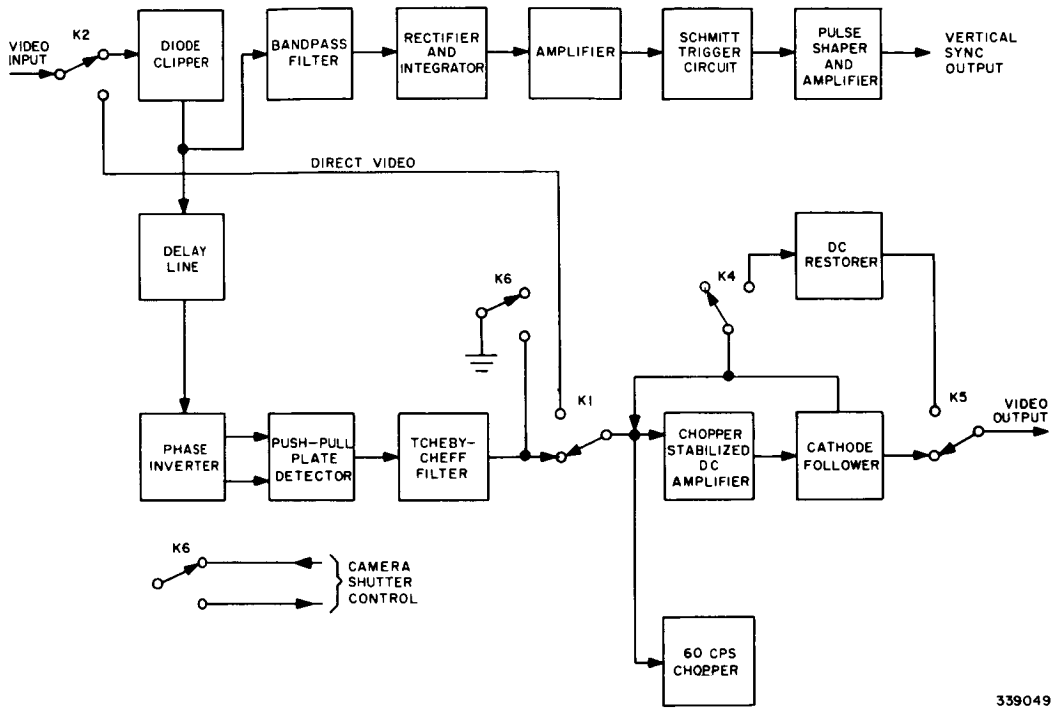

Figure 172. TV-FM Demodulator, Block Diagram

g. Tape and Computer Control

(1) General

The tape and computer control detected the sun-angle tone bursts, detected the video subcarrier envelope for use in the sun-angle computer, provided the source signals for frame identification, provided a central control for the two tape recorders, and provided the readout pulse for the sun-angle computer. (Figure 174 shows the tape and computer control mounted in its associated rack.) The sun-angle tone detectors and the subcarrier envelope detector were designed with equal bandwidths to provide the desired accuracy of 0.1 degree. A certain amount of this accuracy was sacrificed after it was learned, from operational experience, that an accuracy trade-off would be required in order to improve noise immunity.

The source signals indicate to the sun-angle computer the source of the incoming video; that is, "playback" or "direct," "camera 1" or "camera 2." Because of the warm-up time delays in the satellite, equivalent time delays had to be included on the ground. Then, since direct camera picture-taking commands were actually the interruption of the source signals, holding relays had to be added to keep the time-delay relays locked-in during the picture-taking command. The tape recorder controls were set up to operate when the first source signal was received. This automatically put the recorders into the record mode of operation.

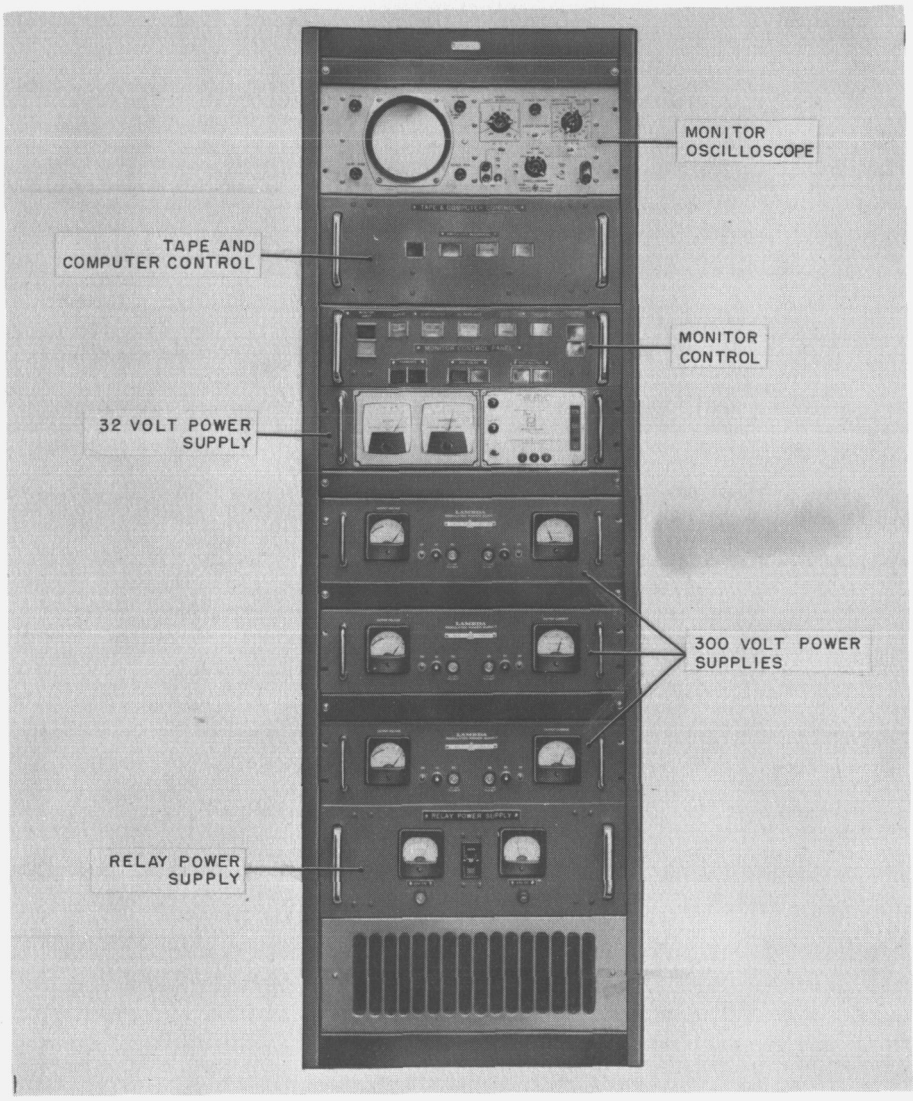

Figure 174. Video Control and Power Rack

One feature was deleted from the control system; that was an automatic stop signal for the tape recorder when the stop signal was received from the satellite ground command equipment. The readout pulse circuitry mixed the normal vertical sync pulse with another pulse for the final data readout. This was required whenever the stop signal was received from the command equipment.

(2) Functional Description

Figure 175 is a block diagram of the tape and computer control. Functionally, the unit is divided into five main sections; namely, the sun-angle pulse circuit, the subcarrier pulse circuit, the read-out pulse circuit, the direct and playback circuits, and the tape control circuits.

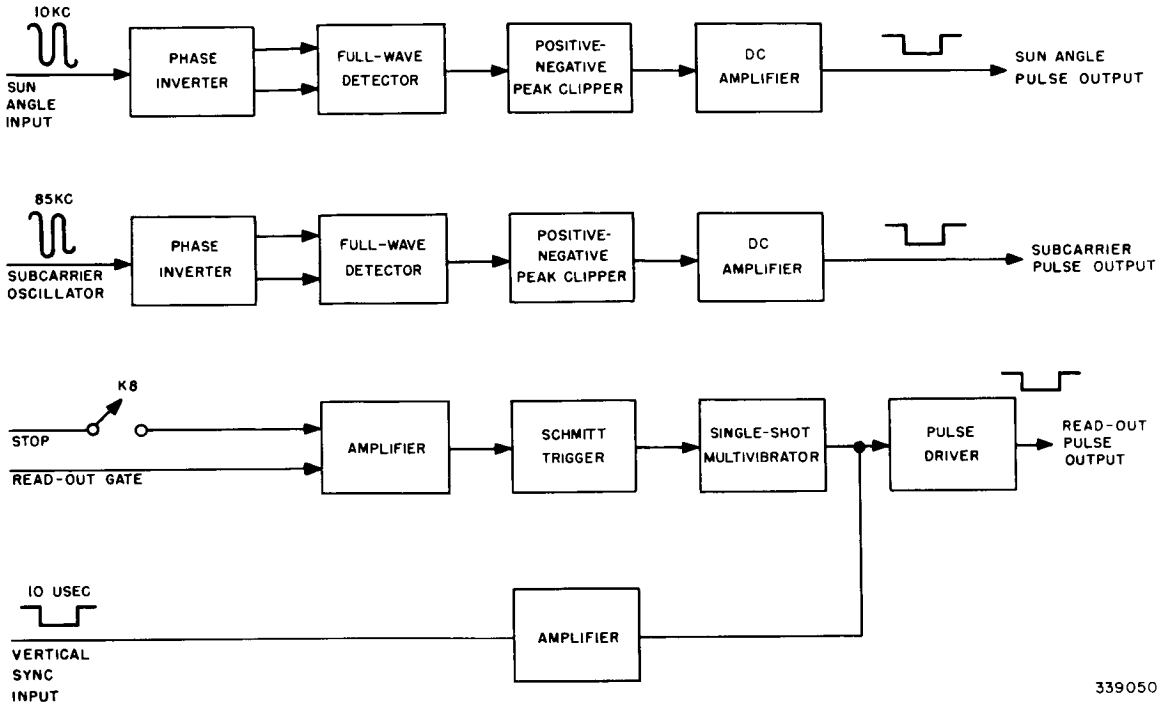

Figure 175. Tape and Computer Control, Block Diagram Part 1 of 2)

The sun-angle pulse circuit receives a sun-angle input, consisting of short, medium, or long 10-kc bursts in various combinations with each other, and delivers pulses, which have the same durations as the burst inputs to the sun-angle detector. Each sun-angle input is applied to the phase inverter; the inverter supplies two out-of-phase inputs to the full-wave detector. The output of the detector is filtered to remove the 10-kc component and applied to the positive-negative peak clipper. The clipper develops sharp leading and trailing edges on the pulse; this pulse is amplified and applied to the sun-angle detector.

The subcarrier pulse circuit receives an 85-kc subcarrier input and supplies the squared video envelope of this signal to the sun-angle detector. Operation of this circuit is the same as the operation of the sun-angle pulse circuit.

The read-out pulse circuit receives one of two inputs; namely, a stop signal from the command programmer or a read-out gate signal from the sun-angle computer. The signal that is present is amplified and applied to the Schmidt-trigger circuit. The output of the Schmidt-trigger circuit, a negative trigger pulse, triggers the single-shot multivibrator to produce a positive-going, 10-microsecond pulse. This pulse is applied to the pulse driver which produces the read-out pulse for the sun-angle computer. The read-out pulse can also be produced by a vertical sync input from the TV-FM demodulator. This input is amplified and then applied to the pulse driver.

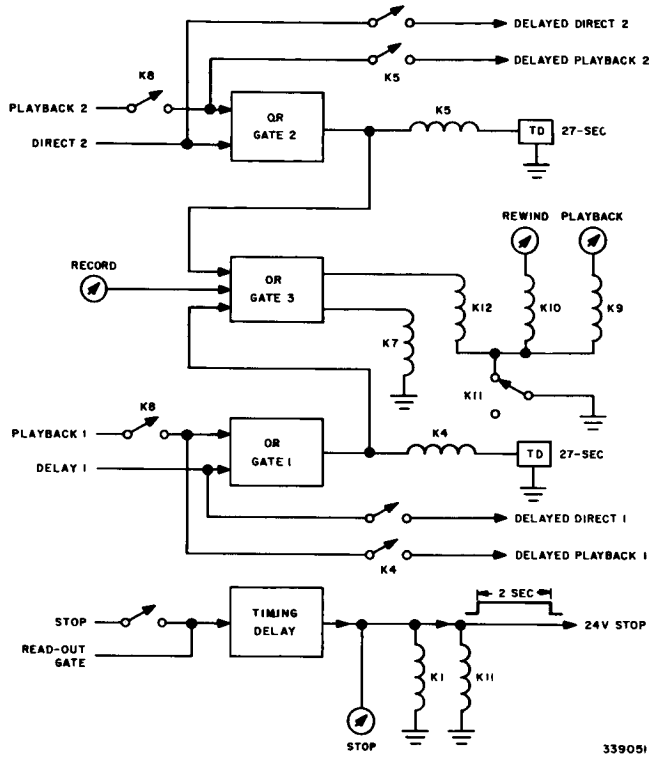

Figure 175. Tape and Computer Control, Block Diagram Part 2 of 2)

The direct and playback circuit receives any one of the direct and playback signals, delays the input signal for 27 seconds, and then applies the signal to the sun-angle computer as a source signal. When either a "direct" or a "playback 1" signal is received, the signal is applied through OR gate 1 to relay K4. Twenty-seven seconds later, the relay energizes and applies the signal to the sun-angle computer. Similar action occurs when "direct 2" or "playback 2" is applied to OR gate 2.

An output from either OR gate 1 or 2 will pass through OR gate 3 and energize relays K7 and K12. When relay K12 picks up, a RECORD indicator lamp lights; when relay K7 picks up, a start signal is sent to the tape recorders.

The tape control circuit controls the start, stop, rewind, and playback functions of the tape recorders. Switch S1 can be used to start the recorders when a direct or playback signal is not present. Stop, Rewind, and Playback switches are

provided for manually controlling each of those functions. Figure 176§ is the schematic diagram of the tape and computer control.

h. Monitor Control

The monitor control provided switches and relays for controlling the inputs of the data processing and display components and for turning on and off the 32-volt power supply, the three 300-volt power supplies, the high voltage power supply, and the sun angle computer power supply. Figure 177 § is the schematic diagram of the monitor control panel; the function of each switch is listed in Table 8. Figure 174 shows the monitor control mounted in its associated rack.

i. Sun-Angle Computer

(1) General

The sun-angle computer (Figure 178) initially was designed to: (a) compute a sun angle; (b) compute elapsed time; (c) provide an index for each photograph; (d) provide a display of computed information for photographic recording and an indexing signal for recording on the instrumentation recorder; and (e) provide the display for playback of data from the instrumentation recorder and a means for selecting readout of single video frames. The elapsed time was to be the time delay between the transmission of the picture taking command and the actual time of exposure of the vidicon. This requirement for the sun-angle computer was cancelled when the side looking, or radially oriented, camera was deleted from the TIROS I system. The precision requirement for the computer was ±0.1 degrees. This, in turn, required an accuracy of 1 part in 400 or 2.5 percent. Each computation was to be made for a 40-degree interval with the multiple of 40 degrees being determined by pulse-width coding.

Initial study phases conducted on the sun-angle computer were directed toward selection of the best approach, digital or analog, for fulfilling the computer requirement. Factors which were considered before selection of the final design approach included the computer precision requirements, the complexity of analog versus digital design, and the compatibility of each technique with other TIROS I subsystems and components. The digital technique was selected because (a) it would be capable of the precision required, (b) design would not be complex since digital modules were available which had excellent reliability figures, and (c) the requirements of the indexing and elapsed time computation were digital in nature and use of the digital approach would permit the entire system to be designed as one unit.

Approximately one second (time between video frames) was available for making the various computations. Since high speed was not a requirement, a serial method of digital computation was implemented. The serial system used fewer components than the comparable parallel systems. Since so much time was available a simple "count up - count down" method of multiplication and division was used.

§ These illustrations are printed on fold-out pages located at rear of this volume.

Table 8. Monitor Control Switching Functions.

Switch	Function
FILM (POS and NEG)	Selects either a positive or a negative picture for filming by energizing the appropriate relay in the display and video amplifier.
DEMOD (IN and OUT)	Determines whether incoming signals to the TV-FM demodulator will be demodulated or not.
DISPLAY (RCVR-TAPE 1, and TAPE 2)	Selects input source for the TV-FM demodulator. When set to RCVR-TAPE 1, the input is either from the TV receiver or tape recorder 1 depending upon the setting of the MONITOR INPUT switch. When the DISPLAY switch is set to TAPE 2, the subcarrier signal from tape recorder 2 is applied to the TV-FM demodulator.
MONITOR INPUT (RCVR and TAPE)	Used in conjunction with DISPLAY switch to select either the TV receiver or tape recorder 1 as the input source for TV-FM demodulator.
TAPE MODE (AUTO and MANUAL)	Turns the program signals which operate the tape recorder on or off.
DC RESTORES (IN and OUT)	Enables the d-c restorer circuit of the TV-FM demodulator when set to IN.
FILAMENTS (ON and OFF)	Turns the tube filaments and blowers in Racks 4 and 5 on or off.
300 VOLTS (ON and OFF)	Turns the three 300-volt power supplies and the 32-volt power supply in Rack 5 on or off.
SUN-ANGLE COMPUTER (ON and OFF)	Turns the sun-angle computer power supply on or off.
HIGH VOLTAGE (ON and OFF)	Turns the high voltage power supply on or off.

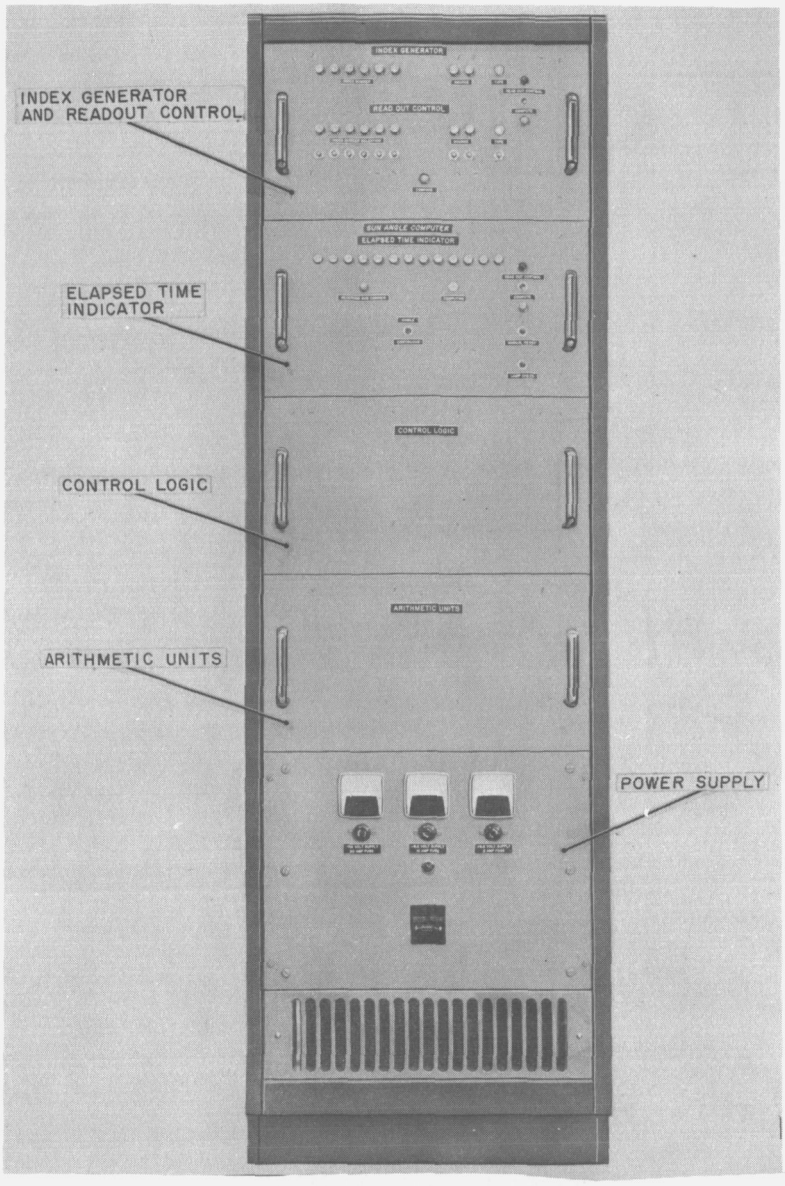

Figure 178. Sun-Angle Computer, Front View

The computer used signals from the command section of the ground station to indicate the source of the incoming video. This information had to come from the ground, since no identifying information was transmitted from the satellite. As each picture was photographed it was counted. Each count sequence started with "1" when the particular data source was initially switched into operation. The one exception to this was when a "direct alternate" camera command was given; in this case, subsequent pictures were counted sequentially, regardless of camera source. This information, along with the sun angle computed from the previous picture, was then recorded on the instrumentation recorder.

The sun-angle computation was not made until the video subcarrier was turned off. Computation had to wait for the end of the subcarrier in order to accommodate the tape playback signal, which was reversed in time; i.e., the first part of the signal corresponding to the shutter pulse was received last.

The data was recorded on the instrumentation recorder on two separate data channels as a series of tone bursts. Each burst was one millisecond long. Since a millisecond space existed between bursts, an index number containing seven binary bits required 13 milliseconds to record. The burst duration was limited to one millisecond so that the data would be recorded within the first 20 milliseconds of the video frame. This was needed for playback purposes. A 70 kc tone was used to correspond to a binary "one" and a 40-kc tone was used to correspond to a binary "zero". These frequencies were chosen to provide as many cycles in the burst as possible, to stay within the recorder bandwidth, and to provide a reasonable spread to make filtering on playback less difficult.

The video subcarrier inputs and the 10-kc bursts of north indicator pulses were amplitude detected. The detection circuitry was designed with vacuum tubes and a transistor output stage. Originally, the signal passed through similar channels consisting of a full wave rectifier, a filter, a diode slicer which acted as a threshold detector, and the driver stage. Later, the diode slicer was replaced by a Schmitt trigger circuit to improve noise immunity and to develop a faster pulse rise time. Initially, in order to stay within the necessary computation accuracy requirements, the bandwidth of this circuitry was established to provide a pulse delay of no more than 1 millisecond. During the operational stages of TIROS I, this pulse delay with its associated noise bandwidth was found to be excessively short. When the transmitters were off, the receiver output noise increased causing false data to be sent to the computer.

Consequently, the pulse detection circuitry was modified to reduce the bandwidth of the north indicator channels to 100 cycles. The subcarrier detector channel was also modified to improve noise immunity.

(2) Functional Description

Figure 179 is a functional block diagram of the sun-angle computer. The index generator provides the frame identification number by counting the read-out pulses; each read-out pulse corresponds to the start of a TV frame. The remaining sections of the computer are used to compute the sun angle, or satellite orientation at the time of picture-taking.

The sun angle is computed by use of the equation $\Theta = 40n - 40t_a/t_b$. The first term, 40n, indicates what section of the satellite is facing the sun; the second term, $40\ t_a/t_b$, refines the section information to provide the actual sun angle.

The index generator consists of a binary counter and a shift register. After each read-out pulse is counted, the pulse number is applied to the shift register where it is shifted out serially to the recording system and to the display indicators.

The sun-pulse decoder categorizes the sun pulses according to length. Each time that a sun pulse is received, it starts a counter and sets a short-pulse flip-flop. The counter continues to count until the sun pulse subsides. If the counter exceeds a specified count, the short-pulse flip-flop is reset and a medium-pulse

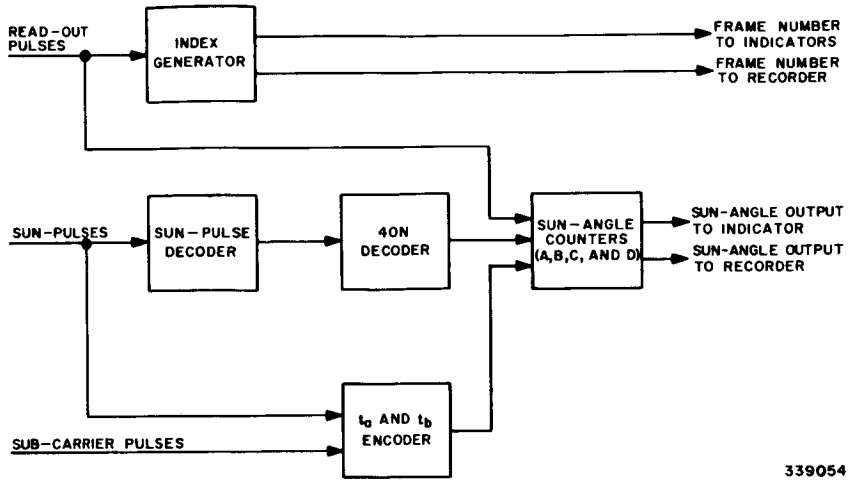

Figure 179. Sun-Angle Computer, Block Diagram

flip-flop is set. Similarly, if the counter exceeds a predetermined maximum count for medium pulses, the medium-pulse flip-flop is reset and a long-pulse flip-flop is set. When the sun pulse terminates, the pulse length data is transferred to a corresponding short, medium, or long 3-bit shift register. Similar action takes place when the second sun pulse is received. The only difference between circuit operation for the first and second pulse inputs is that the length data of the first and second pulses is never applied to the bit of the same shift register. At the end of a subcarrier signal (TV picture) the two bits of pulse-length data are transferred to the 40n decoder.

The 40n decoder checks the length data of each pulse and, when the length data of the pulses is not the same, checks the order of occurrence of the two lengths. Using this information, the decoder computes the coarse sun angle 40n and then ends the computed information to the sun-angle counter. A detailed description of the significance of the pulse lengths and their order in determining 40n, appears in another section of this report.

The t_a and t_b encoder consists of two counter circuits. One counter is gated on by the leading edge of the subcarrier pulse and gated off by the leading edge of the first sun pulse. This counter provides a measure of t_a (Figure 180). The second counter measures t_b. This second counter is turned on by the leading edge of the first pulse and gated off by the leading edge of the second pulse. The rate-of-count of the counters is different in order to make the computation of $40t_a/t_b$ simpler. The 40 t_a and the t_b information is applied to the sun angle counters.

The sun-angle counters do not start computations until the end of a video frame. Thus, the 40n, the 40 t_a, and the t_b information is already stored before the calculations are commenced. Each of the three quantities is stored in a separate counter. When the end-of-frame is sensed, clock pulses are applied to an "add" counter and to the 40 t_a counter. Each pulse increases the "add" counter reading by

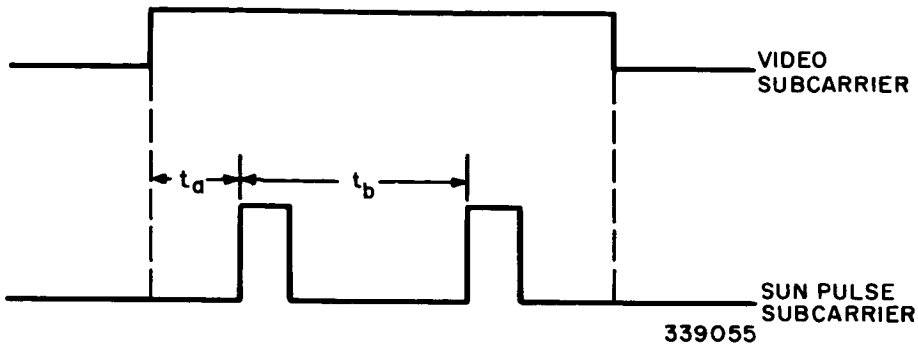

Figure 180. Sun-Pulse Waveforms and Significant Timing

one and decreases the 40 t_a counter reading by one. When the "add" counter reading equals the t_b counter reading, one count is subtracted from the 40n counter and the "add" counter is reset to zero. Successive pulses again advance the "add" counter from zero while also continuing to decrease the $40t_a$ counter reading. When the "add" counter reading is again the same as the t_b reading, another count is subtracted from the 40n counter and the "add" counter is reset. This add-up, subtract-one, and reset operation continues until the reading of the 40 t_a counter is decreased to zero. At that time, the quantity still left on the 40n counter is equal to the sun angle and is read out as such. Thus the computation $40n - 40\ t_a/t_b$ is performed. The computed sun angle is applied to the display indicators and to the instrumentation recorder.

In order to reduce the time required for this computation, certain modifications of this add-up, subtract, and reset operation are used in the actual sun-angle computer. Figure 181[§] is the logic diagram of the sun-angle computer. The schematic diagrams of the index tone generators and the demodulators are shown in Figures 182 through 185. The diagram of the readout control gate is shown in Figure 186.

A detailed description of the circuit operation is given in the Instruction and Operating Handbook, TIROS I Meteorological Satellite System. (Reference 20)

[§] This illustration is printed on a fold-out page located at rear of this volume.

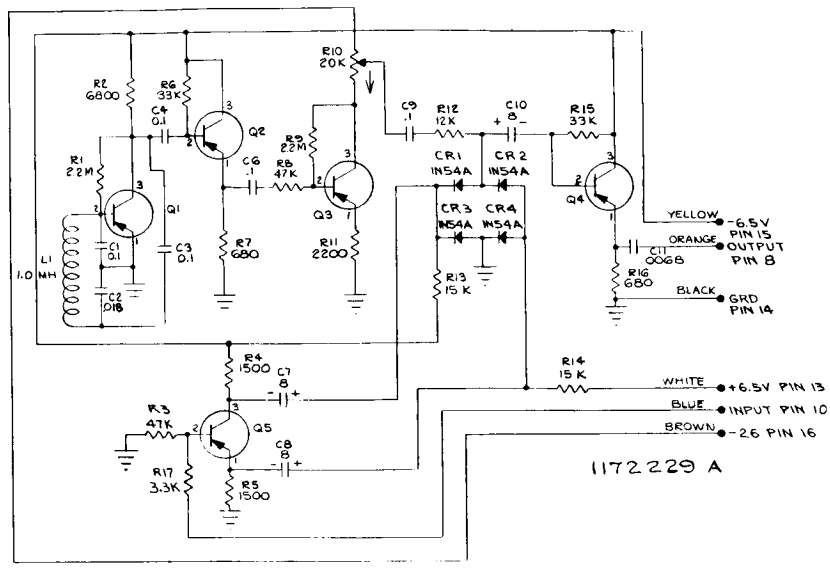

NOTE
ALL RESISTORS $\frac{1}{2}$ W. ± 5% UNLESS NOTED
ALL CAPACITORS IN MICROFARADS
ALL TRANSISTORS ARE TYPE 2N219

ALL RESISTORS ARE IN OHMS UNLESS NOTED
FOR PARTS LIST REFER TO DWG A-1170243.

Figure 182. Index 40-kc Tone Generator, Schematic Diagram

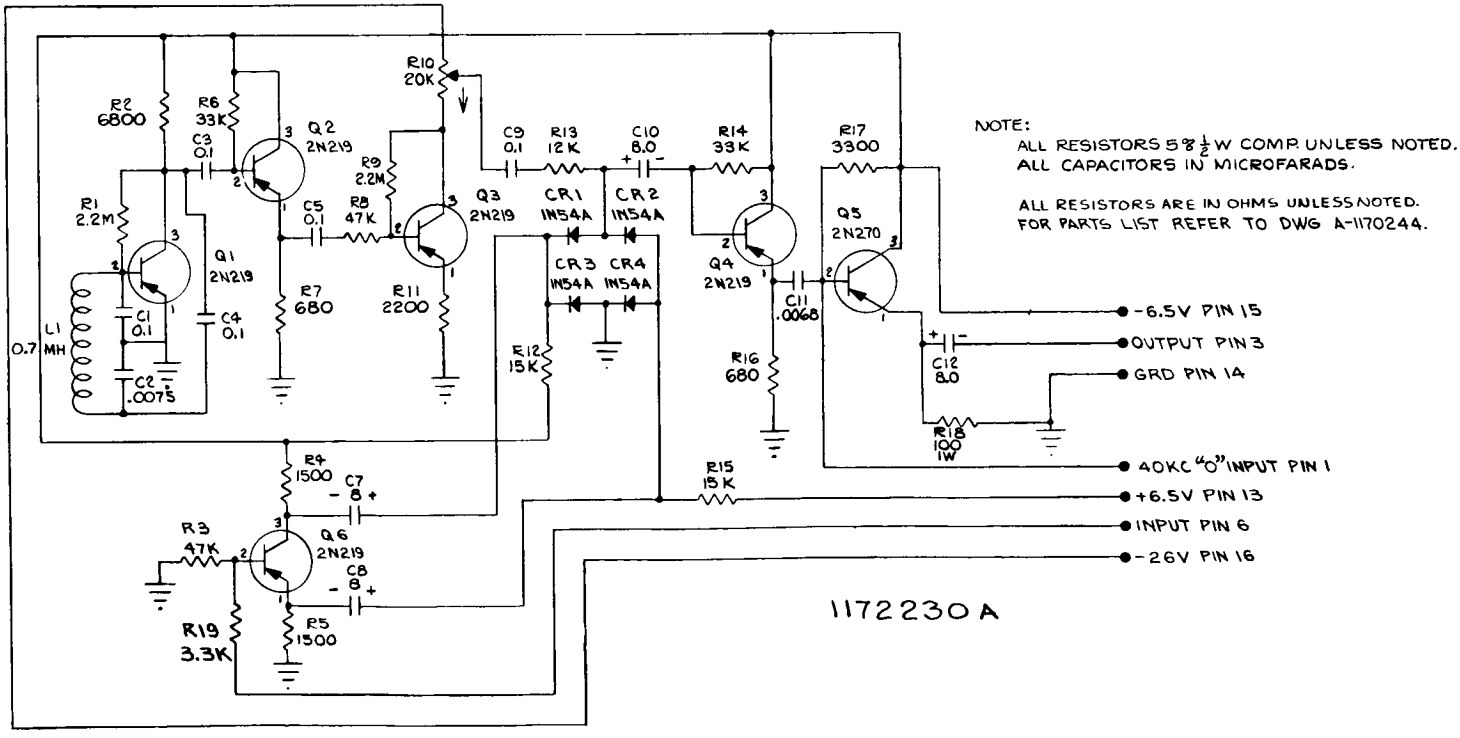

NOTE:
ALL RESISTORS 5% $\frac{1}{2}$ W COMP. UNLESS NOTED.
ALL CAPACITORS IN MICROFARADS.

ALL RESISTORS ARE IN OHMS UNLESS NOTED.
FOR PARTS LIST REFER TO DWG A-1170244.

Figure 183. Index 70-kc Tone Generator, Schematic Diagram

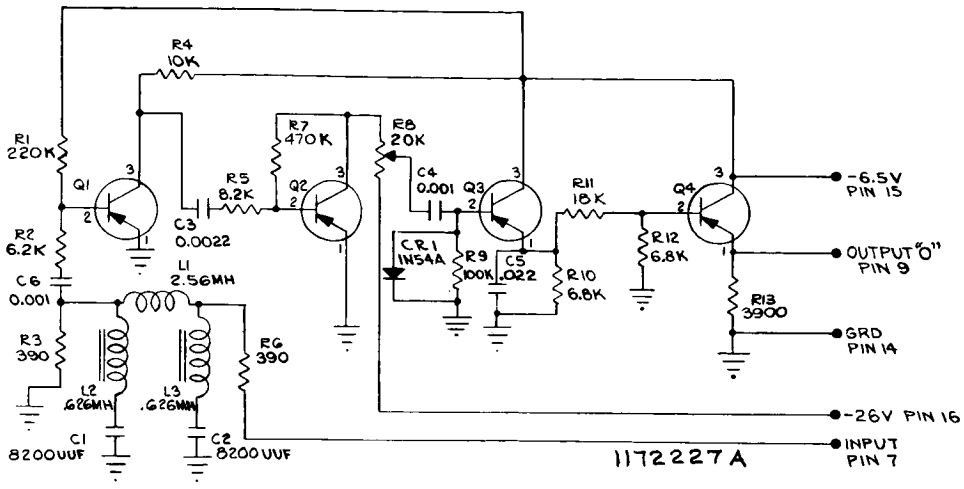

NOTE
ALL RESISTORS ½ W. ± 5% UNLESS NOTED
ALL CAPACITORS ARE IN MICROFARADS
ALL TRANSISTORS ARE TYPE 2N219
ALL RESISTORS ARE IN OHMS UNLESS NOTED
FOR PARTS LIST REFER TO DWG A-1170241

Figure 184. Index 40-kc Tone Demodulator, Schematic Diagram

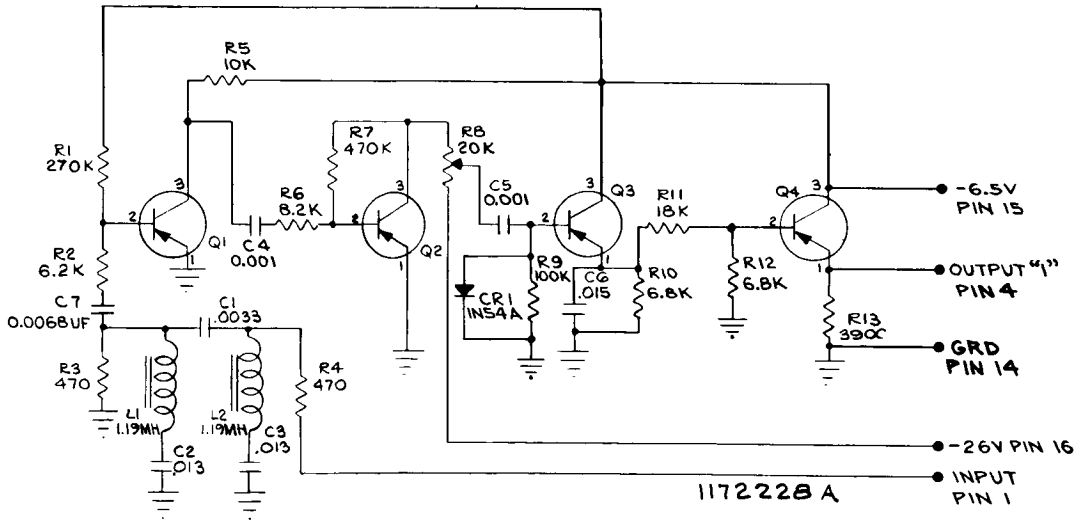

NOTE
ALL RESISTORS ½ W. ± 5% UNLESS NOTED
ALL CAPACITORS ARE IN MICROFARADS
ALL TRANSISTORS ARE TYPE 2N219
ALL RESISTORS ARE IN OHMS UNLESS NOTED
FOR PARTS LIST REFER TO DWG A-1170242

Figure 185. Index 70-kc Tone Demodulator, Schematic Diagram

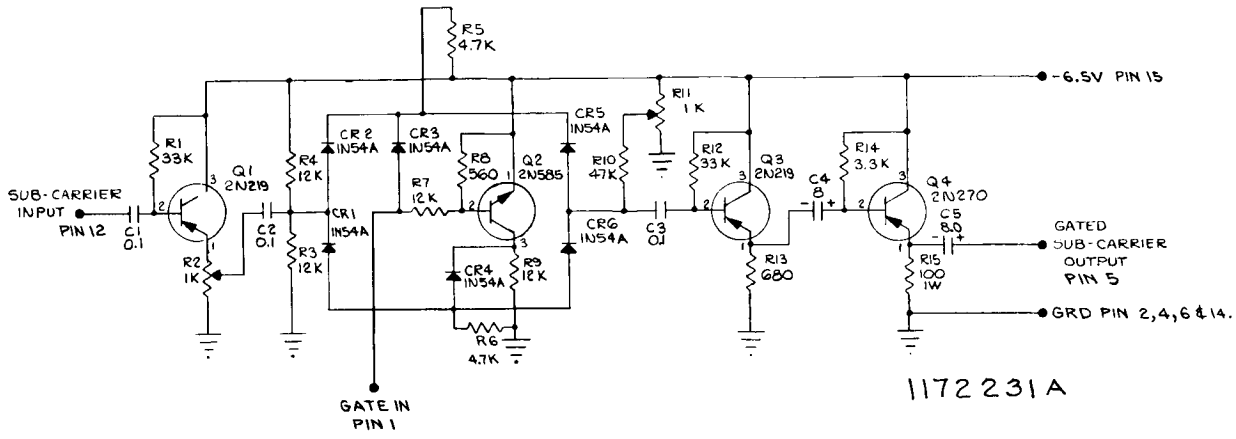

NOTE:
FOR PARTS LIST REFER TO DWG A-1170245.

Figure 186. Readout Control Gate, Schematic Diagram

j Calibrator

(1) General

The operational requirements of the TIROS I ground station called for test and calibration equipment to be used with the primary ground station equipment in three phases of operation. These were the system set-up and calibration, the satellite pre-pass check, and trouble-shooting. These functions overlapped and complemented each other in helping to maintain the equipment in good order. Wherever possible, calibration equipment was designed to be useful in more than one of these phases. Also, the built-in or inherently self-checking features of portions of the ground station were utilized.

The pre-pass check was intended to be a rapid, qualitative verification of ground station performance. This check was also necessary for the determination of station status before launch. The check required a minimum disturbance of station equipment connections and settings, in order to reduce the probability of accidental failure in remaking the connections or in returning controls to their operational settings.

The set-up and calibration tests were designed to allow all necessary qualitative and quantitative adjustments to be made. These tests were to be used after installation of the equipment, and then periodically or as a need for them was indicated by the pre-pass check.

The trouble-shooting tests were intended for use as needed to analyze and verify correction of any difficulties with the ground station equipment. The tests to be used for this purpose were necessarily many and varied because of the difficulty in predicting the type of malfunction which might be encountered.

In most cases these tests and measurements had to be improvised based on an understanding of ground station equipment operation, and had to be made with the assistance of general purpose test equipment.

For much of the ground station equipment, correct operation was either self-evident or amply specified by the applicable instruction book. The ground equipment characteristics which were especially significant and which required specially designed test equipment were as follows:

(a) TV Monitor Synchronizing Circuit Adjustments – These adjustments had to be set for an optimum compromise between stability in the presence of noise and short lock-in time at the beginning of a frame.

(b) Picture Size and Aspect Ratio – The picture "squareness" was an especially stringent requirement since even slight misadjustment caused distortion of the TV pictures. This distortion would greatly increase the difficulty of locating significant picture elements on the earth.

(c) Vertical and Horizontal Sweep Linearity. The linearity of the sweep circuit was not normally adjustable. Non-linearity owing to a malfunction would cause distortion of the TV pictures as outlined in (b).

(d) Brightness Level – It was necessary to set the brightness so that, with the video signal from the satellite ranging between the anticipated maximum black and maximum white levels and with normal film processing, the video information would fall within the usable density range of the film.

(e) Density Linearity – In connection with requirement (d) it was important that equal, small changes in video voltage should effect corresponding equally discernible changes in density of the film over the usable range. Both brightness level and density linearity had to be dependently established for positive and negative pictures.

(f) Focus – Both the electrical focus of the kinescope and the optical focus of the 35-mm camera had to be set for maximum sharpness of the 35-mm film image.

(g) Sun-Angle Computer (SAC) Operation - Independent determination of proper operation was necessary for three phases of the sun angle computation ($40n - 40t_a/t_b$). These were:

1. Measurement of sun pulse duration to determine whether each was a short, medium, or long pulse.
2. Decoding of sun pulse sequence to determine 40n.
3. Measurement of 40 t_a and t_b, division of 40 t_a by t_b, and subtraction of the quotient from 40n.

To meet most of the pre-pass check, setup, and calibration objectives for the TV and sun-angle subsystems, a signal simulation method was used. To allow substitution of signals at the key points in the TV system signal path, certain cables were routed through pairs of normally jumpered connectors on a patch-panel. Removal of a jumper on this panel interrupted the signal at that point and gave access to the incoming and outgoing signal lines for substitution or observation.

Jumpered in this manner on the patch panel were the r-f input cables of the two TV and two IR receivers, the outputs of the TV and IR diversity combiners, and the output of the high-pass filter that fed the TV subcarrier to the TV-FM demodulation circuitry. The latter could be used for substitution of TV subcarrier or, bypassing the TV-FM demodulator circuitry with a relay provided internally for this purpose, a video signal could be substituted directly.

The diversity combiner output jumpers allowed the TV and IR receivers to be interchanged or allowed simulated TV subcarrier and sun pulses to be substituted. Finally, for the most comprehensive check, an r-f signal, modulated with TV subcarrier and sun pulses, could be substituted for the antenna signal at one of the receiver inputs. With signal substitution at the above points, the two tape recorders could be checked for proper recording and playback of TV subcarrier, index, sun pulses, etc.

The simulated video, subcarrier, and sun pulses used in the substitution checks were generated by a calibrator unit which modulated an FM signal generator to establish the simulated composite TV signal.

The video generator portion of the calibrator was originally designed to be capable of generating two types of signal:

1. a pattern of equidistant vertical and horizontal lines for checking kinescope display size, aspect ratio, sweep linearity, and focus; and
2. a pattern of areas of graduated brightness for checking brightness level and density linearity.

It was found possible, however, to combine the necessary features into a single test pattern (Figure 187) consisting of vertical bars graduated in brightness from

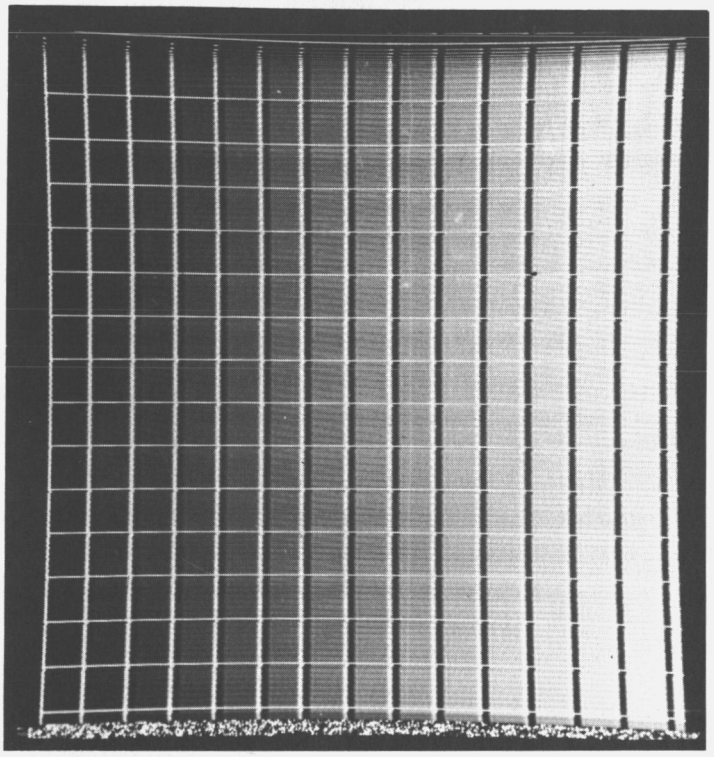

Figure 187. Video Test Pattern

one end of the pattern to the other. Between each pair of bars, or density steps, two narrow adjacent lines were added, one black and the other white, to provide a sharply visible edge between the two for focus and resolution checks. The uniform spacing of these pairs of lines allowed horizontal linearity to be checked; another set of uniformly spaced white lines was superimposed on the pattern in the horizontal direction to allow vertical sweep linearity to be checked.

The calibrator video generator was built with digital counting circuits. These counting circuits, used to generate the timing intervals necessary to ensure consistent spacing between horizontal and vertical lines in the video test pattern, were built up by interconnecting standard transistorized circuit modules to realize high reliability and minimize the amount of new circuit design necessary. The power supply for these modules, and the chassis assembly to house them, were also standard units. The non-digital portions of the calibrator were mounted on the same chassis as the circuit modules and were designed with transistors to allow use of the same power supply.

The subcarrier oscillator (SCO) was an astable multivibrator with an oscillating frequency variable from 70 kc to 100 kc by controlling the voltage applied to the base resistors of the two transistors. To obtain modulated subcarrier, the output of

the calibrator video generator (or any other video test signal) was connected to the input of the SCO portion of the calibrator where it was amplified and then used to control the multivibrator bias voltage.

The sun-pulse portion of the calibrator used some of the timing signals of the video generator section, and some of the same types of digital modules. Two successive timing pulses were generated at predetermined intervals from the beginning of the two-second subcarrier gate. Each of these pulses could be made to trigger any one of the three one-shot circuits. Selection of the desired triggering sequence was made by use of a nine-position switch. The three one-shots were adjusted to give pulse durations equalling those of short, medium, and long sun pulses, respectively. Finally, the one-shot outputs were used to gate the output of a 10-kc oscillator. The resultant sun-pulse tone bursts were combined in the calibrator with the output of the 70- to 100-kc subcarrier oscillator in approximately a 1 to 10 ratio.

To allow inclusion of the TV receivers in overall system tests and to permit other tests and calibration of the TV and IR receivers, an SG-3/U signal generator was employed. This unit was chosen primarily because of its capability of modulation at the TV subcarrier frequency. For simulating the TV signal of the satellite, the generator was externally FM modulated at 150-kc deviation with the calibrator SCO output.

For the determination of proper ground station TV subsystem focus, as well as for a proper camera shutter and magazine operation, the most positive and accurate method was to take a series of test frames on 35-mm film. Thes test frames were then processed and examined under magnification. To permit a more rapid check of focus, two special features were provided in the ground equipment. First, a relay was provided on the sawtooth and deflection unit to permit removal of power from the vertical deflection circuit; the relay could be energized by a push-button on the front panel of the unit. When so actuated, the kinescope display was reduced from a complete raster to a single stationary line across the center of the screen. The electrical focus control could then be adjusted to minimize the width of this line.

Second, a magnifying eyepiece was designed to mount in place at the viewing hood on the display unit. This gave an enlarged view of the line on the face of the kinescope. To check camera focus as well, an adapter plate, with a ground glass surface located in what would normally be the film plane, was mounted on the camera instead of the film magazine. The magnifying eyepiece could then be used to view the image of the kinescope display line on the ground glass surface.

Another special circuit was built into the ground station to provide a simple check on kinescope brightness, film development, and any other factors affecting image density on the film. A push-button actuated relay could be energized to replace the video signal by a d-c voltage which was midway between the normal picture black level and white level. Another set of contacts on this relay opened the camera shutter and initiated a vertical sweep of the kinescope.

(2) Functional Description

The calibrator is composed of three major sections; namely, the video generator, the subcarrier escillator, and the sun-pulse simulator. Figure 188[§] is a block diagram of the calibrator.

The video generator generates a video test pattern; each test frame consists of 500 lines and has a duration of two seconds. The test pattern lines are shaded in steps from black to white for checking linearity, contrast and resolution.

The basic calibrator operating frequency is generated by the 4-kc clock generator, which is adjusted by the FRAME PERIOD control to establish a frame period of 2 seconds. The output of the clock generator is fed to a series of 13 flip-flops (2 through 14) which count down to the frame period in steps of two. Outputs are taken from various groups of these flip-flops to produce horizontal blanking, vertical blanking, white lines, and black-to-white staircase signals.

Horizontal blanking signals are produced for each line when flip-flops 3 through 5 and either the clock generator or flip-flop 2, or both, are in the "one" state (-12 volts output) as determined by AND gates 1 and 2. The outputs of these AND gates are inverted by amplifier-inverter 5 and then applied to the combining gate where the composite video is developed.

Shading of the horizontal lines is produced in steps by a staircase signal which is developed in a resistance ladder from the combination of the outputs from flip-flops 2 through 5. The level of the resistor ladder output decreases in steps from its maximum (black) level, in which all flip-flops are in the "zero" state, to its minimum (white) level, in which all flip-flops are in the "one" state. Table 9 lists the status of each flip-flop for each step of the ladder; the minimum or white level is controlled by the "step margin" control. The output of the resistor ladder is applied to the combining gate where it is used to develop the shading of the horizontal lines.

A white spike followed by a black spike precedes the step changes on each line of the composite video (Figure 189). The white spike is developed by one-shot multivibrator A which is triggered by the clock generator; the black pulse is produced by one-shot multivibrator B which is triggered by the trailing edge of the white spike. The width of the black and white spikes are adjusted by the "spike width" controls on their respective multivibrators. The outputs from the one-shot multivibrators are applied to the combining gate and take precedence over the staircase signal in the composite video.

Every 32nd line of the composite video is all white. The white lines are produced when AND gate 3 receives a "one" input from each of flip-flops 6 through 10 (Table 9). The white line input to the combining gate takes precedence over the black spike staircase signal (Figure 189). The "white level" control sets the white level of the line.

[§] This illustration is printed on a fold-out page located at rear of this volume.

TABLE 9. LOGIC TABLE FOR COMPOSITE VIDEO

A STATUS OF STAGES					LADDER	B STATUS OF STAGES					
CLOCK GENERATOR	Flip Flop 2	Flip Flop 3	Flip Flop 4	Flip Flop 5	OUTPUT	Flip Flop 6	Flip Flop 7	Flip Flop 8	Flip Flop 9	Flip Flop 10	
0	0	0	0	0	black	0	0	0	0	0	
1	0	0	0	0	level	1	0	0	0	0	
0	1	0	0	0	1st	0	1	0	0	0	
1	1	0	0	0	step	1	1	0	0	0	
0	0	1	0	0	2nd	0	0	1	0	0	
1	0	1	0	0	step	1	0	1	0	0	
0	1	1	0	0	3rd	0	1	1	0	0	
1	1	1	0	0	step	1	1	1	0	0	
0	0	0	1	0		0	0	0	1	0	
1	0	0	1	0		1	0	0	1	0	
0	1	0	1	0		0	1	0	1	0	
1	1	0	1	0		1	1	0	1	0	
0	0	1	1	0		0	0	1	1	0	
1	0	1	1	0		1	0	1	1	0	
0	1	1	1	0		0	1	1	1	0	
1	1	1	1	0		1	1	1	1	0	
0	0	0	0	1	4th to	0	0	0	0	1	
1	0	0	0	1		1	0	0	0	1	
0	1	0	0	1	13th	0	1	0	0	1	
1	1	0	0	1	steps	1	1	0	0	1	
0	0	1	0	1		0	0	1	0	1	
1	0	1	0	1		1	0	1	0	1	
0	1	1	0	1		0	1	1	0	1	skip
1	1	1	0	1		1	1	1	0	1	
0	0	0	1	1		0	0	0	1	1	
1	0	0	1	1		1	0	0	1	1	
0	1	0	1	1		0	1	0	1	1	
1	1	0	1	1		1	1	0	1	1	
0	0	1	1	1	14th	0	0	1	1	1	
1	0	1	1	1	step	1	0	1	1	1	
0	1	1	1	1	Horiz.	0	1	1	1	1	white
1	1	1	1	1	blank.	1	1	1	1	1	line

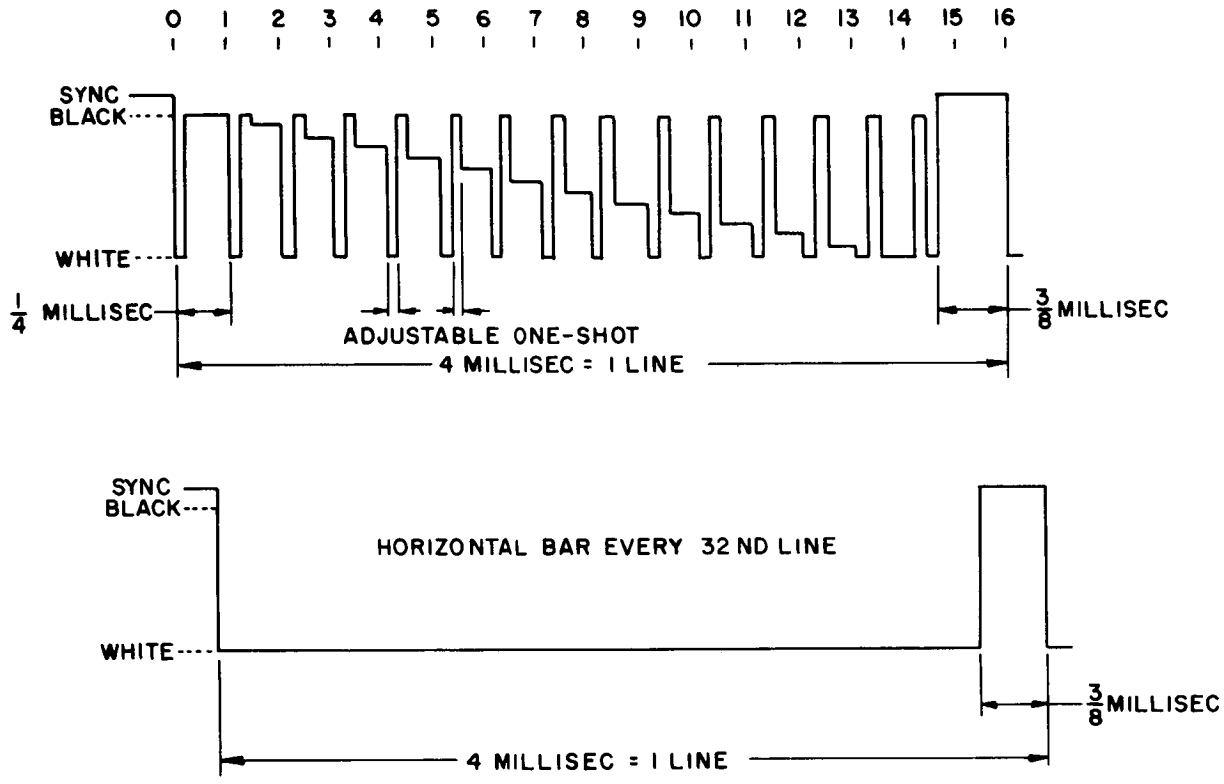

Figure 189. Composite Video for One Line

Vertical blanking is produced for each frame period when flip-flops 11 through 14 are in the "one" state as determined by AND gate 4 (Table 10). The AND gate output is inverted by amplifier-inverter 6 and applied to the combining gate. To limit the frame period at 500 lines, a skip signal is provided to eliminate the last 12 lines of the possible 512. The frame period consists of 15 groups of 32 lines each and 1 group of 20 lines. The skip signal is developed by AND gate 5 when flip-flops 7 and 10 are in the "one" state and cause flip-flops 8 and 9 to change to the "one" state during vertical blanking.

The output of the combining gate is fed through several emitter follower stages and applied to the output as a video test pattern. The 85-kc subcarrier oscillator produces a c-w signal whose frequency is variable between 70 and 100 kc. This signal, provided for checking the monitor system, is modulated by the video composite signal developed in the video generator.

The video composite signal is used only to frequency-modulate the 85-kc oscillator when switch S2 is in the "ungate" position. When the switch is in the "gate" position, the oscillator is turned on for two seconds and then off for two seconds by flip-flop 1 in addition to the frequency modulation. Flip-flop 1 is triggered

TABLE 10. LOGIC TABLE FOR VERTICAL BLANKING AND SUN PULSES

FLIP - FLOP STATUS				OUTPUT
11	12	13	14	
0	0	0	0	2 SECONDS (ONE FRAME)
1	0	0	0	
0	1	0	0	
1	1	0	0	FIRST SUN PULSE
0	0	1	0	
1	0	1	0	
0	1	1	0	
1	1	1	0	
0	0	0	1	
1	0	0	1	SECOND SUN PULSE
0	1	0	1	
1	1	0	1	
0	0	1	1	
1	0	1	1	
0	1	1	1	
1	1	1	1	VERTICAL BLANKING

by the output of flip-flop 14. The subcarrier is switched off for two seconds to provide time for the camera to advance the film and cock the shutter. Adjustment controls are provided for adjusting the symmetry of the subcarrier waveform, the oscillator center frequency, and the subcarrier amplitude.

The sun-angle simulator section of the calibrator generates 10-kc bursts which simulate the sun pulses. Two sun pulses (in one of nine combinations of short, medium, and long duration) are generated at different times during the two-second frame period.

When flip-flops 11 and 12 are in the "one" state and flip-flops 13 and 14 are in the "zero" state, AND gate 6 initiates the first sun pulse (See Table 9). When flip-flops 11 and 14 are in the "one" state and flip-flops 12 and 13 are in the "zero" state, AND gate 7 initiates the second sun pulse. The sun-pulse outputs of these

two AND gates are inverted by their respective amplifier inverters and applied to a 9-position two gang selector switch. The switch permits selection of any one of nine sun-pulse combinations; for example, pulse 1 short and pulse 2 medium, etc.

The selector switch routes the first and second sun pulses to the selected OR gate-multivibrator combination. Each sun pulse triggers the multivibrator to which it is applied to produce the corresponding short, medium, or long pulse. The outputs of the OR gate multivibrator circuits are passed through OR gate 2, inverted and applied to AND gate 8. When a sun pulse is present, the AND gate passes a 10-kc burst of oscillations from the 10-kc generator to the output. The length of the burst is the same as the length of the pulse input; that is, short, medium, or long. Controls are provided for setting the actual width of each of the three types of pulses as well as the amplitude of the pulses.

Figure 190[§] is the schematic diagram of the calibrator.

k. Attitude Pulse Demodulator

(1) General

The attitude pulse demodulator (Figure 191) was designed to receive the 3-kc output pulses from the telemetry receivers, to demodulate and re-form these pulses, and then to apply these pulses to the elapsed time counter-scanner. The unit also received an input from the WWV receiver which was used as a time reference for the elapsed time counter-scanner.

In order to make the demodulator insensitive to the desired receiver volume level, the input was controlled by an audio AGC circuit which used a transistor as a variable impedance for shunting the input. A special sampling circuit, consisting of a delay multivibrator and an AND gate, was included in the unit to prevent the demodulator from sending triggers to the elapsed time counter-scanner in response to short bursts of noise. The outputs of the demodulator were 0.5 millisecond, negative-going pulses.

A front panel selector switch was provided to permit input selection. In one position of the switch, the 3-kc attitude signals from the telemetry receiver were applied to the demodulator input; when the switch was in the other position, the 1-kc tone bursts which originated in the WWV receiver were applied to the input. The attitude pulse demodulator was designed to have the same output, regardless of which input was selected. This ensured that one-second readings could always be produced on the counter-scanner punched-tape output.

(2) Functional Description

Figure 192 is a block diagram of the attitude pulse demodulator. A 3-kc, 100-millisecond tone burst is applied to the amplifier input of the attitude pulse demodulator. After amplification the 3-kc burst is applied to the 3-kc bandpass filter

§ This illustration is printed on a fold-out page located at rear of this volume.

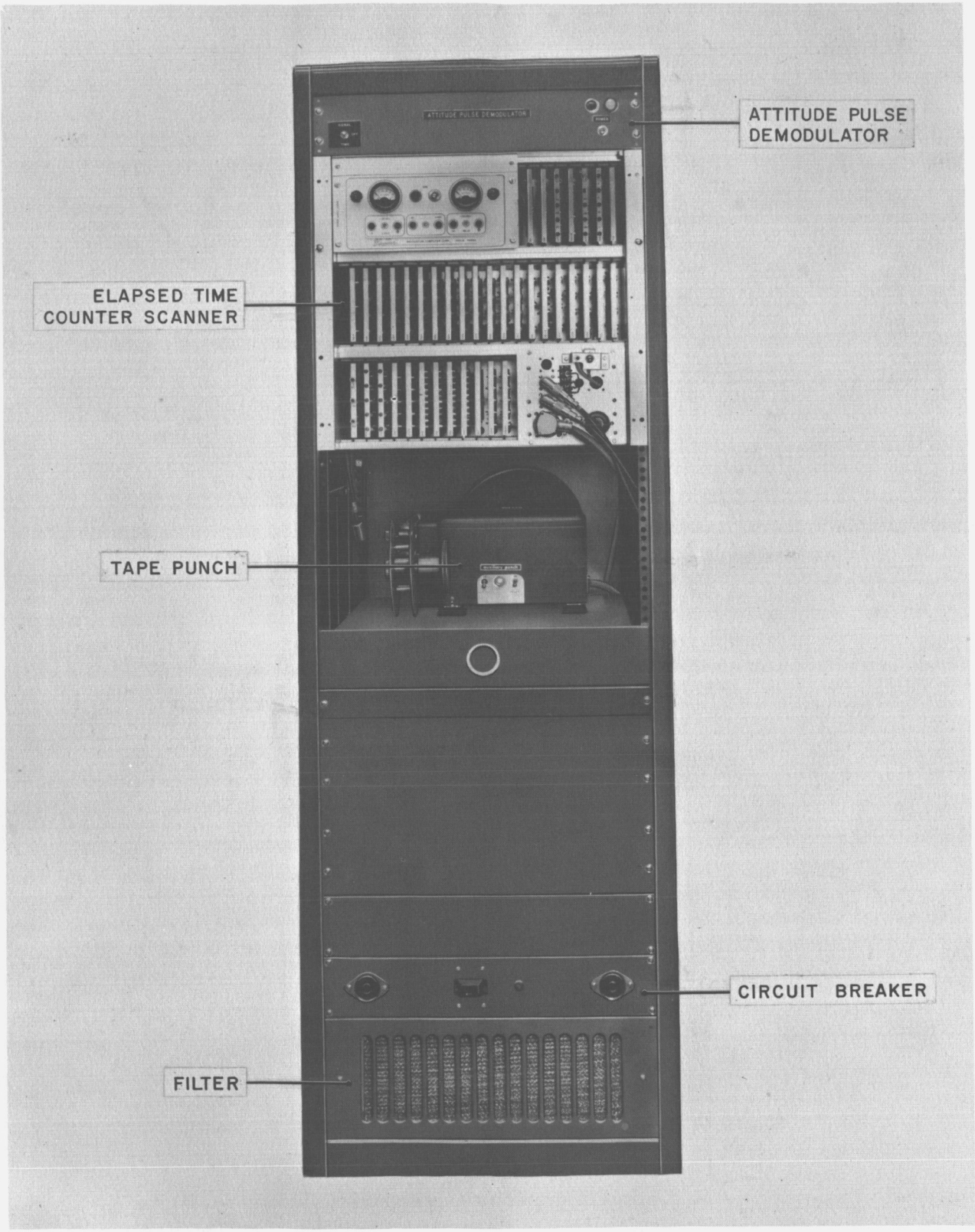

Figure 191. Attitude Recorder Rack

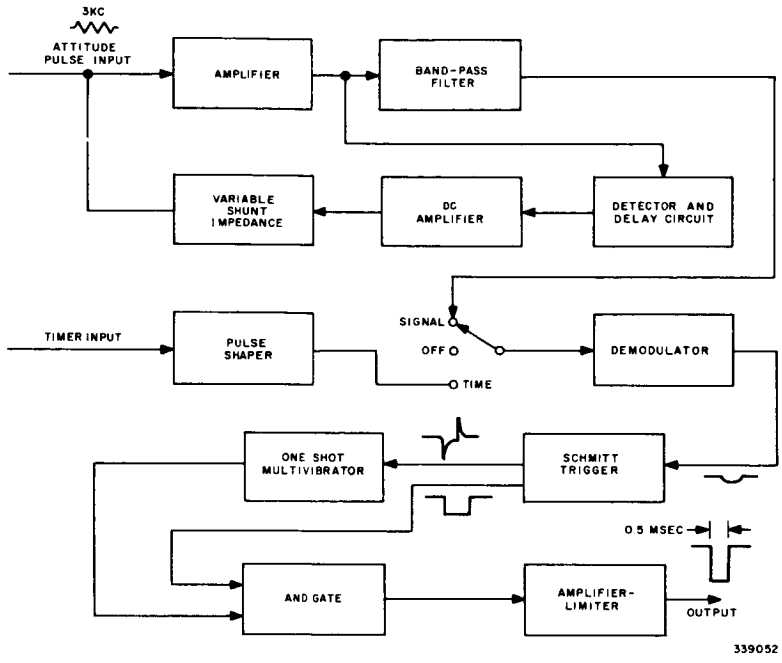

Figure 192. Attitude Pulse Demodulator, Block Diagram

and to the detector and delay circuit. The detector and delay circuit, the d-c amplifier, and the variable shunt impedance form an audio AGC. The AGC circuit effectively reduces the average input level to the amplifier; the delay circuit prevents AGC action from affecting the relatively short attitude pulses.

Timer inputs (from the WWV receiver) are shaped by a pulse shaper and then applied to the TIME contact of a three-position selector switch. The selector switch permits selection of either the "signal" input or the "time" input and applies the selected signal to the demodulator circuit. The output of the demodulator circuit is integrated and applied to the Schmitt-trigger where it is shaped into a negative-going squarewave. Adjustment controls, provided within the Schmitt-trigger circuit, to permit control over the triggering level and thus prevent premature triggering due to noise signals. The Schmitt-trigger has two outputs. One output, a squarewave, is applied to the AND gate. The other output, a differentiated version of the same squarewave, is used to trigger the one-shot multivibrator. The one-shot provides a 2.5-millisecond delay; the output of this multivibrator is applied to the AND gate.

The AND gate ensures that the output from the one-shot is a result of an actual signal input to the Schmitt-trigger and not the result of a noise input. The output of the AND gate is applied to an amplifier-limiter which develops the negative-going, 0.5 millisecond output pulse.

A 24-volt power supply module is also contained on the attitude pulse demodulator. An ON/OFF switch, a fuse, and an indicator lamp which are associated with this power supply are located on the front panel of the attitude pulse demodulator. Figure 193§ is the schematic diagram of the attitude pulse demodulator.

I. Elapsed Time Counter — Scanner

(1) General

The elapsed time counter-scanner was used to measure the time interval between the attitude pulse outputs of the horizon sensing circuit in the satellite, and to drive a tape punch which presented this information, in teletype code, on paper tape. In addition, the counter-scanner had to provide a means of determining the "real time" at which each attitude pulse was received. It was required that the unit measure the time interval to within one millisecond and that the unit be capable of measuring intervals of up to 10 seconds. Figure 191 shows the elapsed time counter-scanner mounted in its associated rack.

The 1-millisecond resolution requirement was met by using a 1-kc clock generator to drive 4-stage decimal counters. Each decimal counter was equipped to provide binary outputs for use by the tape-punch control circuits. A tape-punch mechanism was selected over other read-out media because the punched tape could be inserted into a standard message reader and the attitude data could be immediately transmitted to the NASA Space Operations Control Center.

Due to the speed limitations of ordinary tape-punch mechanisms, up to 700 milliseconds was required for the tape punch to read out the time interval information. Since the time between successive attitude pulses was expected, in some cases, to be less than the 700-millisecond read-out time, a system had to be developed that would permit one time interval to be read out while a second interval was being stored and while a third interval was being counted. Accordingly, a three-counter scheme, in which storage was provided by the third counter stage, was adopted for use in TIROS I.

Use of this scheme permitted simpler logic and at the same time provided added interchangeability of parts. The elapsed time counter-scanner which resulted was one in which sequential switching of counters was used. Switching logic was included so that each of the counters could be read out in turn, and so that read out of one counter could not be started until read out of the previous counter had been completed.

Provisions were made to have the unit recycle as soon as any counter reached its maximum capacity of 10 seconds. This facilitated keeping track of real time in that, in the absence of inputs, the counter-scanner produced 10-second read-outs on the punched tape.

In order to ensure that the counter-scanner would not lose track of real time, input control logic was added to the unit. The control logic sampled storage

§ This illustration is printed on a fold-out page located at rear of this volume.

memories and, whenever two intervals were already in storage, inhibited any additional attitude pulse inputs. The control logic was designed to maintain this inhibit condition until one of the intervals was fully read out and the associated counter was ready to begin counting another interval. Although this technique resulted in the loss of certain attitude pulses, it prevented loss of real-time.

(2) Functional Description

Figure 194 is a block diagram of the elapsed time counter-scanner. The input to the unit is either attitude pulses or timing pulses from the attitude pulse demodulator. The output of the unit, the time interval between successive inputs, is presented in Baudot code to the tape punch. In addition to the Baudot-coded output, the unit supplies line feed, carriage return, and figures inputs to the tape punch.

When power is applied to the unit, 3-kc pulse signals are applied to the 3-to-1 divider and emerge as a series of 1-kc pulses. These 1-kc pulses are applied through the gating circuit to counter A and to memory circuit A. Each pulse causes the counter to advance one step (1 millisecond). The first pulse sets memory circuit A to the memory state. When an attitude or timing pulse is received, it is applied through the input control circuit to the input gating circuit. In response to this input, the gating circuit cuts off the 1-kc pulse inputs to counter A and applies them to counter B and memory circuit B. Counter A stops counting and counter B starts counting.

The pulse inputs to memory circuit B set that circuit to the memory state. The scan logic circuit senses that both A and B are in memory and that the A count is complete while the B count is in process. Accordingly, the logic circuit sends a scan counter-A signal to the counter gating circuit and a start-scan signal to the scan control gate. Upon receipt of these signals the counter gating circuit connects the binary output of counter A to the decimal encoder and the scan control gate connects the 10-pps output of the 100-to-1 divider to the shift register.

The first four shift pulses from the shift register cause the decimal encoder to read out, in most-to-least significant order, the seconds, deciseconds, centiseconds, and milliseconds stored in counter A. The encoder converts the binary outputs of the counter into their decimal, 10-line equivalents. The teletype encoder receives each set of decimal inputs and converts them to the Baudot system. The output of the teletype encoder causes the tape punch to record, in most-to-least significant order, the time interval counted by counter A.

The fifth shift pulse causes the tape punch to advance the tape one line. The sixth and seventh shift pulses, respectively, cause the tape punch carriage to return and cause the tape punch to prepare for punching out the time-interval figures counted by counter B. Thus, at the end of 0.7 seconds (700 milliseconds), the readoutprocess is completed. Upon completion of the readout, the shift register sends an end-of-scan signal to the scan logic circuit, which causes the logic circuit to turn

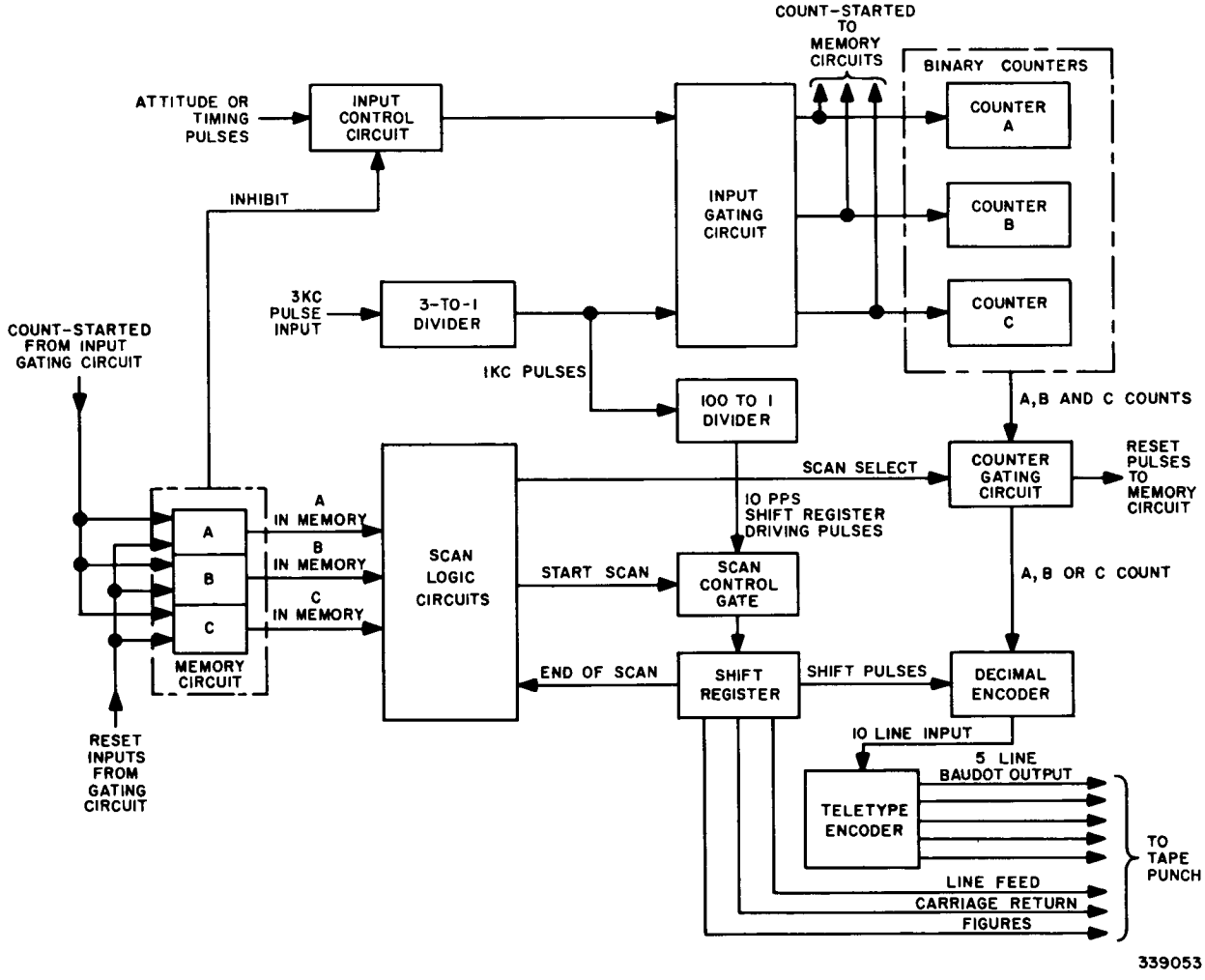

Figure 194. Elapsed Time Counter-Scanner, Block Diagram

off the scan gate. Also at the completion of readout, the counter gating circuit sends a reset pulse to memory circuit A which removes the A-in-memory input to the scan logic. In addition, each time that a readout is completed, the counter which was read out is reset.

When another attitude or timing pulse input is received, counter B is turned off and counter C starts. If this third input is received before readout of counter A is completed, the memory circuit senses that all three counters are in use and sends an inhibit signal to the input control circuit. This inhibit signal remains, and any additional inputs are blocked, until counter A readout is completed and memory circuit A is reset. Once counter A has been reset, the succeeding pulse input will cut-off counter C and start counter A. Thus, although an input might be lost, counter C is not turned off until counter A is again ready to start counting. This ensures that real-time continuity is not lost. Readout and inhibit operations are the same regardless of which counters are counting or are being read out.

For the schematic diagram of the elapsed-time counter-scanner and a detailed description of circuit operation, refer to the Instruction and Operating Handbook for TIROS I Meteorological Satellite System. (Ref. 20)

7. Ground Station Antenna System

Discussion of the antenna system installations at the Fort Monmouth, Kaena Point, and Princeton Command and Data Acquisition Stations involve classified information and therefore is included in the classified supplement to this report.

8. Tape Recorders

Two four-channel magnetic tape recorders were used at each TIROS I Command and Data Acquisition station for storage of the received video data. Recorders having suitable characteristics, such as low "wow" and flutter, wide bandwidth, high signal-to-noise ratio, and adequate recording time, were available commercially. The recorders selected were the Ampex Model FR 104.

It was recognized at the outset that the greatest problem would be the recording of the subcarrier video, which is 70 kc for white signals and 100 kc for black signals. Little trouble was anticipated in recording of the index and computed sun angle information which was in the form of binary coded bursts of 40 and 70 kc. Similarly, very little trouble was anticipated in the recording of the 10-kc raw sun pulse information.

The maximum deviation rate of the subcarrier was 62.5 kc. Since the nominal frequency of the subcarrier was 85 kc, the deviation rate resulted in upper and lower sidebands of 147.5 kc and 22.5 kc respectively. The frequency response of the tape recorder was essentially flat between 100 cycles and 100 kc, decreasing to a gain of essentially zero at 150 kc. This response resulted in a vestigial side-band type of FM operation. This vestigial operation resulted in amplitude modulation of the FM signal as well as a degradation in signal-to-noise ratio of 3 db.

The amplitude modulation, although undesirable, presented no real problem because of the type of TV-FM demodulator which was used in the system. The demodulator, using multiple symmetrical clippers, effectively eliminated the AM. The small degradation in signal-to-noise ratio, caused by the high frequency roll-off in the recorder, was not apparent.

The data, recorded by the two AMPEX tape recorders, was:

Recorder Channel	TAPE RECORDER	
	1	2
1	Video Subcarrier	Video Subcarrier
2	Index Number	Index Number
3	Raw Sun Angle	Computed Sun Angle
4	Not Used	Not Used

9. Events Recorder

a. General

The Kaena Point ground station was equipped with a 20-channel Esterline-Angus events recorder (Model AW). Subsequently, as a result of its proven applicability, RCA installed the same model recorder at the Fort Monmouth ground station. Each recorder, equipped with 20 relay-operated pens, provided an on-off indication versus time on a paper chart. These on-off indications provided a direct, real-time record of the set-up of the command program for use in checking equipment malfunctions or operator failures prior to a pass, and also provided a permanent record of the commands sent during an actual pass.

The recorder was equipped with both manual and automatic start features. Manual start was used during station trouble-shooting and maintenance operations. Automatic start was used for normal operation of the equipment.

b. Functional Description

In automatic start, the chart is set under the pens to a one-minute interval mark. When alarm 1 is received by the command programmer, a start signal, applied to the recorder, starts the chart in motion. Real-time start of the chart is therefore the alarm 1 time of the particular pass. This time, along with a rubber

stamped indication of the various functions, including orbit number, is placed on the record for identification. The recorder pens provide on-off indications for twenty programmer sequences and components. These are:

PEN NUMBER	FUNCTION RECORDED	
1	Direct 1	PROGRAM A
2	Direct 2	
3	Playback 1	
4	Playback 2	
5	Set Clocks	
6	Start Clocks	
7	Fire Spin-Up	
8	Marker	
9	Direct 1	PROGRAM B
10	Direct 2	
11	Playback 1	
12	Playback 2	
13	Set Clocks	
14	Start Clocks	
15	Fire Spin-Up	
16	Monitor Shutter	
17	TV Receiver 1	
18	TV Receiver 2	
19	Telemetry Receiver	
20	Program Run	

C. SATELLITE CHECKOUT EQUIPMENT

C. SATELLITE CHECKOUT EQUIPMENT

1. Introduction

The checkout equipment, commonly called the Go, No-Go equipment, was essentially a simplified ground station used for checking out the TIROS I satellite. The equipment was first utilized at Princeton for pre-delivery checkout of the satellite. It then was transferred to the launch site at Cape Canaveral for operational checkout of the satellite during pre-launch and launch operations. The operational checks were made on the satellite at a pre-launch facility in Hanger AA and Launch Pad 17A. Checkout at Hangar AA was performed by cable connections between the satellite and the Go, No-Go van. Final checkout was performed via an r-f link between the Go, No-Go van in Hangar AA and the satellite located on the launch pad.

2. Development and Design

During the initial study phase, two types of checkout systems were considered. One type was an operational checkout system which would perform checks on the overall operation of the satellite. The second type was a quantitative checkout system which would perform detailed checks on each subsystem in the satellite to determine whether or not its operation was within specific tolerances. The first type of system, the operational checkout system, was selected because it would speed up the checkout procedure and because it provided operational conditions similar to those that the satellite would experience while in orbit.

Three major functions were necessary in order to perform operational checks on the satellite. These functions consisted of commanding the satellite, receiving and recording the telemetry data from the satellite and receiving and displaying the satellite TV video.

In the command subsystem, a commercially available three-watt transmitter, manufactured by Communication Company Incorporated, was selected for the r-f command link between the Go, No-Go van and the satellite at the launch pad. The distance between the van and the launch pad was two miles. A manually operated programmer, which used most of the circuitry designed for the ground station control tone generator, was developed to provide modulating signals to the transmitter. The reason for selecting a manually operated programmer instead of one controlled automatically was to provide more flexibility during countdown.

The same type of telemetry subsystem used in the ground stations was selected for the checkout system. The telemetry subsystem comprised two Tape-Tone frequency converters, two R-390A receivers, and a two-channel Sanborn chart recorder.

The FM Demodulator and Monitor developed for the TIROS I camera subsystem was used in the Go, No-Go video subsystem. A Nems-Clarke 1411A receiver was used for receiving the video carrier. Although the picture quality obtained from this subsystem was not as good as the picture quality displayed by the ground station video subsystem, the quality was considered to be adequate for a Go, No-Go check.

When the various subsystems were integrated into a complete system, a number of problems developed. These problems consisted of: monitor hum, monitor overheating, transients at the beginning of the video signal, noise triggering of the horizontal sync circuit in the monitor, and frequency drift in the telemetry converter.

In order to minimize 60-cycle monitor hum, the monitor was enclosed within a mu metal case. To alleviate monitor overheating, a blower, which maintained the temperature within the operating limits of the transistor circuits, was installed. It was concluded that the cause of the transients, which occurred at the start of each video signal, was the a-c coupling in the video amplifier. A feedback circuit was added to the video amplifier to eliminate this transient problem. Noise triggering of the horizontal sync separator was eliminated by replacing the original circuit with the flywheel type separator which was used in the primary and secondary ground stations. The final problem, frequency drift in the telemetry converter converter, was corrected by placing the local oscillator crystal in an oven.

3. Functional Description

The operation of the Go, No-Go checkout equipment is divided into two phases; namely, the command transmitting phase, which consists of programming the satellite for its various modes of operation, and the receiving phase, which consists of displaying the satellite video signal on a slow-scan monitor and recording the telemetry data on a two-channel Sanborn chart recorder. A simplified block diagram of the checkout equipment is shown in Figure 195.

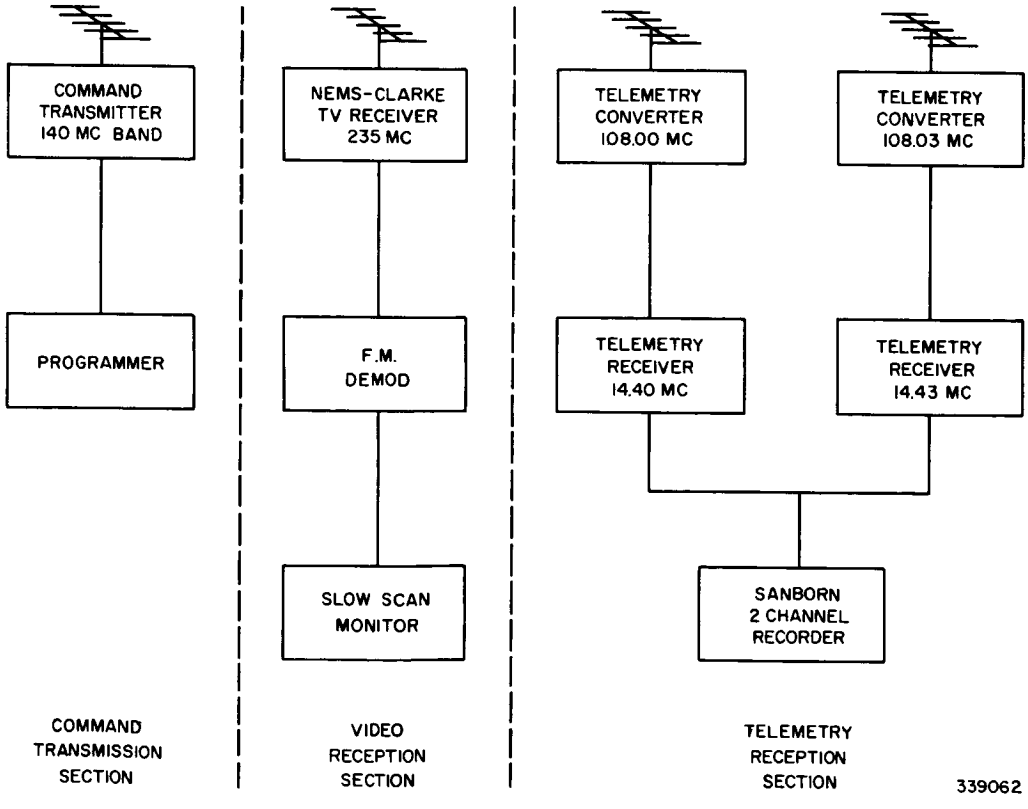

Figure 195. Checkout Equipment, Simplified Block Diagram

The satellite command signals consist of an r-f carrier modulated by audio frequency tones. A manually-operated programmer is used to supply the proper command tone for a given satellite operation. The command operations consist of programming the satellite to take pictures and send them directly back to the ground station, to playback pictures which were taken and then stored on magnetic tape, to set and then start the clocks for remote picture storage, and to fire spin-up rockets. The command transmitter has a power output of three watts. The transmitter frequency is crystal controlled.

The receiving phase of the Go, No-Go equipment is divided into two parts: telemetry reception and TV reception. The telemetry information is received on two carriers (108.00 and 108.03 Mc), which are converted to 14.40 and 14.43 Mc respectively. The telemetry data, in the form of a 1.3-kc ± 0.1-kc FM subcarrier, is demodulated and then recorded on a two-channel Sanborn chart recorder.

The video signal is transmitted from the satellite on a 235-Mc carrier. The video signal is in the form of a 85-kc ± 15-kc FM subcarrier with modulation frequencies from 0 to 62.5 kc. This subcarrier is demodulated to obtain the 0 to 62.5-kc video signal for display on a slow-scan monitor which uses a long-persistence kinescope. Photographs of the kinescope display are taken using a polaroid camera.

Figure 196 § is a detailed block diagram of the Go, No-Go equipment. Figures 197 § and 198 § are the relevant schematic diagrams. The basic operation of these circuits is similar to those of a ground (Command and Data Acquisition) station. A detailed explanation of these circuits is given in the "Operation and Maintenance Handbook for the TIROS I Satellite System".

4. Operational Checks for the TIROS I Satellite

The following Go, No-Go checks were made to determine whether or not the satellite was functioning correctly.

Command checks were made to determine the response made by the satellite to a specific command and to determine the time delay between the command and the response.

Telemetry checks were made by placing "standard overlays" over the recorded telemetry data. The overlay was marked off with tolerance limits for each of the 39 telemetry channels.

Video checks were made to determine whether or not the operation of the satellite cameras and tape recorders was satisfactory. A camera target was supplied by a collimated light, with an appropriate lens system, for the initial evaluation.

---

§ These illustrations are printed on fold-out pages located at rear of this volume.

This operation was performed before the satellite's protective shroud was put in place. After the protective shroud was in place, a light source of 1000 foot-lamberts was diffused directly into both camera lenses. Pictures of the video display were made using a Polaroid camera.

The nine north-indicator signals were transmitted from the satellite on the 235-Mc TV carrier in the form of 10-kc tone bursts. The north indicators were activated during checkout by means of a high-intensity light. The output from the 235-Mc receiver was displayed on an oscilloscope, and pictures of the 10-kc tone burst from each indicator were taken with a Polaroid camera.

The horizon scanner signal was transmitted on the 108-Mc telemetry carrier in the form of a 3-kc tone burst. The horizon scanner was activated during checkout by means of a high-intensity light. The output from the telemetry receiver was displayed on an oscilloscope, and pictures of the 3-kc tone burst from the scanner were taken with a Polaroid camera.

The spin-up rockets and Yo-Yo squibs were checked by stepping the rocket switch around to its various positions on command from the Go, No-Go equipment. With the use of a test set plugged into the satellite, currents were measured at the various switch positions. The amount of current was an indication of whether or not the rockets and squibs were properly connected. High resistance inserted in the rocket and squib circuits before third stage separation prevented the rockets and squibs from being fired during this check.

The charge on the satellite batteries was maintained by a battery charger in the block house. This battery charger was connected to the batteries in the satellite through the launch vehicle. The battery charger unit also powered and controlled the lights in the protective shroud.

5. Checks Made on the Go, No-Go Equipment

Daily checks were made on the checkout equipment in order to ensure its proper operation. Checks were made on the various supply voltages, transmitter power and frequency, programmer command frequencies and clock set pulses, telemetry system calibration, and video system calibration. In addition, general checks were made on the above systems before each checkout of the payload. No major difficulties were encountered during these checks on the Go, No-Go checkout equipment.

6. Antennas and R-F Propagation

Four ten element yagis, with approximately 10-db gain, were used for the four receiving and transmitting frequencies (108.00 Mc, 108.03 Mc, 140-Mc band, 240-Mc band). The three receiving antennas were horizontally polarized to receive the horizontal component from the satellite transmitting antennas, and the command

transmitting antenna was vertically polarized since the satellite receiving antenna was vertical when the satellite was mated to the vehicle. The following list gives the r-f propagation measurements made at Cape Canaveral between Hangar AA and Launch 17A immediately after these antennas were installed:

Frequency	Minimum Required Signal Level	Power Transmitted	Signal Level Received
108 Mc	0.2 v	20 mw	72 v
140-Mc band	1 v	8 watts	500 v
240-Mc band	10 v	2 watts	200 v

In all cases the signal level received was more than adequate.

D. THE IMAGE ENHANCEMENT CONSOLE

1. Introduction

Successful analysis of satellite-returned, TV cloud pictures is dependent, to a great extent on the resolution of the TV system, the noise in the system, and the ability of photo-interpreters to read and interpret the synthesized pictures. In pictures synthesized from electronic data, it has been found practical to introduce "image-enhancement" (i.e., alteration of the contrast in all, or portions of, the picture).

Three types of enhancement have been shown to aid in image interpretation: edge-enhancement, contouring, and gamma-slicing (and stretching). Image enhancement equipment, of general utility, with accessory equipment to facilitate its use with TIROS I data, was developed and constructed under the TIROS I contract.

The Image Enhancement Console is the device which utilizes electronic techniques to alter or emphasize selected features of visual images to facilitate their recognition or readability. In its basic form, it is designed to accept images on film transparencies, which are converted to electronic waveforms by means of television techniques. The electronic waveforms then may be altered, as necessary, to produce a pictorial display of the enhanced image on the video-monitor display. The TIROS Tape Readout Equipment is the supplementary equipment provided to accept tapes recorded by the TIROS I Satellite System, and produce from them continuously the electronic waveforms of any one image, for direct input to the enhancement circuits of the Console. A photograph of the complete equipment is shown in Figure 199.

2. Equipment Design

a. General

The Image Enhancement Console is a desk-type structure arranged in a horse-shoe configuration. It is designed to synthesize an image on a kinescope display from electronic video data. A photographic film scanner unit included in the Console develops

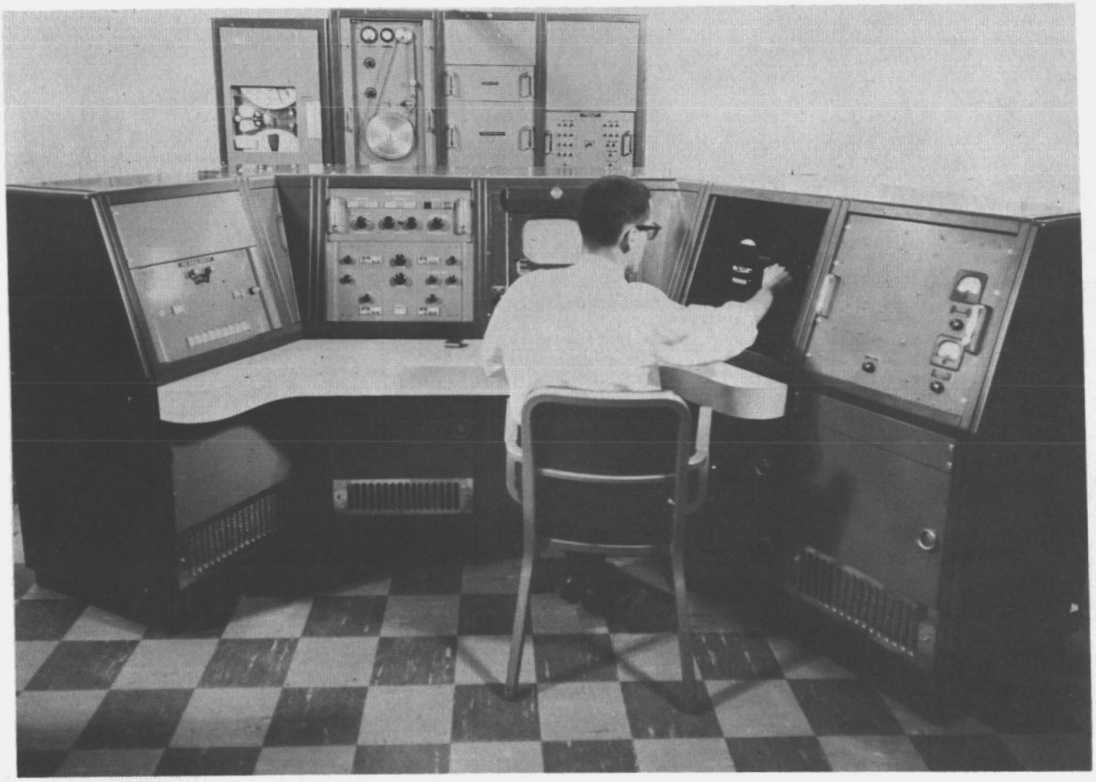

Figure 199. The Image Enhancement Console Equipment

such video data from slides or film strips. By means of enhancement controls, the image may be altered to secure the most informative presentation. A front view of the console, (with access doors open) is shown in Figure 200.

The TIROS Tape Readout Equipment is contractually considered part of the Console, but is actually an assembly of rack-mounted accessory equipment, shown in Figure 201, provided to permit video data from TIROS library tape to be fed into the console in electronic form, rather than requiring an intermediate translation to film-slide format. It consists of a tape recorder-playback unit, and three additional racks of equipment to provide a continuous electronic-waveform input, to the console, of a selected TIROS image and its associated information display. A standard TIROS tape may be placed in the equipment; and a particular frame called for. This frame, and its associated index and sun-angle data, will then automatically be transferred to a tape loop, which is subsequently read out continuously into the console for as long as the operator desires that particular display.

b. Image Enhancement Console

(1) Mechanical Construction

The console consists of standard-size module cabinet sections. Electronic-equipment chassis units are mounted in sliding drawers for easy accessibility. Each cabinet module is cooled by forced air. The console layout places all operating controls

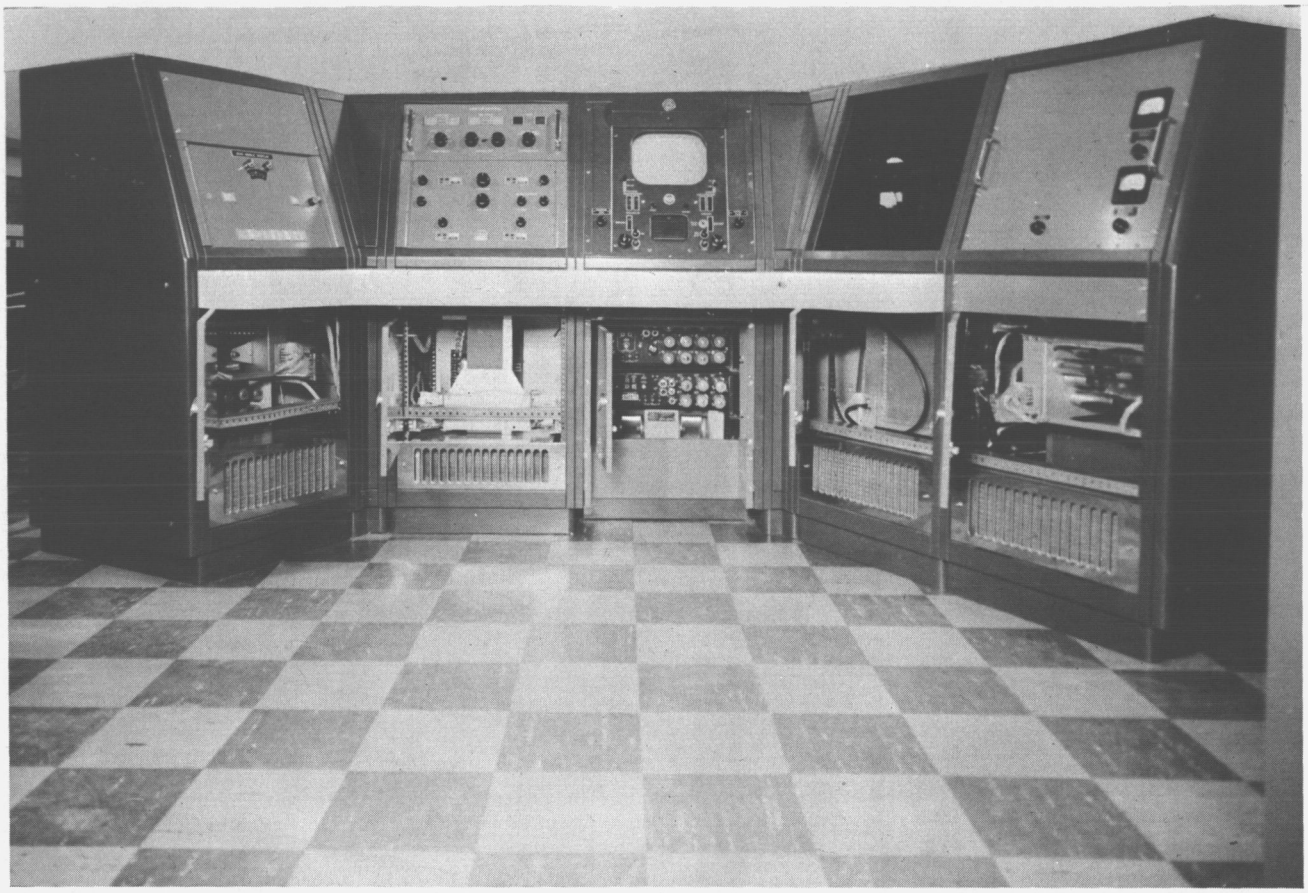

Figure 200. The Image Enhancement Console with Front Access Doors Open

NOTE

The Image Enhancement Console was designed to have a general utility, that is its use is not confined to operation with a TIROS system. However, it was designed and constructed for first-use with TIROS I cloud-picture data, and an auxiliary unit was developed to permit the direct use of TIROS tape-recorded images, and thus eliminate the intermediate steps of reproducing them on photographic slides and inserting these at the Console optical "input." Also, it is contractually related to the TIROS I project. Therefore a discussion of the design and function of the Image Enhancement Console is included in this report.

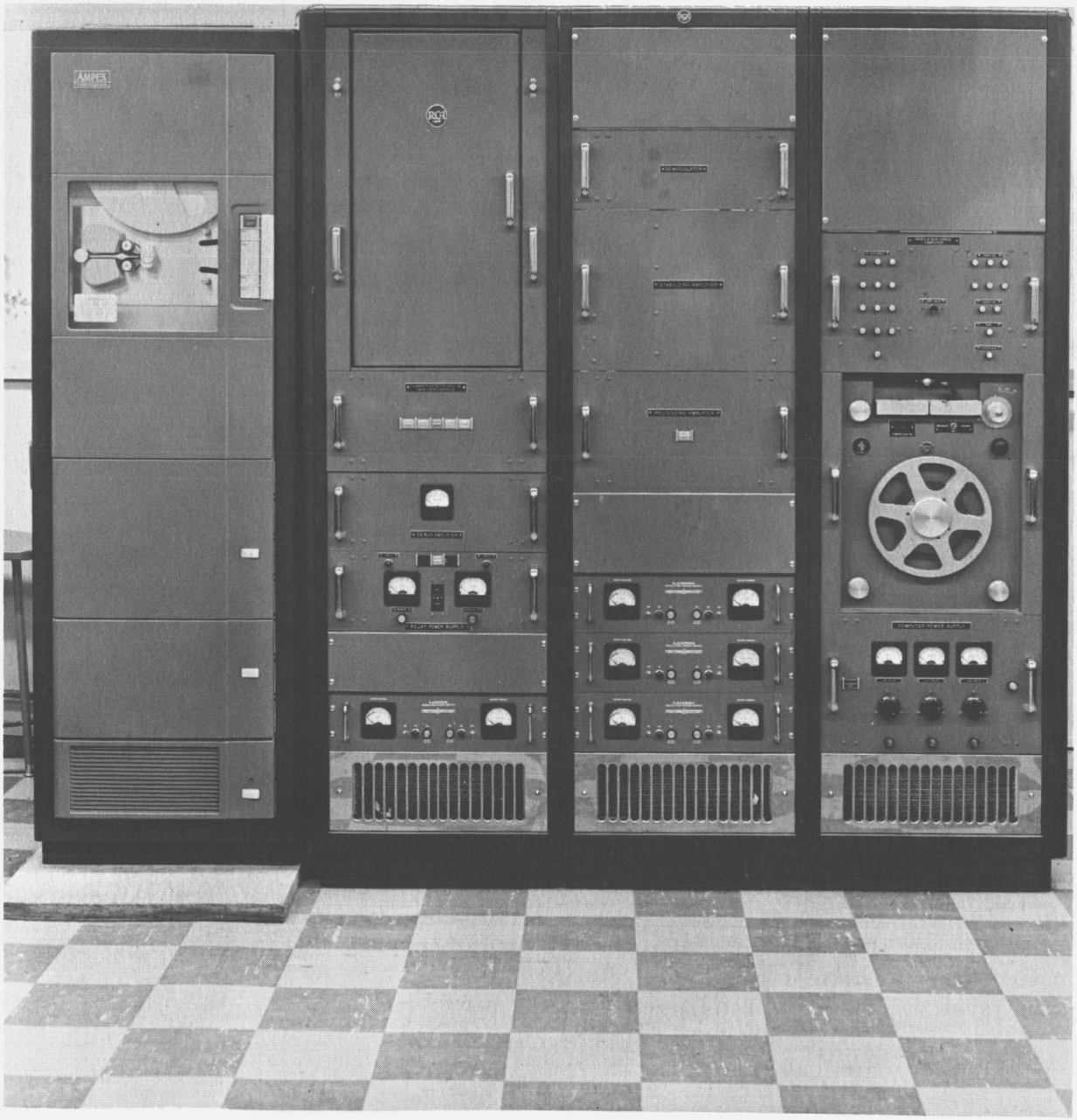

Figure 201. The TIROS Tape Readout Equipment

within easy reach, with service adjustment controls mounted inside the individual drawers. All components are easily accessible for maintenance, although the conservative design should hold the necessity for maintenance to a minimum.

(2) Optics and Electronics

(a) The Scanning Equipment

The scanning equipment is located in the right-hand wing of the console. It consists of the scanner kinescope with its control and deflection circuits, the optical and slide handling mechanisms, the multiplier phototube and preamplifier and a video processing chassis. All operations are controlled by the sync generator. A photograph of the optical unit of the scanning equipment, removed from the console, is shown in Figure 202a.

1. The Flying-Spot Scanner. In principle, the flying-spot scanner is probably the simplest of all television cameras. A diagram illustrating its operation, is shown in Figure 202b. The basic element is a kinescope, causing the beam to scan the face of the tube in a raster, or pattern of horizontal lines. The light produced by the spot is focused on a transparency of the desired image by a lens system. The light beam is modulated in intensity by the variation in film density from point to point in the image. The modulated light is then collimated by a condenser lens system and caused to fall on a light-sensitive surface.

The device used for this purpose is the multiplier phototube. The light passing through the film falls on the face of this tube, which is coated with a material which emits electrons in direct proportion to the incident light. The electron beam thus produced is multiplied by secondary emission from a number of electrodes, and at the output becomes a voltage waveform which reproduces the variations of film density seen by the flying spot.

In the Console, the kinescope is a modified type, electrically equivalent to the RCA Type 5ZP16, which is a 5-inch flat-face tube capable to 1000 TV lines resolution. The P16 phosphor emits most of its energy in the near ultraviolet, with a peak at about 3800 Angstroms. The multiplier phototube is a selected RCA Type 6342-A having an S-11 response peaking in the range 3900 to 4900 Angstroms.

Two lens systems are supplied, along with a simple means to change from one to the other without readjustment. The primary lens is a 2-inch f/2 Wollensak TV Raptar. Essentially the whole 35-mm slide format is "seen" by this lens. For higher magnification, (ratio about 3:1), a 1-inch f/1.5 Wollensak Cine Raptar is provided, along with a second condenser lens.

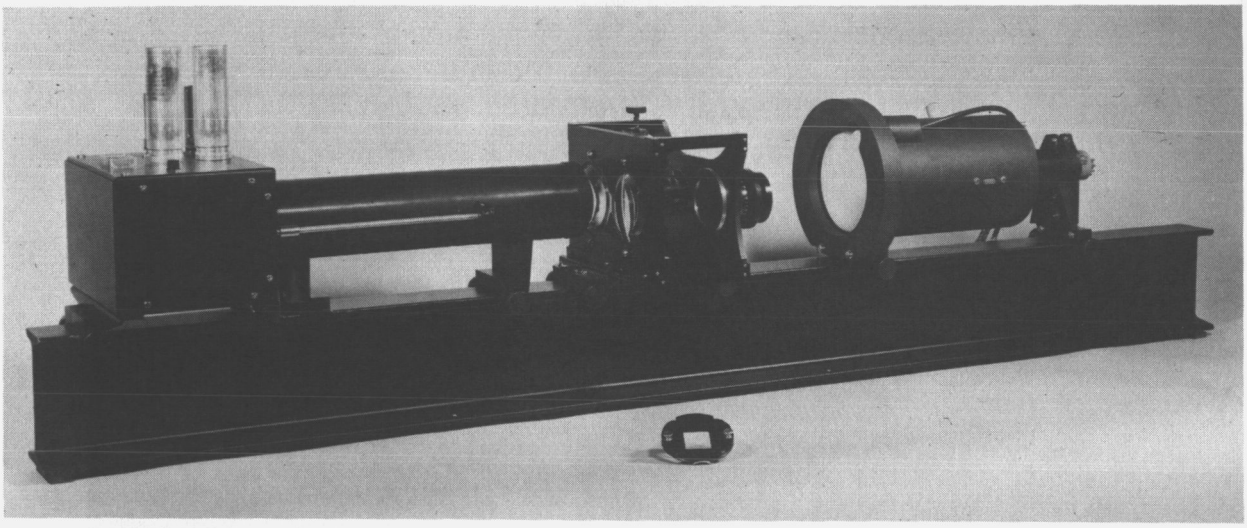

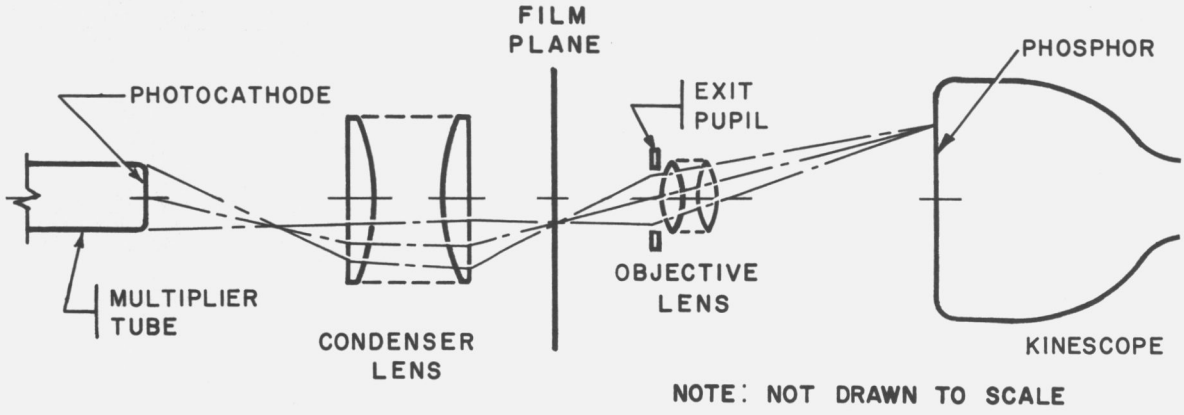

Figure 202. The Hard Copy (Flying Spot) Scanner (a) Assembly (b) Diagram

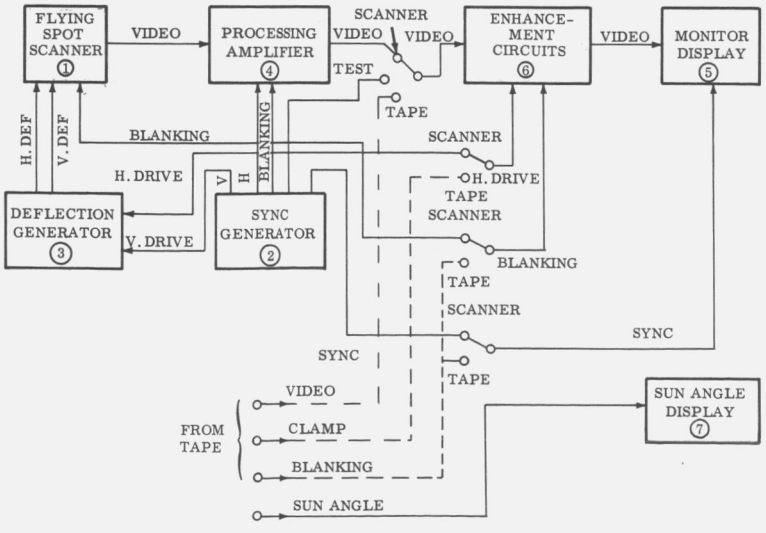

Figure 203. The Scanner and Video Circuits, Block Diagram

The input material may be either slides or strip film. Means are provided to move the film left and right, up and down, or to rotate it. Thus the operator may examine any section of a picture using high magnification. Resolution, referred to the picture, is of course improved by using the high magnification.

All components of the scanner are rigidly mounted on a 5-inch aluminum I-beam. Only the optical components and slide mount are normally accessible to the operator.

2. Video Circuitry. A block diagram of the scanner and associated video circuitry is shown in Figure 203. Included with the Scanner, as part of block No. 1, is the blanking and kinescope protective circuitry. The blanking circuit turns off the kinescope beam while the spot retraces. The protective circuitry prevents damage to the kinescope in the event of failure of scanning.

The Sync Generator, block No. 2, is a standard unit (RCA Type TG2-A) and supplies pulses to synchronize all operations in the "slide" mode. The sync generator also supplies a grating signal useful in testing system performance.

The Deflection Circuits, block No. 3, supply currents to the magnetic-deflection yoke of the kinescope. Timing of the deflection is controlled by pulses from the sync generator.

The Scanner Processor, block No. 4, performs several functions compensating for limitations in other parts of the system. These include the decay characteristic of the kinescope phosphor, which continues to glow for a short time after the electron beam has moved on. If not compensated, this would result in a smear following a sharp edge in the picture. To correct for the transfer characteristics, or gamma, of the monitor kinescope the contrast is stretched near the black region by the gamma corrector. Blanking is added in this unit to remove any noise present in the retrace interval. Blanking is also necessary after polarity reversal, since in a negative picture the retrace interval would become white, rather than black. The waveforms involved in this operation are shown in Figure 204.

(b) Output Equipment

The output equipment consists of the Enhancement Unit, block No. 6, the Monitor Unit; block No. 5, and the Sun-Angle Display, block No. 7. The Master Control Unit, block No. 8, and Master Control Relay Unit, block No. 9, control all operations.

The sun-angle display, when it receives (from TIROS I tape) digital data representing sun-angle from the computer, converts the digital number to a dial reading which is retained for the operator's reference while viewing a picture in the

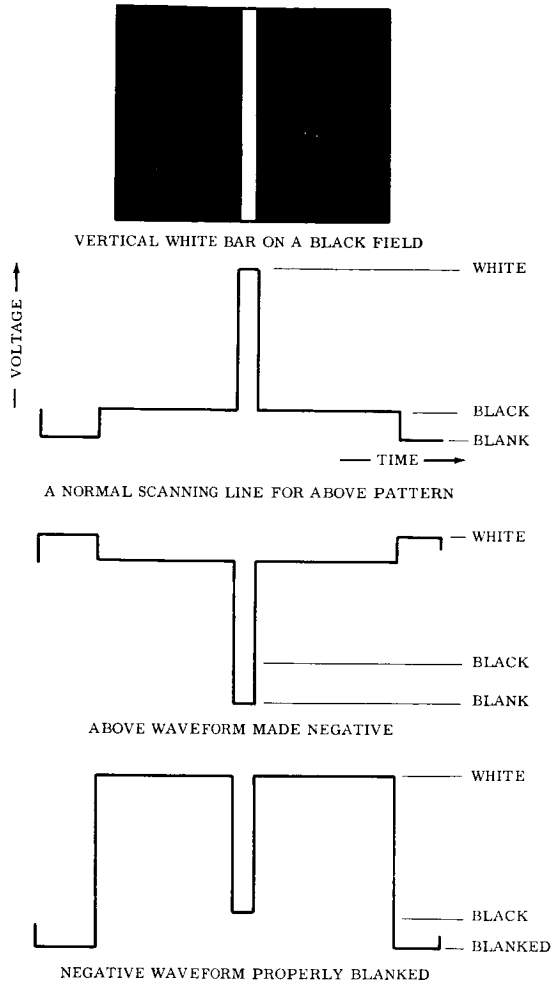

Figure 204. Typical Image Waveforms

tape mode. The video monitor is basically a high-quality standard broadcast TV unit (RCA Type TM6C). It has been modified slightly to permit non-interlaced scanning in the tape mode. The picture is displayed on a 10-inch kinescope, capable of resolution in excess of 600 lines. In addition, the video voltage waveform is displayed on a second cathode ray tube. This display is used to help the operator maintain the same signal level at all times.

The enhancement chassis is flexibly designed to permit a wide degree of operator control over the output picture. The picture may be displayed without enhancement, and with various types or degrees of three enhancement effects. These four possible outputs may be mixed in any proportion, either as photographically positive or negative images. Input and output level controls, used in conjunction with the waveform monitor, assure a constant brightness and contrast in the picture on the monitor kinescope.

The three types of electronic image enhancement provided are identified as "differentiation," "outlining," and "slicing."

The differentiate channel generates and adds a signal proportional to the rate of change (i.e., the derivative) of brightness along a horizontal line of the picture. This combination "sharpens" the appearance of the edges of objects in the picture. The degree of sharpening can be controlled by changing the time constant of the differentiating circuit, and a selection of three time constants is provided. The signal output of this channel can be controlled in amplitude, and can be changed from positive to negative.

The slice channel passes only a portion (or "slice") of the black-to-white scale, and amplifies (or "stretches") this to produce a full range of black-to-white on the monitor display. For this channel, the POSITION potentiometer determines the location of the gray scale between black and white, and the THICKNESS control selects the width of the scale to be passed. The channel output can be attenuated, and changed from positive to negative.

The outline channel generates a pulse during each video line when the video signal passes through a value equivalent to a selected gray-level range. These pulses are displayed in two dimensions on the monitor, and give the appearance of constant-brightness contour lines. A THICKNESS potentiometer varies the width of the gray scale included in the working range, and a POSITION control selects the location between black and white occupied by this width of gray scale. The output of this channel also can be attenuated, and changed from positive to negative.

(c) Control Equipment

The Master Control Unit, works in conjunction with the Control Relay Unit, to control and sequence power application and circuit switching.

The upper section of the Master Control Unit panel contains the controls and indicators for power application, selection of the operational mode, and selection of a particular frame on the TIROS library tape for viewing. The lower section contains the enhancement controls and indicators.

A FUNCTION SELECTOR switch starts automatic sequencing of power application and circuit interconnections for either the "tape," "slide," or "test" mode of operation. The CAMERA SELECTOR and INDEX SELECTOR switch permit the unique identification of a particular frame on the library tape desired for viewing, and the LIBRARY TAPE switch group enables the fast wind or rewind of the library tape to a position near where the desired frame is located. The TAPE CONTROL switch group permits initiation of the frame search, and subsequent recording of the desired frame on the tape loop. The VIEW switch then permits readout of the tape loop for the monitor display of the desired picture.

A set of controls for viewing an unchanged picture, and other controls for introducing the various kinds of enhancement are contained on the lower panel.

c. The TIROS Tape Readout Equipment

The tape readout equipment accepts pictures transmitted from the TIROS satellite. A block diagram of its circuits is shown in Figure 205. As received, these pictures are on a frequency-modulated carrier at (nominally) 85 kilocycles. This carrier is recorded on magnetic tape in the TIROS ground station. Also recorded, on separate channels on the same tape, are frame identification codes and information about the angle between the sun and the camera when the picture was taken.

The TIROS pictures are synthesized too slowly (two seconds per picture) for detailed observation. The purpose of the tape equipment of the enhancement console is to speed up the rate of transmission of the TIROS pictures, displaying the same picture 30 times per second. At this speed the effect of the various enhancement controls is immediately evident.

(1) The Tape Loop

The change in speed mentioned above is accomplished by re-recording on an endless tape loop, a single picture selected from the original or library tape. The loop is then speeded up in the ratio of 60:1 for readout. The nominal carrier frequency then becomes 5.1 megacycles, and the resulting picture is very similar to a standard TV picture. (A major difference is lack of "interlace." Interlacing divides the raster into two fields, one containing odd numbered lines and the other even numbered lines. The effective flicker frequency of an interlaced picture is doubled.)

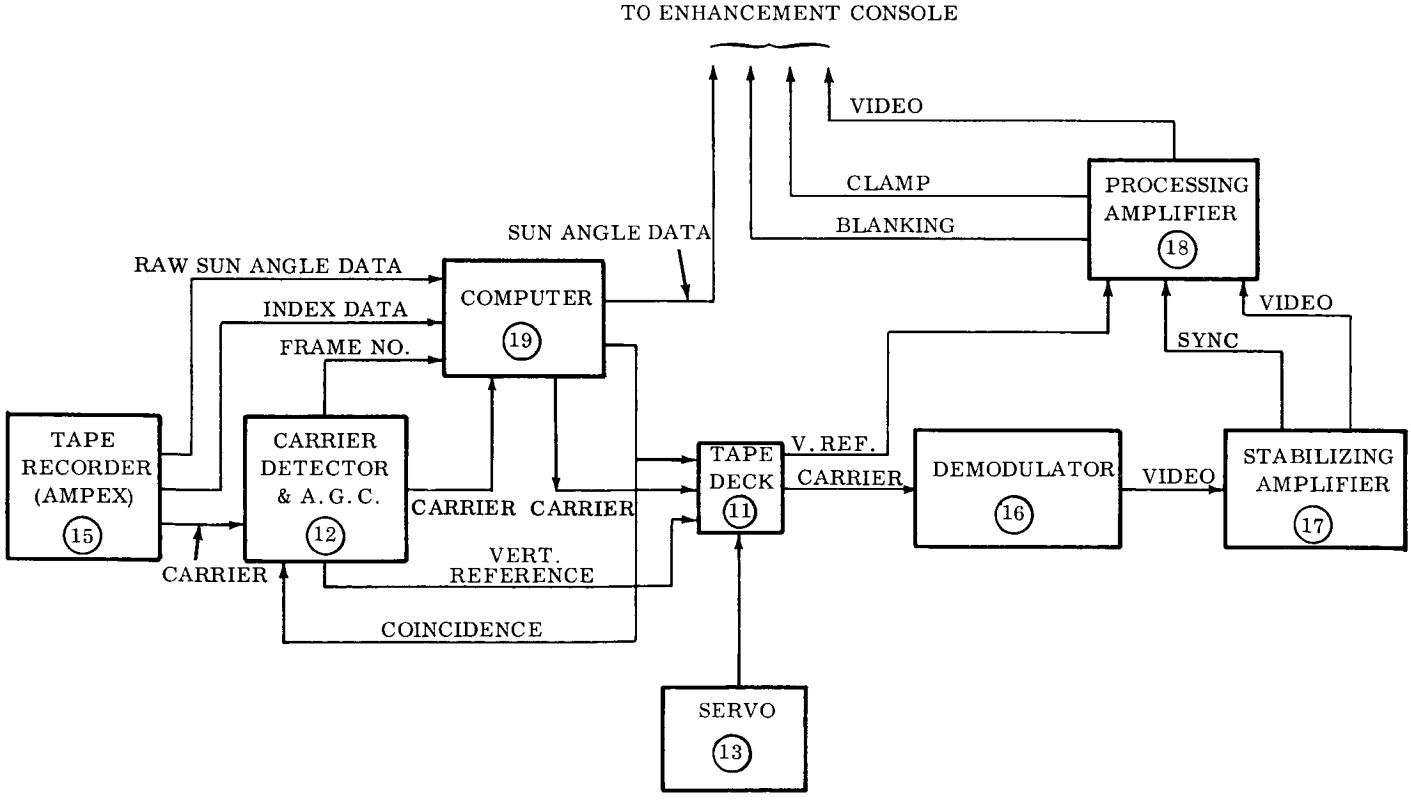

Figure 205. The TIROS Tape Readout Circuits, Block Diagram

The tape loop is supported at the top by air flowing through a set of holes in a stationary idler, and at the bottom by the capstan. An air pad just above the record-playback head reduces flapping of the tape and steadies it to pass smoothly over the head. Two channels are used in recording. The first is the carrier channel, while the second is used for a pulse to record the beginning of the frame. A d-c erase head also is provided.

The tape deck contains the record and playback electronics for both channels as well as the two drive motors for the capstan. The high speed motor is a hysteresis-synchronous type which drives the capstan directly at 3600 rpm. The low speed motor drives the capstan at 60 rpm by means of a rubber disc engaging the capstan. A solenoid is used to "engage" the drive disc during low speed operation.

The low speed operation is servo-controlled, using a brake on the capstan shaft to vary the load on the motor and hence its speed. The speed is measured by comparing the frequency generated by a tone wheel, which is also mounted on the main shaft, with a crystal-generated reference frequency, and any error signal developed then actuates the servo loop.

(2) Peripheral Equipment (Record Mode)

The Servo Unit, No. 13, contains the speed reference circuitry mentioned in the preceding section as well as the circuitry required to complete the servo operation.

Selection of the desired frame is made by the operator, who sets the number into the search circuits by means of dials on the master control panel. As the library tape plays back, each frame number is compared with the desired number by the computer, Unit No. 19. The computer opens a gate when the desired frame is reached. The carrier detector and AGC unit, No. 12, detects the beginning and end of each frame and operates a gate coinciding exactly with the frame. When both gates are open, the picture is recorded. The AGC, or automatic gain control, assures that each picture will be recorded on the loop at the optimum level.

After recording, all units continue to run until the sun angle information is received, when they automatically stop. The computer then decodes the sun angle and actuates the associated sun-angle display, Unit No. 7, in the output equipment.

(3) Peripheral Equipment (Playback Mode)

When the library tape and the loop stop, the equipment is ready for the playback mode. In playback, the carrier is read from the loop at high speed. In the demodulator, Unit No. 16, the video is recovered from the carrier. It will be recalled that the carrier was frequency modulated in the satellite by the picture, or video, information. The video goes to the stabilizing amplifier where sync is detected and certain transient effects at the ends of the frame are reduced. This unit, No. 16, is a standard commercial amplifier (RCA Type TA9), slightly modified.

In the processing unit, No. 18, the sync information is processed to reduce the effects of noise. The vertical sync is generated from the pulse recorded on the second channel of the tape loop, (it may be adjusted by the operator to compensate for variations in loop length and picture time). Vertical and horizontal sync are combined into a mixed blanking voltage.

The video is then blanked, either for positive or negative as in the scanner processor. Various pulses from the processor , as well as the video, are then sent to the console output equipment.

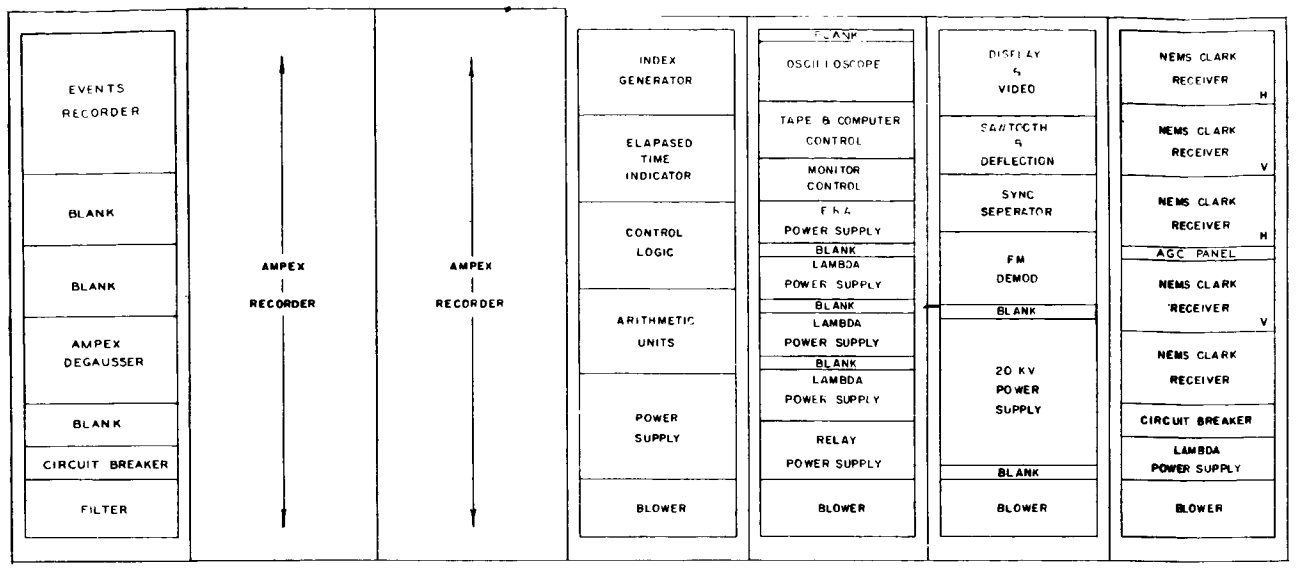

RACK 18 EVENTS RECORDER

RACK 9 TAPE RECORDER 1

RACK 10 TAPE RECORDER 2

RACK 6 SUN ANGLE COMPUTER

RACK 5 VIDEO CONTROL & POWER

RACK 4 VIDEO MONITOR

RACK 11 TV & IR RECEIVERS

VIEW NORTH

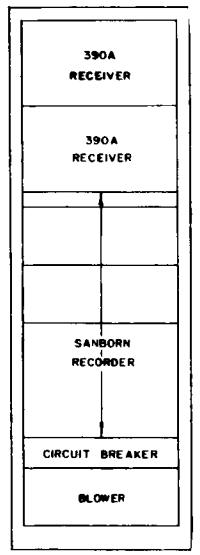

RACK 8 TELEMETRY RECORDER

VIEW SOUTH

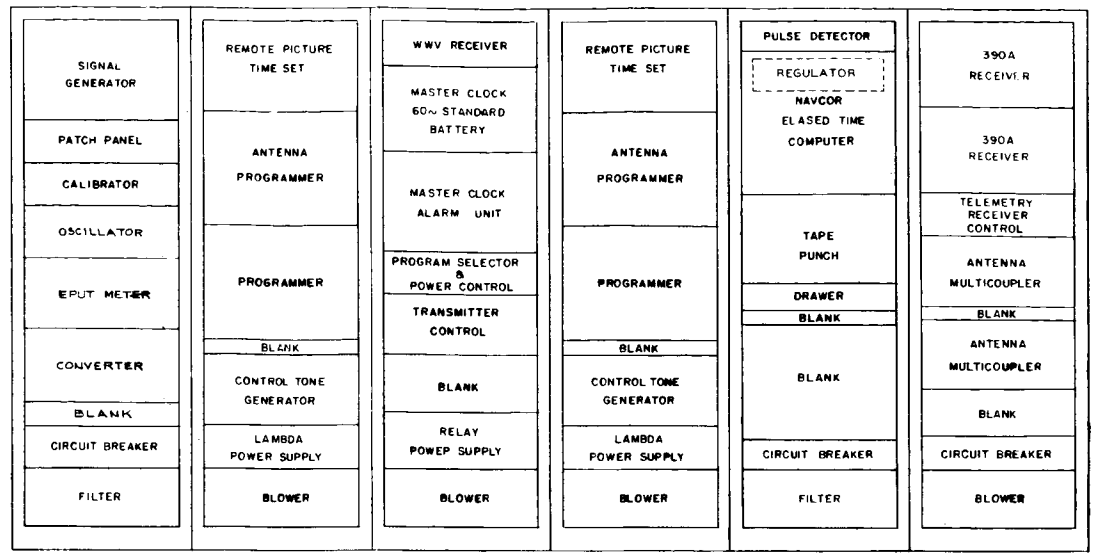

RACK 12 CALIBRATION

RACK 1 COMMAND CONTROL PROGRAM A

RACK 2 COMMAND CONTROL TIMING

RACK 3 COMMAND CONTROL PROGRAM B

RACK 13 ATTITUDE RECORDER

RACK 17 TELEMETRY RECEIVER & CONTROL

VIEW EAST

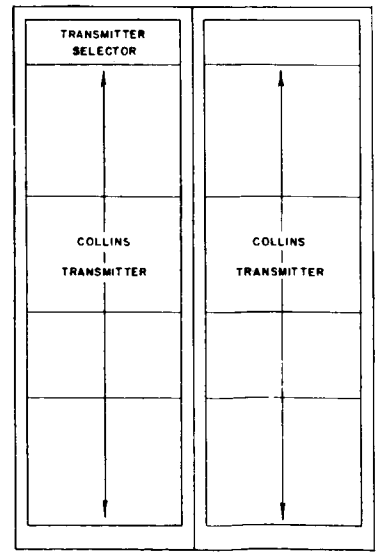

RACK 14 COMMAND TRANSMITTER A & SELECTOR

RACK 15 COMMAND TRANSMITTER B

THESE RACKS LOCATED IN DISH TOWER

1173108D

Figure 134. Ground Station Components

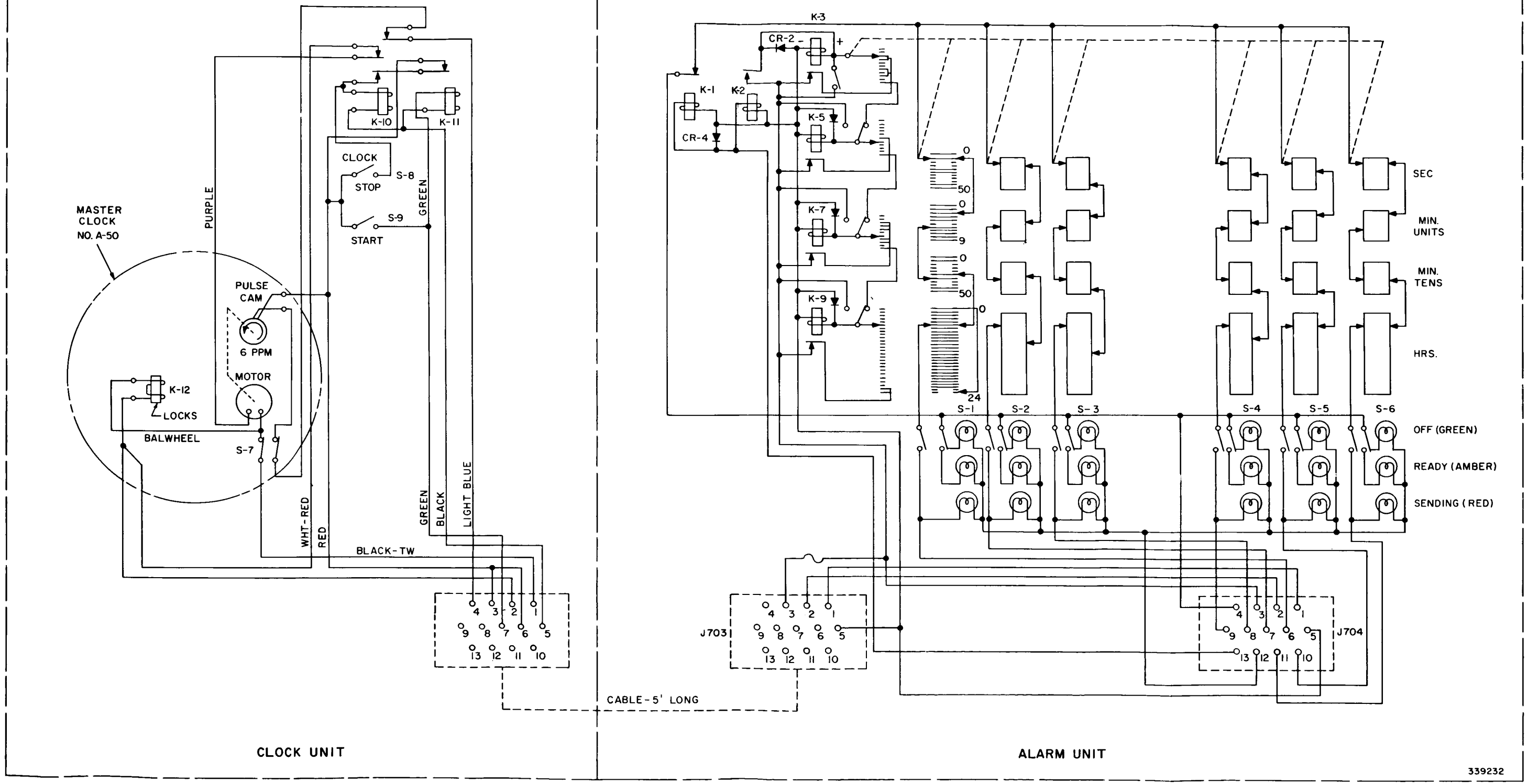

Figure 140. Master Clock, Schematic Diagram

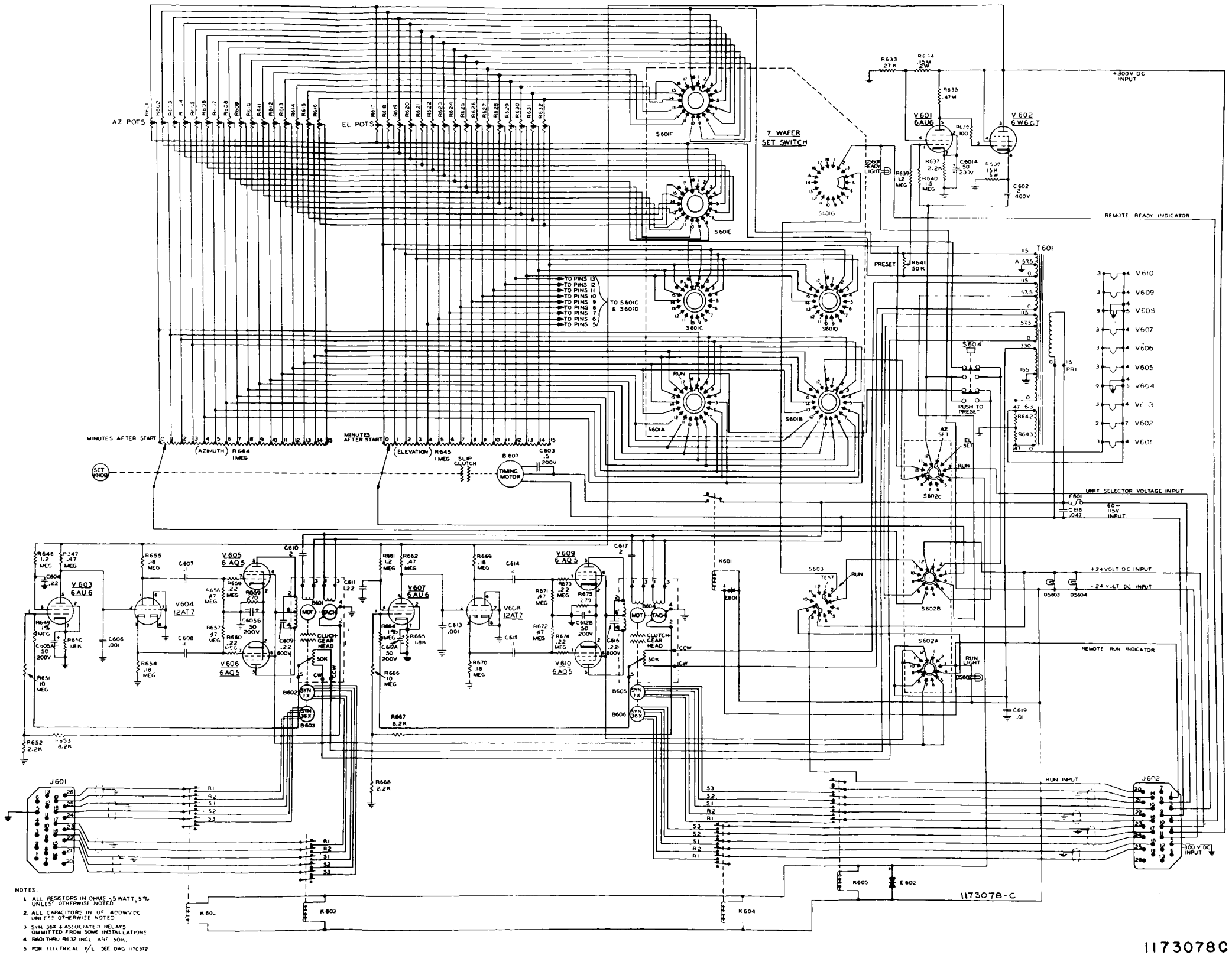

NOTES.
1. ALL RESISTORS IN OHMS, .5 WATT, 5% UNLESS OTHERWISE NOTED
2. ALL CAPACITORS IN UF, 400WVDC UNLESS OTHERWISE NOTED
3. SYN. MOT & ASSOCIATED RELAYS OMMITTED FROM SOME INSTALLATIONS
4. R601 THRU R632 INCL ARE 50K.
5. FOR ELECTRICAL F/L SEE DWG 1170372

1173078C

Figure 143. Antenna Programmer, Schematic Diagram

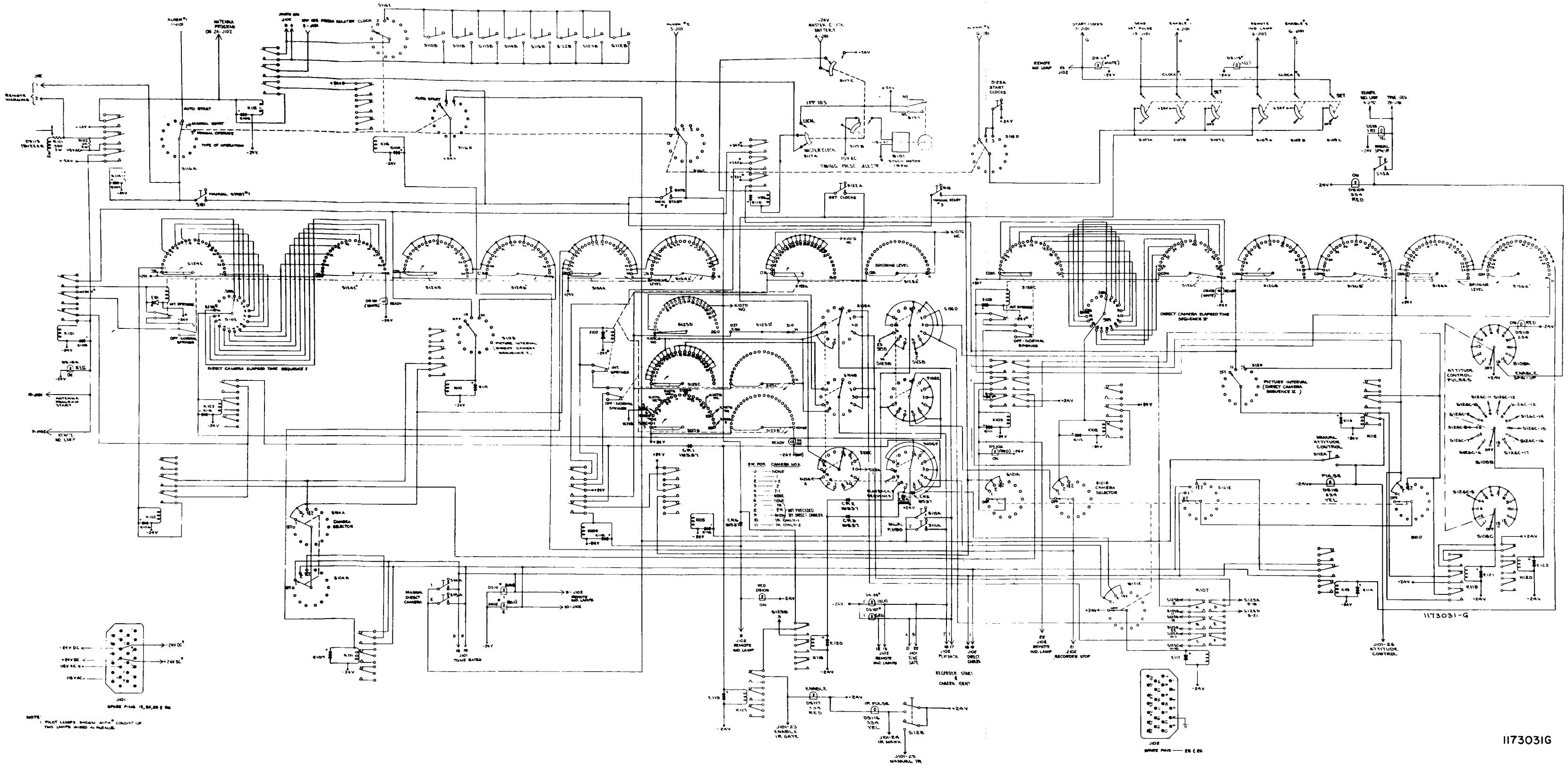

Figure 151. Command Programmer, Schematic Diagram

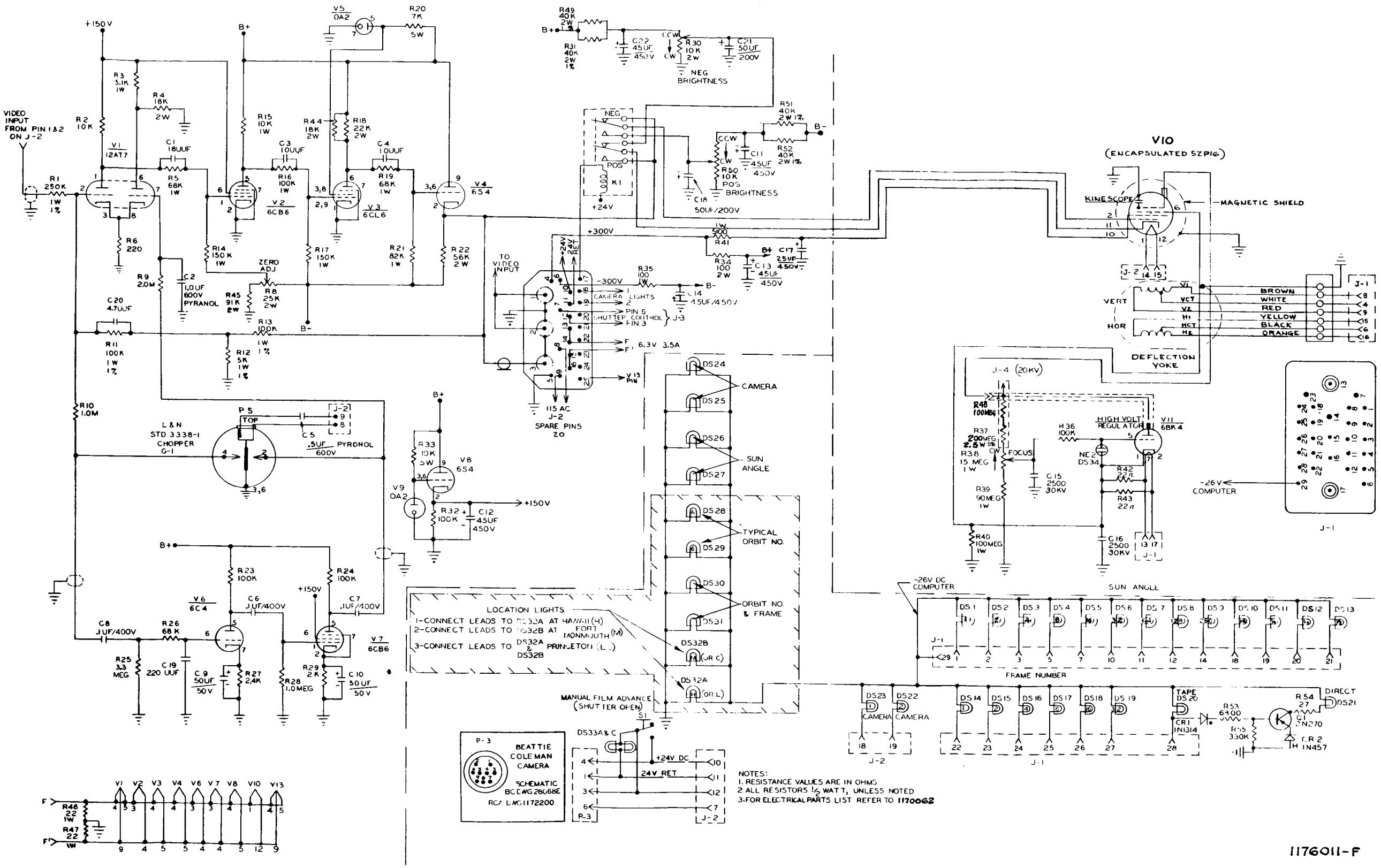

Figure 163. Display and Video Amplifier, Schematic Diagram

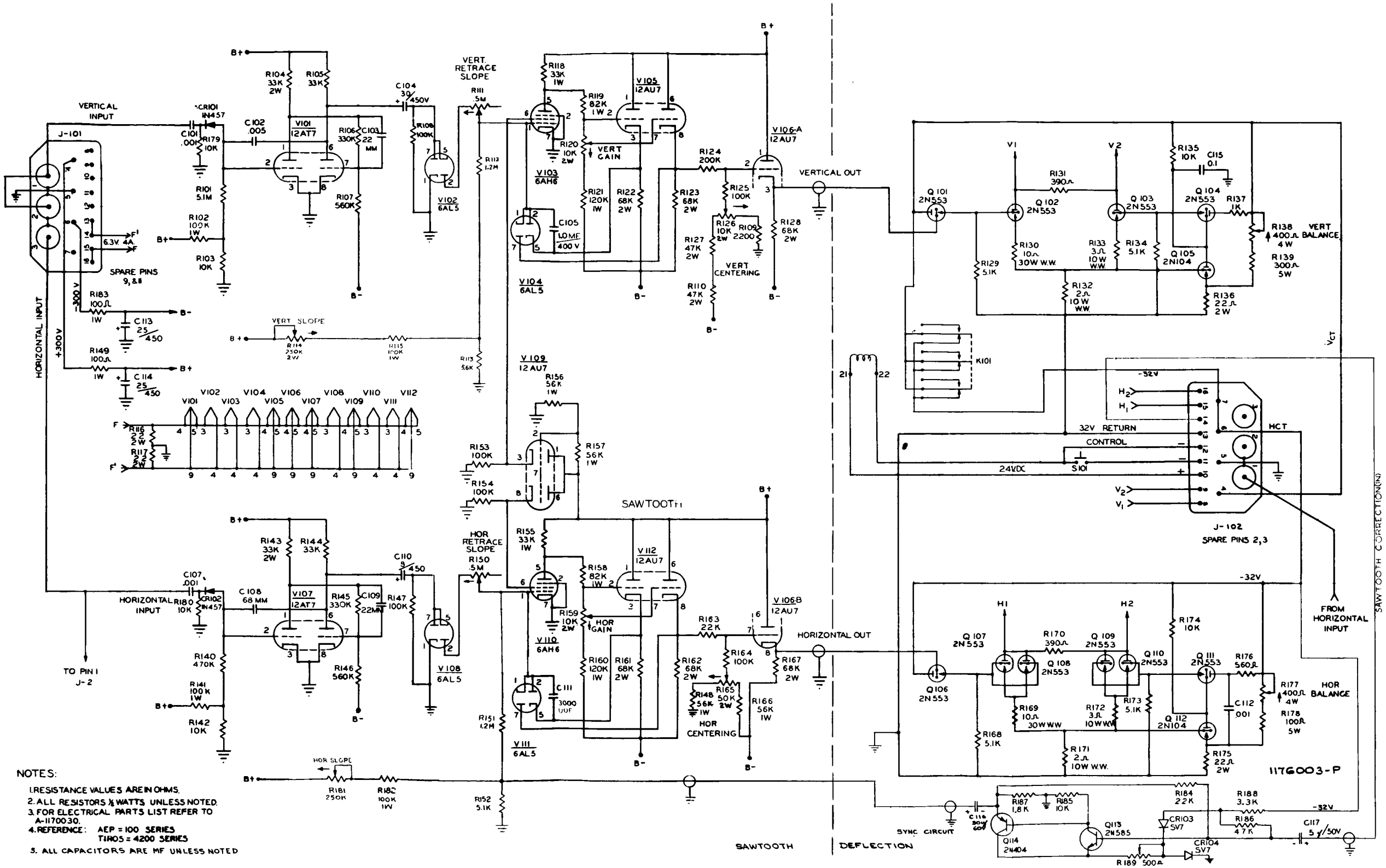

Figure 168. Sawtooth Generator and Deflection Amplifier, Schematic Diagram

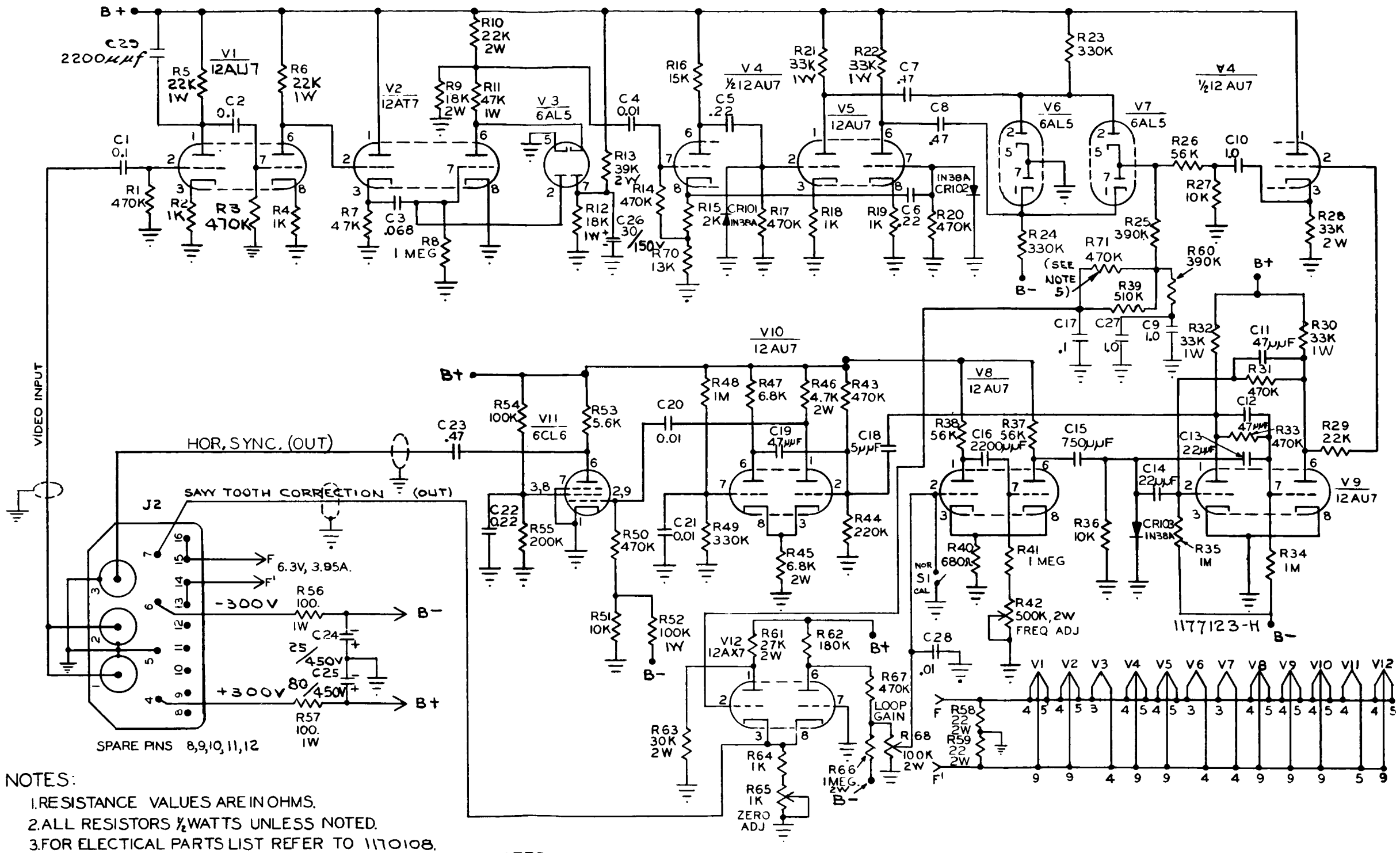

NOTES:

1. RESISTANCE VALUES ARE IN OHMS.
2. ALL RESISTORS ½ WATTS UNLESS NOTED.
3. FOR ELECTICAL PARTS LIST REFER TO 1170108.
4. ALL CAPACITORS IN MICRO FARADS UNLESS NOTED.
5. RESISTOR R 71 IS USED IN HAWAII GRD. STATION ONLY.
6. REFERENCE: AEP-200 SERIES
   TIROS 4300 SERIES

1177123H

Figure 171. Horizontal Sync Separator, Schematic Diagram

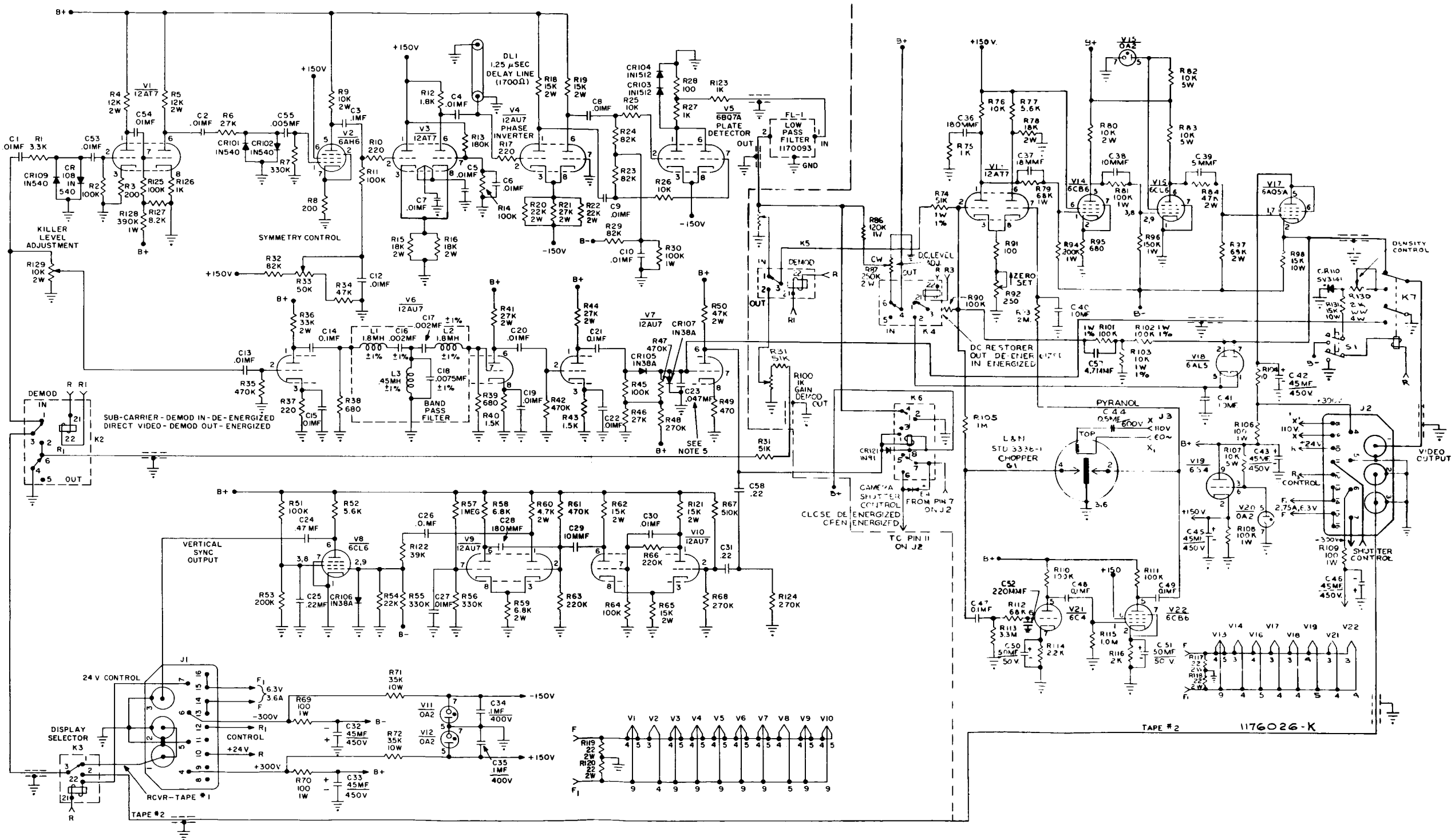

NOTES:

1. ALL RESISTORS VALUES ARE IN OHMS AND 1/2 WATT UNLESS NOTED
2. FOR LIST OF MATERIALS REFER TO DWG 1170094
3. RELAYS SHOWN IN DE-ENERGIZED POSITION
4. REFERENCE: AEP-500 SERIES
   TIROS-4400 SERIES
5. C23 IS .033 MF IN AEP GROUND STATION

Figure 173. TV-FM Demodulator, Schematic Diagram

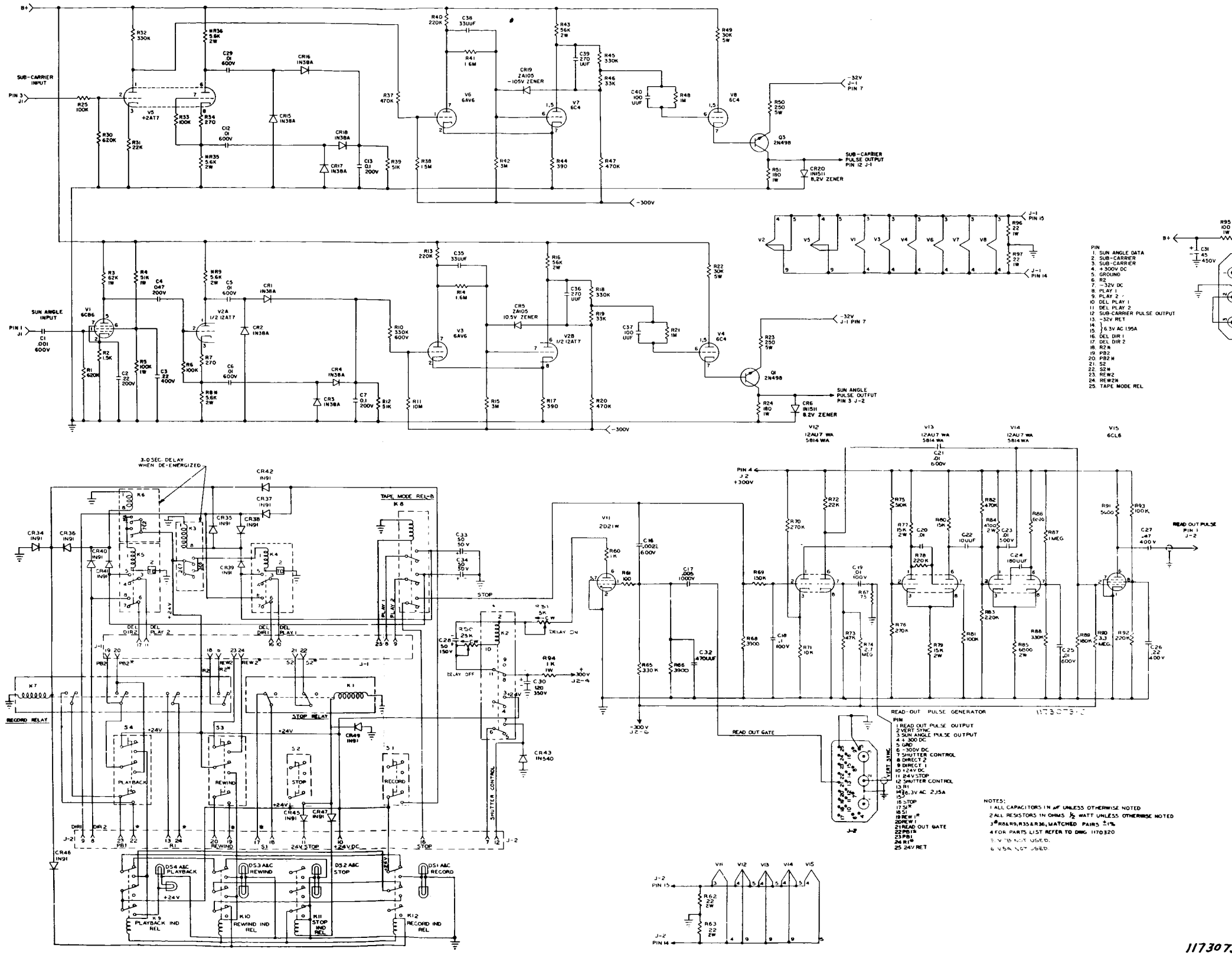

1173073 G

Figure 176. ***Tape and Computer Control, Schematic Diagram***

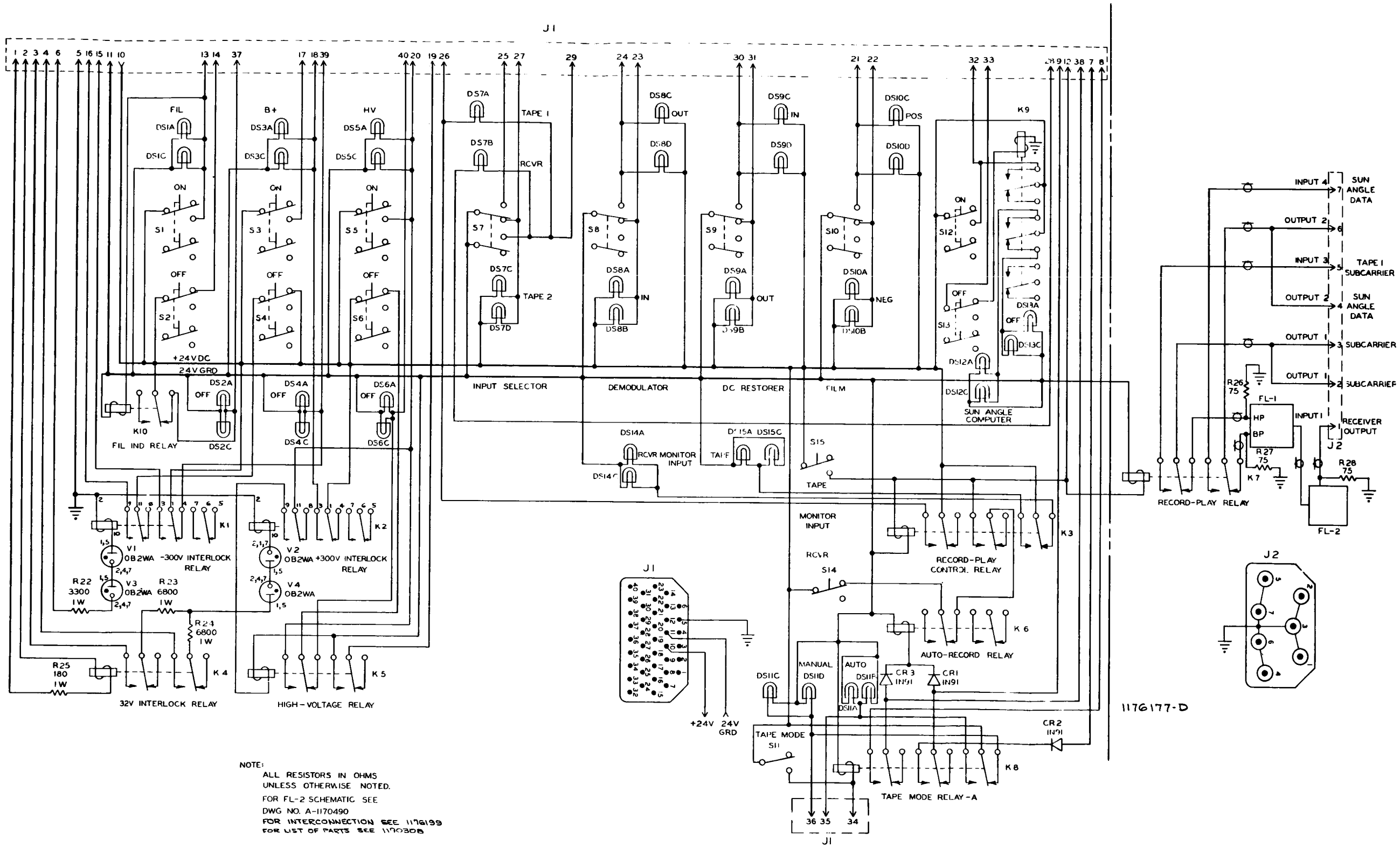

NOTE:
ALL RESISTORS IN OHMS
UNLESS OTHERWISE NOTED.
FOR FL-2 SCHEMATIC SEE
DWG NO. A-1170490
FOR INTERCONNECTION SEE 1176199
FOR LIST OF PARTS SEE 1190308

1176177D

Figure 177. Monitor Control, Schematic Diagram

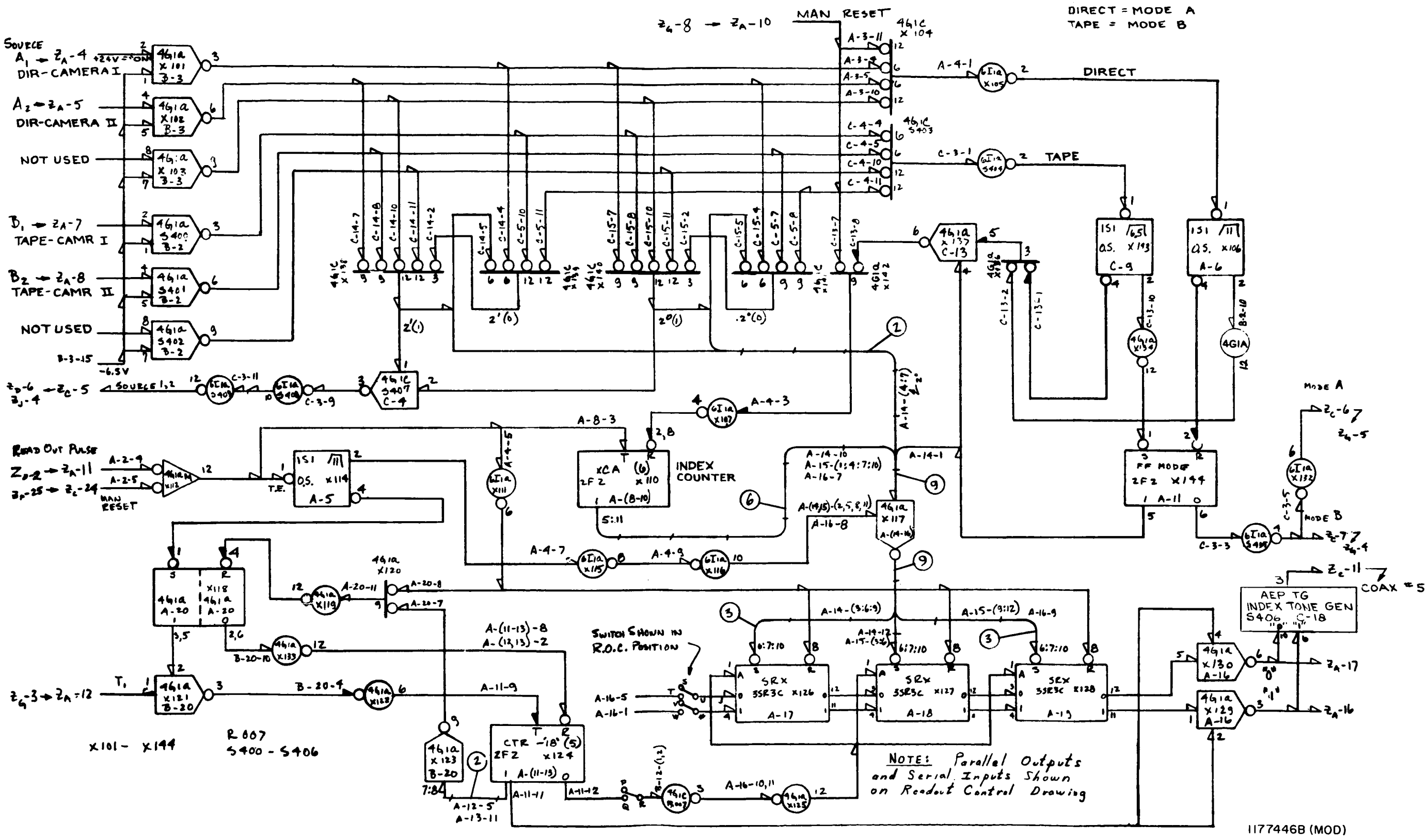

Figure 181. Sun-Angle Computer, Logic Diagram (Sheet 1 of 12)

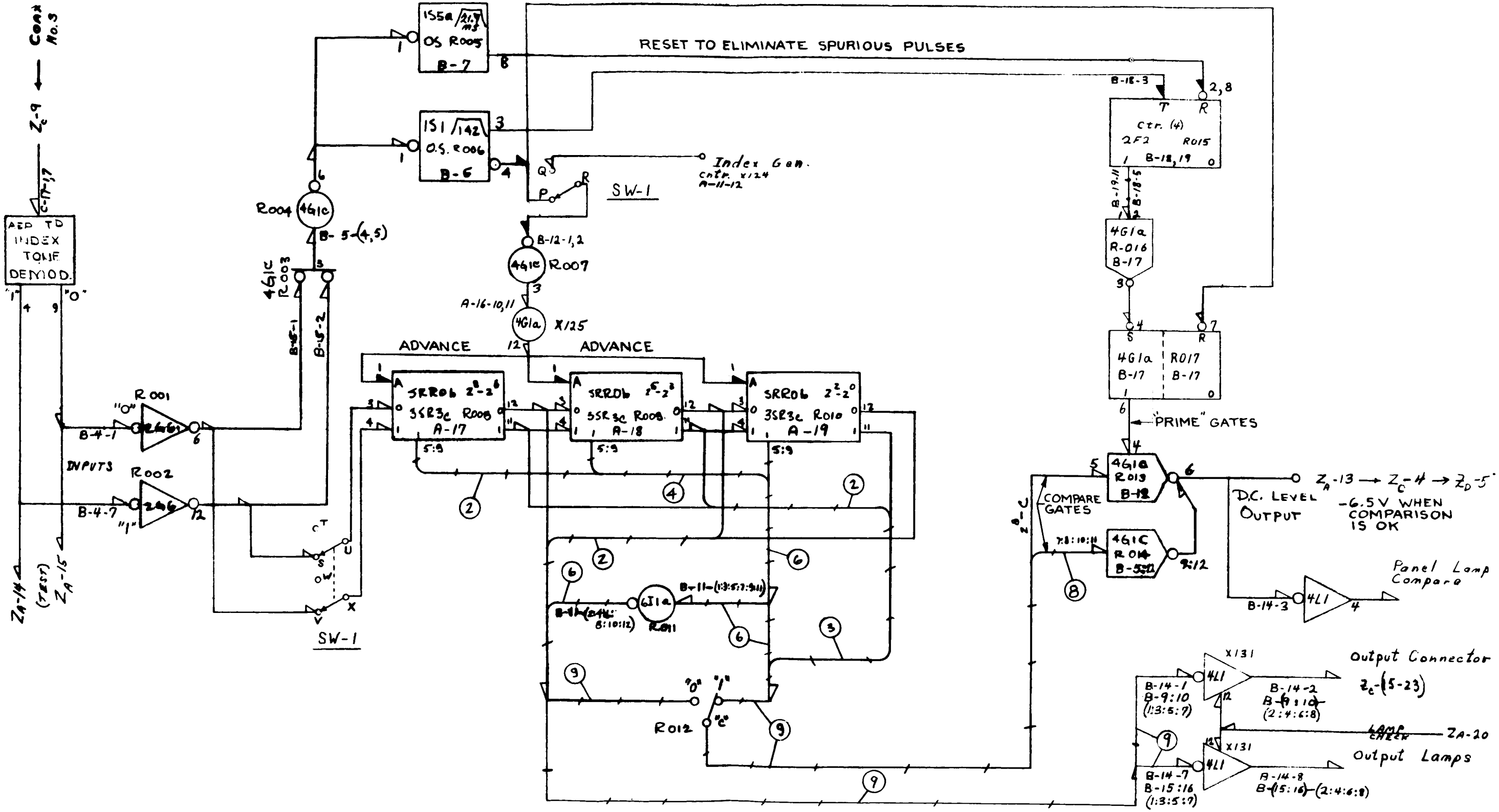

1177447A (MOD)

Figure 181. Sun-Angle Computer, Logic Diagram (Sheet 2 of 12)

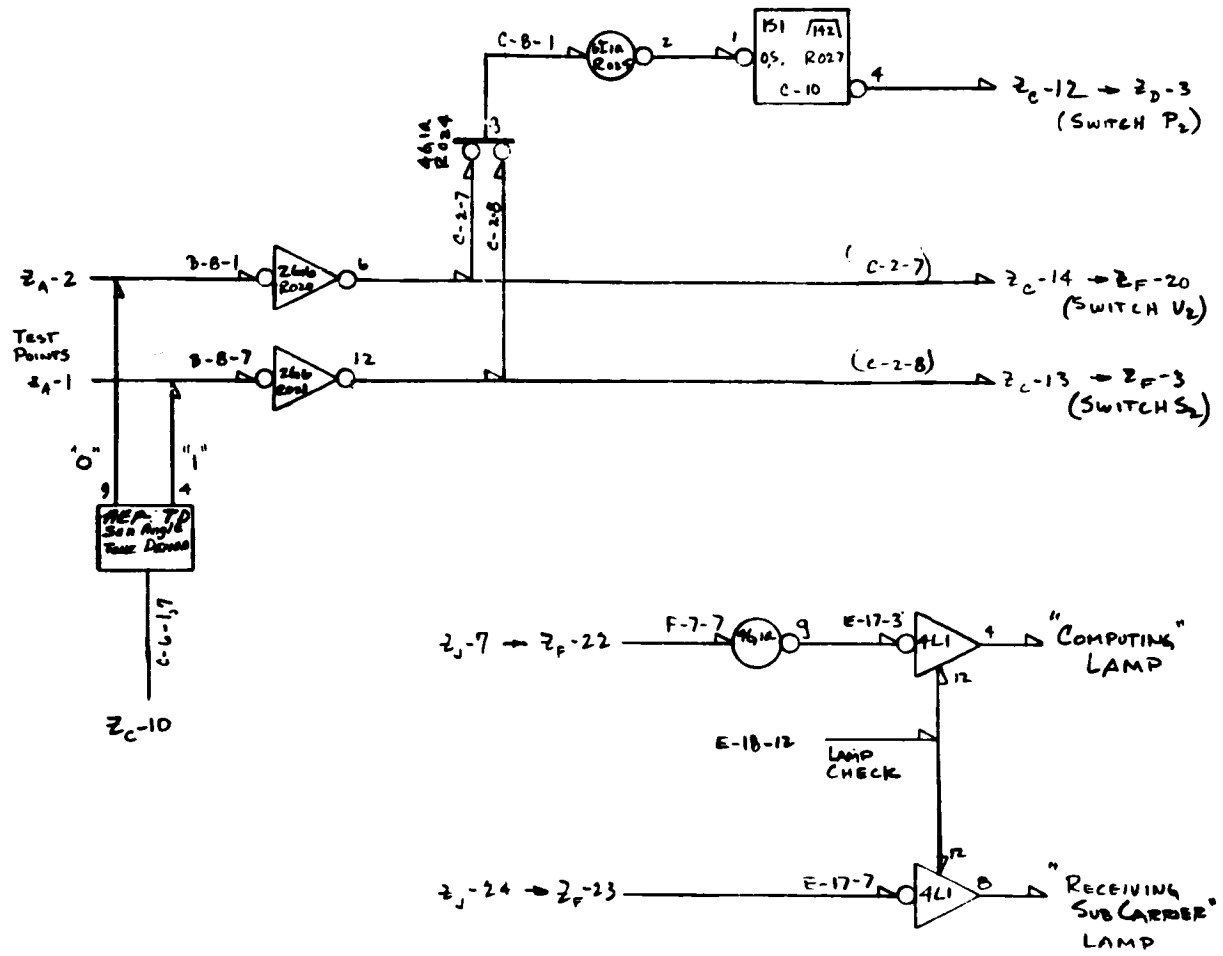

1177448A (MOD)

Figure 181. Sun-Angle Computer, Logic Diagram (Sheet 3 of 12)

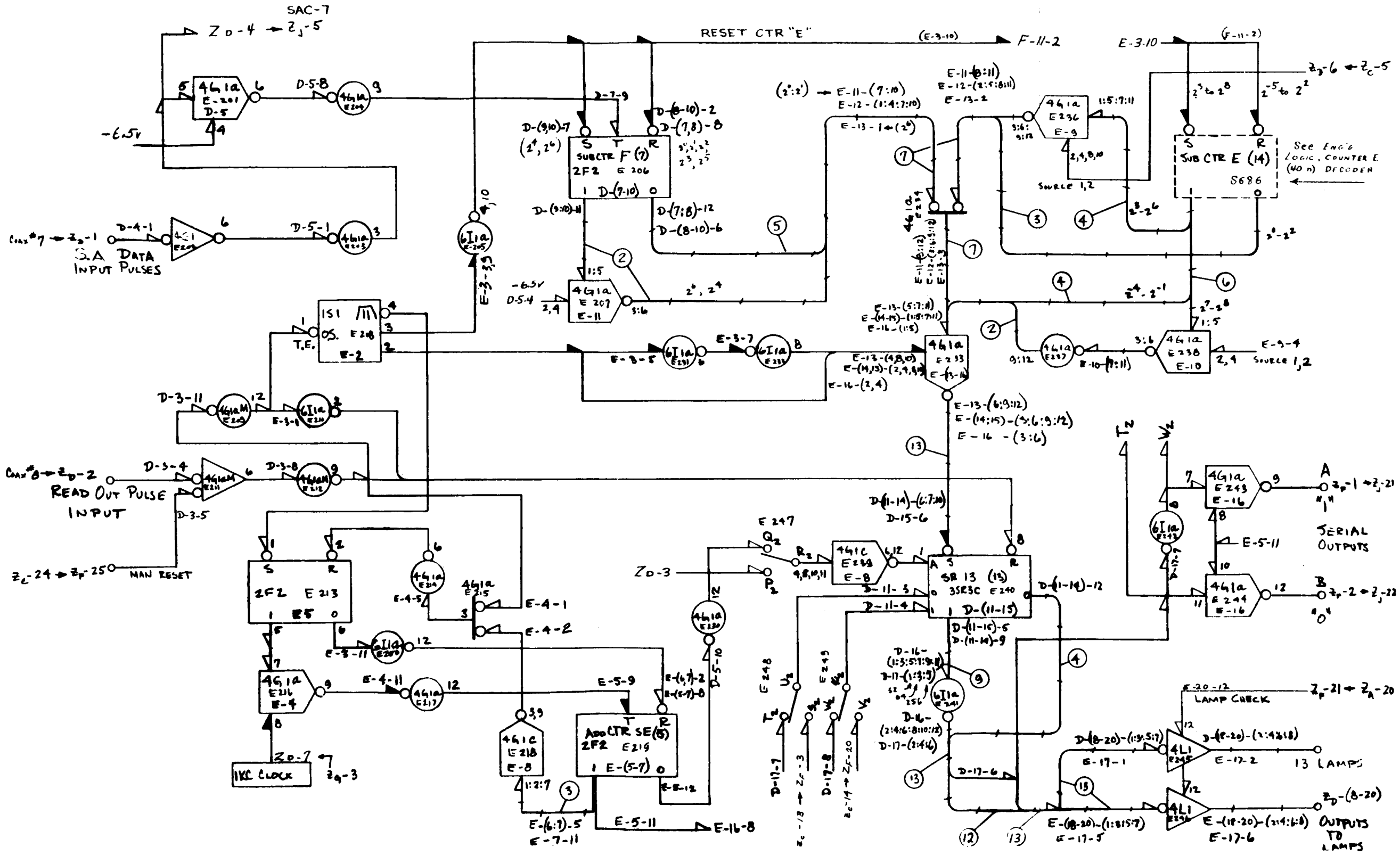

1177449A (MOD)

Figure 181. Sun-Angle Computer, Logic Diagram (Sheet 4 of 12)

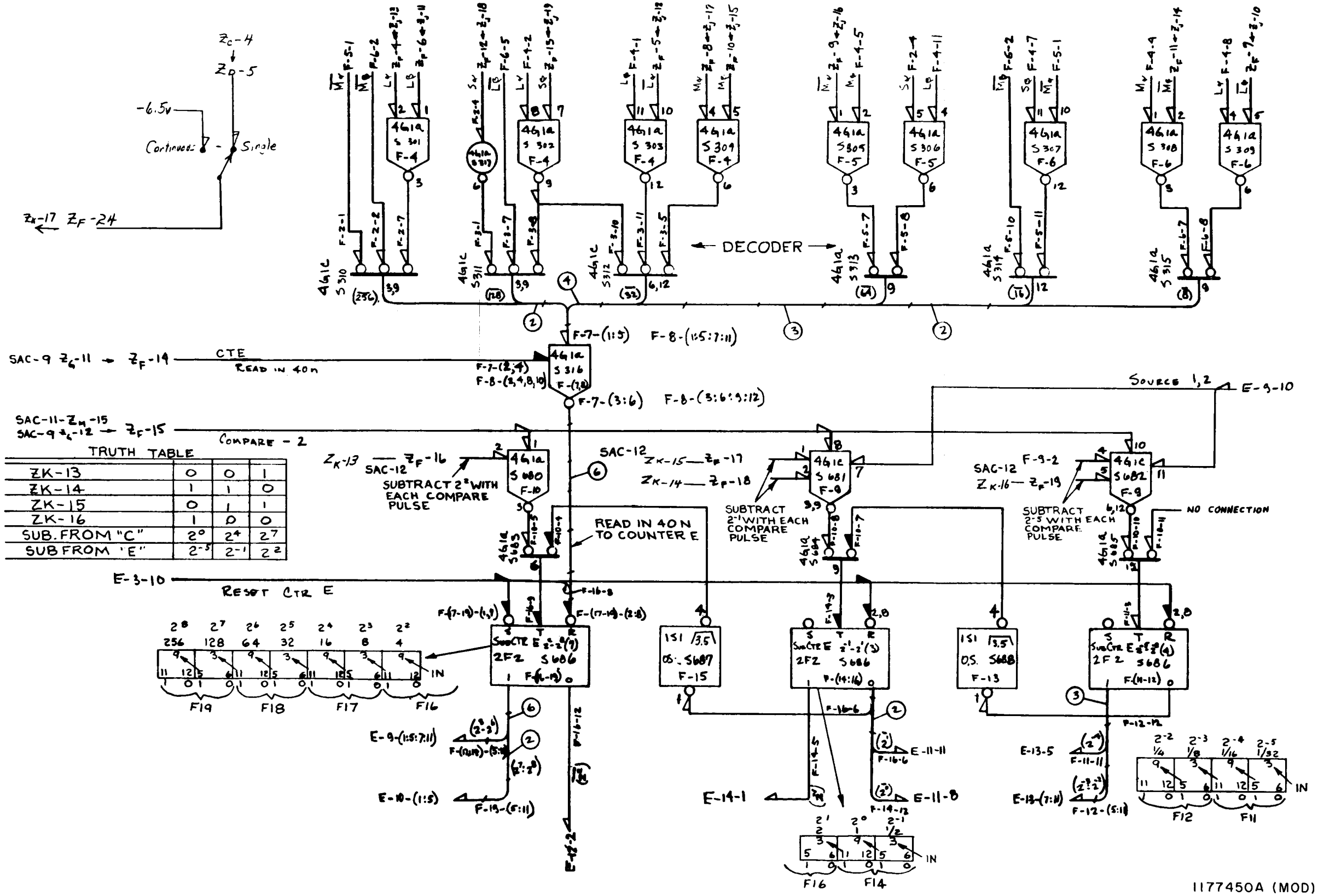

1177450A (MOD)

Figure 181. Sun-Angle Computer, Logic Diagram (Sheet 5 of 12)

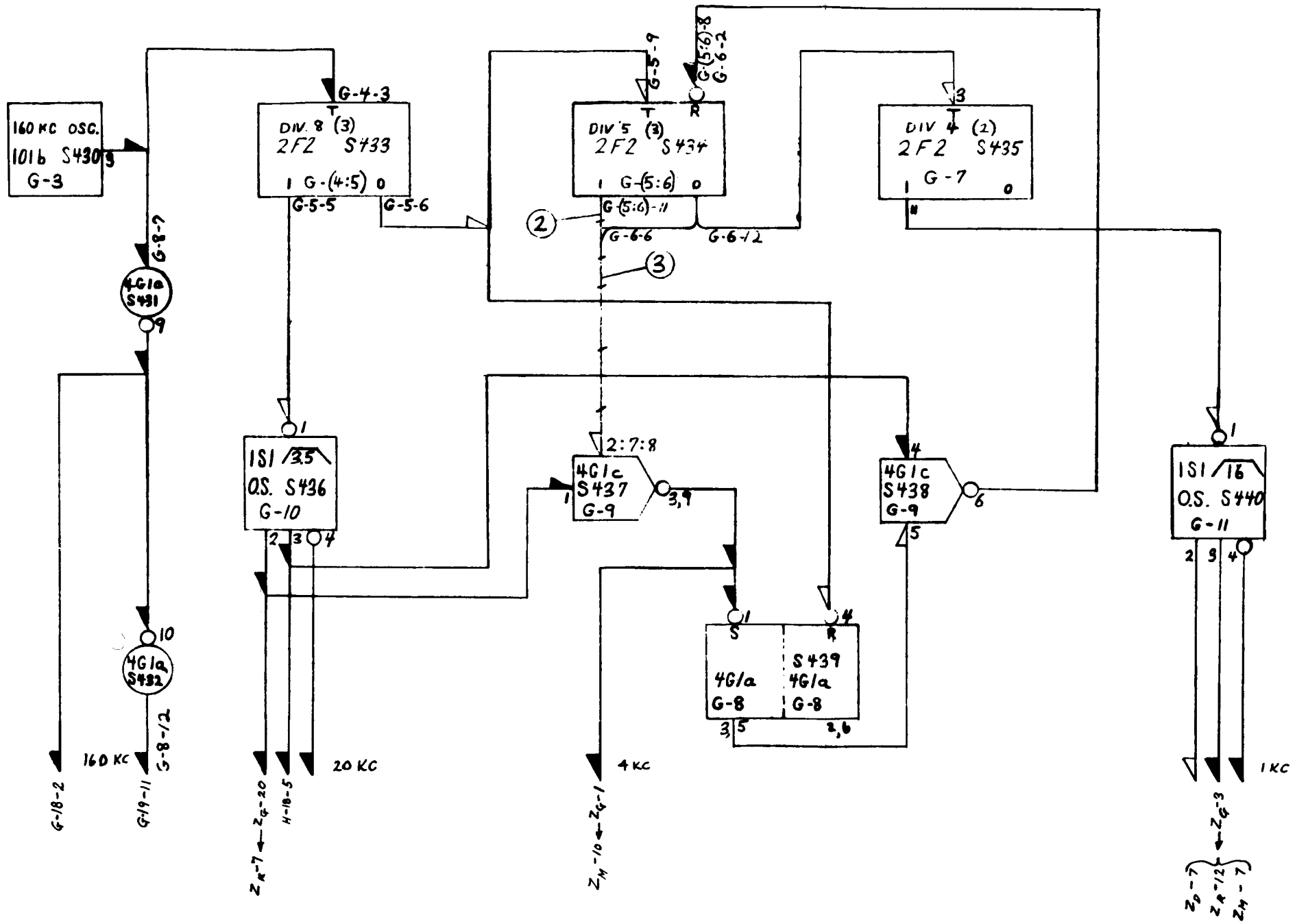

1177451A (MOD)

Figure 181. Sun-Angle Computer, Logic Diagram (Sheet 6 of 12)

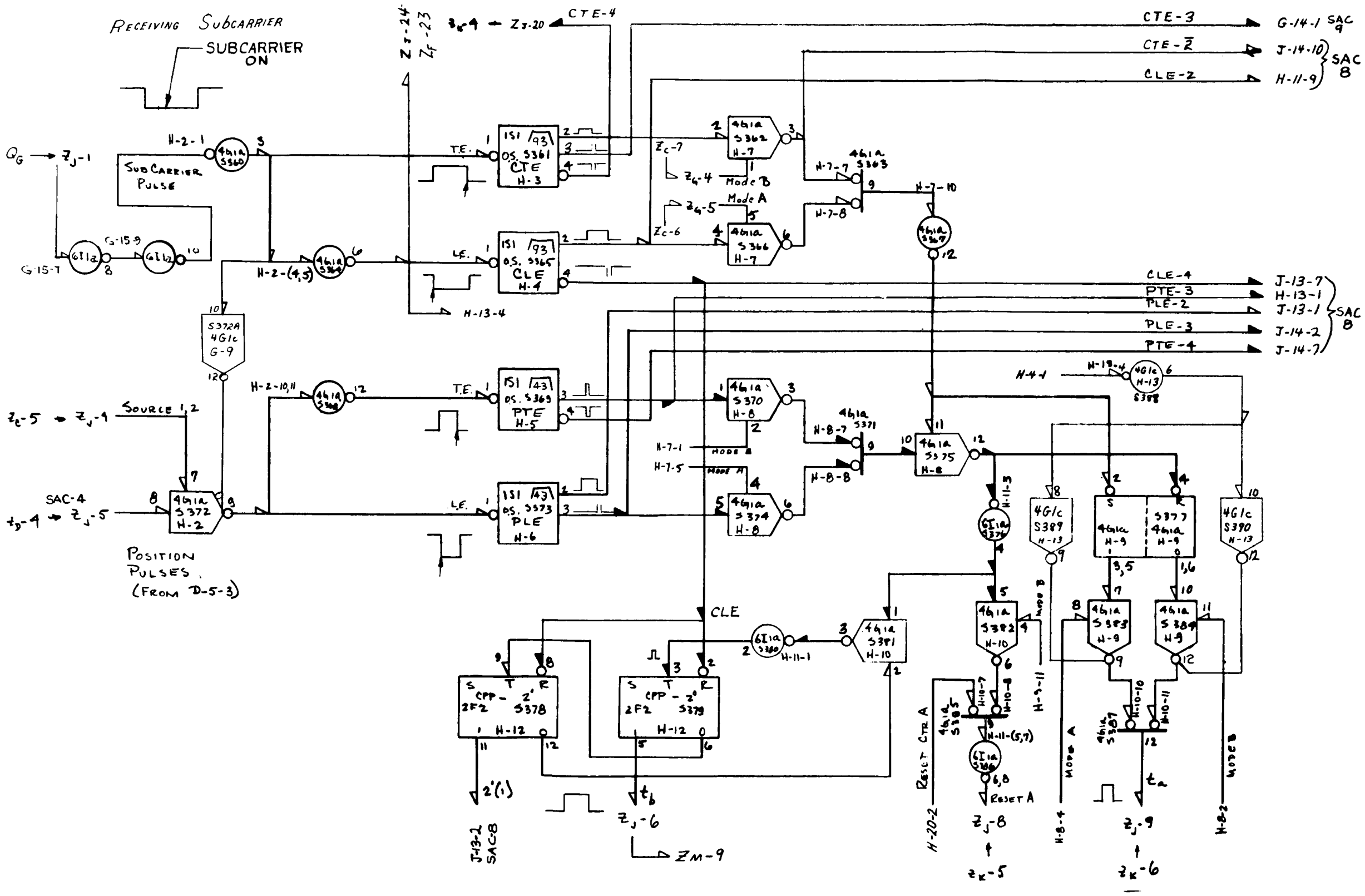

1177452A (MOD)

Figure 181. Sun-Angle Computer, Logic Diagram (Sheet 7 of 12)

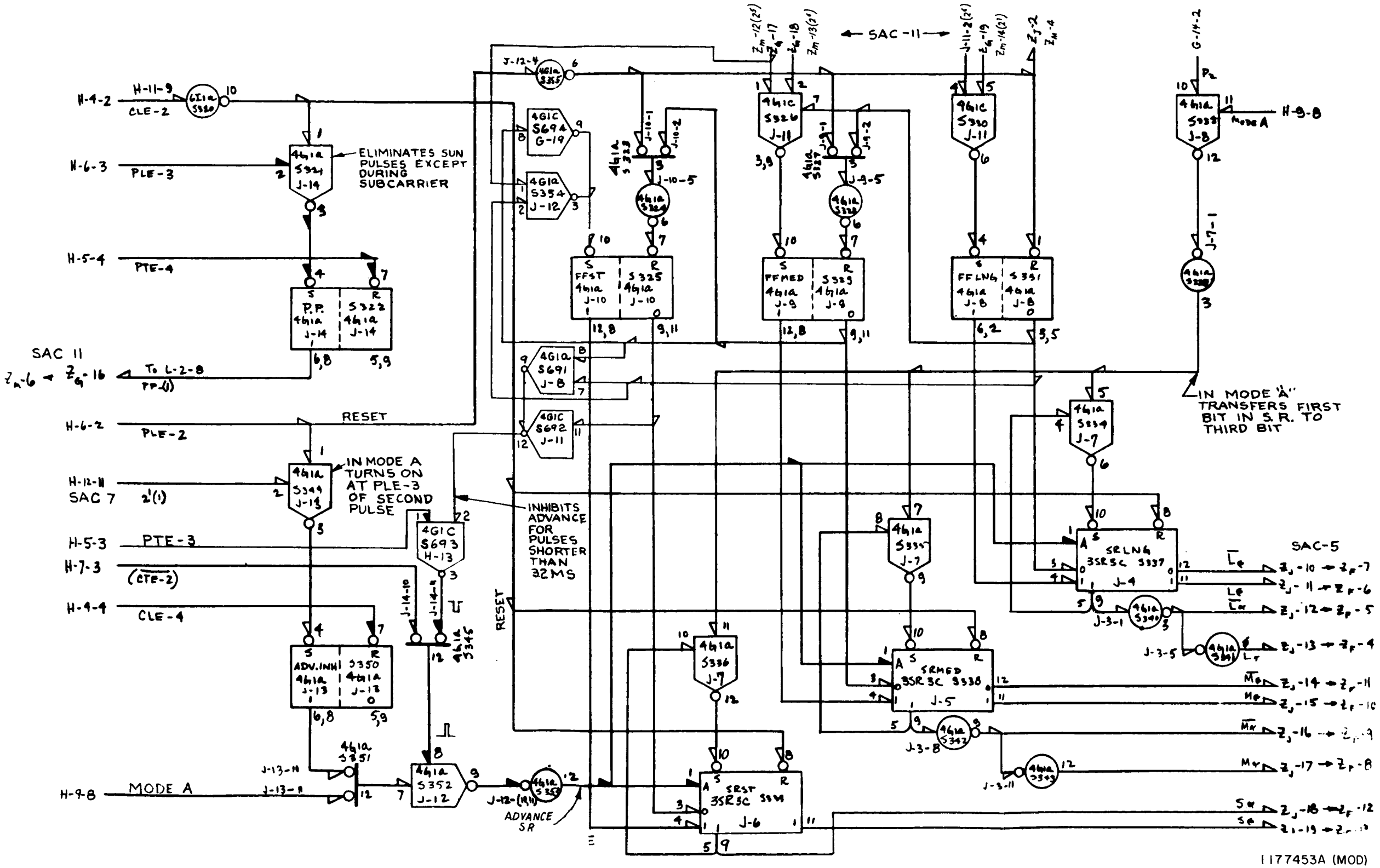

Figure 181. Sun-Angle Computer, Logic Diagram (Sheet 8 of 12)

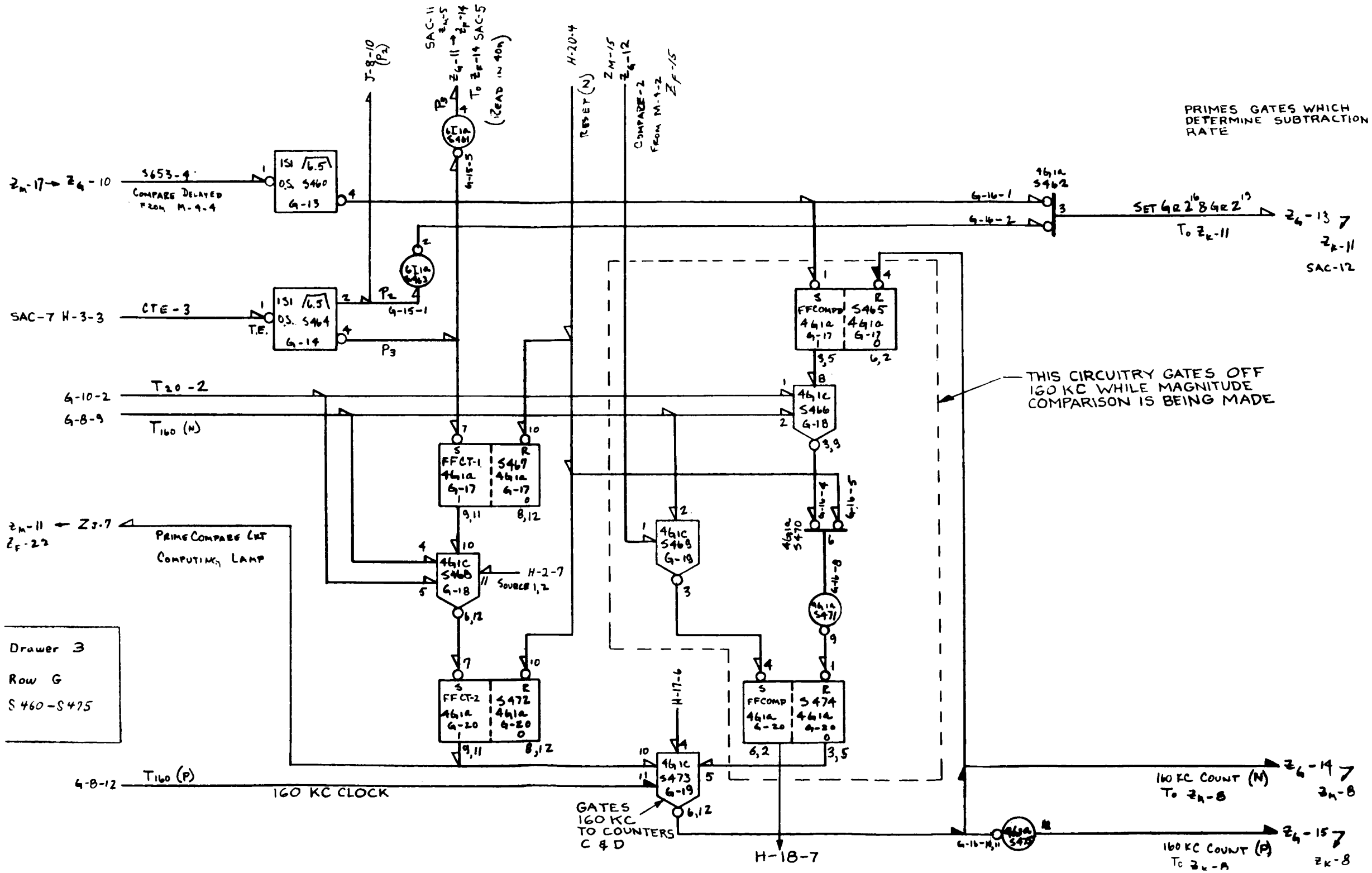

Figure 181. Sun-Angle Computer, Logic Diagram (Sheet 9 of 12)

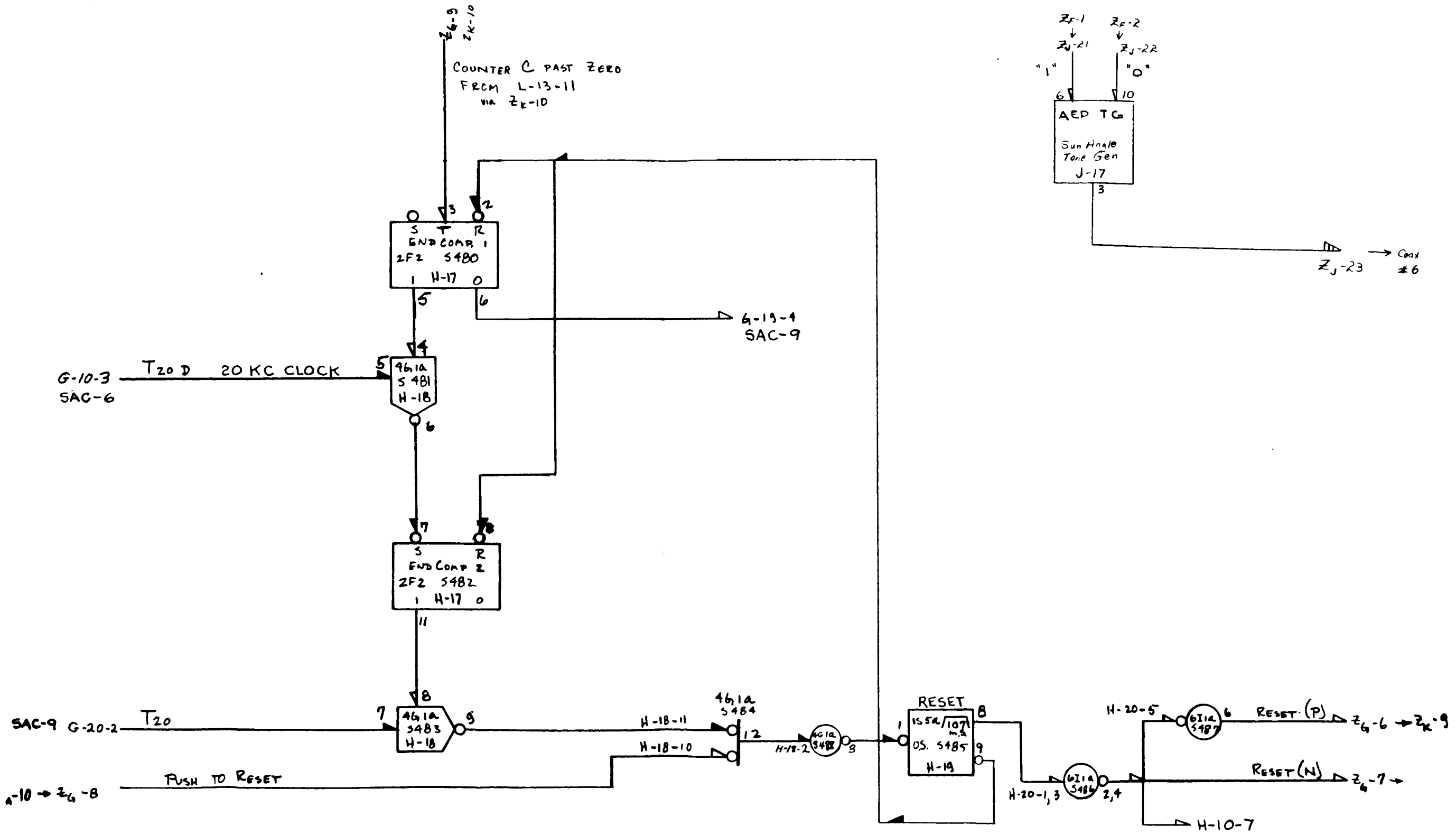

1177455A (MOD)

Figure 181. Sun-Angle Computer, Logic Diagram (Sheet 10 of 12)

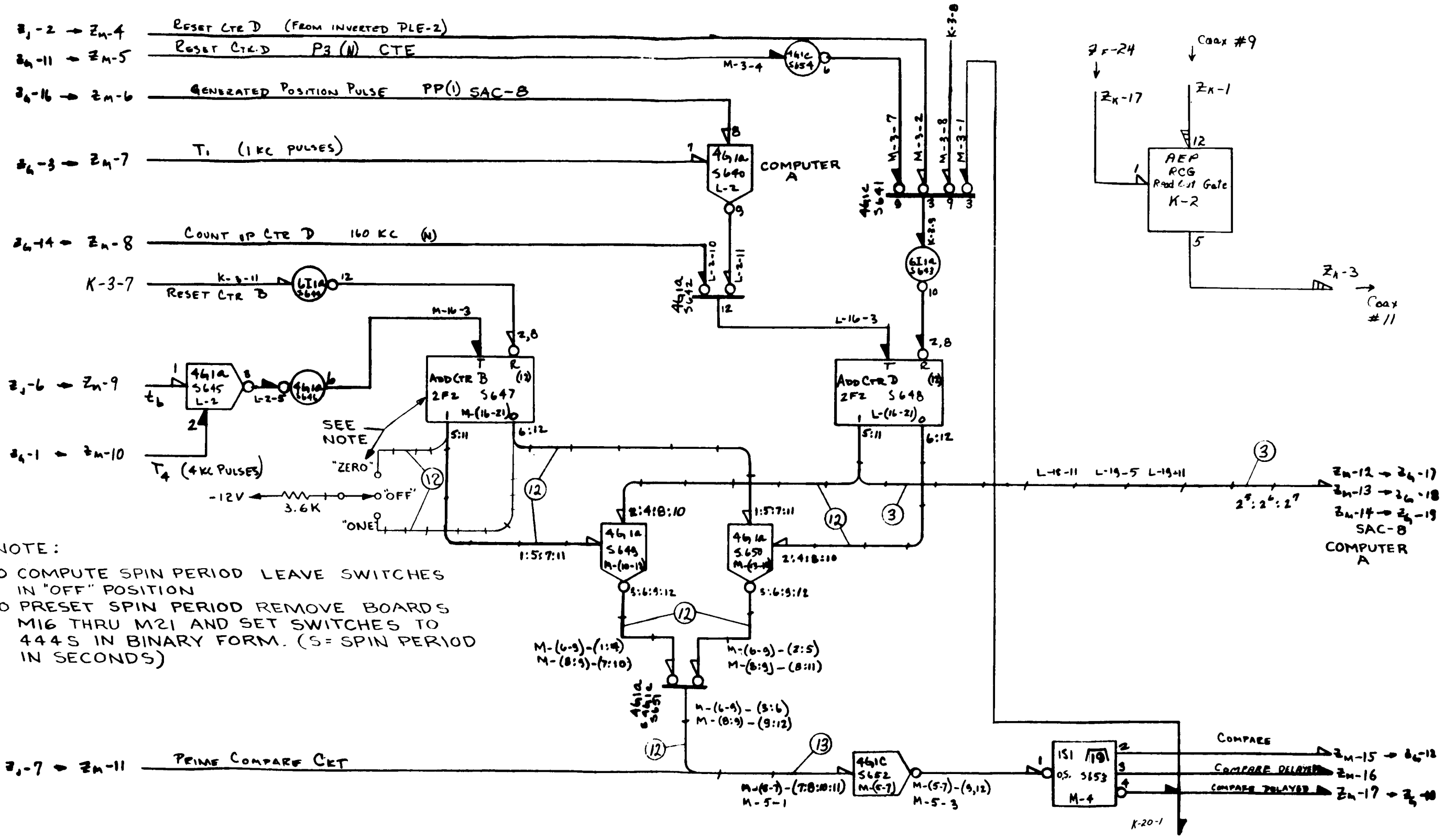

NOTE:

TO COMPUTE SPIN PERIOD LEAVE SWITCHES IN "OFF" POSITION

TO PRESET SPIN PERIOD REMOVE BOARDS M16 THRU M21 AND SET SWITCHES TO 4445 IN BINARY FORM. (S = SPIN PERIOD IN SECONDS)

1177456A (MOD)

Figure 181. Sun-Angle Computer, Logic Diagram (Sheet 11 of 12)

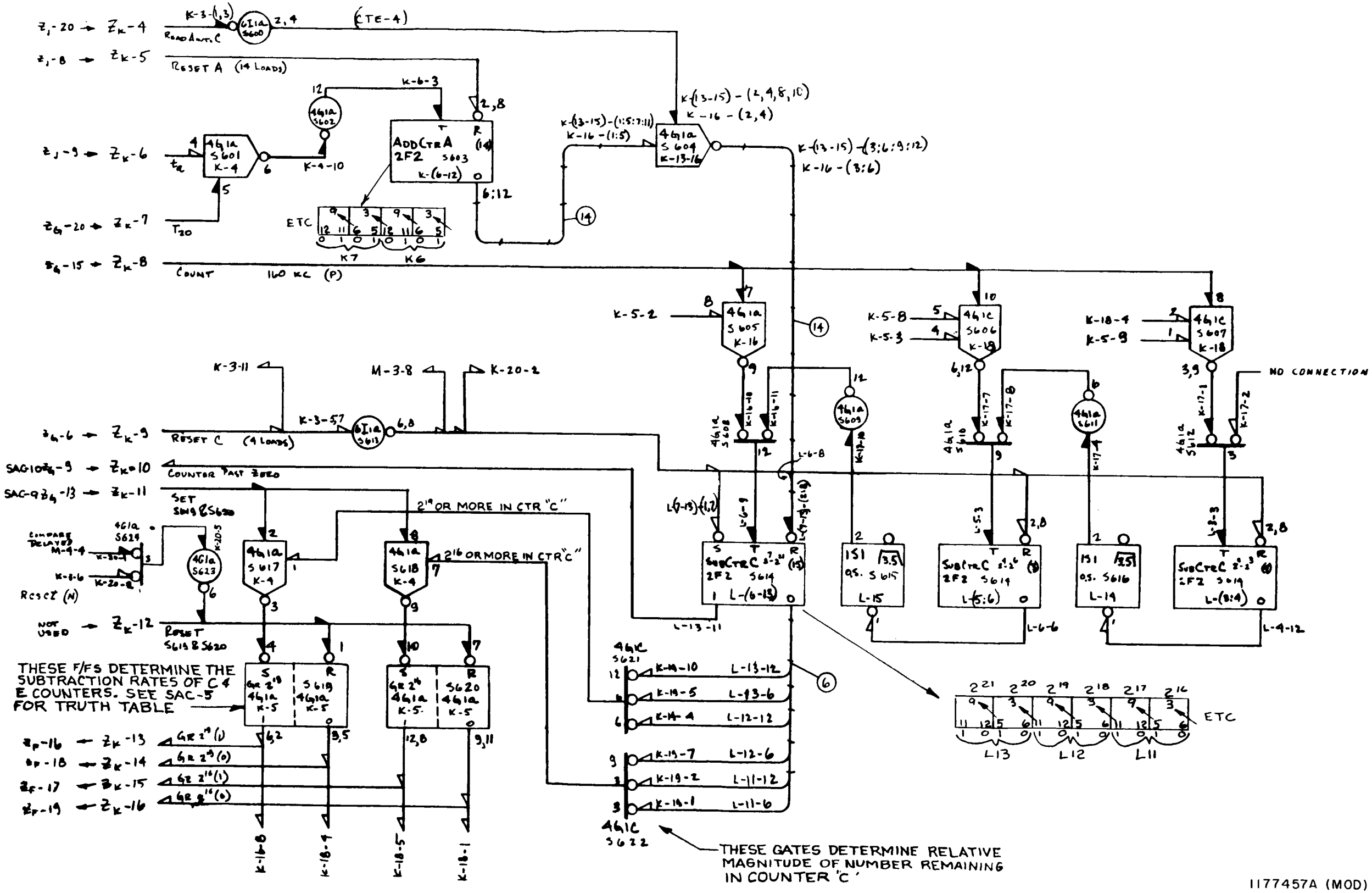

1177457A (MOD)

Figure 181. Sun-Angle Computer, Logic Diagram (Sheet 12 of 12)

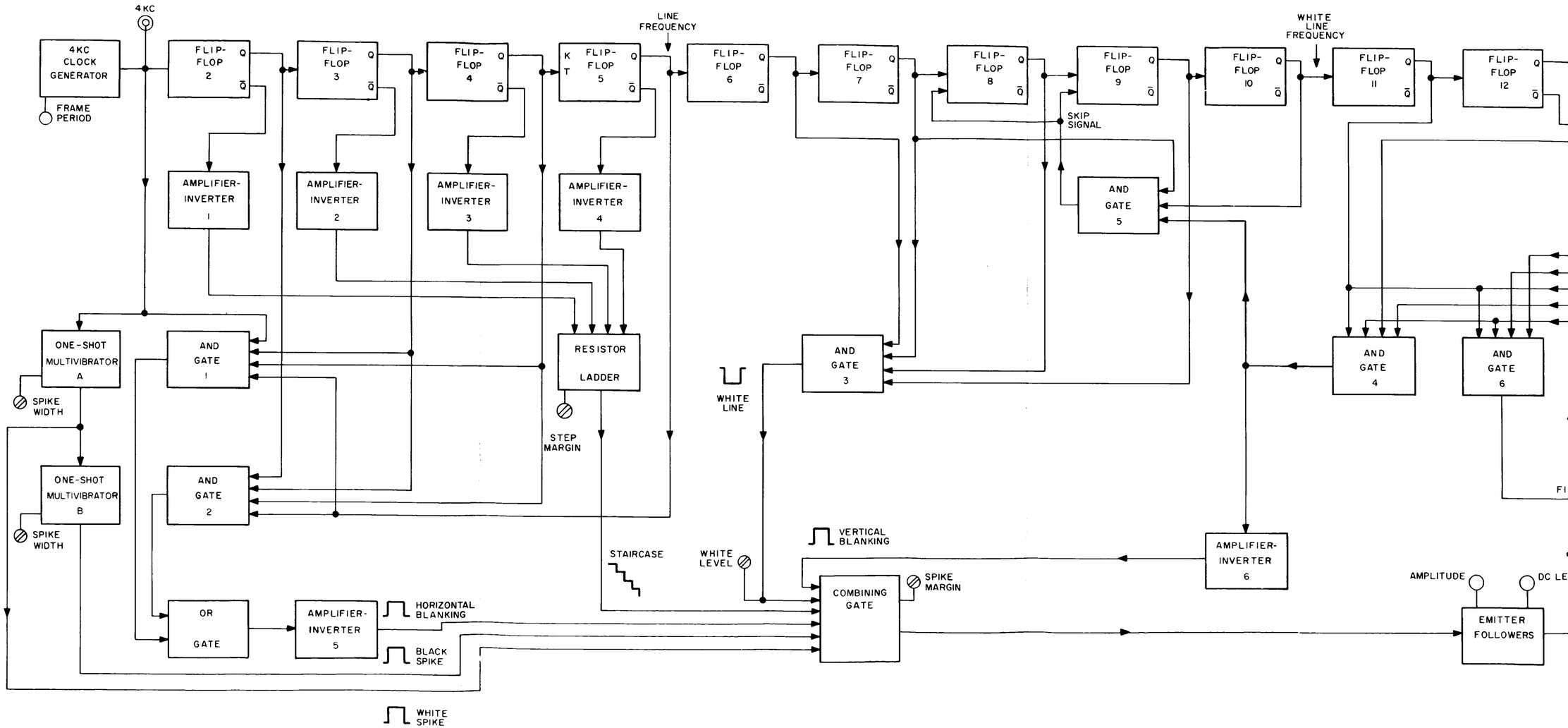
4KC
4KC CLOCK GENERATOR
FRAME PERIOD
FLIP-FLOP 2
FLIP-FLOP 3
FLIP-FLOP 4
KT FLIP-FLOP 5
LINE FREQUENCY
FLIP-FLOP 6
FLIP-FLOP 7
FLIP-FLOP 8
FLIP-FLOP 9
FLIP-FLOP 10
WHITE LINE FREQUENCY
FLIP-FLOP 11
FLIP-FLOP 12
SKIP SIGNAL
AMPLIFIER-INVERTER 1
AMPLIFIER-INVERTER 2
AMPLIFIER-INVERTER 3
AMPLIFIER-INVERTER 4
AND GATE 5
ONE-SHOT MULTIVIBRATOR A
SPIKE WIDTH
AND GATE 1
RESISTOR LADDER
STEP MARGIN
AND GATE 3
WHITE LINE
AND GATE 4
AND GATE 6
ONE-SHOT MULTIVIBRATOR B
SPIKE WIDTH
AND GATE 2
VERTICAL BLANKING
AMPLIFIER-INVERTER 6
STAIRCASE
WHITE LEVEL
COMBINING GATE
SPIKE MARGIN
AMPLITUDE
DC LE
OR GATE
AMPLIFIER-INVERTER 5
HORIZONTAL BLANKING
BLACK SPIKE
EMITTER FOLLOWERS
WHITE SPIKE

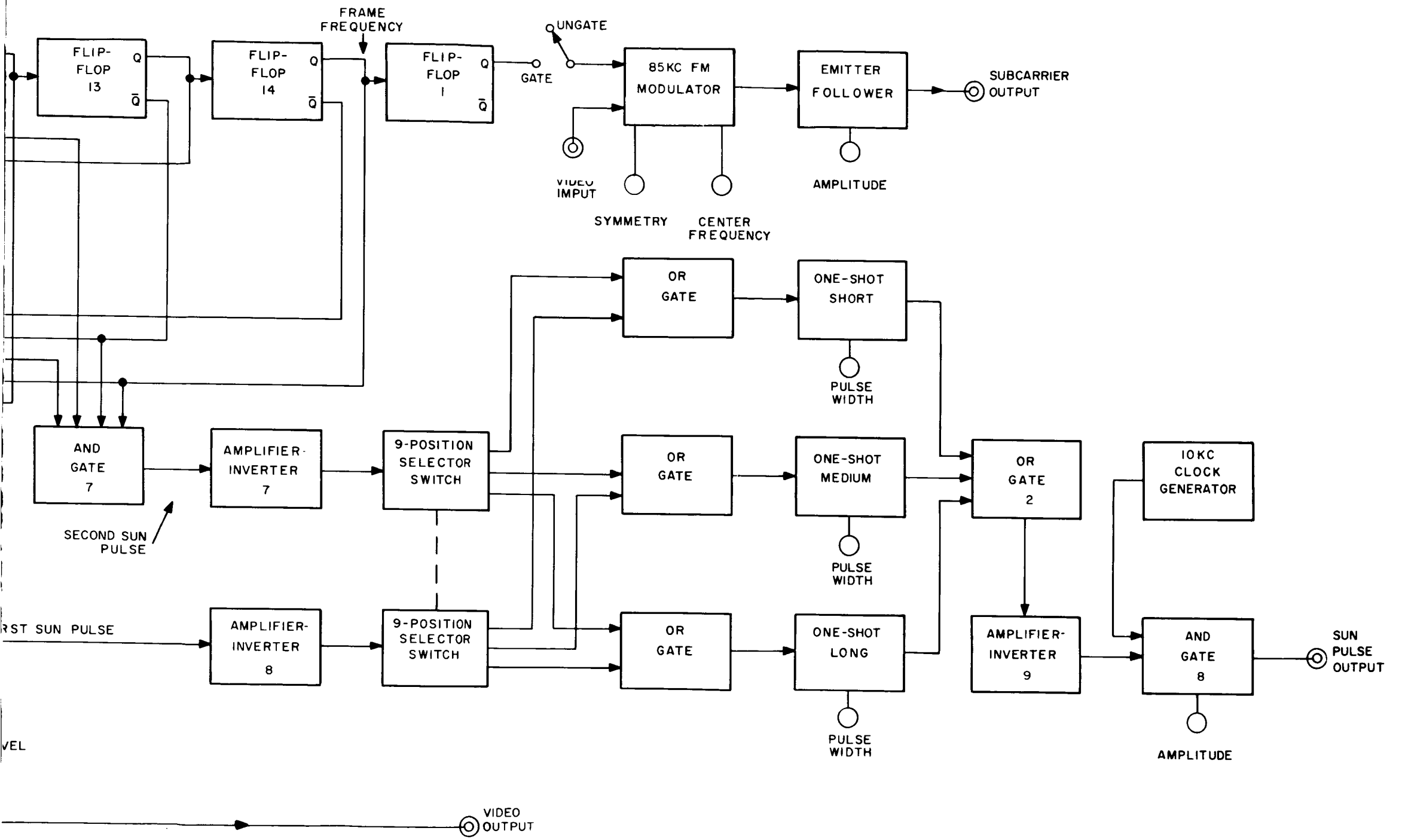

339064

Figure 188. Calibrator, Block Diagram

CONNECTIONS TO PACKARD-BELL MODULAR UNITS			
CONNECTION		VIA WIRE	TO PIN
STAIRCASE DRIVERS	MOST SIGNIFICANT	Z8	V2
		Z7	V4
		Z6	V6
	LEAST SIGNIFICANT	Z5	V9
WHITE CLAMP VOLTAGE		Y8	D2
COMBINING BUSS		Y7	D3
+6V		Z2	C1
GRD		Z3	C8
-12V		Z4	C15
FRAME PERIOD		Z1	P11
BLACK SPIKE COMBINER	WHITE LINE	Y12	K4
	BLACK COMBINER GATE	Y13	U9
	BLACK SPIKE	Y14	Q10
GATE TO 85KC SCO		Z9	R6
		Z10	R3
GATES TO SUN PULSE SELECTOR SWITCH	FIRST	Y10	H4
	SECOND	Y11	H6
TO SUN PULSE GATES	SHORT SECOND	Y2	G7
	SHORT FIRST	Y1	G6
	MEDIUM SECOND	Y6	K10
	MEDIUM FIRST	Y5	K9
	LONG SECOND	Y4	E7
	LONG FIRST	Y3	E6
KEYED 10KC SUN PULSE BYPASS		Y9	D5
		Y15	D4
SUN PULSE KEYING		Z12	D6
HOR SYNC		Z13	U12
4KC CLOCK		Z11	P4

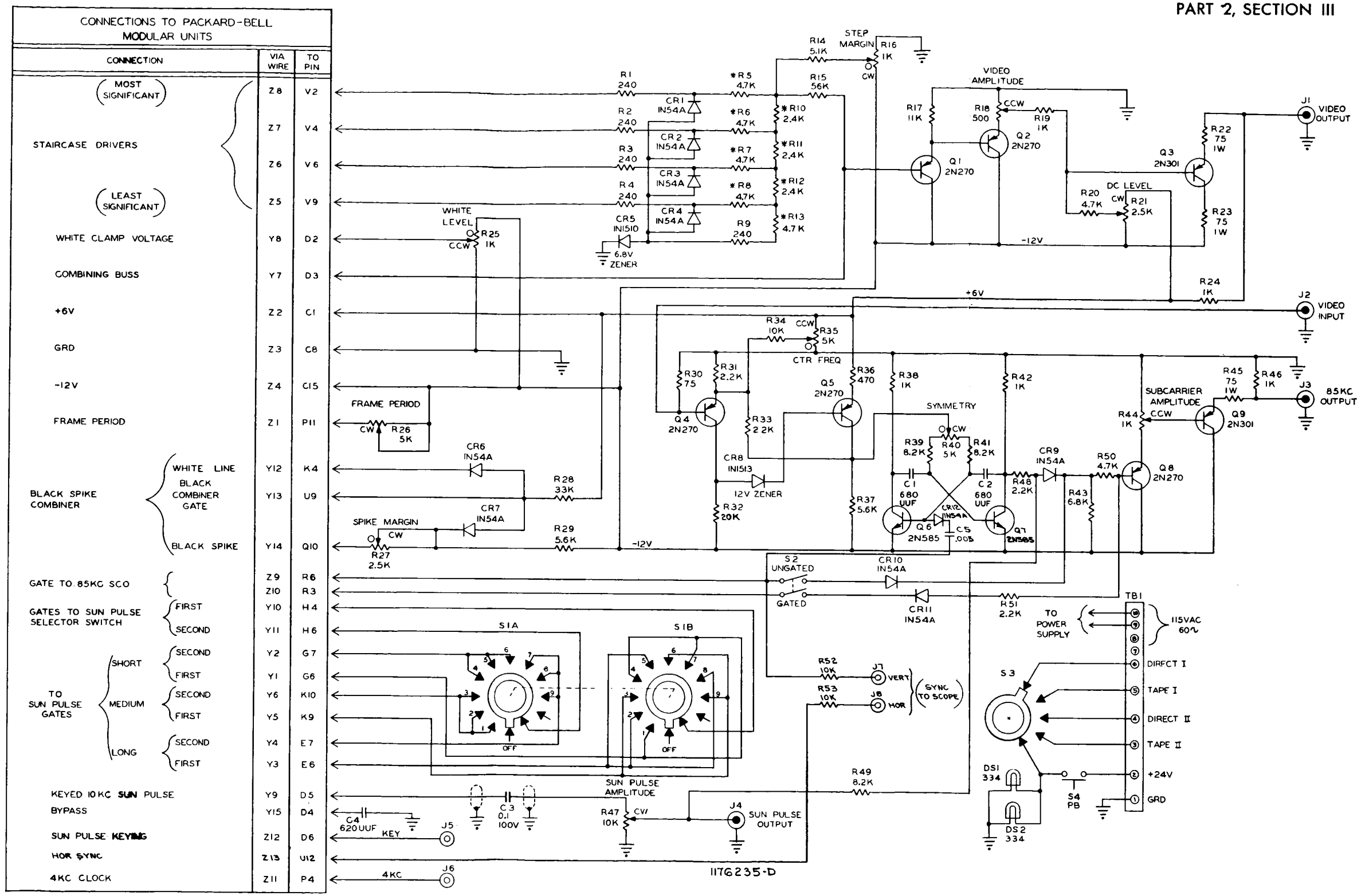

NOTE:
- ALL CAPACITORS IN UF UNLESS OTHERWISE NOTED.
- ALL RESISTORS IN OHMS UNLESS OTHEWISE NOTED.
- * THESE RESISTORS SPECIALLY SELECTED & MATCHED.
- ROTARY SWITCHES SHOWN AS VIEWED FROM REAR OF PANEL.

1176235D

Figure 190. Calibrator, Schematic Diagram (Sheet 1 of 2)

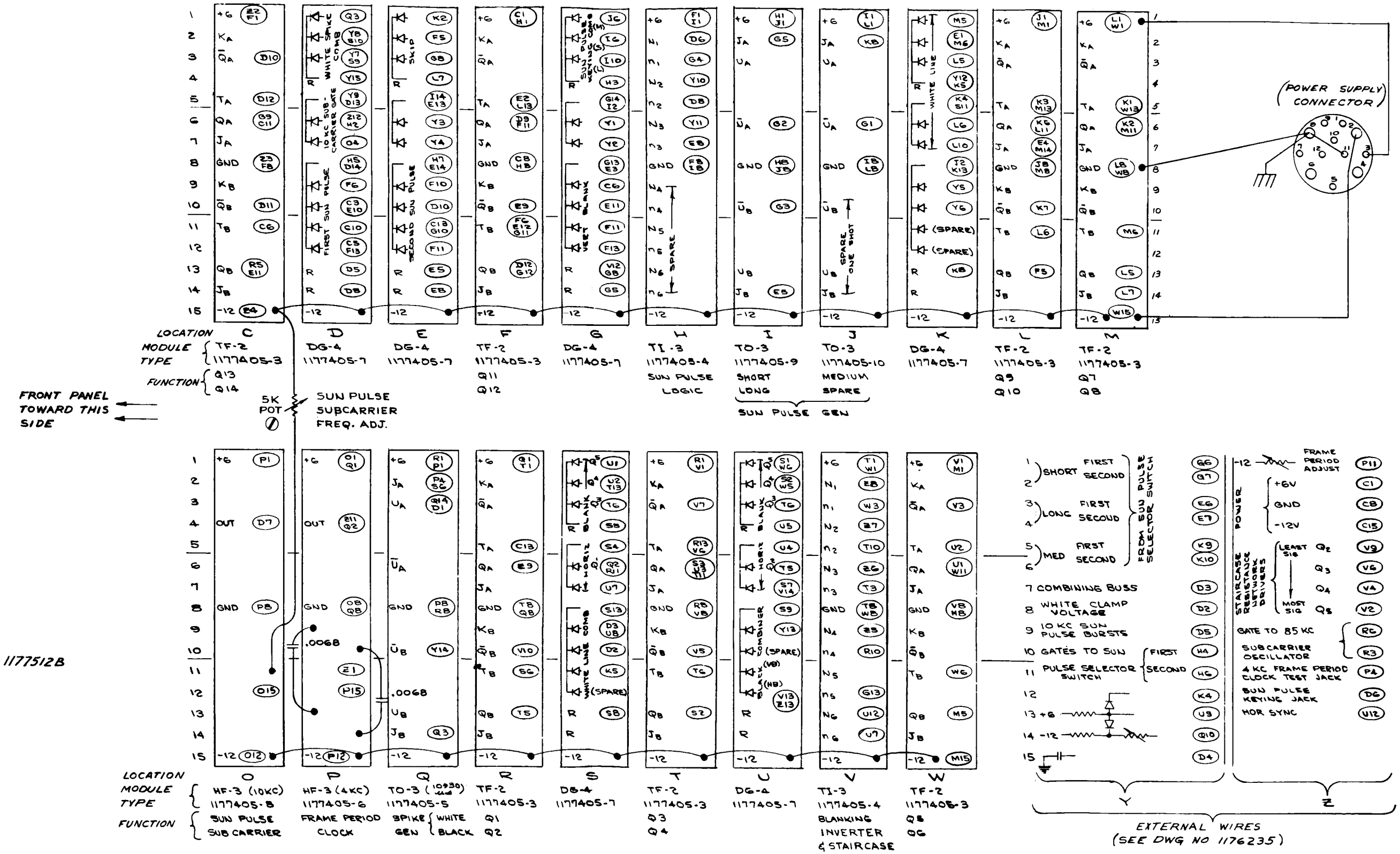

Figure 190. Calibrator, Schematic Diagram (Sheet 2 of 2)

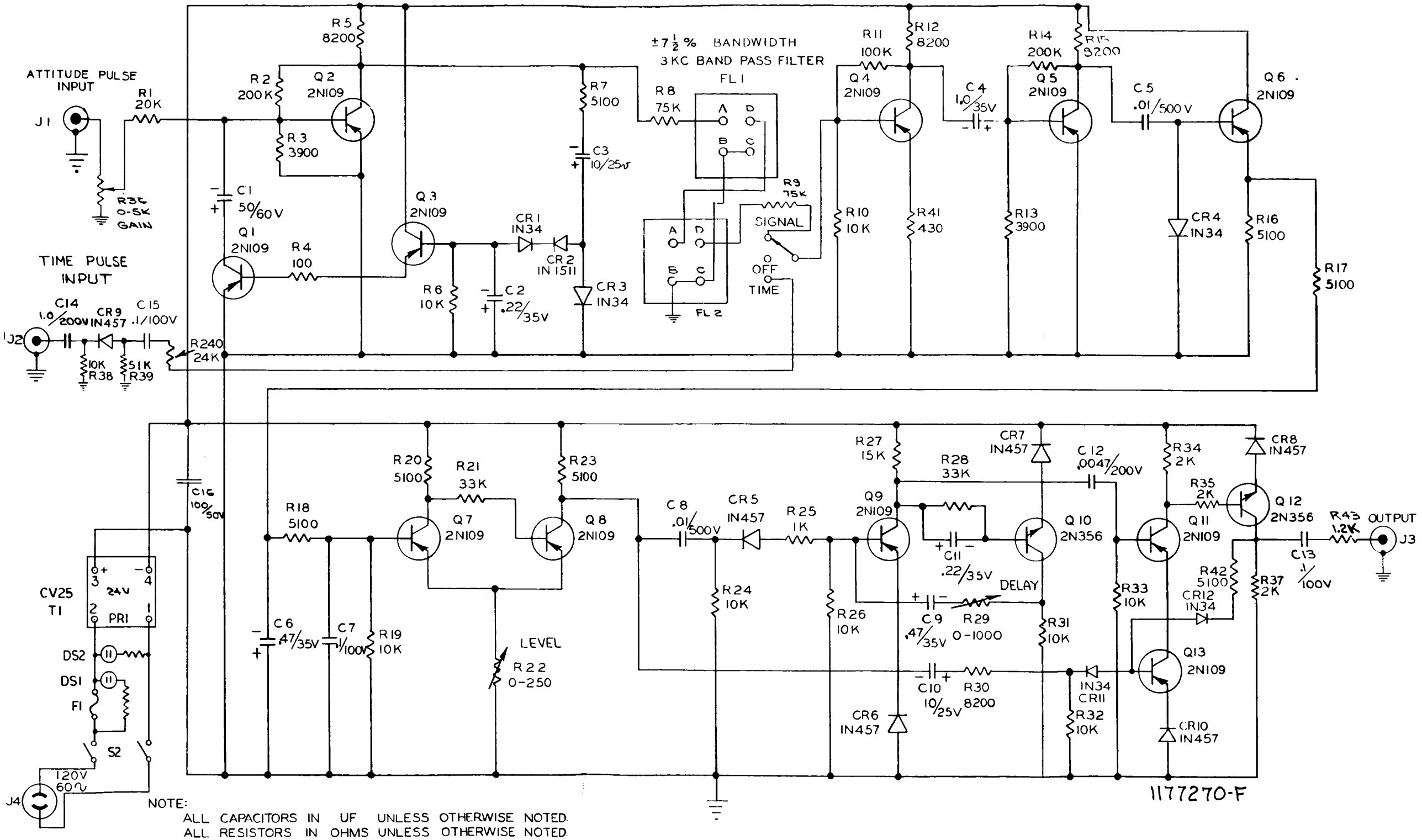

NOTE:
ALL CAPACITORS IN UF UNLESS OTHERWISE NOTED.
ALL RESISTORS IN OHMS UNLESS OTHERWISE NOTED.
FOR PARTS LIST REFER TO DWG 1170377
FOR WIRING DIAGRAM SEE DWG 1176378

1177270F

Figure 193. Attitude Pulse Demodulator, Schematic Diagram

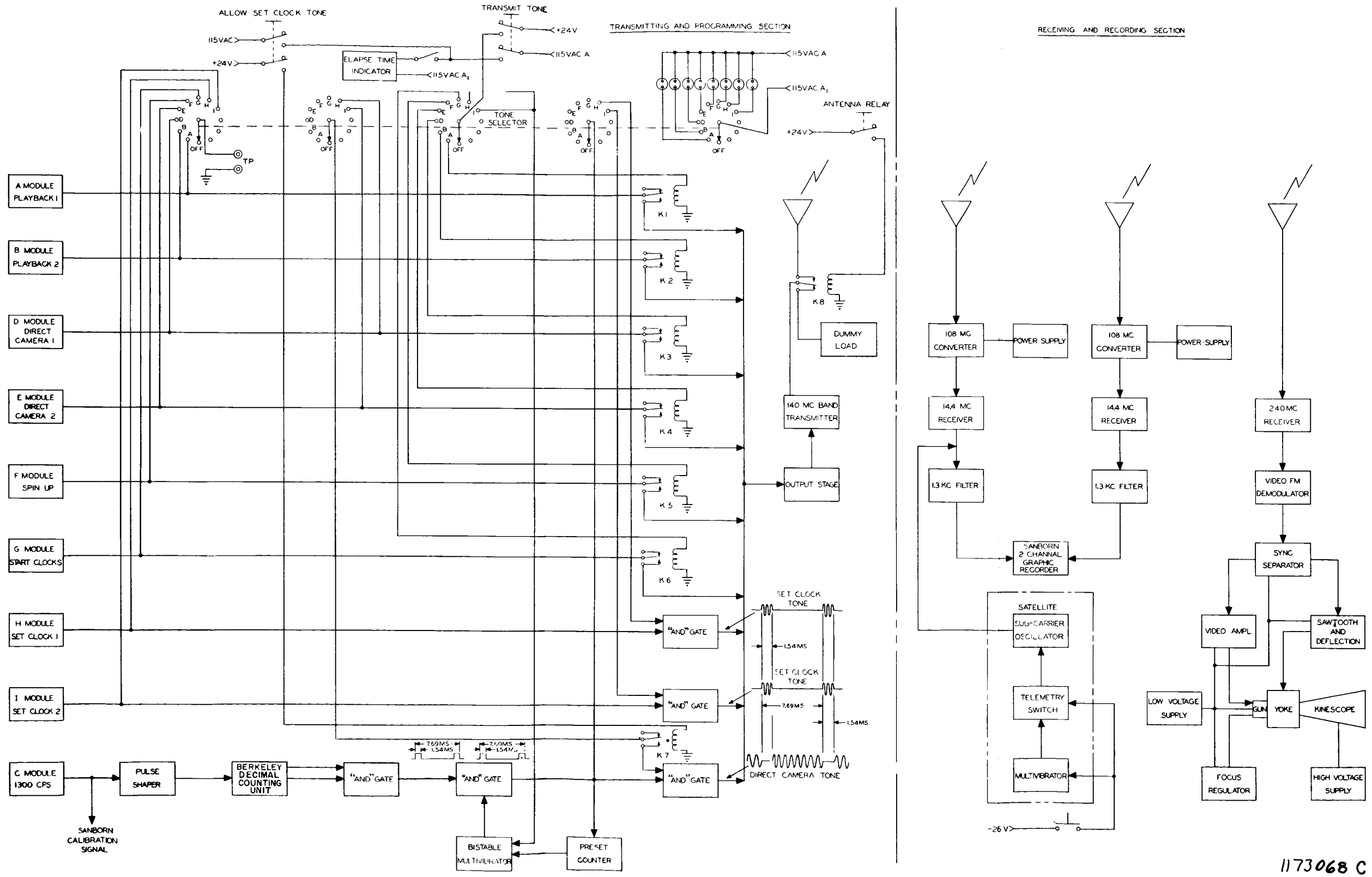

1173068 C

Figure 196. Checkout Equipment, Block Diagram

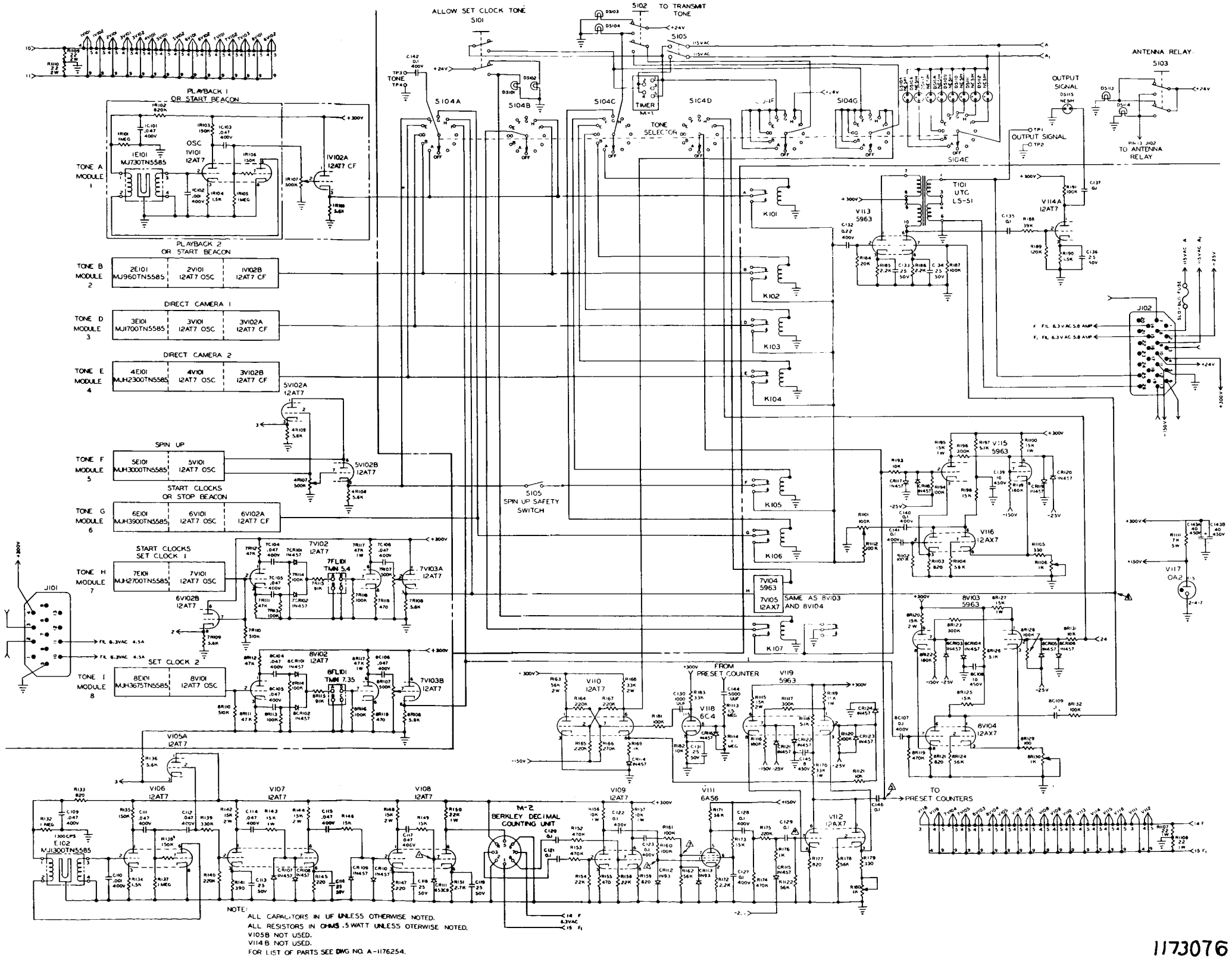

1173076D

Figure 197. Checkout Programmer, Schematic Diagram

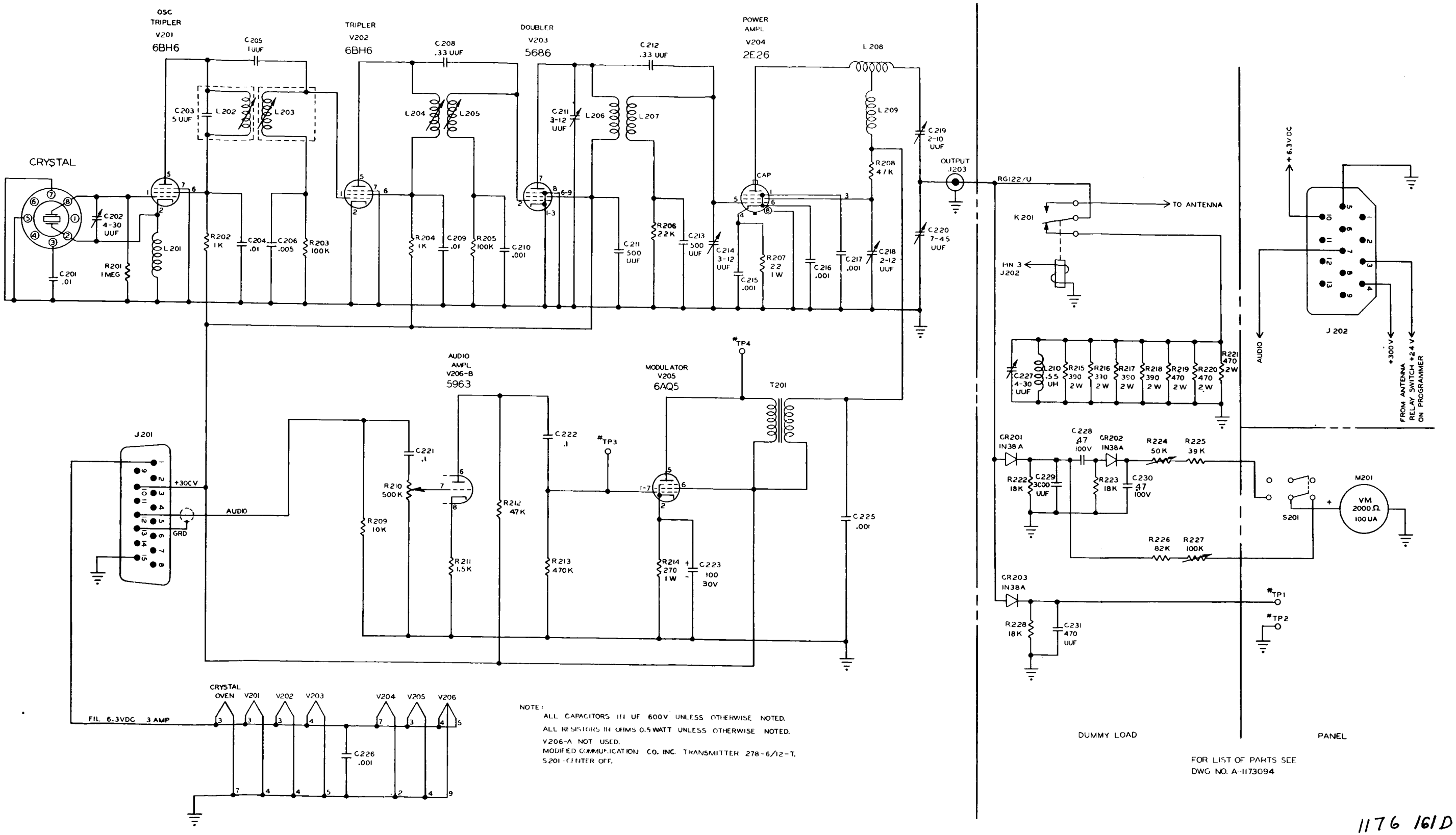

NOTE:
ALL CAPACITORS IN UF 600V UNLESS OTHERWISE NOTED.
ALL RESISTORS IN OHMS 0.5 WATT UNLESS OTHERWISE NOTED.
V206-A NOT USED.
MODIFIED COMMUNICATION CO. INC. TRANSMITTER 278-6/12-T.
S201 - CENTER OFF.

FOR LIST OF PARTS SEE DWG NO. A-1173094

1176 161D

Figure 198. Checkout Command Transmitter, Schematic Diagram